Waveguide properties of thin polymer films

Yitao Ren

Waveguide Properties of Thin Polymer Films

Yitao Ren

A thesis submitted for the degree of

Doctor of Philosophy

at the

University of Durham, Department of Physics

March 1999

Abstract

Some basic concepts and principles of optical dielectric slab waveguiding and experimental methodology involving characterisation of waveguide films are introduced. Results from the characterisation of thin polymeric waveguide films and measurements of refractive indices of the films are presented. The birefringence of some polymer films is analysed and discussed.

The photostabilities of several dopants (DEMI, Ultra-DEMI, Dicyclohexyl-DEMI, Mor2, Morpip and DCM) are investigated in a polymer matrix (PMMA), and their measured photostabilities are presented. These organic chromophores change their properties in the course of photodegradation. Degradation experiments are carried out by exposing the doped waveguide films to light in air, vacuum and nitrogen environments. The degradation mechanisms of these chromophores are discussed. It is found that the degradation of the DEMI, Ultra-DEMI, Dicyclohexyl-DEMI and DCM are due to photooxidation, their photostabilities are much higher in vacuum than in air. The Mor2 and Morpip degrade by direct photodecomposition, their photostabilities are in the same order when exposed to light in their main absorption bands. The oxygen free environment (e.g. vacuum) is essential to increase their photostabilities. A beam branching effect in DCM doped waveguide film is observed.

Stacked multi-layer waveguides are investigated as possible humidity sensors. Symmetric structure (PMMA/P-4VP/PMMA/P-4VP/PMMA) (P4VP-I) and unsymmetric structure (SiO_2/P-4VP/Zeonex/P-4VP/Air) (P4VP-II) are studied. Special procedures and process have been developed to fabricate multi-layer waveguide structures in experiments. It is found that both structures have good reversibilities and show reasonable stabilities. 30 ppm concentrations of water vapour can be detected by the P4VP-II structure. The experimental results show that the overall response of P4VP-II structure exhibits good linearity with increase of the concentration of water vapour. The structures can not only measure the phase shift of interference, but also can measure the direction of fringe movement. The sensitivity of the structure can be further improved by using different combinations of polymers in the structure.

Acknowledgements

First and foremost I would like to express my sincere gratitude to my supervisor Dr. Graham Cross for his trust, guidance and full support throughout this research; and for his modelling on the propagation of laser beam along a multi-layer waveguide structure. I would not be in a position to submit without his continuous supervision, his inspiration and ideas in discussions allow me to understand many aspects of my studies and broaden my horizons. I am deeply grateful to Professor David Bloor for his help and advices during my studies. It has been a privilege for me to be a member of optoelectronics research group of the University of Durham and to have an opportunity to study in the active and creative atmosphere of the group here.

I would like to express my special thanks to Dr. Marek Szablewski for his reading, language correction and comments on my thesis, and for the synthesis of nonlinear optical materials for my studies. I enjoyed and benefited from discussions on chemistry with him. His understanding, kindness and patience has also been exemplary.

I would also like to thank Dr. Ken Durose for the SEM pictures of multi-layer waveguide structure; Dr. Dave Healy for his help on refractive index measurements; Dr. Phil Thomas and Mr. Akira Masutani for much help on computing techniques; Dr. Yasuyuki Kagawa for the synthesis of nonlinear optical materials. I would also like to thank Nancy-Ann Hackam and other members of optoelectronics research group for making my study period very enjoyable. I am also grateful to Norman Thompson and David Patterson for their excellent technical support in my research and perseverance in the labs.

I am also grateful to the committee of vice-chancellors and principals (CVCP) for its overseas research students award, the department of Physics for its partial financial support; the Graduate Society for its free accommodation award during my 3 years' study; Dr. N. J. Freeman from Farfield Sensors Ltd. for his help on waveguide sensor studies.

Finally, I would like to pay my deepest and overwhelming gratitude to my wife Li, who did her best to support my studying, for her love, understanding, sacrifice and efforts; to my parents, brother and sisters for their encouragement and support.

Declaration

I hereby declare that the work presented in this thesis has not been previously submitted for any degree and is not being currently submitted in candidature for any other degree.

Signed.....

The work reported in this thesis was carried out by the candidate. Any work not carried out by the candidate is acknowledged in the main text.

Signed.....
Ph.D. Supervisor

Signed.....
Candidate

Statement of copyright

Contents

List of figure captions

Chapter 2

Chapter 3

Chapter 4

Chapter 5

List of tables

Chapter 3

Chapter 4

Chapter 5

CHAPTER 1 INTRODUCTION

The transmission of information by light is not a new idea, as a matter of fact the idea is quite old. It was only a dream and it was impossible to implement a practical optical transmission system before the invention of the laser (a coherent light source) in the 1960s.[1-3] As science and technology develops, it is becoming increasingly more important today for communication to be faster and more efficient, the transmission and processing of optical information has been an intensive research area since the invention of the laser.

The birth of the laser changed the situation dramatically. These coherent light sources are an essential requirement for practical transmission of information by light and allow conventional optical communications systems to have much greater capacity than that of other systems. Furthermore light-waveguiding optical fibres act as high-capacity, reliable, efficient and economical media to allow optical signals propagating over a very long distance with small losses.

In order to transmit and process optical information, the idea for manipulating a laser beam was borrowed from microwave technology and proposed by E. Snitzer and H. Osterberg [4] based on their observation of waveguide modes propagating in optical fibre, and by Amnon Yariv [5] and W. L. Bond [6] from their analysis and observation of planar dielectric waveguide in a p-n junction. In 1964, D. F. Nelson showed the phase of guided light in a p-n junctions could be modulated by the electro-optic effect, which led to a fast development in the field of dielectric waveguides,[7, 8] particularly when new coupling techniques such as the prism coupler [9, 10] and the grating coupler [11] were developed, significant progress had been made since then in this field.

There is little doubt that optical waveguide devices have an ever growing impact on electronic engineering, this trend will continue and the process will be faster. Guided-wave optics and waveguide structures offer significant advantages in applications, the major advantages are:

- Low-loss transmission and large bandwidth
- Immunity from electromagnetic interference and outside vibrations
- Small size, light weight and low cost
- Lower power consumption and more reliability
- Strong beam confinement and large nonlinear interaction
- Compatible with modern microelectronics

Of course there are some disadvantages in dielectric waveguides, such as high research and development costs and no transmission to electrical power.

In nonlinear optics[12], the strong beam confinement, in which the beam of light is confined and compressed to the regions of the order of wavelength in one (slab waveguide) or two (channel waveguide) dimensions, means that high power densities can be achieved with small power (e.g. a 100 mW laser can result in a power density of the order 10 $MWcm^{-2}$ in an area 1 $\mu m \times 1$ μm), in this situation the nonlinear effect can be realised and studied even using a small or moderate power laser. A large second-harmonic conversion rate can be achieved for waveguide structures compared to bulk interaction because of large nonlinear interactions in the waveguide structure, and the ratio is [13]

$$\eta_{wg} \sim t^{-2} L^2 P^{(\omega)}, \quad \eta_b \sim \lambda^{-1} L P^{(\omega)}$$

$$\frac{\eta_{wg}}{\eta_b} \sim \frac{L}{\lambda} \tag{1.1}$$

where t is the thickness of the waveguide, L indicates the length of the waveguide or bulk crystalline length involved in the interaction, $P^{(\omega)}$ is the total fundamental power, λ is the light wavelength.

The ratio can of be the order of 10^4 (when L 1 cm and λ 1 μm) in theory. In practice, the ratio of the order of 10^2 can be implemented. This is highly in favour of the waveguide

configuration. The phase velocity of light in a waveguide depends on the parameters of structure (thickness of film, refractive index of film and substrate). This implies that phase-matching can be achieved with some degree of freedom by a proper choice of these parameters (using dispersion to compensate for the effective index dispersion).

Nowadays optical waveguiding or guided-wave optics is a subject which has drawn considerable attention from researchers and is still under rapid development. Many new subjects (e.g. integrated optics, nonlinear waveguide optics and optical fibres) have developed from optical waveguiding. In optical waveguides, polymer waveguide and organic materials or chromophore doped waveguides have been energetically studied and have achieved significant progress because of their potential advantages over other materials.[14-16] Various optoelectronic technologies have been widely used in practical applications.[17-21] Much work has been carried out and is being undertaken in this field to explore new materials and to develop new techniques, to improve the properties of materials and the functions of techniques available.

Therefore with the current trends in polymer waveguides, the aim of this work was to investigate the waveguide properties of thin polymer films. Particularly focusing on: 1) Photostability of organic chromophores in a polymer matrix, 2) waveguide sensing effects using multi-layer structures.

Photostability to prolonged light exposure is one of the most desirable properties for organic chromophore containing polymer systems or the devices made from them, when they are used in practical applications. Photodegradation occurs when an organic chromophore system is exposed to optical radiation, which leads to changes in the physical and chemical properties of the system. Responses and behaviour are different for organic chromophore systems under different environments and irradiation of different wavelengths. The molecular structures can be changed to improve their stabilities and the photostability of the organic chromophore system is enhanced in oxygen free environment as shown in this thesis. The quantum yields of photodegradation of chromophores are reported.

As a new and fast developing field, waveguide sensing and its techniques, including the waveguide interferometric sensor are studied. Symmetric and unsymmetric vertically

integrated waveguide sensors were fabricated and were used in applications to humidity sensors. By employing the different properties of polymer and the various combinations of polymer layers in the waveguide structures, the detection of humidity concentration was greatly improved and enhanced.

Chapter 2 describes some basic concepts and principles of waveguiding; presents the fundamental theory of dielectric slab waveguides and introduces the material requirements for waveguide fabrications and experiments. The transverse field patterns in three-layer structures (symmetric and unsymmetric) involved are described. Several coupling techniques are described, end-fire and prism coupling are portrayed in more detail.

Chapter 3 introduces some elementary and important methods used to fabricate and characterise thin polymer waveguide films. Dip coating and spin coating are discussed in detail. More attention is paid to the process of multi-layer waveguide structures for sensing applications. The characterisation of polymer waveguide and experiments performed (refractive indices measurement, birefringence of thin polymer films, linear loss and extinction coefficient measurements) are presented. The purpose is to provide direct and necessary technique training, to familiarise the reader with the basic properties of materials used in the experiments, and furthermore to accumulate necessary data for the design of new waveguide structures.

Chapter 4 describes the formation of an organic chromophore polymer system and the mechanism of photodegradation. In order to evaluate some organic nonlinear optical chromophores synthesised in our group, the DEMI-series chromophores and several yellow chromophores were studied under different environments under exposure to varied wavelengths. The responses from these materials are observed and analysed. The results from the experiments are presented. This will help to improve the structures of the materials, to choose a proper working environment and to achieve a higher photostability from a better understanding of the characteristics of the materials and photodegradation mechanisms of organic chromophores.

Chapter 5 presents a short review on classification, and specification of sensors. Particular attention is paid to optical sensors, their technology, and waveguide

interferometric sensors. Details of design, modelling, fabrication and characterisation of vertically stacked waveguide humidity sensors are reported and discussed. A special procedure and process for fabricating multi-layer waveguide structures was developed. The results from experiments show a promising potential for this integrated waveguide sensor.

Chapter 6 draws some conclusions on the studies performed and proposes future work.

1.1 References

1. T. H. Maiman, *Stimulated optical radiation in ruby*, Nature, **187**, 493-494 (1960).
2. T. H. Maiman, *Stimulated optical emission in fluorescent solids. I. Theoretical considerations*, Phys. Rev., **123** (15), 1145-1150 (1961).
3. T. H. Maiman, R. H. Hoskins et al, *Stimulated optical emission in fluorescent solids. II. Spectroscopy and stimulated emission in ruby*, **123** (15), 1151-1157 (1961).
4. E. Snitzer and H. Osterberg, *Observed dielectric waveguide modes in the visible spectrum*, J. Opt. Soc. Am., **51** (5), 499-505 (1961).
5. Amnon Yariv and R. C. C. Leite, *Dielectric-waveguide mode of light propagation in p-n junctions*, Appl. Phys. Lett., **2** (3), 55-57 (1963).
6. W. L. Bond, B. G. Cohen, R. C. C. Leite, and A. Yariv, *Observation of the dielectric-waveguide mode of light propagation in p-n junctions*, Appl. Phys. Lett., **2** (3), 57-59 (1963).
7. D. F. Nelson and F. K. Reinhart, *Light modulation by electro-optic effect in reversed-blased GaP p-n junctions*, Appl. Phys. Lett., **5** (7), 148-150 (1964).
8. Henry F. Taylor and Amnon Yariv, *Guided wave optics*, Proceedings of the IEEE, **62** (8), 1044-1060 (1974).
9. P. K. Tien, R. Ulrich, and R. J. Martin, *Modes of propagating light waves in thin deposited semiconductor films*, Appl. Phys. Lett., **14** (9), 291-294 (1969).
10. P. K. Tien and R. Ulrich, *Theory of prism-film coupler and thin-film light guides*, J. Opt. Soc. Am., **60** (10), 1325-1337 (1970).
11. M. L. Dakss, L. Kuhn, P. F. Heidrick, and B. A. Scoff, *Grating coupler for efficient excitation of optical guided waves in thin films*, Appl. Phys. Lett., **16** (15), 523-525 (1970).
12. George I. Stegeman and Colin T. Seaton, *Nonlinear integrated optics*, J. Appl. Phys. **58** (12), R57-78 (1985).
13. J. Zyss, *Nonlinear organic materials for integrated optics: a review*, Journal of molecular electronics, **1**, 25-45 (1985).
14. Toshikuni Kaino and Satoru Tomaru, *Organic materials for nonlinear optics*, Advanced materials, **5** (3), 117-123 (1993).
15. C. P. Wong (Ed.), Polymer for electronic and photonic application, Academic press, Inc. 1993.

16. Paras N. Prasad and David J. Williams, Introduction to nonlinear optical effects in molecules and polymers, John Wiley and Sons, Inc., 1990.

17. Theodor Tamir (Ed.), Guided-wave optoelectronics, Springer-Verlag, 1990.

18. Lawrence A. Hornak (Ed.), Polymer for lightwave and integrated optics, Marcel Dekker, Inc., 1992.

19. Toshikuni Kaino, et al., *Development of polymer optical waveguides for photonic device applications*, from Photonic and optoelectronic polymer (ACS Symposium Series 672), American chemical society, Washington, DC, 1997.

20. Allan W. Snyder and John D. Love, Optical waveguide theory, Chapman and Hall, 1983.

21. R. Levenson, J. Liang et al, *Advances in organic polymer-based optoelectronics*, from Polymer for second-order nonlinear optics (Editor: Geoffrey A. Lindsay and Kenneth D. Singer), American chemical society, Washington, DC, 1995.

CHAPTER 2 WAVEGUIDE THEORY

Preface

The aim of this chapter is to present and to introduce some preliminary concepts and fundamental theory of dielectric slab waveguides. Some basic dielectric waveguide structures will be studied by ray optics. These studies will lead to some conclusions as to requirements for direct waveguide fabrication and experiments. The slab waveguide structure is of great importance in the area of integrated optics and optoelectronics, where it is a basic component in the construction of many devices. The special case of a symmetric three-layer structure, having equal refractive indices above and below the guiding layer, is presented. The discussion of unsymmetric three-layer structure is described also. Several different forms of coupling techniques and their theories are studied. Among them the techniques of prism coupling and end-fire coupling that are used in my experiments are explained in detail.

2.1 Introduction

With the fast progress and development in optical communications, optical interconnection, integrated optics and electro-optic devices, etc., great interest has been stimulated in optical guided wave technology over the last 20 years. Great efforts have been made in the research and development of optical devices which employ surface-guided optical waves and guide light in sheets or strips of a thin dielectric film. Much progress has been made in this field.

Optical waveguides, or dielectric waveguides, are structures that are used to confine and guide the light in the guided-wave devices. In order to realise its function as a fundamental element in such a device, there are two basic requirements for a waveguide structure:

1. It is necessary, but not sufficient, that the refractive index of the waveguide region must be greater than that of its surroundings (substrate and superstrate), which is based on the phenomenon of total internal reflection.
2. The region to guide the light must be transparent at the wavelength of interest.

In waveguides, the light can be confined either in one dimension in a planar waveguide or in two dimensions in a channel waveguide or fibre. The size of the confinement region is normally of the order of the wavelength of light. The guided wave field is maximum in the region with high index and decays with distance into the surroundings with lower index.

2.2 Generation of guided modes

In order to obtain an intuitive feeling, a clear physical principle and a general understanding of the nature of light propagation in an optical waveguide, without allowing the physics to be lost in the mathematics, a theory that combines geometrical ray optics and waves, but mainly geometrical ray description, is used to analyse and to discuss the generation of an optical guided mode and its propagation in a waveguide.[1 - 4]

An optical waveguide is generally formed by three media, a film, a cover above and a substrate below. To make analysis easy, the most typical and simplest structure, a stacked slab waveguide with three layers, is discussed. Fig. 2.1 shows a slab waveguide, consisting of a high index dielectric film (the guide film of index, n_1) sandwiched between two other optical materials, cover and substrate with refractive index n_2 and n_0, respectively. The guide film has a uniform thickness d through the whole plane. The waveguide has parallel planar boundaries (confinement), it is confined in the x direction and is assumed to be semi-infinite in the positive and negative x directions, it is infinite in the z direction which is the propagation direction of the guided modes and is assumed to be also infinite in the lateral direction y because the width of a waveguide is normally wide enough, implying that no electromagnetic quantity will vary in this direction. The resulting guided modes propagate in the positive z direction.

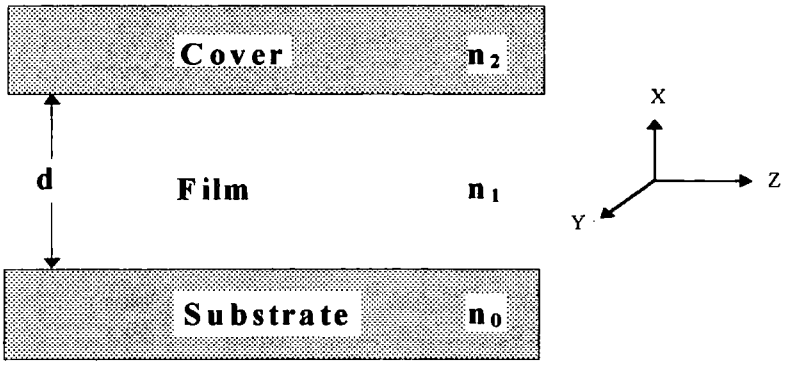

Fig. 2.1 A diagram of the three-layer slab waveguide structure

The propagation of light in a waveguide in ray optics, reflection and refraction of incident light at a dielectric interface must be considered. If light is incident at an angle θ_i on an interface separating two isotropic and homogenous dielectric media of refractive index n_1 and n_2, it will be partially reflected and refracted. The incident, reflected and refracted (transmitted) waves are represented by $\mathbf{E}_i(\mathbf{r})$, $\mathbf{E}_r(\mathbf{r})$ and $\mathbf{E}_t(\mathbf{r})$, their corresponding wave vectors are $\mathbf{k}_i$, $\mathbf{k}_r$, and $\mathbf{k}_t$, i.e.

$$\begin{aligned}\mathbf{E}_i(\mathbf{r}) &= \mathbf{A}_i e^{-j(\mathbf{k}_i\cdot\mathbf{r})}\\ \mathbf{E}_r(\mathbf{r}) &= \mathbf{A}_r e^{-j(\mathbf{k}_r\cdot\mathbf{r})}\\ \mathbf{E}_t(\mathbf{r}) &= \mathbf{A}_t e^{-j(\mathbf{k}_t\cdot\mathbf{r})}\end{aligned} \tag{2.1}$$

According to boundary conditions, the tangential components of the electric field must be continuous across the dielectric interface, thus we have,

$$[\mathbf{E}_i(\mathbf{r})+\mathbf{E}_r(\mathbf{r})]_{tan} = [\mathbf{E}_t(\mathbf{r})]_{tan} \tag{2.2}$$

Which implies that at all points (x=0) along the boundary,

$$\left[\mathbf{A}_i e^{-jk_{iy}y} e^{-jk_{iz}z} + \mathbf{A}_r e^{-jk_{ry}y} e^{-jk_{rz}z}\right]_{tan} = \left[\mathbf{A}_t e^{-jk_{ty}y} e^{-jk_{tz}z}\right]_{tan} \tag{2.3}$$

and require that [21]

$$\begin{aligned}k_{iy}=k_{ry}=k_{ty}\equiv k_y\\ k_{iz}=k_{rz}=k_{tz}\equiv k_z\end{aligned} \tag{2.4}$$

Physically this means that the incident, reflected and transmitted wave vectors lie in the same plane or are coplanar. The equation (2.3) does not depend on the choice of (y, z), so we can chose these three wave vectors which lie in the xz plane (the plane of incidence) as shown in Fig 2.2. Therefore we obtain

$$\begin{aligned}\mathbf{k}_i &= +k_{ix}\hat{x} + k_{iz}\hat{z}\\ \mathbf{k}_r &= -k_{rx}\hat{x} + k_{rz}\hat{z}\\ \mathbf{k}_t &= +k_{tx}\hat{x} + k_{tz}\hat{z}\end{aligned} \tag{2.5}$$

where

$$k_{ix} = k_1 \cos\theta_i, \quad k_{iz} = k_1 \sin\theta_i$$
$$k_{rx} = k_1 \cos\theta_r, \quad k_{rz} = k_1 \sin\theta_r$$
$$k_{tx} = k_2 \cos\theta_2, \quad k_{tz} = k_2 \sin\theta_2$$

and

$$k_1 = n_1 k_0, \quad k_2 = n_2 k_0, \quad k_0 = 2\pi / \lambda_0$$

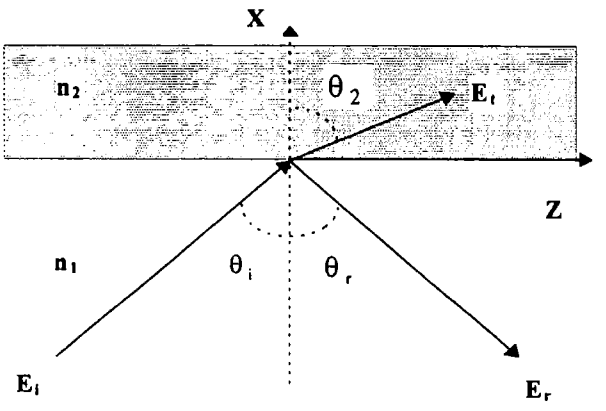

Fig. 2.2 Reflection and refraction of a incident ray at a interface between two dielectric media

Therefore from equation (2.4) we obtain

$$\sin\theta_i = \sin\theta_r$$

and (Snell's law)

$$k_1 \sin\theta_1 = k_2 \sin\theta_2 \quad \text{or} \quad n_1 \sin\theta_1 = n_2 \sin\theta_2 \tag{2.5}$$

if $n_1 > n_2$, then $\theta_i < \theta_2$ from equation (2.1). When $\theta_2 = 90°$, $\theta_i = \theta_c$ (critical angle), $\sin\theta_c = n_2/n_1$. since

$$\cos\theta_2 = (1 - \sin^2\theta_2)^{\frac{1}{2}}$$

so that

$$k_2 \cos\theta_2 = \sqrt{k_2 - k_2 \sin^2\theta_2}$$
$$k_{tx} = \sqrt{k_2 - k_1 \sin^2\theta_i} \tag{2.6}$$

For $\theta_1 > \theta_c$, k_{tx} becomes wholly imaginary, the power reflection coefficient is unity.[6] This indicates that a plane wave is totally internally reflected with no net power flow into the less dense medium, refracted light disappears when it is incident upon a dense/less dense dielectric interface from the dense medium, all incident light turns back to the media with high index by total reflection.

It is the total reflection of light at the interface of two different dielectric media that is the basis of the dielectric waveguide, the waveguide structures are used to confine and guide the light in the guided-wave devices. Light is bounded in the waveguide with total internal reflection of the light occurring at the film/substrate and film/cover interfaces, and propagates in the waveguide (z direction) following a zig-zag path. More than one mode of light can be confined in the structure, where a mode of the waveguide represents a spatial distribution of optical energy in physical study. Each zig-zag path represents a mode in the waveguide and the angle of reflection in the path is different for each mode.

Considering an asymmetric slab waveguide structure shown in Fig. 2.1, we normally have $n_1 > n_0 > n_2$, so there are two critical angles of interest for total reflection, θ_s for the film /substrate and θ_c for the film /cover interfaces, respectively.

$$\theta_c = \sin^{-1} n_2/n_1 , \qquad \theta_s = \sin^{-1} n_0/n_1 , \qquad \theta_s > \theta_c \tag{2.7}$$

As the incident angle in the waveguide is increased, the light can radiate from the film into both the cover and the substrate as shown in Fig.2.3.

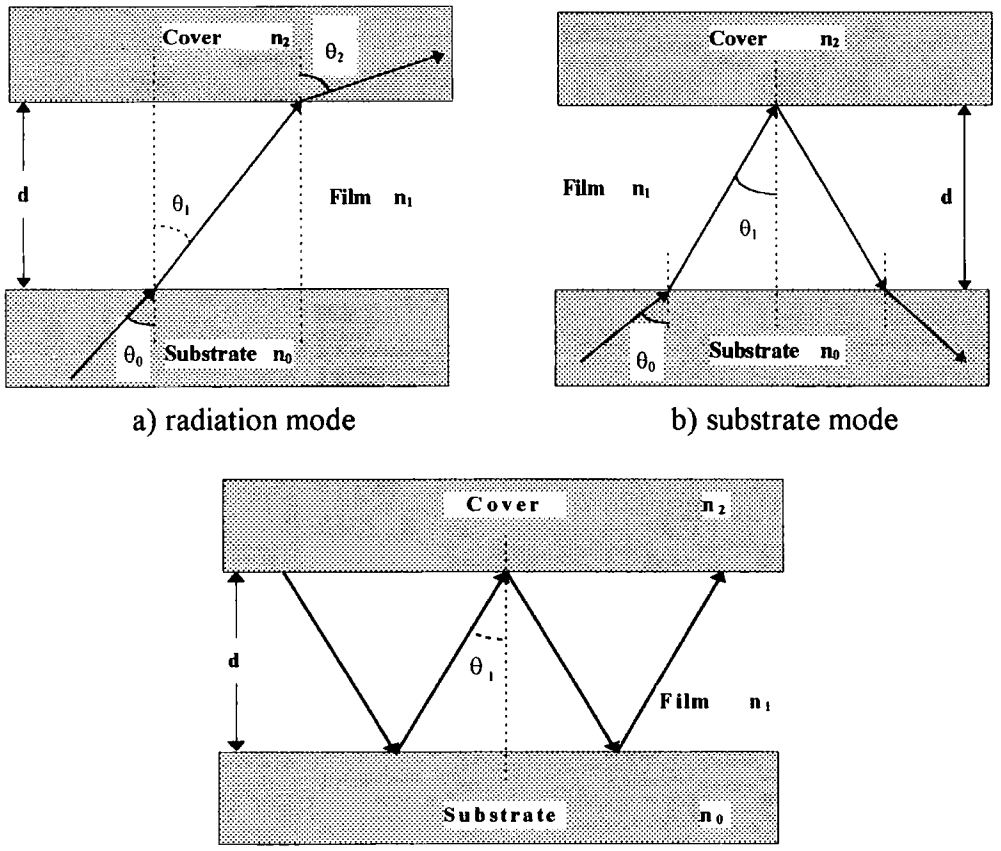

Fig. 2.3 A zig-zag ray diagram for the three possible modes in waveguide

When $\theta < \theta_c$, light goes freely through the film from the substrate side by refraction and escapes from the cover as the radiation mode, there is no light confinement. When θ increases to $\theta_c < \theta < \theta_s$, the light incident from the substrate by refraction is totally reflected at the film/cover interface and returns back into the substrate where the light escapes as the substrate mode, there is partial light confinement, light can occur both in the film and the substrate. Eventually when θ is large enough, $\theta_c < \theta_s < \theta$, total internal reflection occurs at both upper (film/cover) and lower (film/substrate) interfaces. In this case waveguiding occurs. Light is totally confined in the film with high index and propagates along the z direction in a zig-zag path.

In principle, once $\theta > \theta_s$, total internal reflection should occur in the film at all angles, the corresponding modes in the waveguide should be continuous. However not all of these modes can be supported by the waveguide. Actually, only certain modes are formed in the waveguide because of the limitation of particular waveguide structure. These modes must obey the propagation condition.

A guided mode following a zig-zag path in a waveguide can be represented by two wavevectors which are denoted by bold typeface, $\mathbf{A}_1$(down) and $\mathbf{B}_1$(up) which can be divided into two components along z (horizontal) and x (vertical) direction as in Fig. 2.4.

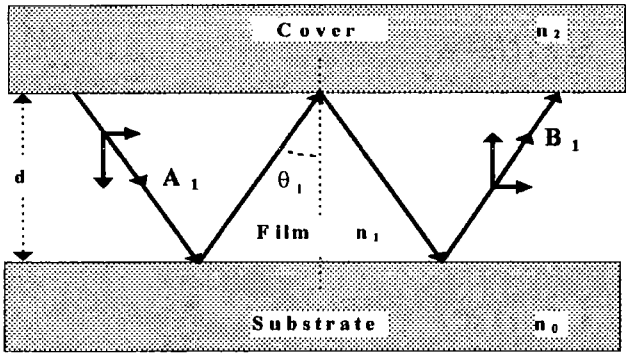

Fig. 2.4 The zig-zag path of a guided mode in waveguides

Equal horizontal components for $\mathbf{A}_1$ and $\mathbf{B}_1$ indicate that the guided waves propagate along the film in the z direction with the same constant velocity. The vertical components of $\mathbf{A}_1$ and $\mathbf{B}_1$ represent waves, they overlap and interfere to form a standing wave across the film thickness d in order to avoid decay of their energy due to destructive interference. The waves discussed above are planar. They are TE (E_y, H_z, H_x) modes (transverse electric) and

TM (H_y, E_z, E_x) modes (transverse magnetic). The propagation constant of guided modes along upward- and downward-travelling path is $\beta = kn_1 (k = \omega/c)$, k, ω and c are the free space wave vector, the angular frequency of the light and the velocity of light in vacuum, respectively.

When the guided wave propagates along the zig-zag path upwards and downwards, the vertical components of $\mathbf{A_1}$ and $\mathbf{B_1}$ have a magnitude $kn_1\cos\theta_1$, the phase change for the wave to cross the thickness d of the film twice (up and down) is thus $2kn_1 d\cos\theta_1$. Additionally a phase shift is introduced from total reflection at the film/cover and film/substrate interfaces, $-2\Phi_{12}$ and $-2\Phi_{10}$, which represents the Goos-Hanchen shift and can be interpreted as the penetration of the zig-zag ray into the cover and substrate before it is reflected. Consequently, the total phase shifts in each cycle should be equal to $2m\pi$ in order to develop standing waves in the x direction or to interfere constructively for the guided waves in the waveguide.

$$2kn_1 d\cos\theta_1 - 2\Phi_{12} - 2\Phi_{10} = 2m\pi \tag{2.8}$$

Equation (2.8) is the condition for all guided modes in a waveguide structure. Here m is an non-negative integer (m=0,1,2, ...) and the order of the guided mode. The phase shifts, Φ_{12} and Φ_{10}, can be obtained from the theory of total reflection.[5]

$$\tan\Phi_{12} = \frac{\sqrt{n_1^2\sin^2\theta_1 - n_2^2}}{n_1\cos\theta_1} \qquad \tan\Phi_{10} = \frac{\sqrt{n_1^2\sin^2\theta_1 - n_0^2}}{n_1\cos\theta_1} \tag{2.9}$$

for TE modes and

$$\tan\Phi_{12} = \frac{n_1^2\sqrt{n_1^2\sin^2\theta_1 - n_2^2}}{n_2^2 n_1\cos\theta_1} \qquad \tan\Phi_{10} = \frac{n_1^2\sqrt{n_1^2\sin^2\theta_1 - n_0^2}}{n_0^2 n_1\cos\theta_1} \tag{2.10}$$

for TM modes.

The characteristic equation (2.8) determines the permitted angles θ_1 for constructive interference which is characterised by β, for other angles waveguiding in the film is not possible. It is clear that a series of β can be obtained for a given wavelength and waveguide structure, choice of indices (n_0, n_1, n_2) and guide thickness d. Each β represents a possible guided mode in the structure. There is a cut-off condition on allowed m values to limit the number of β for each set of n_0, n_1, n_2 and d. Below it, those possible modes correspond to the radiation or the substrate modes. Thus, there are only a

limited number of guided modes that can exist in a given waveguide beyond the cut-off condition. The β-values permitted for the guided modes are bounded in the range

$$kn_0 \leq \beta_m \leq kn_1 \tag{2.11}$$

For each discrete guided mode, the corresponding z direction propagation constant β_m is given by

$$\beta_m = kn_1 \sin\theta_m = \omega/v_p \tag{2.12}$$

where v_π (the phase velocity) is the velocity of light parallel to the waveguide and is determined by the horizontal components of propagation constant β (or wavevectors A_1 and B_1). An effective guide index is defined by

$$N_m = \frac{c}{v_p} = \frac{\beta_m}{k} = n_1 \sin\theta_1 \tag{2.13}$$

which is bounded by

$$n_0 < N_m < n_1 \tag{2.14}$$

Two distinct mode types (TE and TM) can exist, depending on the orientation of the electric and magnetic field of the plane wave. In wave optics, the TE and TM modes are the solutions of Maxwell's equations that match certain boundary conditions at the film/substrate and the film/cover interfaces. Propagation in the z direction is characterised by the wave vector component (propagation constant) $\beta = \omega/v_p = ck/v_p = nk$, v_π denotes phase velocity in the z direction, n is the effective index for propagation of the wave.

A transverse magnetic (TM) mode has the electric field polarised in the xz plane, the magnetic field lies entirely in the transverse plane (along the y axis). The opposite situation occurs when the magnetic field lies in the xz plane, leaving the electric field in the transverse plane, resulting in a transverse (TE) mode as shown in Fig. 2.5.

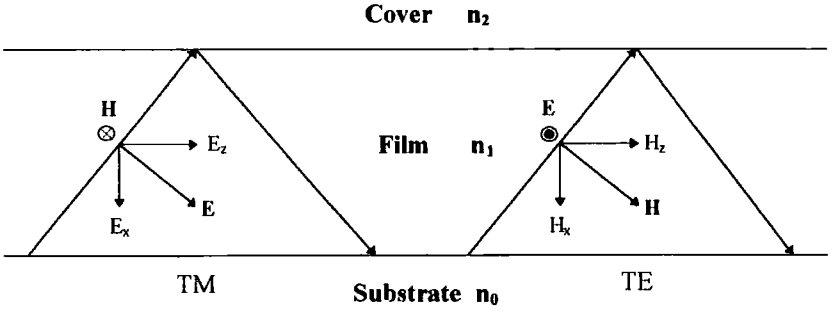

Fig.2.5 The two types of slab waveguide modes

The waveguide is called single-moded if just one mode (the fundamental mode) is supported in it. When a finite number of modes can propagate in it, the waveguide is multi-moded. Any mode that cannot propagate is described as being cut off. The higher the order of the modes, the smaller the value of the incident angle θ and the greater the number of reflections between the upper and lower interfaces in a unit propagation distance.

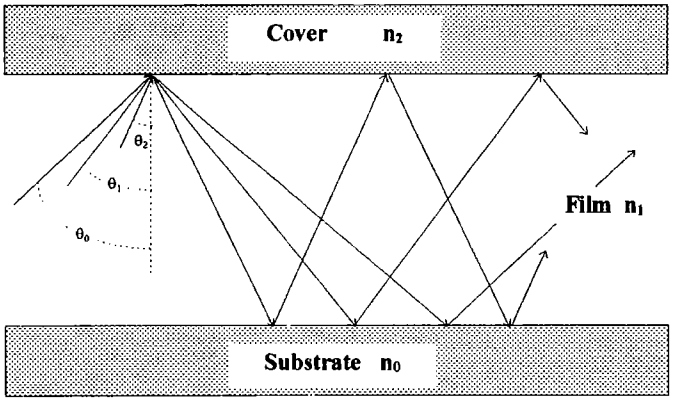

Fig.2.6 Discrete bounce angles for the first three guided modes

2.2.1 Goos-Hanchen shift[1]

A ray (plane wave) that is incident upon an interface from an optically denser medium at an angle greater than the critical angle, experiences not only total internal reflection but also a phase shift that is a function of the angle of incidence. The phase shift was used in equation (2.9) to obtain the condition for the guided modes. The equation expresses that the reflected ray is shifted laterally relative to the incident ray shown in Fig.2.7. This means the axis of a beam of light with some well-defined cross-section should be considered. The incident beam is composed of a set of plane waves, each wave having a slightly different angle of incidence. As the phase change on reflection depends on the angle of incidence, the reflected beam will not be a perfect reconstitution of the incident beam at the point of incidence. Therefore a lateral shift of light occurs.

For different polarised light, the lateral shift is given by

TE modes:
$$z_s = \frac{\tan\theta_1}{k(n_1^2 \sin^2\theta_1 - n_0^2)^{\frac{1}{2}}} \qquad (2.15)$$

TM modes:
$$z_s = \frac{n_0^2 \tan\theta_1}{k(n_1^2 \sin^2\theta_1 - n_0^2)^{\frac{1}{2}}(n_1^2 \sin^2\theta_1 - n_0^2 \cos^2\theta_1)} \tag{2.16}$$

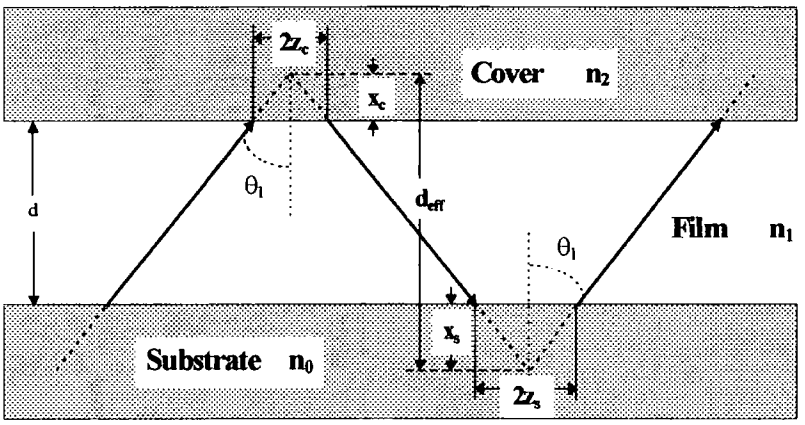

Fig.2.7 Ray picture of reflection in a slab waveguide showing a lateral shift.

The shift corresponds to the penetration depth of the ray given by

$$x_s = z_s / \tan\theta_1 \tag{2.17}$$

Because of the Goos-Hanchen shift at interfaces, or ray penetration, the guide appears to be larger than its real thickness d and to posses an effective thickness d_{eff}.

$$d_{eff} = d + x_s + x_c \tag{2.18}$$

Therefore in a waveguide, the guided light is not only confined in the guide with thickness d, the light will penetrate into the cladding layers (substrate x_s and cover x_c) before it is reflected. In ray optics the guide becomes thicker with an effective thickness which represents the effective waveguide width as measured between the imaginary boundaries above and below the waveguide core associated with the Goos-Hanchen shift as shown in Fig.2.8. This indicates that the field of the guided light will extend into the cladding layers (the substrate or the cover) by the evanescent fields which their corresponding decay constants (p and q) are given by,

$$x_s = \frac{1}{p}, \qquad x_c = \frac{1}{q} \tag{2.19}$$

In view of these considerations, the field of the guided light penetrates the true boundaries into the cladding layers when the guided light propagates along the waveguide with propagation constant β. The total power carried by guided modes is confined within the guide with thickness d_{eff}. The rate of decay depends on the constant p for the substrate and q for the cover. The bigger the value of p and q, the faster the decay of the field, then the more shallow the penetration (x_s and x_c). For a unsymmetric waveguide and $n_1 > n_0 >$

n_2, where p is bigger than q, the evanescent field extends into the substrate more than into the cover as shown in Fig.2.11.

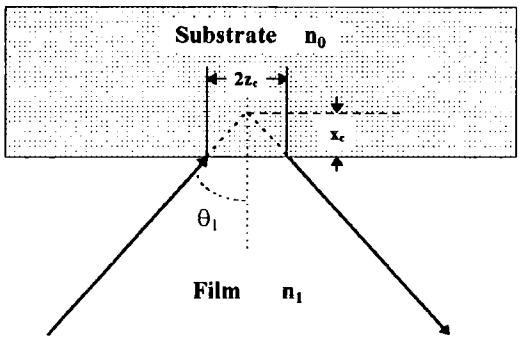

Fig.2.8 Ray picture of effective guide thickness and penetration

2.2.2 Transverse field patterns[6, 7]

Each guided mode, which can be obtained from the solution of the Maxwell's equations for the corresponding boundary condition, has its own particular transverse field distribution across the thickness of the film. This field pattern is determined by the refractive indices of the cladding layers (substrate n_0 and cover n_2, $n_1 > n_0 \geq n_2$) and the guiding layer, and the thickness of the guiding layer. That is decided by the vertical component of propagation constant $\beta(= kn_1\cos\theta_1)$, or wavevectors A_1 and B_1.

For a well-confined mode, most of its energy will be confined in the guiding region, a small part of it will go outside the guiding region and will be lost in the cladding regions. The amount is dependent on the thickness and mode number. A significant amount of its energy will propagate in the evanescent field outside the guiding region for a poorly-confined mode. One typical sample is the 0 mode (the lowest-order mode) which is very useful in many waveguide applications. Fig.2.9 shows a field pattern of the 0 mode in a symmetric structure, its field distribution is symmetric and is characterised by a maximum in the middle of the waveguide. The field varies cosinusoidally inside the guide and exponentially decays outside the guide (the evanescent field).

The field patterns of the first three guided modes (TE) in a symmetric slab waveguide with three layers are shown in Fig.2.10. A similar situation exists for the TM modes. Note that

the lowest-order mode has no sign reversals, the first mode has one and the second mode has two, etc.

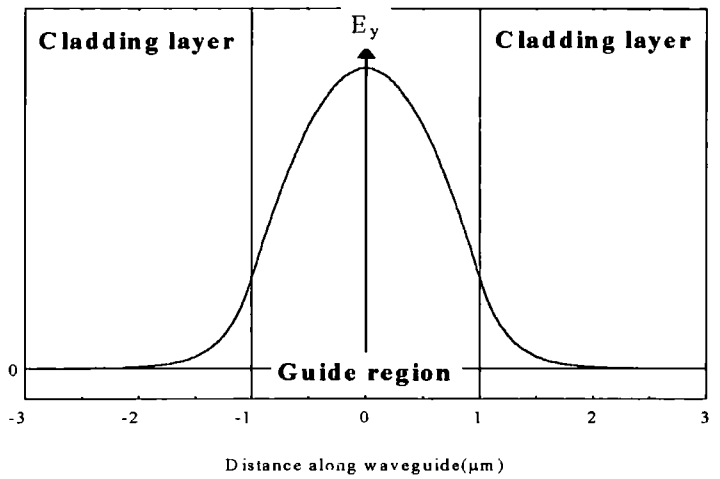

Fig.2.9 Normalised field distribution of the lowest-order mode (TE_0) in a three-layered, symmetric slab waveguide

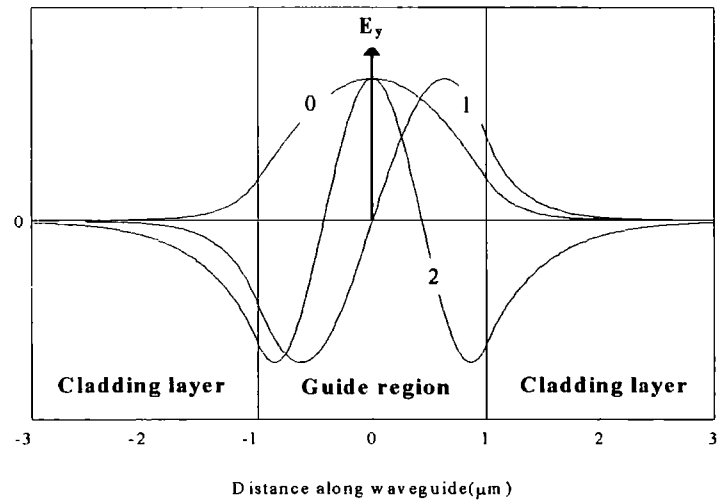

Fig.2.10 Normalised mode patterns for a three-moded (TE) symmetric slab waveguide

We can see from Fig.2.11 that 1) field distribution is unsymmetric even for the lowest-order mode, 2) more field of the guided modes extends into the cladding layer with high index. The confinement of modes is better on the side of the cladding layer with low index because of larger index differences with the guide layer. Field distribution of guided modes in a waveguide is mainly determined by the refractive indices of the guide layer and the cladding layer. The cladding layer region (substrate and cover) should normally be thick enough for the evanescently decaying waves to be sufficiently attenuated before

reaching further possible interfaces. The thickness of a typical single-moded guide layer amounts to a few tenths of a micron to about 1 micron, the cladding layer should be at least 1 to 2 microns thick. Improving confinement of the modes is advantageous to reduce the propagation loss and energy exchange with cladding layer for a waveguide. It can be implemented by increasing the difference of refractive index between the guide and cladding layer in a certain range. For a single-moded symmetric waveguide shown in Fig.2.12, as the index difference increases, the mode field concentrates more towards the centre of the guide (from curve 0 to 3), and the tail of the evanescent field becomes smaller. As the difference rises further, the one-moded waveguide may become a multi-moded one. General features of TM modes are similar to those of TE modes except that TM modes have a lower degree of confinement. A larger fraction of the total TM mode energy thus is propagated in the external media compared to a TE mode of the same order.

In some practical situations, it is more difficult to make a symmetric structure than an unsymmetric one where air can normally be used as the upper cladding layer (cover) of the structure. It is simpler and allows for a wider choice of materials, if an unsymmetric structure can meet the requirements of the application. Fig.2.11 shows the field patterns of the first three TE and TM modes for a similar unsymmetric slab waveguide with three layers.

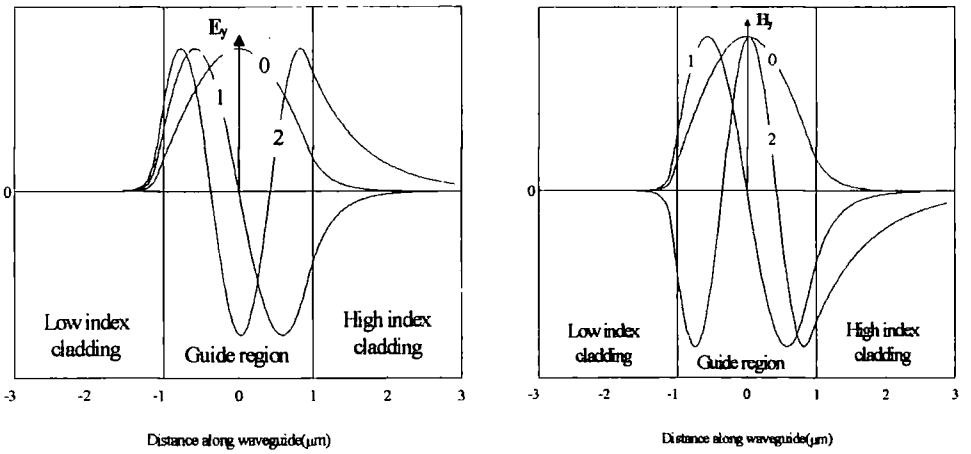

(a)TE modes (b)TM modes

Fig.2.11 Normalised field patterns for a three-moded unsymmetric slab waveguide structure with three layers. a)TE modes, b)TM modes

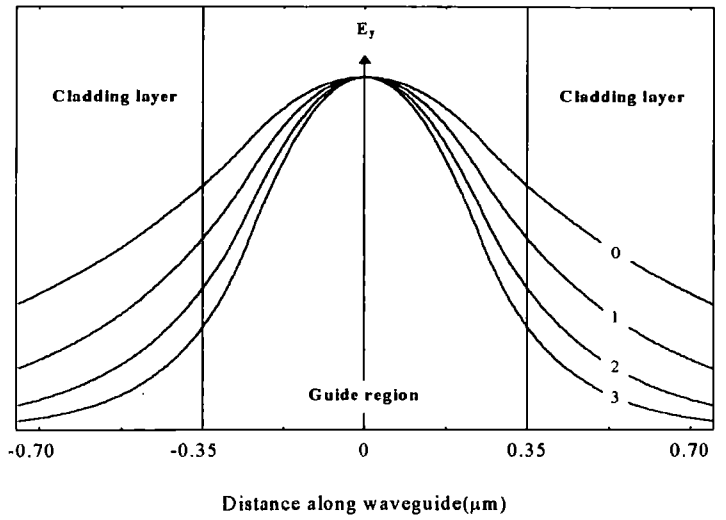

Fig.2.12 The changing trend of the lowest-order mode versus the index difference between the guide layer (n_1) and the cladding layers (n_0 or n_2) in a symmetric structure with three layers. 0) $\Delta n=n_1-n_0=0.03$, 1) 0.06, 2) 0.11, 3) 0.18

Lower order modes are characterised by propagation with higher effective index. Higher order modes penetrate more deeply into the cladding layers compared with the fundamental mode. High amplitudes of field (high light intensities) inside the waveguide are obtained for the lowest-order mode (m=0). However, one cannot increase the amplitude or intensity arbitrarily by simply decreasing the film thickness, as the field then extends more and more deeply into the substrate and the cover region. Changing the optical wavelength has a similar result. When the optical wavelength changes from long (low optical frequency, low k) to short wavelength (high optical frequency, large k) in a single-moded symmetric waveguide, more field of the mode will distribute towards the centre of the guide, and confinement is improved. However, as the wavelength becomes shorter (frequency rises further), the original one-moded waveguide may change to a multi-moded one.

2.2.3 Cut-off conditions

Subject to appropriate boundary conditions at the interfaces, only limited, discrete values of the propagation constant β are allowed in the range, $kn_1 \geq \beta \geq kn_0$, this was discussed in section 2.2 and shown in Fig.2.6. Such β values correspond to the various TE and TM modes in a waveguide. The number of guided modes that can be supported by the structure and their propagation constants depend on the thickness, d, of the guide layer,

wavelength, λ, of the light and the refractive indices of the waveguiding media (n_0, n_1, n_2). For a known combination of these parameters, there is a cut-off condition below which no modes can be guided in the waveguide. The cut-off condition can be expressed in several ways as is shown below.

1. For a given wavelength λ and indices (n_0, n_1, n_2), the minimum thickness required for a waveguide to support a mode of TE polarization of order m is given by [8]

$$d_{min} = \frac{\left[m\pi + \tan^{-1}\left(\frac{n_0^2 - n_2^2}{n_1^2 - n_0^2}\right)^{\frac{1}{2}} \right]}{k(n_1^2 - n_0^2)^{\frac{1}{2}}} \qquad (2.20)$$

for a symmetric waveguide (n_0=n_2) and m=0, $d_{min} \to 0$, the film can be infinitesimally thin

2. To permit waveguiding for a given wavelength in the three-layer structure of a given mode, refractive indices should be chosen for TE modes as follows,

symmetric structure: $$\Delta n = (n_1 - n_0) > \frac{m^2\lambda^2}{4d^2(n_1 + n_0)} \qquad (2.21)$$

unsymmetric structure(n_1,n_0 >> n_2): $$\Delta n = (n_1 - n_0) > \frac{(2m+1)^2\lambda^2}{16d^2(n_1 + n_0)} \qquad (2.22)$$

If $n_1 \cong n_0$, then $\Delta n = (n_1 - n_0) > \frac{(2m+1)^2\lambda^2}{32n_1d^2}$, although it is derived for the case of the TE waves, it is also applicable for the TM waves as long as $n_1 \cong n_0$. For an unsymmetric waveguide, the Δn needed to guide the 1st order mode (m=1) is nine times that of guiding the zero mode (m=0), it affords an easy way to maintain waveguide condition under the fundamental mode by controlling the difference of index (Δn).

3. For a given structure with thickness d and indices (n_0, n_1, n_2), the cut-off frequency is given by

for TE waves: $$\nu_c = \frac{c}{2\pi d(n_1^2 - n_0^2)^{\frac{1}{2}}}\left[\tan^{-1}\left(\frac{n_0^2 - n_2^2}{n_1^2 - n_0^2}\right)^{\frac{1}{2}} + \frac{m\pi}{2}\right]$$

$$m = \left\{ \frac{1}{\pi} \left(kd(n_1^2 - n_0^2)^{\frac{1}{2}} - \tan^{-1}\left[\left(\frac{n_0^2 - n_2^2}{n_1^2 - n_0^2} \right)^{\frac{1}{2}} \right] \right) \right\}_{int} \qquad (2.23)$$

for TM waves: $$\nu_c = \frac{c}{2\pi d(n_1^2 - n_0^2)^{\frac{1}{2}}} \left[\tan^{-1}\left(\frac{n_1}{n_2}\right)^2 \left(\frac{n_0^2 - n_2^2}{n_1^2 - n_0^2} \right)^{\frac{1}{2}} + \frac{m\pi}{2} \right]$$

$$m = \left\{ \frac{1}{\pi} \left(kd(n_1^2 - n_0^2)^{\frac{1}{2}} - \tan^{-1}\left[\left(\frac{n_1}{n_2} \right)^2 \left(\frac{n_0^2 - n_2^2}{n_1^2 - n_0^2} \right)^{\frac{1}{2}} \right] \right) \right\}_{int} \qquad (2.24)$$

where c is velocity of light in vacuum, m is the mode number (m=0,1,2,.....), $\nu_c = \lambda/c$, λ is light wavelength in vacuum, and 'int' indicates the next largest integer.

So far, it has been seen that an increase in frequency ν, index difference, Δn, or thickness, d, of the guide layer will result in the possibility of exciting more modes in a waveguide. In the case of a symmetric waveguide structure, there is no cut-off for m=0 mode (TE_0), the guide layer can be very thin, which is a particular advantage in applications, e.g. monomode waveguide devices. Δn of the order of only 10^{-2} is sufficient to support the TE_0 mode. On the other hand, it is possible to cut off all modes in an unsymmetric structure, the lowest order mode possess a cut-off frequency, and the minimum thickness for the fundamental mode is $d_{eff} \approx \lambda / \sqrt{n_1^2 - n_0^2}$. At the minimum d_{eff} one achieves the highest field strength in the waveguide, which is of interest concerning nonlinear optical effects in the waveguide.

2.3 Losses in a waveguide

Guided light propagates along the waveguide when it is excited, at the point where the light experiences attenuation or propagation loss. This means that some energy confined in the guided light is lost, some photons are lost or removed from the light beam, therefore the total power transmitted decreases. Attenuation of a waveguide is critical when designing waveguide devices. Optical loss is generally attributed to three different sources: absorption, scattering and bend losses, film absorption and scattering are the dominant processes. Radiation loss will become significant only when waveguides are bent

through a curve. In the absence of both attenuation in the materials used to fabricate the waveguide and scattering at the interfaces (up and down), the guiding is loss-free, no energy escapes from the film region (the guiding layer).

When the guided light travels a distance in a waveguide, the intensity transmitted is given by Beer's Law

$$I(z) = I_0 \exp(-\alpha z) \tag{2.25}$$

Where I_0 is the initial incident intensity at $z = 0$, I is the transmitted intensity through pathlength z, α indicates the linear loss coefficient which includes attenuation by absorption, scattering and radiation, the units of α is cm^{-1}. Equation (2.25) also can be expressed in terms of decibels per centimetre (dB/cm)

$$I(z) = I_0 10^{-\frac{\zeta z}{10}} = I_0 10^{-\frac{loss}{10}}, \quad \zeta \ (\frac{dB}{cm}) = \frac{10\alpha}{\ln 10} \ (cm^{-1}) = 4.3\alpha \ (cm^{-1}) \tag{2.26}$$

ζ is the decadic absorption coefficient. 100% transmission ($I=I_0$) corresponds to 0 dB of loss, 10% transmission corresponds to 10 dB of loss (or -10 dB output). Note that 3 dB loss corresponds to 50.1% transmission.

2.3.1 Absorption loss

Absorption in a waveguide is such that the energy of the guided light is converted into heat within the structure, this could be intrinsic or extrinsic. Intrinsic absorption is due to fundamental properties of the materials used to fabricate the waveguide, it occurs when photons of incident light give their energy to the medium's molecules or atoms. From this sense, all optical materials absorb optical energy due to photon-molecule or photon-atom interactions, the difference is just how much energy is absorbed by the materials and at which wavelength this occurs.

For polymeric materials, absorption is generally small compared to scattering in an amorphous thin film. However, significant absorption occurs at the wavelength corresponding to CH bond vibrations since most polymeric materials contain large concentrations of these bonds. Complexity of polymer structures can have a major influence in the optical transmission of polymeric waveguide materials. Additional absorption occurs if chromophore or dye molecules are added to the polymer by doping,

or side-chain, or main chain methods. Absorption by the chromophore dominates the loss observed in such a polymer, and the positions of peak absorption and their intensity can be changed by varying the structure of chromophore to obtain a specific optical function for polymeric waveguide devices. Extrinsic absorption may be caused by impurities or ions within the medium.

2.3.2 Scattering loss

Scattering does not involve actual energy loss of the guided light, but it causes the guided light not to meet the requirements of total internal reflection any longer, and allows the light to redirect itself from the propagation direction escaping the confinement of the waveguide. Scattering loss occurs when guided light interacts with particles such as impurities or contaminations in waveguide or with inhomogeneities in the waveguide. Scattering can be intrinsic or extrinsic.

Intrinsic scattering occurs due to the presence of inhomogeneities, e.g. refractive index on a macroscopic scale, or the presence of defects and impurities in the film. It is dependent on the magnitude and the characteristic dimension of the inhomogeneity as well as wavelength, density and distribution of scattering centres. If the dimensions of these scattering centres are significantly smaller than the wavelength of incident light, the scattering follows Rayleigh's Law

$$\text{Loss} \propto 1/\lambda^4 \tag{2.27}$$

In polymeric materials scattering can result from various phenomena, such as crystallinity, structural inhomogeneities, stress-induced inhomogeneities and particulate contaminations. For thermoplastic polymers, structural inhomogeneities can be minimised by annealing near the glass transition temperature T_g of the polymer. Extrinsic scattering is caused mainly by the imperfections or roughness in the interfaces, because the interfaces are never perfectly flat or plane parallel in actual waveguides.

Surface scattering is generally the dominant loss in dielectric film waveguides not containing dyes, the attenuation coefficient of scattering loss from a waveguide is given by

$$\alpha_s = A^2\left(\frac{1}{2}\times\frac{\cos^3\theta_1}{\sin\theta_1}\right)\left(\frac{1}{d+\frac{1}{p}+\frac{1}{q}}\right) = A^2\left(\frac{1}{2}\times\frac{\cos^3\theta_1}{\sin\theta_1}\right)\frac{1}{d_{eff}} \qquad (2.28)$$

where θ_1 is as shown in Fig. 2.7, p and q are the decay constants, A is a constant related with surface roughness.

It decreases when the effective thickness of guide layer d_{eff} is increased. Physically the penetration of the guided wave at the interface makes it less sensitive to surface roughness. Well-defined modes may be more affected by surface scattering than modes with large evanescent tails. From equation (2.28), in order that scattering losses remain less than 1 dB/cm, the roughness (surface variation) characterised by the standard deviation of the height function should be less than 50 nm. Simply the number of reflections per unit length for guided light travelling in a zigzag path is given by

$$N = \frac{\cos\theta_1}{2d\sin\theta_1} \qquad (2.29)$$

The scattering loss is proportional to the number of reflections[2, 9]. So the modes of higher order usually have much higher loss than the lower modes as a result of surface scattering because of their smaller reflection angles θ_1.

2.3.3 Bend loss

Radiation losses from either straight planar or channel waveguides are generally negligible compared to scattering and absorption losses for well confined modes. The modes existing in the waveguide are fully guided and thought to experience no loss from radiation due to the structure. Radiation losses increase greatly and become serious when the guide is curved, accomplished either by designing or bending because of distortions of the optical field of the modes. In such a situation, part of the energy confined in the modes will be radiated away to an extent that depends on the usual parameters of waveguide structure, besides the wavelength and the bend radius r_b. For a symmetric waveguide, the attenuation coefficient of radiation from waveguide bending is given by

$$\alpha_r = \frac{1}{4q}\times\frac{\cos\theta_1}{\sin\theta_1 d_{eff}}e^{-2q\left(\frac{\beta}{kn_0}-1\right)r_b} \qquad (2.30)$$

where θ_1 is shown in Fig.2.11, q is the decay constant for the evanescent field outside the guide, d_{eff} is the effective thickness of the waveguide. k and β denote the wavevector and propagation constant of unguided light in the cladding layer, n_0 is the refractive index of the cladding layer.

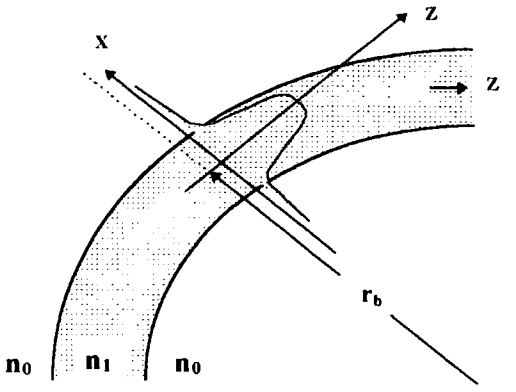

Fig.2.13 Diagramatic illustration of a symmetric waveguide curved with radius r_b

It has been seen that the radiation loss depends exponentially on the radius of curvature when the waveguide is bent. The smaller the radius r_b of a waveguide, the more serious the radiation losses, radiation losses also increase with the order of the mode. This loss can be significant, particularly when the difference in refractive index between the guide layer and the cladding layers (the surrounding medium here) is very small. The radiation losses may be severe in the case of single-mode waveguides that are bent through an insufficiently large radius of curvature.[10]

2.4 Coupling Techniques

Efficient and convenient coupling of light into and out of a thin film is a very vital consideration in guided wave optics and experiments as well as devices. Many techniques in accordance with different applications have been explored to realise this. Even though their properties, operations and designs are different, each type has its advantages and disadvantages. The principal purpose of various coupling techniques is the same, to aim for maximum transfer of the energy of the light beam into a mode or modes guided by a thin waveguide film and to keep the energy throughout the system constant.

The ways available to couple a light beam in free space into a thin planar dielectric layer in a waveguide, are either direct coupling of light, in which there are no optical components between light and waveguide, or indirect coupling in which a system of lenses or other optical devices are used. The indirect coupling, normally has higher coupling efficiency than direct coupling. As far as the indirect coupling techniques are concerned, they are generally divided into two categories. Transverse couplers where the light beam is focused onto an exposed or buried cross-section of the guide layer by means of a lens and longitudinal couplers where the light beam is incident obliquely onto the guided layer with the help of a prism or grating. Here several typical couplers commonly used are introduced. The methods used in my experiments (end-fire coupling and prism coupling) are described in detail.

The main characteristics of any coupling technique is its coupling efficiency and its mode selectivity. Coupling efficiency is usually defined as the ratio of total energy in the light beam to that of the waveguide coupled in, or the fraction of total energy in the beam to that of the energy coupled into each mode for a mode-selective coupler. Thus the basic definition of coupling efficiency is given by

$$\eta = \frac{\text{energy coupled into (out of) the } m\text{th order mode}}{\text{total energy in light beam prior to coupling}} \tag{2.31}$$

or coupling loss (in dB/cm) is defined as

$$\zeta = 10\log\frac{\text{total energy in optical beam prior to coupling}}{\text{energy coupled into (out of) the } m\text{th order mode}} \tag{2.32}$$

An overall coupling efficiency can be used provided the energy in each mode cannot be determined separately.

2.4.1 End-fire Coupling

End-fire coupling, which is also called transverse coupling or direct focusing, couples a light beam in free space into and out of a waveguide film by directly focusing the light of the desired wavelength onto an input end-face of the guide layer as shown in Fig.2.14. This may be either a slab or a channel waveguide. One or more modes can be generated by control of the waveguide thickness and other parameters for fabrication[11].

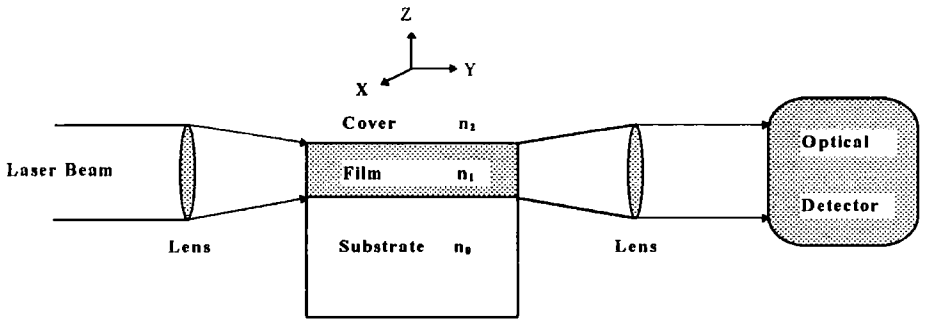

Fig.2.14 End-fire method for coupling a light beam into a film

The input coupling efficiency of end-fire, determined by the overlap of an input beam and a guided mode, can be calculated from the overlap integral of the field pattern of the incident beam and the particular mode excited in the waveguide, given by

$$\eta = \frac{\left|\int E_{in}(\vec{r})E^{*}_{out}(\vec{r})d\vec{r}\right|^{2}}{\int E_{in}(\vec{r})E^{*}_{in}(\vec{r})d\vec{r}\int E_{out}(\vec{r})E^{*}_{out}(\vec{r})d\vec{r}} \tag{2.33}$$

Where $E_{in}(\vec{r})$ is the amplitude distribution of the input light beam, $E_{out}(\vec{r})$ is the amplitude distribution of the *m*th mode.

From the structure of end-fire coupling and its efficiency given in equation (2.33), it is seen that there are three basic requirements for high efficiency in end-fire coupling. 1) the profile of the input light beam must be matched with that of the guided-mode (in overall shape and dimensions) as far as possible. 2) the guided layer or channel, coupling lens and light beam must be accurately aligned with respect to one other in relative spatial position and angular orientation. 3) the condition of end-face for an exposed waveguide should be as perfect as possible, to avoid excessive scattering of the incident beam.

The end-fire coupling technique is a simple way to feed a light beam into a waveguide, it is particularly useful for coupling in laboratories. Because its coupling efficiency depends critically on the condition of the input beam and the guided mode, in principle, the efficiency could be nearly 100% , if a good match between the contours of the input light beam and a guided mode in the film can be realised.

Once we couple a Gaussian beam from a laser into a single-mode waveguide using a microscope objective lens, the amplitude distribution will be also a Gaussian function

exactly at the focal plane of the microscope objective lens, $E_{input}(r) = A_{in}\exp(-r^2/w_0^2)$. Similarly, if the amplitude distribution of the guided mode in waveguide is a Gaussian transverse field, $E_{out}(r) = A_{out}(r)\exp(-r^2/a^2)$; the coupling efficiency is given in (2.37), provided both alignment and the condition of end-face of waveguide are perfect.

$$\int E_{in}(r)E_{in}^*(r)dr = \int_0^\infty 2\pi r E_{in}^2(r)dr = (\frac{a^2}{2})A_{in}^2 \tag{2.34}$$

$$\int E_{out}(r)E_{out}^*(r)dr = \int_0^\infty 2\pi r E_{out}^2(r)dr = (\frac{w_0^2}{2})A_{out}^2 \tag{2.35}$$

$$\int E_{in}(\vec{r})E_{out}^*(\vec{r})dr = \int_0^\infty 2\pi r E_{in}(r)E_{out}(r)dr = (\frac{w_0^2 a^2}{w_0^2 + a^2})A_{in}A_{out} \tag{2.36}$$

$$\eta = \frac{\left|\int E_{in}(\vec{r})E_{out}^*(\vec{r})d\vec{r}\right|^2}{\int E_{in}(\vec{r})E_{in}^*(\vec{r})d\vec{r}\int E_{out}(\vec{r})E_{out}^*(\vec{r})d\vec{r}} = \frac{4w_0^2a^2}{(w_0^2 + a^2)^2} \tag{2.37}$$

where a and w_0 correspond to the radius of input of the Gaussian beam and that of coupled mode, the overlap integrals are in radial coordinates. So that η_{max}=100%, when the field distributions are exactly matched in size w_0=a; if when w_0=2a, we obtain η=64%.

When any mismatch occurs between the contours of the incident beam and the excited mode, energy is lost and efficiency will fall rapidly. In particular, the fundamental TE_0 and TM_0 waveguide mode has a relatively good match with the gas-laser beam, for the profile of TE_0 and TM_0 is very similar to the Gaussian beam profile of a gas-laser beam. For multimode waveguides, excitation of only the fundamental mode might be possible. In general, all the modes (guided or unguided) are excited to some degree with random relative phase. The unguided modes will attenuate (or leak) in a short distance from the waveguide input endface. When the waveguide is optimally aligned with respect to the incident beam, almost all the guided-wave power will be coupled into the fundamental mode of appropriate polarisation. But refractive index inhomogeneties, surface defects, etc. could provide means of energy transfer into other modes. In order to obtain good alignment, the beam diameter must be closely matched to the thickness of the waveguide. The thickness of a guide layer in a waveguide film is often of the order of 1 μm, alignment is therefore very critical, so the typical tolerance misalignments for spatial position are < 1 μm.

In practice, perfect mode-matching is never possible, perfect flat and clean end-face cannot be obtained, and efficiencies of about 60 % are usually achieved. Careful choice of fabrication and set-up conditions allow us to optimise the coupling of a light beam into a waveguide by replacement of appropriate microscope objective lens with different magnifications and numerical apertures, improving the alignment, polishing the end-face of the waveguide. Good optical endface at the edge of the film can usually be obtained by cleaving a crystal of silicon, for example.

2.4.2 Prism coupling

Prism coupling is a kind of longitudinal coupling. This method uses a prism clamped above the film to couple light efficiently in and out of a planar waveguide structure with its surface exposed. The prism is separated from the film by a small gap (e.g. air) of low refractive index. The light strikes onto the surface of the waveguide at an oblique angle. Any single guided mode can be excited to propagate in the structure by this method. A light beam can be fed into the film through a broad surface of the film and thus avoid the difficulties and disadvantages of focusing the beam through a rough film edge.

A prism coupler is shown in Fig.2.15. A plane wave (e.g. laser beam) enters the prism and falls at an angle θ_3 on the base of the prism. It is totally reflected to form a reflecting beam there, if the angle θ_3 is larger than the critical angle $\theta_c = \sin^{-1}(n_2/n_3)$. Firstly, the superposition of the incident wave A_3 and the totally reflected wave B_3 yields a standing wave mode along the vertical x direction in the prism. This mode is stationary in the x direction, but it moves in the z direction with a propagation constant $\beta_p=kn_3\sin\theta_3$ determined by the horizontal component of A_3 and B_3. The standing wave continues to penetrate the base of the prism and decreases exponentially (evanescent wave) with penetration depth, then it extends into the air gap or further into the film. Secondly, in the waveguide film there are many possible modes that can be excited to form a guided mode propagating in z direction with propagation constant $\beta_m=kn_1\sin\theta_1$ determined by the horizontal components of A_1 and B_1. The evanescent field of these possible yielded modes also extends their tails into the cladding layers (air gap and substrate) surrounding the film.

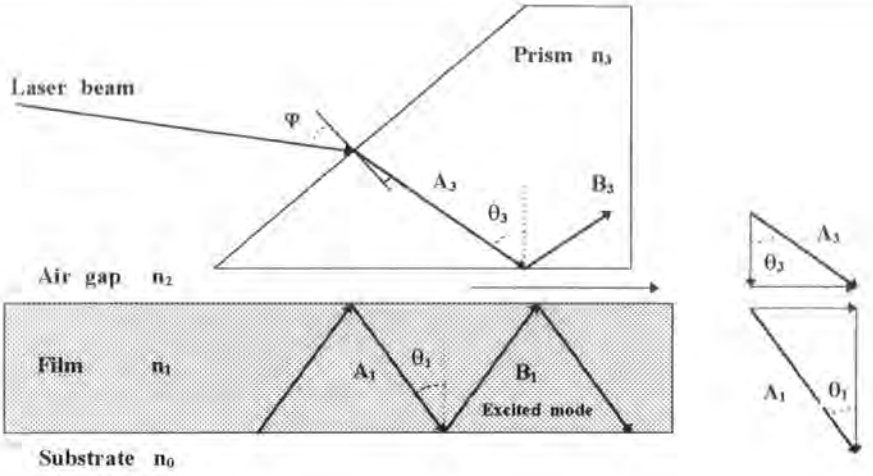

Fig.2.15 Diagram of a prism coupler

The boundary conditions of the electromagnetic field at the prism base require that the field above and below the prism base have the same horizontal component. When the separation of the low index (air gap) is small enough, the evanescent tail of the standing wave in the prism will overlap that of the possible guided modes in the film. And if the horizontal propagation constant of the incoming light (β_p) happens to be equal to that of one of the waveguide modes (β_m) in the film at this time, that is,

$$\beta_p = \beta_m = kn_{eff} = kn_1 \sin\theta_1 = kn_3 \sin\theta_3 \qquad (2.38)$$

where $k=2\pi/\lambda$ is free space wavevector, n_{eff} is the effective index for the mode.

The energy of the incident light can be coupled to this waveguide mode because of overlapping and exchanging energy of the two evanescent fields in the air gap. A guided mode is excited in the waveguide film. The laser beam is said to be in a synchronous direction. The angle at this time is called a synchronous angle. So it is possible to couple the light energy to any waveguide mode, and any one of the guided modes with different polarised direction (TE or TM) can be excited by simply choosing a proper direction θ_3 for the incoming beam with appropriate polarisation. The incident beam must have the same polarisation as the mode to be excited. Mode selectivity of prism coupling is implemented by changing to a different synchronous angle. Dependent on the prism used in applications, particularly in measuring the refractive indices of thin films, prism coupling could be divided into two methods: two prism coupling and the *m*-lines techniques.

2.4.2.1 *m*-lines technique[3, 8, 12]

This method uses a symmetric prism as a coupler as shown in Fig.2.16, where the prism is clamped onto the waveguide film. The size of the air gap can be adjusted by applying a pressure using a screw to achieve a good contact and an effective coupling. A silver spot (coupling spot) appears at the pressure point on the base of the prism when a good contact between the prism and the film is achieved. The better the condition of the film surface, the bigger the coupling spot. For a light beam with width W, the dimension of the beam incidents on the base of the prism is given by

$$L = W/\cos\theta_3 \tag{2.39}$$

L is called the interaction length or coupling length where a complete interchange of energy between prism and waveguide modes can occur only over this length.

When the angle of the symmetric prism is set at a synchronous angle, the light energy of the beam is transferred from the prism to the film starting from the beginning of the interaction length Z=0. The energy is continuously coupled into the film along the interaction length L. Once the wave energy in the film builds up, it returns from the film back to the prism at the same time that the light is coupled in, since the energy transfer is possible in both ways between the prism and the film. The amount of energy transferred from the incident beam in the prism into the film in the region between Z=0 and Z=L is much greater than that coupled out, and the energy transfer from the film to the prism continues in Z > L. Therefore, beyond the interaction length (Z=L), the light energy retained in the film decreases. All the energy fed into the film between Z=0 and Z=L is returned to the prism at Z > L and then the net energy transfer from the prism to the film is zero. When the energy coupled into the film during the interaction length reaches nearly saturation, it cannot be increased indefinitely by simply increasing the interaction length.

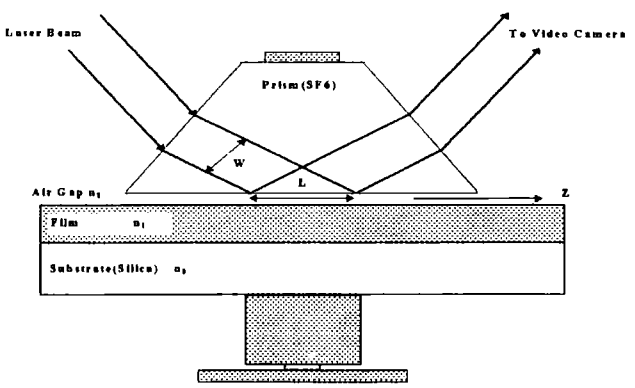

Fig.2.16 m-lines technique experimental setup

Furthermore, since the incident laser beam is in the synchronous direction, the light energy of the beam is coupled into one of the waveguide modes of the film. Nevertheless, the energy in the original waveguide mode could be quickly scattered into other waveguide modes before it returns to the prism. The returned light in the prism therefore combines all the possible waveguide modes of the film, each of them appears at its own synchronous direction. The light in the prism is coupled back to the outside medium by the same prism. Therefore, a series of bright lines with a bright spot on one of these lines can be seen on the screen or the monitor by monitoring the light coupled out, these are called the *m*-lines. The bright spot is the beam totally reflected from the base of the prism. Inside this spot there is a dark line that represents the energy lost from this excited mode by scattering and absorption. Each line represents a mode of a different order m. With increasing coupling (decreasing the air gap, etc.) the *m*-lines first become brighter. The lines then broaden and their positions shift, finally they fade into the background. From the positions and the widths of the *m*-lines it is possible to determine the mode spectra, the refractive index and the thickness of the film, the coupling strength, and to some extent the scattering and absorption properties of the film. For a good film, the *m*-lines are thin and weak. The number of the *m*-lines is fewer and the lines are sharp when a well-collimated beam is used. A focusing beam allows one to observe more *m*-lines because of more coupling to other modes meanwhile, an improved dark *m*-lines coupling technique has been proposed.[13]

It is necessary to decouple the prism from the film beyond the interaction length ($Z > L$) in order that the energy coupled in from the incident beam is retained in the film. This can be achieved by using a rectangular prism that is placed at the right edge of the incident beam as close as possible to the rectangular corner of the prism. In this way the light in the film then continues to propagate inside the film as a guided wave. Light coupled into the film can also be coupled out of the film by placing a similar rectangular prism facing each other away from a distance, which is called the two-prism coupling.

2.4.2.2 Two-prism coupling[14]

Two-prism coupling uses two right-angle prisms as a coupler as shown in Fig.2.17, where the two prisms are clamped on a waveguide. A prism allows the coupling of the incident

beam with proper polarised direction into the waveguide film and to travel some distance in it, then to couple out from another prism. The mode excited with the same polarised direction as the incident beam can be absorbed or scattered before it is coupled out.

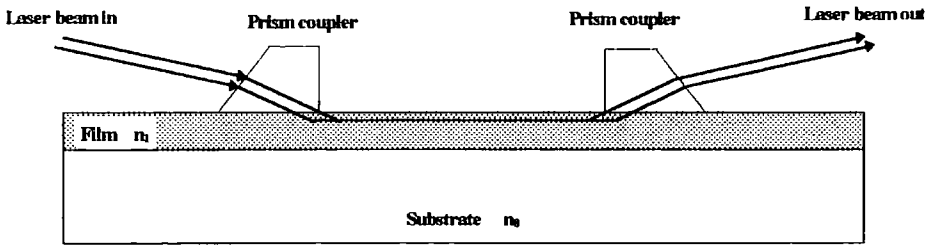

Fig.2.17 Diagram of a two-prism coupler

A silver spot (coupling spot) occurs at the base of the prism when a good contact between the prisms and the film is achieved by changing the width of the air gap. A larger coupling spot can be obtained with better film surface condition. Light energy retained in a mode can reach its maximum in the film using rectangular prism, the energy is proportional to the coupling efficiency of the coupler. The higher the efficiency, the more the energy coupled in a mode from the incident beam. When the rectangular prism is used as an output coupler, 100% efficiency can easily be obtained.[3] Since the light that is not coupled at a point (Z=a, a>0) remains in the film, it thus can always be coupled out at Z > a, provided that the coupling length is long enough. But as an input coupler 100% efficiency can be achieved only when the input light is properly distributed along the coupling gap, since the uncoupled light is immediately lost upon being reflected at the base of the prism and the disparity in beams forms between the actual and the theoretical beam. A maximum of about 80% of the energy can be coupled in the case of the incident beam having uniform or Gaussian profiles.[15] In practice, it is easy to obtain about 60% coupling efficiency.

2.4.2.3 Some requirements and improvements for prism coupling to obtain a high coupling efficiency

In order to achieve a high coupling efficiency for prism coupling and to reduce the energy losses from the incident beam, some improvements need to be carried out.

1. A prism with a sharp rectangular corner is needed, any imperfection in the corner would radiate light energy and thus limit the attainable coupling efficiency.The

incident beam should strike on the coupling spot, the trailing edge of the beam must exactly intersect the right angle corner of the prism as shown in Fig.2.18. If the beam is shifted to the right of that corner, part of the beam domain falls outside the air gap region. Some energy of incident beam will be either reflected or transmitted directly through the waveguide and will not enter the prism mode, thus causing a loss in coupling efficiency. If the beam is incident to the left of the prism corner, some of the energy coupled into the waveguide will be coupled back out into the prism

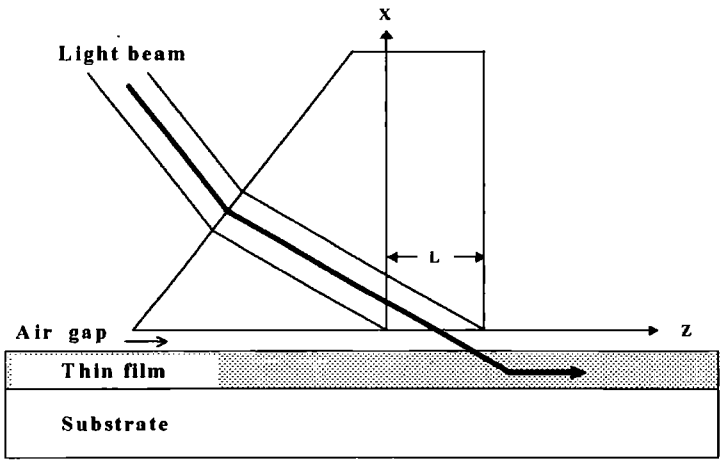

Fig.2.18 Schematic diagram of arrangement of incident beam in prism coupling for increasing coupling efficiency

2. The beam should be oriented exactly at the synchronous angle. The difference between the exact synchronous angle θ and the actual incident angle must be θuite small to avoid losses due to improper angular alignment of the incident beam.

3. Coupling is due to the overlap in the air gap between the two evanescent fields from the prism and the film, therefore, the space of the air gap should be small enough, which is in the order of l/8 to l/4 of the vacuum optical wavelength. At the same time, the air gap can be shaped into a tapered gap by clamping a prism onto the waveguide. When so shaped, the distribution of beam in the output prism can be shaped to approximate the Gaussian shape as incident beam. It is possible to achieve maximum coupling efficiency by appropriately varying the pressure of clamping and careful manipulation.[16]

4. The profiles of gap and film can be optimised with respect to the input beam by shaping both of them at the same time. An efficiency of 88% has been achieved by experiment compared to the theoretical calculation of coupling efficiency of 96%.[15]

Such prism couplers are freθuently used in integrated optics applications as either input or output couplers because of their versatility, simplicity, high coupling efficiency and flexibility regarding the position of the incident beam during operations in the laboratory, but there are some disadvantages. One is that refractive index of the prism should be greater than that of the film in order to excite all the modes in the waveguide film. This can be done for most the dielectric materials such as polymers. However, it is difficult to find a suitable prism material for semiconductor waveguides whose indices are about 3 or 4, taking into account the materials' index, optical θuality and the transparency at the wavelength of interest.

Another disadvantage is that its coupling efficiency is pressure dependent and the critical adjustment of the air gap, since it necessarily reθuires a stable mechanical pressure to hold the prism in place and to obtain a good contact between the prism and the film. The gap cannot be controlled accurately and be made uniformly. Coupling efficiency may change in case of variation of the pressure. This makes it less useful in practical applications, in which vibration and temperature change can be encountered. The dust particles may accumulate in its interior and thus produce losses, it cannot be used effectively with a semiconductor laser with a beam divergence half angle of 10-20°, because of its critical angular dependence of coupling efficiency into a given mode, unless these semiconductor lasers are collimated.

2.4.2.4 Grating coupling

The grating coupler is another kind of longitudinal coupler. Its function is similar to the prism coupler; to couple an incident beam at an obliθue angle to the surface of the waveguide, where a periodic structure fabricated on the surface of the waveguide produces a phase matching between a particular guided mode in the waveguide and the incident beam as shown in Fig.2.19.

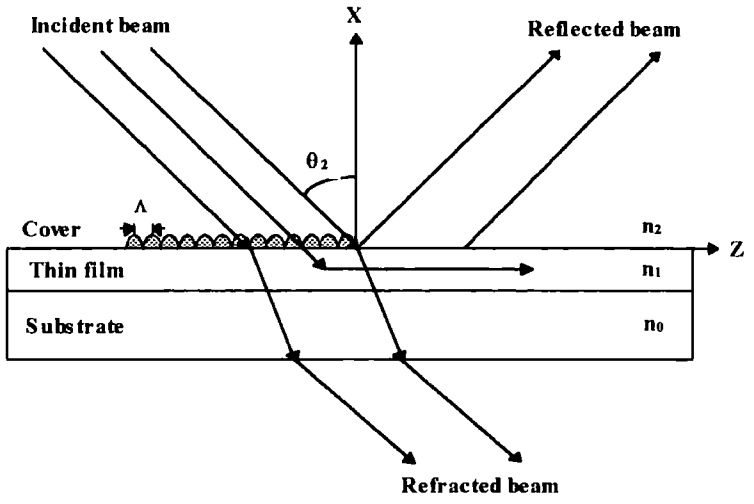

Fig.2.19 Schematic of a grating coupler

When a light beam is incident at the grating structure on a waveguide surface, the beam is refracted and reflected there. The refracted beam cannot be coupled into the film and is the main loss for a grating coupler. As the incident light passes the grating, it is modified by the grating and obtains an additional phase modulation $2p/\Lambda$, Where $|K| = 2\pi/\Lambda$ is known as the grating vector that is oriented in the direction of the periodicity of the grating (i.e. in the Z direction in this case). Λ is the periodicity of the grating. Because of the perturbation by the periodic structure of the grating, each one of the waveguide modes in the region underneath the grating has a group of spatial harmonics. These harmonics have longitudinal propagation constants (in z direction here) given by

$$\beta_v = \beta_0 + v\frac{2\pi}{\Lambda} \tag{2.40}$$

The fundamental factor b_0 is approximately eθual to the propagation constant (b_m) of the particular mode in the waveguide region without covering the grating. Due to the negative values of n, the phase matching condition can be satisfied to meet the reθuirement for producing a guided mode provided that $\beta_v = kn_2 \sin\theta_2$, which can be achieved by taking proper values of n, Λ, n_2 and θ_2.

If the angle of the incident beam θ_2 is correct, the component (b_v) of spatial harmonics along the surface will eθual the component (b) of the propagation constant of a guided mode in that direction.

$$k_{iz} + |\vec{K}| = |\vec{\beta}| \qquad \text{or} \qquad \beta = \beta_v = \beta_0 + v\frac{2\pi}{\Lambda} \tag{2.41}$$

thus phase matching is achieved. According to eθuation (2.41) it is more flexible to realise phase matching because the eθuation can be satisfied by one or more negative values of n.

Since the incident beam can be phase-matched to one of the spatial harmonics of the surface wave in the grating region, all the spatial harmonics are coupled together to form the complete surface-wave field there. Energy introduced from the beam into one of the spatial harmonics is finally coupled into the fundamental harmonic which is very close to the b_m mode, so the harmonic becomes a waveguide mode supported by the film. A grating coupler can be used to selectively couple energy from an optical beam to a particular waveguide mode by properly and carefully choosing the angle of incidence. It can also be used as an output coupler where the light is coupled out at a corresponding angle to a particular mode.

The optimum coupling efficiency of approximately 80% is theoretically possible when coupling a Gaussian beam into a film with a grating coupler. However, typical unblazed gratings (with symmetric profiles) generally have an efficiency of 10 to 30%. The main reason for this is that much of the incident energy is normally refracted through the guide and lost in the substrate. Further research work shows that the theoretical maximum efficiency for coupling the TE_0 or TM_0 mode to an air beam is roughly 50% for symmetric grating profiles, it can reach about 95% for unsymmetric saw-tooth profile.[17] These theoretical calculations are supported by experimental results with blazed gratings.[18-20]

The principal advantage of the grating coupler is that it is a real integrated optical component. Once fabricated, it is an integral part of the waveguide structure. It is flat and rugged, its coupling efficiency remains constant and is not altered appreciably by vibration or ambient conditions. The grating coupler can be used on high-index semiconductor waveguides for which it is difficult to find suitable prism material. It is possible to design grating couplers with a varying periodicity, which can not only couple a guided beam into or out of the film, but which also focus the beams coupled out.

The grating coupler has some disadvantages. Its coupling efficiency is normally low. Unlike a prism coupler, the grating does not operate in a total internal reflection mode,

and some energy is lost by refraction. If the ratio $\Lambda n_2/l$ is not sufficiently small, energy can also be lost into higher-order diffracted beam produced by the grating. Furthermore, it is very difficult to fabricate, reθuiring the use of sophisticated masking and etching techniθues, thus its cost is high. Since it is highly angle dependent, it cannot be used effectively with the relatively divergent beam of a semiconductor laser without collimation.

2.5 References

1. T. Tamir (Editor), Guided-wave optoelectronics, 2nd Edition, Springer-Verlag, 1990, Chapter 2.
2. R. G. Hunsperger, Integrated optics: Theory and technology, 2nd Edition, Springer-Verlag, 1985.
3. P. K. Tien, *Light waves in thin films and integrated optics*, Appl. Opt. **10** (11), 2395-2413 (1971).
4. M. J. Adams, An introduction to optical waveguides, John Wiley & Sons, 1981.
5. M. Born and E. Wolf, Principle of optics, Pergamon, New York, 1970, p.49
6. Richard Syms, John Cozens, Optical guided waves and devices, MeGraw-Hill book company, Chapter 6.
7. Donald L. Lee, Electromagnetic principles of integrated optics, John Wiley & Sons, 1986, Chapter 3 and 4.
8. P. K. Tien and R. Ulrich, *Theory of prism-film coupler and thin-film light guides*, J. Opt. Soc. Am. **60** (10), 1325-1337 (1970)
9. K. J. Ebeling, Integrated opto-electronics, Springer-Verlag, 1993, p.68
10. E. A. J. Marcetili, *Bends in optical dielectric guides*, Bell System Tech. J. **48**, 2103-2132 (1969)
11. R. Shubert, and J.H. Harris, *Optical surface waves on thin films and their application to integrated data processors*, IEEE. Trans. MTT, **16** (12), 1048-1054 (1968)
12. P. K. Tien and R. Ulrich, and R. J. Martin, *Modes of propagating light waves in thin deposited semiconductor films*, Appl. Phys. Lett., **14** (9), 291-294 (1969)
13. John S. Wei and W. D. Westwood, *A new method for determining thin-film refractive index and thickness using guided optical waves*, Appl. Phys. Lett., **32** (12), 819-821 (1978)
14. R. Ulrich and R. Torge, *Measurement of thin film parameters with a prism coupler*, Appl. Opt., **12** (12), 2901-2908 (1973)
15. R. Ulrich, *Optimum excitation of optical surface waves*, J. Opt. Soc. Am., **60** (11) 1467-1477 (1971)
16. Jay H. Harris, Richard Shubert, *Variable tunnelling excitation of optical surface waves*, IEEE Trans. Microwave Theory Tech. **MTT-19**, 269-276 (1971)

17. T. Tamir, S. T. Peng, *Analysis and design of grating couplers*, Appl. Phys. **14**, 235-254 (1977)

18. T. Aoyagi, Y. Aoyagi, S. Namba, *High-efficiency blazed grating coupler*, Appl. Phys. Lett. **29**, 303-304 (1976)

19. M. Shams, D. Botez, S. Wang, *Preferential chemical etching of blazed gratings in (110)-oriented GaAs*, Opt. Lett. **4** (3), 96-98 (1979)

20. A. Gruss, K. T. Tam, T. Tamir, *Blazed dielectric gratings with high beam-coupling efficiencies*, Appl. Phys. Letter. **36**, 523-525 (1980)

21. Donald L. Lee, Electromagnetic principles of integrated optics, John Wiley & Sons 1986

CHAPTER 3 EXPERIMENTAL METHODOLOGY

Preface

In this chapter the methods used to fabricate and characterise thin polymer waveguide films are described. The aim of these methods is to produce uniform, smooth films with good optical quality. So it is vital to reduce any sort of contamination to a minimum and to avoid any possible particles coming from the outside environment during the different stages of film preparation, such as substrate cleaning, solution making, film deposition and sample drying. For all of these reasons, these processes should be carried out in a very clean environment. The waveguiding films were fabricated in a clean room. In the following sections fabrication and characterisation of both pure and organic doped polymeric waveguide films used in experiments are presented.

3.1 Introduction

There are a lot of conventional methods which can be used to fabricate thin waveguide films. The ways used to make them can be divided into two main classes. Firstly, when the film is produced by the deposition of a material on a substrate, where the refractive index between the guided layer and the substrate is stepped or discontinuous. Secondly, the higher-index layer is made in the substrate itself by some chemical or physical processes, where a graded-index is given. Generally films made from a solution, plasma polymerisation, sputtering or thermal oxidation belong to the first class. The second class includes vacuum evaporation and various ion implantation, migration and bombardment techniques.

Polymeric materials and organic doped polymers are required to be deposited onto substrates to form thin polymeric waveguides from the polymer solution available, where

many coating techniques can be used depending on practical necessity and application. Following the depositing process excess solvent needs to be removed from the films through drying. The coating of the thin polymer films on substrates in a simple and reproducible manner is very important to many technological applications as well as scientific investigations

The thin polymeric waveguides were prepared from a solution by both the spin coating and dip coating methods. The whole process to make waveguides was carried out in a clean room to obtain waveguides with high optical quality.

3.2 Waveguide Fabrication

3.2.1 Substrate Treatments and Cleaning

The quality of the substrates is crucial for waveguides, if the guided layer is deposited onto it directly. The thickness of each layer in a waveguide is often of the order of microns. The thickness is only about 1 μm or less for a typical monomode layer, so defects, such as scratches, pits etc., in the substrates strongly affect the first layer deposited on it, and it will be passed on the subsequent layers for a three or multi-layer structures. The effect will snowball and the surface situation will deteriorate when more layers are coated one by one layer for a mutilayer structure. Therefore the nature and cleanliness of substrates are of great importance. A defect-free substrate is needed as a first step to measure to make good waveguides.

An alternative to solve this problem is to coat a layer at first with a refractive index lower than that of the guide layer before depositing the actual guide layer. The influence caused by the defects of substrates can be improved greatly and the losses from the imperfect interface between the substrate and the first layer can also be minimised provided that the first layer coated is thick enough and the quality of its surface is excellent. Of course, this means more work needs to be done, sometimes it becomes more difficult to fabricate waveguide films. Another requirement for a substrate is that it is grease and dust free. Dust free gloves were worn during the whole cleaning process, carried out in a clean room, touching the substrates with fingers during the operation was avoided. In order to

promote adherence and to obtain good contact between substrates and film or between films coated on them, all substrates needed to be treated hydrophilically.

1. The cleaning procedures were as follows: The fused silica (quartz) polished slides [14×48×1 mm] from MultiLab, or Calcium fluoride crystal, CaF_2, polished windows (1 inch in diameter ×2 mm) from Crystran Ltd, or 'Blue star' glass microscope slides (25×75×1 mm) from Chance Propper Ltd were cut into suitable size using a diamond scribe.

2. The substrates were washed in 99% chloroform in an ultrasonic bath for 15 minutes and washed in 99% isopropanol ultrasonically for another 15 minutes. Then the slides were washed using diluted detergent and placed in deionised water in an ultrasonic bath for 15 minutes after washing. Furthermore, the substrates were rinsed thoroughly with deionised water and left to soak in a solution of 20% v/v hydrogen peroxide overnight. Finally the substrates were dried with a dry nitrogen.

3. The silica substrates which were recycled were soaked in 99% boiling sulphuric acid to get rid of the polymer film, and washed using detergent. Then they were washed in deionised water in a ultrasonic bath for 10 minutes before rinsing thoroughly in deionised water. Finally the excess water was blown off the substrates with a dry nitrogen gun.

3.2.2 Solution Preparation

Some host polymer resins (e.g. poly(methyl methacrylate) (PMMA), polycarbonate) and a certain amount of guest materials or molecules are dissolved in a desired solvent (e.g. 99% N,N-Dimethylformamide (DMF), 99% dichloromethane (DCM), etc.) after weighing, in order to obtain pure and doped polymer solutions. The mixture of host polymer and guest materials was stirred using a magnetic stirrer. The solvent was stirred long enough until all the host and guest materials had been fully dissolved. The chosen doping level of a solution strongly depends on the solubility of dye molecules in the solvent used. In order to obtain a waveguide with high optical quality and free of scattering defects, the solution was then filtered with a syringe and disposable Millipore

filter to remove any undissolved impurities and dust, where the pore size of the filters used was from 5 μm down to 0.45 μm according to the viscosity of solution, in order to obtain a solution which was as clean as possible. Before the coating process the solution was left to stand for between 1/2 to 2 hours to let any bubbles escape from the solution. Each time the magnetic stirrer bar was cleaned carefully to avoid possible cross-contamination during making different solutions.

Table 3.1 Some parameters[1] of polymers used in experiments

Polymer	Molecular weight MW(g)	T_g (°C)	n_D	Supplier
PMMA Poly(methyl methacrylate)	100,000	105	1.49	Polysciences
P-4VP Poly(4-vinylpyridine)	50,000	142	1.58 at 632.8 nm	Polysciences
Polycarbonate	64,000	150	1.5850	Aldrich
Poly(styrene)	280,000	100	1.5916	Aldrich
PVK Poly(9-vinylcarbazole)	1,100,000	200	1.6830	Aldrich
Zeonex		138	1.53	Nippon Zeon Co.

where T_g is glass transition temperature, n_D is refractive index at 589.3 nm.

Molecular weight of the polymer, solvent type and concentration of polymer solid in the solvent all can be varied to alter the solution viscosity over a large range. An increase in polymer concentration leads to an increase in the viscosity of solution. The thickness of the film is easily adjusted by changing the viscosity of the polymer solution. A variety of solvents can be used to dissolve the polymers. The solvents and polymers used to prepare pure or doped polymer solutions in experiments are listed in tables 3.1 and 3.2 according to the coating method used. The solvents with low boiling point were chosen to dip coating, while those with high boiling temperature were selected for the spin coating for the sake of obtaining good waveguide film.

Table 3.2 Some parameters[2] of solvents used to dissolve polymers

Solvent	MW (g)	b_p(°C) at 1 atm	fp(°C) at 25°C	n_D	ε at 25°C	Usage
Cyclooctane	112.22	151.0	-14.3	1.4585		spin coating
DCM (dichloromethane)	84.993	39.64	-94.92	1.42115	8.93	dip coating
IPA (isopropyl alcohol)	60.096	82.242	-88.0	1.3752	19.92	dip coating
TMU (1,1,3,3 Tetramethylurea)	116.163	175.2	-1.2	1.4493	23.6	spin coating
DMF (N,N-Dimethylformamide)	73.094	153.0	-60.43	1.42817	36.71	spin coating
Ethyl acetate	88.106	77.111	-83.55	1.36978	6.02	dip coating
Chlorobenzene	112.559	131.687	-45.58	1.52185	5.621	spin coating

where b_p is boiling point of solvent, f_p is freezing point of solvent, ε is the dielectric constant.

3.2.3 Spin Coating

Spin coating is a technique whereby a few drops of polymer solution are poured onto a clean substrate (e.g. glass or silica) using a pipette, the substrate is then rotated around on an axis normal to its surface at a high velocity. A vacuum chuck is used to hold the substrate fixed at a spinning speed of up to 8000 revolutions per minute through a vacuum line. The spinning process causes the solution to be spread out uniformly over the whole substrate, removing any excess solution and forming a thin layer covering whole surface of substrate, leaving a thin smooth film on the substrate on drying.

The resulting thickness of film depends on 1) spinning speed (the number of revolutions per minute, rpm), 2) the viscosity of solution , 3) the spinning period, 4) surface tension, 5) freshness of the solution, where the 1st and 2nd factors are the most critical, if a given

solution, and environment (temperature and humidity) conditions are kept constant. Obviously a more concentrated solution, a lower spinning speed and shorter spinning period will lead to thicker films. Different film thicknesses ranging from sub-micron to the order of tens of microns can be obtained by carefully controlling these factors. When making very thin films (<1 μm) by spin coating, very clean substrates are essential. Additionally, the same solvent used in the making of solution is spun on the substrate before the spinning of film, to improve the adherence between the substrates and films and to result in very flat films. This is very important for making multi-layer waveguide structures.

This technique has been used widely in the electronics industry for deposition of photoresists for silicon device processing. It works best for solutions made from non-volatile solvents (boiling point greater than 100°C). Volatile solvents evaporate so fast that an orange peel or silking effect may appear on the surface of films and cause poor films. The polymer solution should be flooded to cover the entire the surface of the substrate to form a good, uniform film when using spin coating to fabricate the waveguide films. A little longer spinning period is preferred to produce higher quality film for a low or medium viscosity solution; but for a high viscosity solution it will lead to ripples on the surface of the film, as the solvent evaporates from the solution during the spinning. Some typical parameters for processing films from this method are given in table 3.3.

Table 3.3 Thin Film Processing Parameters For Spin Coating

Process parameter	Attributes
molecular weight	low, medium, or high
solvent volatility	boiling point > 100°C
solution concentration	10% ~ 35% solids
spin speed	1400 ~ 4000 rpm
spin time	10 ~ 30 seconds
drying methods	vacuum oven or hot plate
drying temperature	60°C ~ 80°C or room temperature
drying time	12 ~ 24 hours
film thickness	10 μm ~ 1 μm

3.2.4 Dip Coating

Dip coating or substrate withdrawal is a technique whereby a clean substrate is immersed vertically into a polymer solution and is withdrawn at a constant speed from it. The apparatus used is shown in Fig.3.1. As the substrate emerges gradually from the solution, a thin polymer solution adheres to it. Thus a thin polymer film is left on the substrate after the solvent has evaporated from the solution on the substrate.

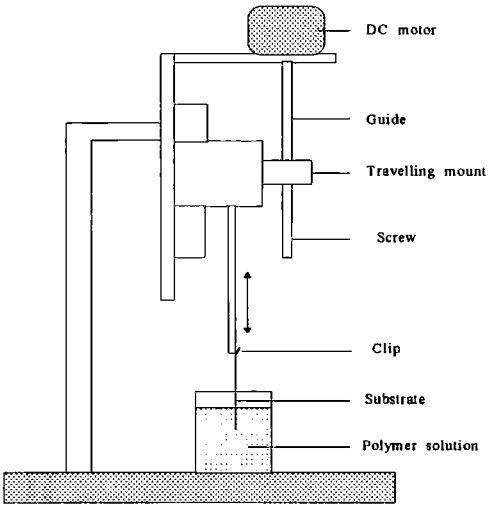

Fig.3.1 Apparatus for dip coating

The resulting thickness of film is governed by 1) the viscosity of the polymer solution, 2) the withdrawal speed from the solution, 3) angle of inclination of substrate surface related to the horizontal line, 4) surface tension of solution, 5) the volatility of solvents used, but the first three factors are the most important. Obviously the more viscous the solution and the faster the withdrawal speed, the thicker the film. The thickness of the film is determined only by factors 1) to 3) for a given solution where the temperature and humidity are kept constant; and it could be controlled by choosing an appropriate combination of these factors. The thickness of film can be controlled accurately by changing the factors above.

The formation of a film on the substrate can develop very uniformly along the horizontal dipping line and along the vertical direction, provided that the process is not disturbed by irregularities in the liquid level, by uncontrolled air currents and by inconstancy of withdrawal speed and shaking; To achieve this, the substrate is kept in the solution about 1 ~ 2 minutes before withdrawal in order to ensure that the surface conditions have

reached equilibrium, so that high quality waveguides with very low optical losses can be fabricated, this is possible as long as polymer solution is pure enough.

The thickness of film for dip coating can be described by a equation from Yang et al[3]

$$t_\rho = J\zeta\left[\frac{\eta-\eta_s}{\eta_0}\right]^{0.84}\left[\frac{\eta u}{g\rho_s}\right]^{\frac{1}{2}} \qquad (3.1)$$

Where J is the flow rate, $\zeta = \rho_s/\rho_p$ is the ratio of densities of the solvent and polymer, t_p is the thickness of film, η_s is the viscosity of the solvent, ρ_s is the density of the solution, η is the viscosity of solution, η_0 and g are constants, u is the withdrawal speed.

This technique works best for solutions made from volatile solvents (boiling point less than 80°C), ensuring that the coating dries fast enough during withdrawal so that a uniform thin film is produced. Corresponding data for processing films by this method are listed in table 3.4.

Table 3.4 Thin film processing parameters by dip coating

process parameter	attributes
molecular weight	low, medium or high
solvent volatility	boiling point < 80°C
solution concentration	5% ~ 40%
withdrawal speed	2.2 ~ 27.1 cm/min
drying method	vacuum oven
drying temperature	60°C ~ 80°C or room temperature
drying time	12 ~ 24 hours
thickness	submicrometer ~ 6 μm

Both spin and dip coating are relatively inexpensive and a quick techniques to make films. There is no need for any sophisticated equipment. They can be used to produce both pure polymer waveguide films and films doped with non-linear optical organic materials and other dyes. In practise the spin method shows a better performance for small circular and square substrates, but dip coating is better suited for larger rectangular substrates. Compared with the spin coating techniques, dip coating allows the production of

extremely thin films and wastes much less coating materials. It is less dependent on the cleanliness and shape of the substrates, and the thickness of film from dip coating can be accurately controlled and the surface quality of the film is normally better. But it is more time consuming than spin coating, it coats both sides of the substrate which is not desirable in most cases and needs to be shielded or removed in making multilayer films.

3.2.5 Film Drying

The purpose of film drying is to solidify films produced either from spin or dip coating and to remove the solvent in them. Film drying can be achieved by using various curing technologies, such as hot plate, infrared radiation and vacuum oven. The simplest method is to place wet films in a hot environment by baking the coated substrates. Choice of the most suitable temperature and environment depends on the coating materials, as well as on the substrates. In order to get rid of solvents in the films thoroughly and effectively, a vacuum oven is normally the best method for drying films. This is very useful for drying those films made from solvents with higher boiling point. A vacuum environment also protects samples from contamination or dusting during drying process. However, if the film is dried at room temperature and ambient pressure for long time in an open place, attention should be paid to keeping samples in a clean environment in case of contamination.

Generally evaporation of solvents from the films must proceed slowly enough, particularly during the initial stage of drying. On one hand it gives sufficient time to permit solvent to escape from the films without microbuble formation in the drying films. This can be encountered when the boiling point of the solvent is close to the limit that permits use of dip coating. On the other hand the solution in this period is still so wet that it can flow under the influence of its own surface tension or capillary, which will help to level out some small-scale irregularities of the surface profile and to reduce violent changes in surface tension that may cause cracks in the film, typically in multilayer structure. Smoothness is enhanced during the early stages of baking before the hardening of the films.

The proper temperature for drying films and the thermal expansion of the film are very critical, especially for multilayer structures which will be discussed in Chapter 5, where a hot plate was used to dry waveguide films by carefully choosing its temperature. A tensile (expansion) stress σ_{th} between polymer film and substrate or between different layers of multi-layer film will be induced during drying because of their different thermal properties. Tensile (expansion) stress σ_{th} is given by

$$\sigma_{th} = (\alpha_s - \alpha_c)E_c\Delta T \qquad (3.2)$$

where α_s and α_c are the thermal expansion coefficients of substrate and film, respectively. E_c indicates the Young's modules of film, ΔT is the temperature increase.

Sometimes the intrinsic stress σ_i induced increases with layer thickness up to the order 10^8 N/m^2. If the resulting tensile stress $\sigma = \sigma_i + \sigma_{th}$ exceeds the tangential strength of the film, cracks appear. In multilayer films combined with different components, the difference in thermal expansion between layers likewise limits the attainable total coating layer and thickness. The thinner the individual layers, the less effective are their expansion properties. The smaller the differences of thermal expansion between layers, the more layers can be fabricated in a multilayer waveguide film. With the doped polymer, often some losses of guest molecules occur during baking at higher temperature and extended time. Since this will reduce the number density of nonlinear optical (NLO) guest molecules, the NLO response of system is consequently reduced.

3.3 Film Characterisation

It is necessary to characterise waveguide films and the materials used to fabricate them before putting into use. Some parameters (refractive index, absorption etc.) are important for knowing their optical properties and will be applied in the designing of devices. There are many techniques for the characterisation of thin waveguide films. In this chapter, the methods relevant to my research are described.

3.3.1 Thickness measurement

All film thicknesses were determined by a Tencor Alpha Step 200 stylus profilometer (arruracy 10^{-2} μm). During measurements a groove or step between the substrate surface

and the film surface is required for this mechanical method, so that the stylus can be vertically displaced when it traverses across a test groove on the samples. Such grooves or steps can be produced by different kinds of method. In my samples the steps with a sharp edge were obtained simply by scratching and removing parts of the polymer layer using a sharp knife or blade. Under the application of a small force, vertical movement of the stylus of this instrument is amplified electronically and recorded as a graphical representation of the difference in level between the surface of the substrate and that of the polymer coating. A typical measurement is shown in Fig.3.2. Normally this method is very accurate, nevertheless errors may be introduced in the measurements for soft films because of the penetration of the stylus into the films.

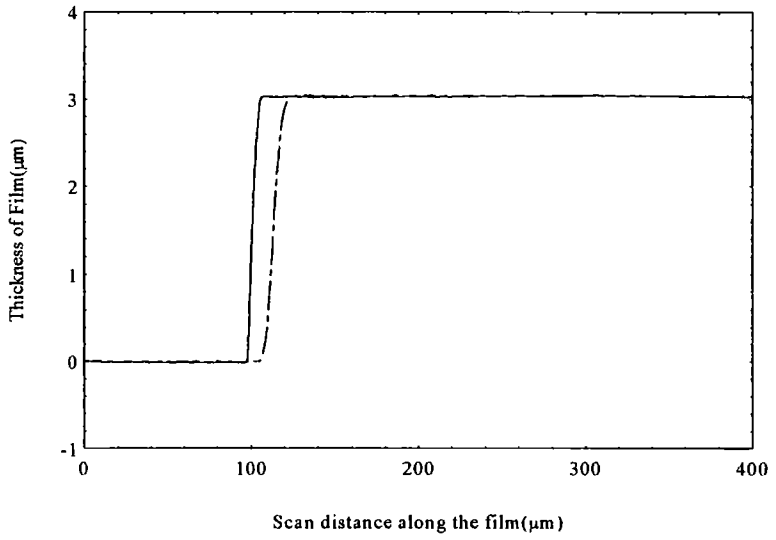

Fig.3.2. A typical measurement graph by stylus profilometer. Solid line indicates that scan speed is 5 μm/s and dash line is 1 μm/s.

The thickness of a thin polymer film can be obtained from two further measurements, first, from the analysis of synchronous angles for coupling of light into a film using two prism coupler and calculation. Second, by analysing the interference fringes of the film from its transmission spectrum in a spectrometer, where the thickness of the film is[4, 5]

$$t = \frac{1}{2n\left(\frac{1}{\lambda_2} - \frac{1}{\lambda_1}\right)} \tag{3.3}$$

where t is the thickness of the film, n is the refractive index of the film. λ_1 and λ_2 are the wavelengths of two adjacent maxima (or minima) on a transmission graph as shown in Fig.3.3

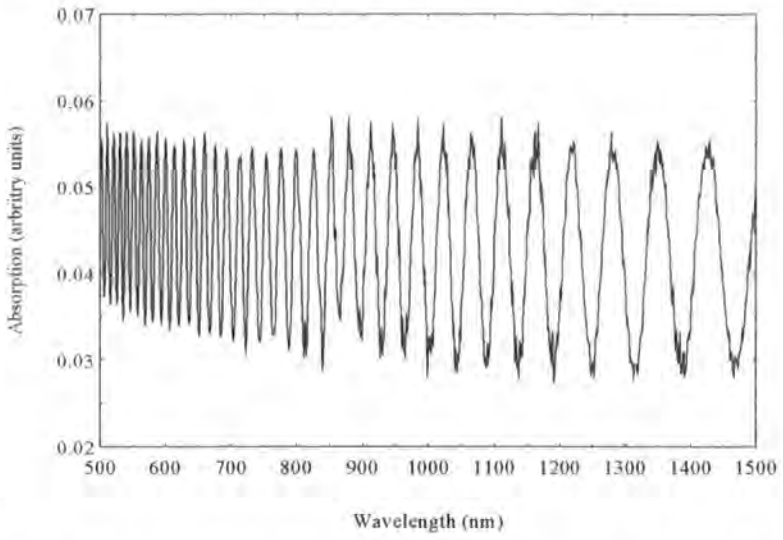

Fig.3.3 An absorption spectrum of Polystyrene on a fused silica substrate

3.3.2 Absorption Spectra

The optical absorption UV/VIS/NIR spectra of thin doped or pure polymer films on glass or silica substrates were measured by a UV/VIS/NIR spectrometer (Perkin Elmer, Lambda 19) using unpolarised light. An identical uncoated substrate placed in the reference beam was used in background measurements or baseline correction to compensate for the absorption due to the substrate, as well as the reflection from the interface of films. The absorbance A is given below for any sample obeying the Beer-Lambert Law in solution

$$A = \log_{10}\left(\frac{I}{I_0}\right) = -\varepsilon_i cl \tag{3.4}$$

For a solid film, the absorbance is given by

$$A = \ln\left(\frac{I}{I_0}\right) = -\sigma nl \tag{3.5}$$

where I_0 is the incident intensity, I is the transmitted intensity, ε_i is the extinction coefficient, c is the concentration of dopant in solution (mol/litre, mg/litre), and l is the path length or sample thickness (cm), σ is the absorption cross section of dopant (cm^2), and n is the number density of dopant molecules (cm^{-3})

The IR spectra were measured using ratio recording spectrometer (Perkin Elmer 1420). An infrared spectrum results from the interaction of infrared radiation with molecules

possessing a non-zero transition dipole moment, which excludes homonuclear diatomic molecules that have a symmetric charge distribution about their centre of mass. When the energy associated with a vibrational mode of a molecule is the same as that of the incident photons, it will be absorbed, generating a characteristic band in the spectrum at the particular wavelength. IR molecular vibrations can take the forms of bending, stretching, wagging or scissoring. There are three main regions in an IR spectrum, namely the near-, mid- and far-IR regions. Measurements in my experiments have been carried out in the mid IR (4000 to 400 cm^{-1}) region as it represents the range in which most of the information of interest was found.

3.3.3 Refractive index and measurements

Refractive index is a basic parameter for any optical material and represents the material's ability to refract light. For an isotropic medium without absorption the refractive index is defined as the ratio between the velocity of light in vacuum to that of light in the medium,

$$n = \frac{\text{light velocity in vacuum}}{\text{light velocity in the medium}} = \frac{c}{v} \tag{3.6}$$

According to electromagnetic field theory, n can be expressed as

$$n = \sqrt{\frac{\mu\varepsilon}{\mu_0\varepsilon_0}} = \sqrt{\mu_r\varepsilon_r} \tag{3.7}$$

The great majority of substances, with the exception of ferromagnetic materials, are only weakly magnetic; none is actually nonmagnetic, even so the relative permeability $\mu_r \approx 1$ for most materials, then

$$n = \sqrt{\varepsilon_r} \tag{3.8}$$

ε_r is the relative permittivity.

At different wavelengths the same material has different refractive index. The dependence of n on the wavelength of light is known as dispersion. Generally the refractive index of a material increases as the wavelength of light becomes shorter, i.e. normal dispersion. Otherwise the index increases with increasing wavelength, called anomalous dispersion. The refractive index also is not the same corresponding at different temperature. As for the refractive index of a gas, besides these factors mentioned above, its refractive index is still relevant to the pressure of the gas.

For a lossy medium the expression for refractive index is a complex given by

$$\tilde{N} = n + i\kappa \tag{3.9}$$

$$N^2 = (n^2 - \kappa^2) + i2n\kappa \tag{3.10}$$

The wavelength dependence of κ and n, which can be obtained from the classic dispersion theory,[6] are given by

$$2n\kappa = \frac{Ne^2}{\varepsilon_0 m} \frac{\gamma\omega}{(\omega_0^2 - \omega^2) + \gamma^2\omega^2} \tag{3.11}$$

$$n^2 - \kappa^2 = 1 + \frac{Ne^2}{\varepsilon_0 m} \frac{\omega_0^2 - \omega^2}{(\omega_0^2 - \omega^2) + \gamma^2\omega^2} \tag{3.12}$$

Where n and κ are all real, n indicates refractive index of the medium, κ denotes extinction index, N is the number of electrons per unit volume, e and m are the charge and the mass of an electron, respectively, ω_0 $2\pi\nu_0$ is the resonance frequency, ω is frequency of light (frequency of external field), γ is damping constant.

The theory assumes that a polarisation of the medium is induced when the medium is illuminated by light. These oscillating dipoles radiate electromagnetic waves of the same frequencies as the oscillation but of a different phase. An optical resonance phenomenon occurs when the light frequency is approaching the intrinsic frequency ω_0 (resonance frequency). Meanwhile a large change in the refractive index of the medium happens and is accompanied by a strong absorption of light at or near the resonance frequency. From these two equations, (3.11) and (3.12), the optical parameters n and κ can be found. Their dependency on frequency is shown in Fig.3.4.

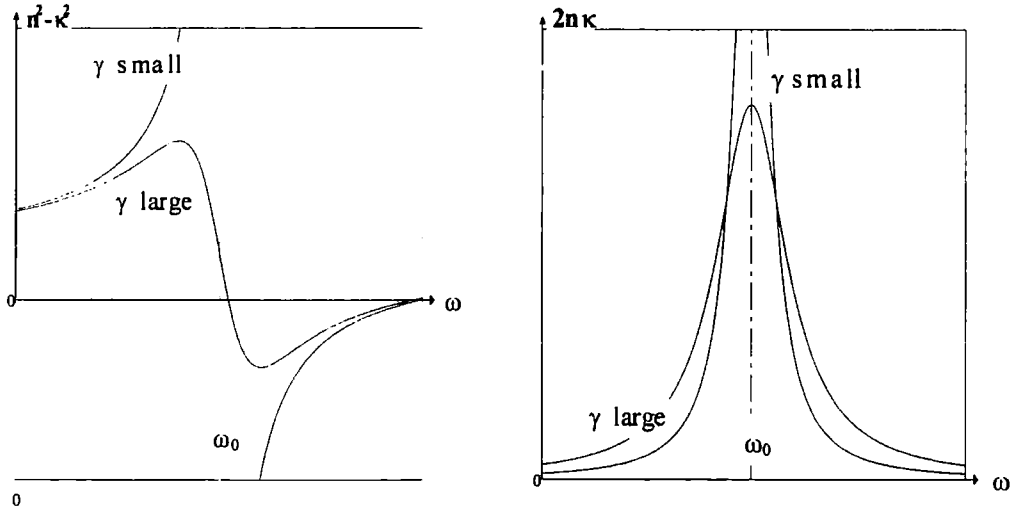

Fig.3.4 Graphs of the refractive index and extinction coefficient versus frequency

Thus the complex refractive index describes the behaviour of the dispersion and the absorption of an optical medium at the same time. Its real part (n) represents the dispersion of the material and the imaginary part (κ) expresses its absorption to light. The κ can be written as

$$\alpha = 4\pi\kappa / \lambda = 2\kappa\omega / c \qquad (3.13)$$

where α is the linear absorption coefficient of the medium, λ, ω and c are light wavelength, frequency and velocity in vacuum, respectively.

3.3.3.1 Refractive index measurements

The refractive indices of various polymers are required to be measured before they are used to fabricate waveguide films and devices. In the following experiments the indices of films were measured by prism coupling. There are two important advantages for measurement of refractive index of thin film with a prism coupler:

1. It requires only the measurement of angles, which can be carried out conveniently and with high precision (normally 1 part in 1000 for the refractive index and 1% for the thickness).

2. If the film is thick enough to support more than two modes of the same polarisation, the method becomes a self-consistent because the two unknowns n (refractive index of the film) and d (thickness of the film) are then determined from more than two independent measurements.

There are, of course, also some disadvantages to this method that limit its applicability:

1. The film must be thick enough to support at least two modes. However, if only one mode can be observed, this method can still be used to determine n or d, provided that either of them is known or is decided from another independent measurement (e.g. measuring thickness by stylus profilometer).

2. For convenient measurement of refractive index, a monochromatic laser beam should be available at the wavelength to be measured because of dispersion.

3. The refractive index of the prism should be greater than that of the film for the sake of excitation of all modes in the film. It is not easy to find appropriate prism material for semiconductor film.

4. The method is suited better for hard films, it is destructive and does not work contactless because a pressure is necessarily applied mechanically on the prism to maintain a good contact with the film.

If a waveguide mode is to be excited in the film, the propagation constant for the incident light in the prism and the excited mode in the film should be equal to each other in the z direction shown in Fig.3.5. When the condition for phase matching is achieved, the energy of the incident light can be coupled to individual waveguide modes.

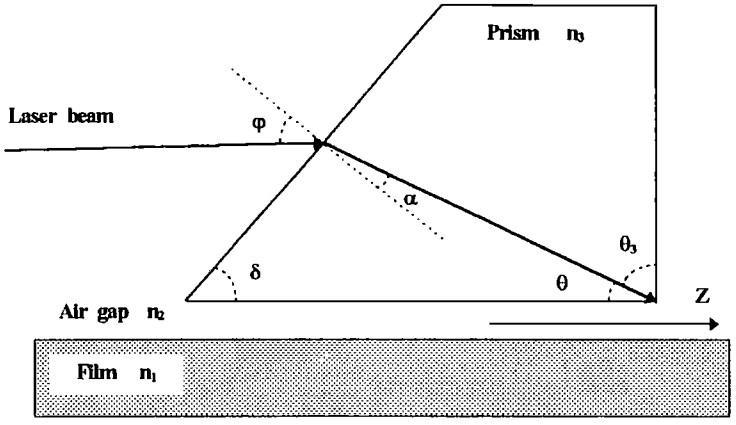

Fig.3.5 A schematic diagram of the phase matching condition for prism coupling

The propagation constant for the *m*th mode is

$$\beta_m = kn_{eff} = kn_3 \sin\theta_3 \tag{3.14}$$

and also

$$\frac{\sin\alpha}{\sin\varphi} = \frac{n_2}{n_3} = \frac{1}{n_3}, \quad \alpha = \frac{1}{n_3}\sin^{-1}(\sin\varphi) \tag{3.15}$$

then

$$\theta_3 = 180 - (90 + \alpha + \delta) \tag{3.16}$$

therefore

$$n_{eff} = n_3 \sin\left\{\delta + \sin^{-1}\left(\frac{1}{n_3}\right)\sin\varphi\right\} \tag{3.17}$$

where $k=2\pi/\lambda$ is wavevector in vacuum, n_{eff} is the effective index for the mode, δ indicates the prism angle.

Substituting equation (3.14)~(3.17) into equation (2.4), for an unsymmetric slab waveguide, the equations used to give the film refractive index and thickness[7] are given by

$$V\sqrt{1-b} = m\pi + \tan^{-1}\left(\sqrt{\frac{b}{1-b}}\right) + \tan^{-1}\left(\sqrt{\frac{b+a}{1-b}}\right) \tag{3.18}$$

for TE modes. Where $V = kd\sqrt{n_1^2 - n_0^2}$, d is the film thickness, m is the mode order (m=0,1,2,.....).

$$b = \frac{n_{eff}^2 - n_0^2}{n_1^2 - n_0^2}, \qquad a = \frac{n_0^2 - n_2^2}{n_1^2 - n_0^2} \tag{3.19}$$

The corresponding equations for TM modes are

$$V\left(\frac{n_1}{n_0}\sqrt{q_0}\right)\sqrt{1-b} = m\pi + tg^{-1}\left(\sqrt{\frac{b}{1-b}}\right) + \tan^{-1}\left(\sqrt{\frac{b+a(1-bd)}{1-b}}\right) \tag{3.20}$$

$$b = \left(\frac{n_{eff}^2 - n_0^2}{n_1^2 - n_0^2}\right)\left(\frac{n_1^2}{n_2^2 q_0}\right), \qquad a = \left(\frac{n_1}{n_2}\right)^4\left(\frac{n_0^2 - n_2^2}{n_1^2 - n_0^2}\right)$$

$$d = \left(1 - \frac{n_0^2}{n_1^2}\right)\left(1 - \frac{n_2^2}{n_1^2}\right), \qquad q_0 = \frac{n_{eff}^2}{n_1^2} + \frac{n_{eff}^2}{n_0^2} - 1$$

where q_0 is called the reduction factor, a is a measure of the asymmetry, b is known as the normalised guide index. n_0, n_1 and n_2 are the refractive indices of the substrate, the film and the cover (here air), respectively.

As a result, the effective index of each guided mode, the film thickness and its refractive index, can be calculated by only measuring synchronous angles or coupling angles (φ), provided that the refractive indices of the prism and the substrate, the angle of the prism and the wavelength of the incident beam, are known.

In the experiments, measurements of refractive indices were carried out from visible to infrared bands at different wavelengths using an argon ion laser (Ar^+ at 457.9 nm, 488.0 nm, 514.5 nm), a helium-neon laser (He-Ne at 632.8 nm), and two infra-red lasers (laser diode at 940.0 nm and 1300 nm), respectively, All films were fabricated on silica substrates (n=1.457018 at 632.8 nm) by spin or dip coating. Proper thicknesses of the films were achieved to support enough guided modes for measurements. A narrow air gap between the prism and the film was provided by dust particles or by the uneven surface.

When measuring at the wavelength of interest where there is no or very little absorption in the film at the wavelength of the incident laser beam, two prism coupling was used, so that the intensity of the out-coupled modes would not be too faint to be observed. One prism was used to couple light into the film and the other one to couple light out, where the two prisms with 60° angle are made from SF6 glass (n=1.79883 at 632.8 nm) in order to excite all the modes in the film. The experimental set-up is shown in Fig.3.6.

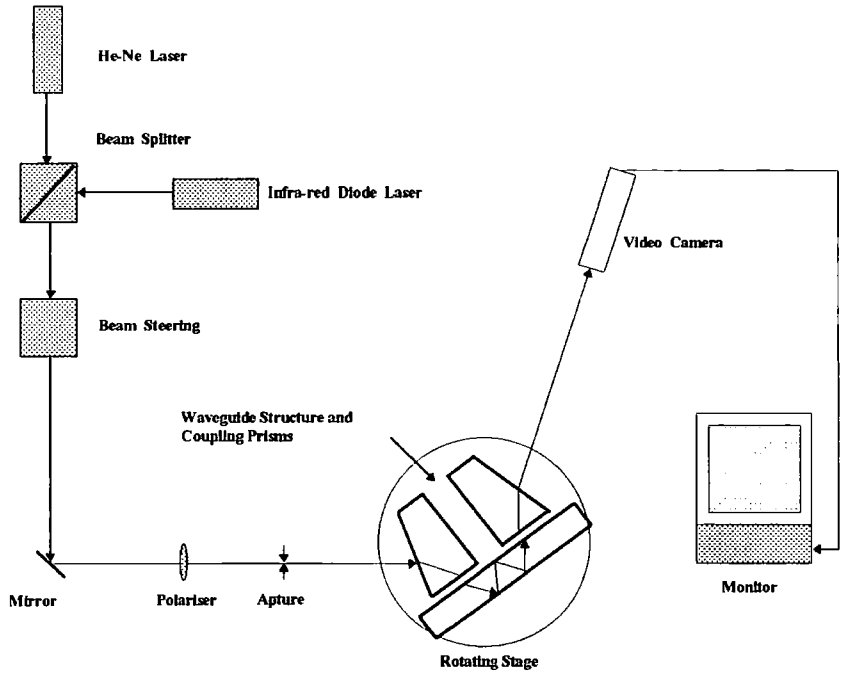

Fig.3.6 Experimental set-up of the prism coupling

The two right angled prisms were clamped directly on the waveguide film and substrate and mounted on a U shaped mount. The U shaped mount was fixed on a rotation stage that could be translated in two dimensions in the horizontal plane. Clamping the prisms was carried out with care, ensuring that no scratches were made on the film. A small area which is silvery in appearance, the coupling spot, occurred on the base of the prism while the prisms were clamped onto the waveguide film with its surface exposed, if a good contact between the film and the prism was reached. A good coupling spot indicated a good optical contact, the bigger the spot, the smoother and better the surface of the film, and a higher coupling efficiency could be achieved easily because of the good contact.

When only a visible laser beam was used in experiments, it was simpler to conduct measurements compared with using an invisible IR beam where another visible beam was needed to direct the IR beam. Firstly all components in the system were aligned. The

incident laser beam was set in a horizontal plane and allowed to strike on the surface of the right angle prism via a polarizer. By carefully adjustments the prism was positioned as close to the centre of the rotation stage as possible to prevent the beam from drifting off the centre during rotation, which would induce a variation in coupling efficiency. The beam was refracted through the prism on to a proper position on the coupling spot to achieve the highest coupling efficiency. Another prism was placed a short distance away from the first one by right angles facing each other, the separation between was as small as possible in order to obtain enough high intensity to couple out. Secondly the stage was rotated until the beam was reflected back to coincide with the incident beam, which meant the incident beam was normal to the sloping face of the prism. The angle reading from the stage was the reference angle or set to zero. All subsequent angle readings were referenced to this angle. The guided modes coupled out from the left prism were monitored directly on a screen or through a camera and a monitor. The TE or TM modes in the film were excited with appropriate light polarised both parallel (for TE) and perpendicular (for TM) to the plane of the film via the polariser.

The rotation stage was roughly rotated clockwise or anticlockwise untill a streak of waveguide light was seen along the film. On the screen the patterns of the light coupled out were displayed, containing several bright vertical lines, the brightest of which represented the mode that was guiding. Other modes (represented by less bright lines) are weakly observed because of surface roughness or multiple couplings. With a good film surface, these lines are thin or sharp. By fine tuning, the optimum position of the *m*th guided mode was decided from observing the maximum intensity of the *m*th line on the screen or detector, this angle was known as the *m*th mode angle.

In this way all the modes supported by the film were excited and the mode angles were found. Furthermore, all the external coupling angles (φ) corresponding to each guided mode were measured experimentally.

$$\varphi = \text{reference angle} - \text{mode angle} \qquad (3.21)$$

The values of φ might be positive or negative depending on the relative values of mode angles that were determined by the refractive indices of the prisms used and the film to be measured.

The $\pm\varphi$ and other parameters necessary were input into a computer, the thickness and the refractive index of the film were obtained at the same time by a calculating program incorporating equation (3.18) and (3.19). The results from the calculation provided a range of thicknesses and refractive indices in the form of a curve. One mode was represented by one curve, over which each waveguide mode could exist. If more than one mode was measured, the curves would intersect because these guided modes were supported by same film. The unique film refractive index and thickness was determined from the crossing points with minimum deviation of these curves. There should be only one crossing point, provided that good measurements were achieved.

In principle the index and the thickness could be decided solely by measuring two guided modes only. But measurement of three modes is preferable since an error could be estimated easily meanwhile. A typical set of the curves for a polymer waveguide film is shown in Fig.3.7.

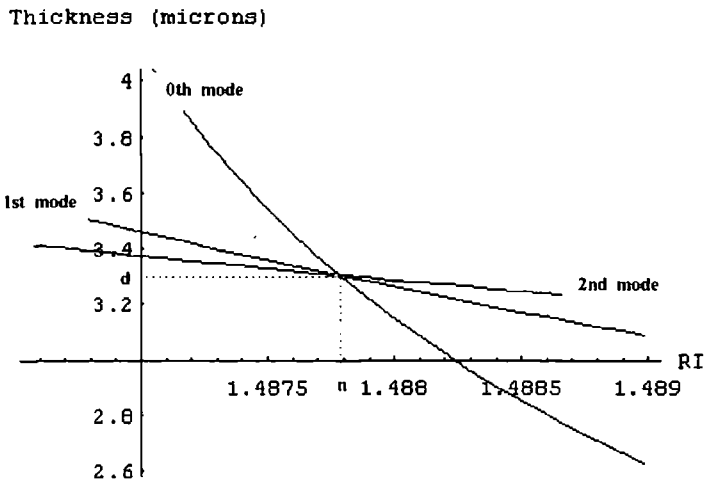

Fig.3.7 A set of typical curves of mode indices for a polymer film. The thickness(d) and the refractive indices of the film are given by the crossing point.

In some measurements wavelengths where there is a small amount of absorption are required, the *m*-line technique is used in these cases. When the *m*th mode was being guided in the film, the dark line inside a bright spot that was on the *m*th line became the dimmest on the screen. At that time the angle reading was the mode angle measured exactly as in the technique of two prism coupling, there the same mathematical analysis could be used. The strong absorption caused the *m* lines to broaden, leading to larger measurement errors. If the transmission was below 80%, all *m* lines would vanish[8].

If an infra-red diode laser was used in measurements where the beam of the laser was very dim or invisible by eye, a visible laser (e.g. He-Ne laser) was required to align the invisible beam with the whole system. In this case the reference angle was determined from the measurement of visible light. All the angles of guided modes were measured by monitoring light coupled out using an infra-red camera.

A typical profile of TE and TM modes from a polymer film is shown in Fig.3.8.

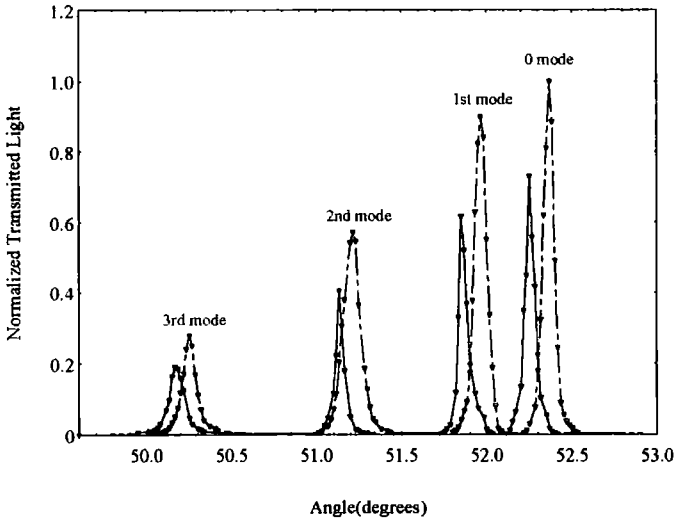

Fig.3.8 Normalised intensity of TE and TM modes vs coupling angles, supported by a poly(methyl methacrylate) (PMMA) film on a silica substrate. The broken line is TM modes and solid line is TE modes.

Indices of various doped or undoped polymer films at different wavelengths are listed in table 3.5 and 3.6, indices of PMMA and PC can be found in reference 9 and 10.

Table 3.5 Measurements of refractive indices for different dyes doped in PMMA

material	coating method	doping level w/w	wavelength nm	refractive index TE	TM
DEMI	spin	0.5%	940.0	1.48805±0.0002	1.48866±0.0002
	spin	1%	940.0	1.49044±0.0002	1.49065±0.0002
Ultra DEMI	spin	0.5%	940.0	1.48804±0.0003	1.48799±0.0003
	spin	1%	940.0	1.49098±0.0003	1.49139±0.0003
DCM	dip	5%	632.8	1.51456±0.0004	1.51462±0.0005
Morpip	dip	6.04%	632.8	1.49844±0.0002	1.49843±0.0002
Mor2	dip	6.27%	632.8	1.50110±0.0003	1.50142±0.0002

Table 3.6 Measurements of refractive indices for different pure polymers

material	wavelength nm	coating method	refractive index TE	TM
PMMA poly(methyl methacrylate)	457.9	dip	1.49889±0.0002	1.50121±0.0002
	488.0	dip	1.49780±0.0002	1.49849±0.0002
	514.5	dip	1.49618±0.0002	1.49686±0.0002
	632.8	spin	1.48894±0.0003	1.48951±0.0003
	780.0	dip	1.48539±0.0002	1.48562±0.0002
	940.0	spin	1.48348±0.0001	1.48415±0.0002
	1300.0	spin	1.48000±0.0002	1.48012±0.0001
PC (polycarbonate)	632.8	dip	1.58389±0.0002	1.57291±0.0003
	940.0	dip	1.56971±0.002	1.56953±0.002
P-4VP poly(4-vinylpyridine)	632.8	dip	1.57759±0.003	1.58224±0.004
	780.0	dip	1.57050±0.003	1.57466±0.003
zeonex	632.8	spin	1.52323±0.0002	1.52214±0.0003

A dispersion graph of pure poly(methyl methacrylate)(PMMA) is shown in Fig.3.9.

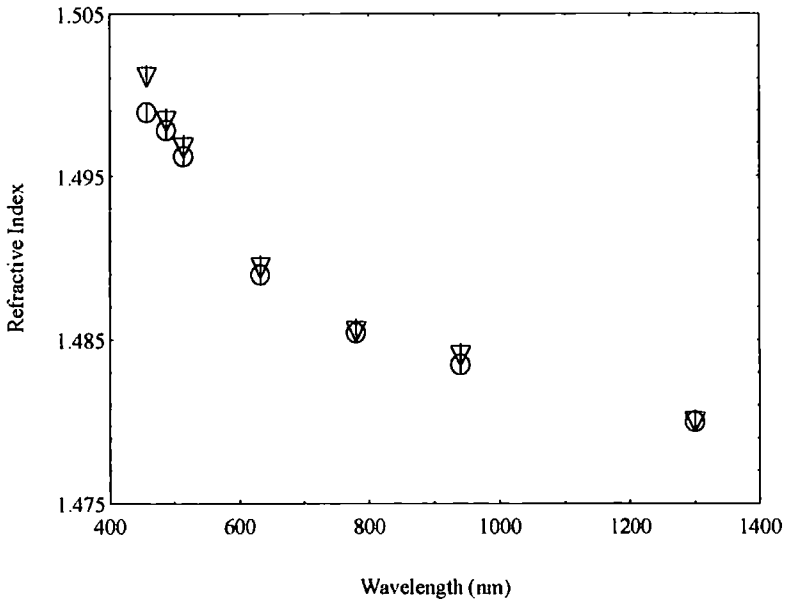

Fig.3.9 Refractive indices of pure PMMA at different wavelengths. Triangle indicates TM mode and circle indicates TE mode.

3.4 Efficiency measurement of two prism coupling from waveguide in polymer films

It is essential to estimate the coupling efficiency of the two prism coupling technique for application. With the limitation in my experiments where it is impossible to measure the coupling efficiency for single prism, the coupling efficiency of both prisms (coupled in and out) as an integral is measured in experiments, which gives us enough accuracy for future calculations. So the total coupling efficiency is given by

$$\eta_{total} = \eta_1 \eta_2 \tag{3.22}$$

Where η_1 is the coupling efficiency of the first prism(coupled in) and η_2 is that of the second(coupled out).

Comparatively speaking, the in-coupled efficiency is normally lower than the out-coupled one. In-coupled efficiency is crucial in experiments because it decides the power of incident beam into the film. For out-coupled efficiency, 100% efficiency[11] can easily be achieved. If the energy of guided light coupled in from the first prism could be coupled out totally from the second one, or η_2=100%, then the in-coupled efficiency measured is the minimum (E_{1min}). Otherwise η_1 reaches its maximum when the efficiency of the in-coupled and out-coupled efficiency are thought to be equal (η_1=η_2).

A 10 mW helium-neon laser emitting at 632.8 nm was used as the light source. A chopper and a lock-in amplifier, a pin-holed detector were employed to find and to detect the maximum output. Polymer films with excellent surface condition were fabricated from either spin or dip coating and were used in measurements. The whole system was aligned so that the laser beam entered the first prism at the coupling spot and was coupled into the film effectively. Then the guided light was coupled out through the second prism and was monitored by a pin-holed detector. Necessary adjustments were carried out for the prisms and the detector during measurements, trying to achieve the maximum in-coupling and to find the maximum out-coupling. A minimum separation (~3 mm) between the two prisms existed during measurements. The absorption caused from it was taken into account. Results were calculated by measuring the intensity of the incident beam before in-coupling and that of out-coupling and are listed in table 3.2.

Table 3.7 Measurements of coupling efficiency of two prism coupling

$\eta_{1\,min}$	$\eta_{1\,max}$
0.71	0.82
0.69	0.81
0.73	0.82
0.69	0.80
0.69	0.81
$\overline{\eta}_{1\,min} = 0.702$	$\overline{\eta}_{1\,max} = 0.812$

From the results listed in the table 3.2, a maximum in-coupling efficiency(~80%) was achieved. At a normal condition, about 70% in-coupling efficiency could be obtained for most ordinary waveguide films used in my experiments.

3.5 Measurement of linear losses in doped polymer film

The attenuation coefficient of a thin film optical waveguide is a significant parameter for the evaluation of its usefulness in applications. Generally the losses need to be as low as possible for a good waveguide material. The losses in materials different from one to another due to their structures, additional losses can be introduced from the fabrication process of device and the degree of contamination in the material. Organic systems consisting of a polymer matrix with a non-linear optical chromophore offer great promise for the creation of new guided-wave devices for use, which the nature of the chromophore determines the non-linear optical properties of system. Both the higher-order susceptibilities and the fundamental optical properties are important for a material for practical applications. In terms of device performance, measurement of linear losses during characterisation is helpful to evaluate the properties of a new material and its potential applications as well as selecting the best system.

Doped poly(methyl methacrylate) (PMMA) waveguide films with DEMI and Ultra DEMI chromophore (see section 4.5.2) as guests in different concentration were used in measurements in order to investigate their possible usage at near infrared wavelengths and to choose appropriate concentration for them in degradation to obtain a whole degradation curve. The set-up of the experiment is shown in Fig.3.10. Two prism-

coupling was used to couple light into and out of the film. An infrared diode laser at 940 nm was used as a light source. A 10 mW He-Ne laser was an alignment beam. A chopper and lock-in amplifier were used to detect minor variations in out-coupled light intensity caused by losses in the film. Slab waveguide films were fabricated by dip coating according to the methods described in section (3.2). Filters with 0.45 μm pore size were used, trying to get rid of any impurities in solution and films.

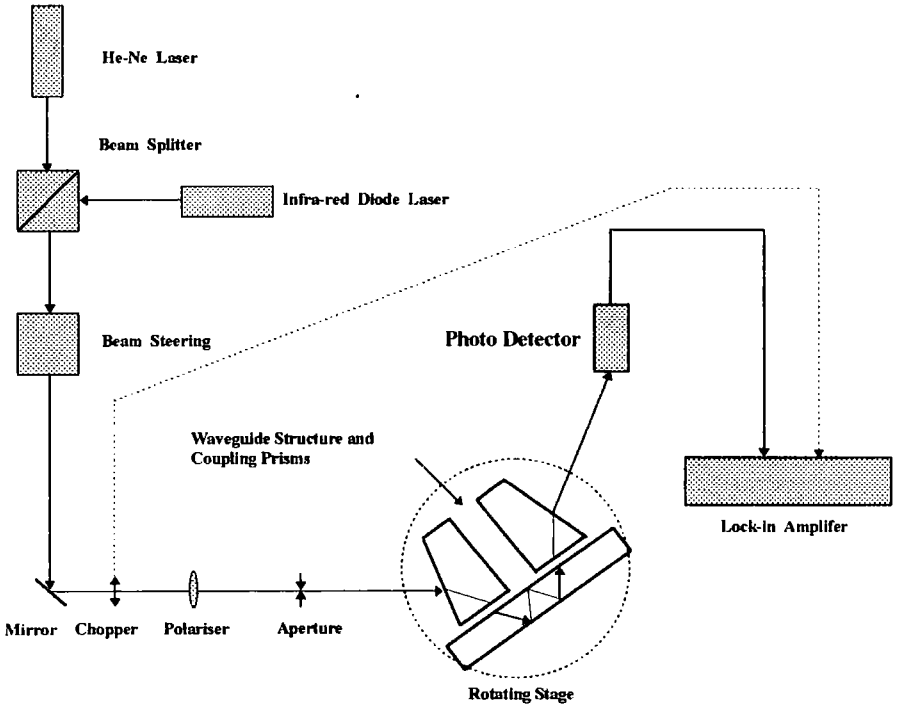

Fig.3.10 Experimental set-up for linear losses measurement

Firstly two laser beams were aligned with whole system. One prism coupled light into the film, a light streak was seen across the film. Then another prism was applied at different positions along the streak. Secondly, out-coupled light was detected by a pin-holed detector and measured by lock-in amplifier. Attenuation coefficients were obtained from the Beer's Law, $I = I_0 e^{-\alpha z}$, by calculating data measured.

During measurements, the in-coupled prism was fixed and kept stable to guarantee the coupling efficiency unchanged. Since the two prisms could not be put together, there was a minimum separation between them. The out-coupled intensity measured at minimum separation was set as I_0, the position of the out-coupled prism was set as $z_0=0$. All the following out-coupled light intensities measured at different points along the streak and the corresponding positions of the prism were I(z) and z referenced to I_0 and z_0. Therefore

the ratios of light power $I(z)/I_0$ were determined from such measurements. To avoid damaging the films the first measurements were carried out at greatest prism spacing, and the output prism was moved in steps toward the input prism shown in Fig.3.11. Each time the spacing between the two prisms was measured with a micrometer. Meanwhile, the pressure of the output coupling prism on the film and substrate should be low and constant in order to prevent changes in the efficiency of the input coupling prism.

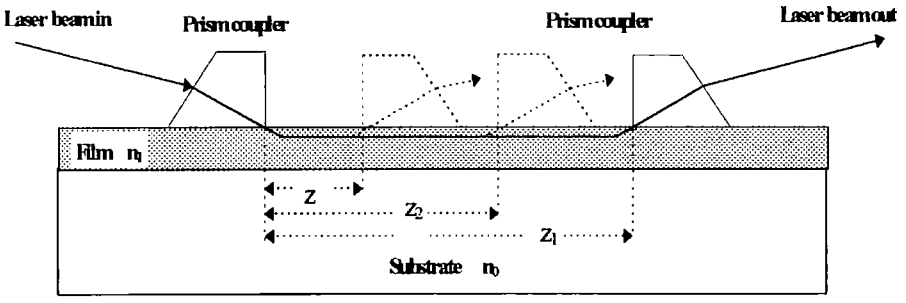

Fig.3.11 Closing view of in- and out-coupled prism in loss measurement

The attenuation coefficient calculated from measurements are listed in table 3.7. Here losses are total loss including the intrinsic and the extrinsic. From UV absorption spectra of these materials shown in Fig.4.6, there is no absorption at 940 nm. From the experiments which have been done the quantity of intrinsic loss from the absorption of doped material still cannot be determined. Further investigation needs to be done.

Loss measurements using two prism coupling is difficult work. It is very sensitive to any changes (contact pressure, surface condition of film, etc.) during operation. Large errors may be from the variation of coupling efficiency, the distance measurements and the uneven surface.

Table 3.8 Attenuation coefficient of doped PMMA film at different concentration

material	doping level w/w	wavelength nm	mode	loss dB/cm
DEMI	1%	940	TE_0	42±4
	0.5%	940	TE_0	16.6±3
Ultra DEMI	0.5%	940	TE_0	16.5±4

3.6 Measurement of extinction coefficients

In order to determine the concentration or doping level of samples and to estimate the absorption cross-section of molecules of different samples in any future experiments, the extinction coefficient (ε) of three materials, DEMI, Ultra DEMI and Dicyclohexyl DEMI, were measured in solution by a UV/VIS/NIR spectrometer (Perkin Elmer, Lambda 19) using unpolarised light. According to the definition of extinction coefficient

$$A = \varepsilon c l \tag{3.23}$$

where c is the concentration of dopant in the solution (mol/Litre or mg/Litre), d is the path length (cm), A is the absorbance of material (dimensionless).

The extinction coefficient was determined from equation (3.23) by measuring the absorbance of sample. In experiments samples were dissolved in dichloromethane (DCM) solvent to make solutions at a certain concentration. Different concentrations of the same sample were obtained by diluting the solution. A standard cell with unit thickness was used to contain the solution to be measured and was placed in the measuring channel of the spectrometer. Another identical cell filled with DCM solvent was put in the reference channel for background correction (absorption due to the solvent and the cell, reflection from the wall of the cell). The absorbance A was given by measuring the peak absorption of each spectrum at same wavelength as shown in table 3.7.

Table 3.9 Measurement of extinction coefficient

material	extinction coefficient in DCM		peak wavelength
	$L.Mol^{-1}.cm^{-1}$	$L.mg^{-1}.cm^{-1}$	nm
DEMI	62941±10%	0.22760±10%	720
Ultra DEMI	55926±13%	0.14870±13%	723
Dicyelohexyl DEMI	69743±16%	0.18138±16%	725

where peak wavelength were measured from their UV absorption spectra.

3.7 Measurements of birefringence in thin polymer films

Normally, optical polymers are amorphous isotropic materials. However the optical anisotropy of polymers can be induced by various methods (molecule orientation and internal stress of film) during film processing. Sometimes polymers with positive or negative birefringence can be transformed to change the sign of birefringence by internal compensation of positive and negative birefringence in copolymerization.[12] The birefringence of a thin film is defined as the difference of refractive index measured between the light polarised parallel (TE) and perpendicular (TM) to the plane of the film,

$$\Delta n = n_{TE} - n_{TM} \tag{3.24}$$

According to the Lorenz-Lorentz equation, equation (3.24) can be written as

$$\Delta n \approx \frac{2}{9}\pi \frac{(\bar{n}^2 + 2)^2}{\bar{n}}(P_{II} - P_{\perp}) \tag{3.25}$$

Birefringence occurs when the material consists of a nonrandom array of optically anisotropic molecules. Its sign can be positive or negative, which is determined if the refractive index in the plane of the film (n_{TE}) is greater, smaller or equal to that normal to the plane of the film (n_{TM}). Birefringence is proportional to the difference between the net polarizabilities per unit volume parallel (P_{II}) and perpendicular ($P_{\perp}$) to the plane of the film, $\bar{n}$ is the average refractive index of the material.

All waveguide films were fabricated on silica substrates in experiments and dried in a vacuum oven below 80°C for 24 hours. Two-prism coupling was used for the characterisation of the films. Measurement of the synchronous angles to $\frac{1}{60} \sim \frac{2}{60}°$ permits the determination of the refractive index to $< \pm 4\times10^{-4}$. N,N-Dimethylformamide (DMF) solvent was used to make the solution for spin coating of films, dichloromethane (DCM) was used in dip coating. The index, mode birefringence and film birefringence of PMMA, polycarbonate (PC) and poly(4-vinylpyridine) (P-4VP) are listed in the following tables, their molecular structure are shown in Fig.3.12.

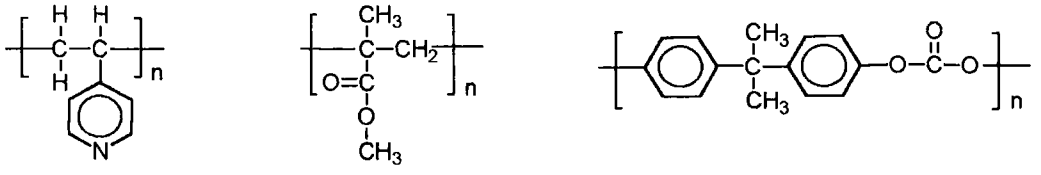

P-4VP PMMA PC

Fig.3.12 Molecular structures of P-4VP, PMMA and PC

Table 3.10 Mode refractive indices and birefringence of poly(methyl methacrylate) (PMMA)

wavelength nm	coating method	polarization	mode	mode index	polarisation	mode	mode index	mode birefringence	film birefringence
457.9	dip	TE	0	1.49743	TM	0	1.49893	-1.5×10^{-3}	-1.61×10^{-3}
			1	1.49023		1	1.49141	-1.18×10^{-3}	
			2	1.47823		2	1.47891	-6.8×10^{-4}	
488.0	dip	TE	0	1.49538	TM	0	1.49604	-6.6×10^{-4}	-7.1×10^{-4}
			1	1.48806		1	1.48856	-5.0×10^{-4}	
			2	1.47596		2	1.47630	-3.4×10^{-4}	
514.5	dip	TE	0	1.49313	TM	0	1.49363	-5.0×10^{-4}	-5.2×10^{-4}
			1	1.48418		1	1.48468	-5.0×10^{-4}	
			2	1.46989		2	1.47023	-3.0×10^{-4}	
632.8	spin	TE	0	1.48651	TM	0	1.48765	-1.14×10^{-3}	-1.15×10^{-3}
			1	1.47997		1	1.48112	-1.15×10^{-3}	
			2	1.46937		2	1.47040	-1.03×10^{-3}	
780.0	dip	TE	0	1.48360	TM	0	1.48376	-1.6×10^{-4}	-1.6×10^{-4}
			1	1.47680		1	1.47696	-1.6×10^{-4}	
			2	1.46565		2	1.46582	-1.7×10^{-4}	
940.0	spin	TE	0	1.48130	TM	0	1.48226	-9.6×10^{-4}	-1.01×10^{-3}
			1	1.47471		1	1.47552	-8.1×10^{-4}	
			2	1.46397		2	1.46462	-6.5×10^{-4}	
1300	spin	TE	0	1.47631	TM	0	1.47664	-3.3×10^{-4}	-3.6×10^{-4}
			1	1.46636		1	1.46668	-3.2×10^{-4}	
			2	1.45100		2	1.45117	-1.7×10^{-4}	

Table 3.11 Mode refractive indices and birefringence of polycarbonate (PC)

wavelength nm	coating method	polarisation	mode	mode index	polarisation	mode	mode index	mode birefringence	film birefringence
632.8	dip	TE	0	1.57751	TM	0	1.56691	1.06×10^{-2}	1.06×10^{-2}
			1	1.55754		1	1.54710	1.04×10^{-2}	
			2	1.52441		2	1.51462	9.79×10^{-3}	
940.0	dip	TE	0	1.56564	TM	0	1.56550	1.4×10^{-4}	1.4×10^{-4}
			1	1.55308		1	1.55308	0	
			2	1.53241		2	1.53227	1.4×10^{-4}	

Table 3.12 Mode refractive indices and birefringence of poly(4-vinylpyridine) (P-4VP)

wavelength nm	coating method	polarisation	mode	mode index	polarisation	mode	mode index	mode birefringence	film birefringence
632.8	dip	TE	0	1.57807	TM	0	1.58472	-6.65×10^{-3}	-6.86×10^{-3}
			1	1.56520		1	1.57133	-6.13×10^{-3}	
			2	1.54398		2	1.48880	-4.9×10^{-3}	
780.0	dip	TE	0	1.56850	TM	0	1.57416	-5.66×10^{-3}	-5.87×10^{-3}
			1	1.54904		1	1.55422	-5.18×10^{-3}	
			2	1.51034		2	1.52048	-4.14×10^{-3}	

From the data in these tables, it can be seen that

1. Within experimental errors, the PMMA film exhibits negative birefringence. Its birefringence is small. The data measured are independent to the wavelength and have no indication relevant to any coating methods. They do not show have solvents dependence either.

2. For the three polymers considered, the mode birefringences of PMMA and P-4VP have decreasing tendency with increasing of mode order.

Some observed variations in index measurements are probably caused by residual solvent and by the pressure applied by the prism coupler. The contribution of the residual solvent to the film index is expected to be isotropic therefore not affecting significantly the film birefringence.

From previous studies of polystyrene and other polymers.[13,14] It is believed that the birefringence of a thin polymer film is caused by preferential orientation of the polymeric backbone in the plane of the film during the solvent casting process. The sign of the birefringence is shown to depend on the orientation of the dominating polarizable group, relative to the chain backbone. That is controlled by the angle between the principal polarizability of the monomer and the chain direction. The birefringence is independent of molecular weight,[15] but film birefringence is solvent dependent for polystyrene.[16] Meanwhile, the orientation or alignment of the polymer molecules due to stresses during processing will induce film birefringence to a certain degree when polymer chains are relatively mobile.

The optical properties of PMMA, P-4VP and PC are dominated by the anisotropic polarizabilities that are determined mainly by their optically anisotropic groups (methyl ester, pyridine and phenyl group). Since the anisotropic groups of PMMA and P-4VP, methyl ester and pyridine group, are perpendicular to their backbone as a pendent group, a large portion of these strong polarizable groups of molecules will be aligned in the direction normal to the plane of the film, when the polymeric chain backbones are preferentially aligned in the plane of the film during the solvent coating and drying process. Therefore, they give negative birefringence. On the contrary, polycarbonate (PC) exhibits positive birefringence because its dominating polarizable group (phenyl group) is contained in the main chain. However the magnitude of birefringence reflects both the optical anisotropy of the group and the steric constraints to its free rotation. Thus the optical anisotropy is the direct result of the drying process produced in plane orientation of the molecular chains in the solvent plasticized melt.

As to birefringence induced by stresses, it depends on temperature, solvent and substrate,[14] sometimes it is affected by method of film making. Birefringence will decrease or may disappear by weakening the alignment of anisotropic groups of molecules or releasing the stresses in the films. Particularly for the polymer film whose birefringence is purely due to stresses, the film becomes isotropic through releasing the stresses by heating and subsequent cooling process, where the film is baked at or above the softening point for a certain time and followed by decreasing temperature gradually.

3.8 References

1. Data from the catalogue of Aldrich and Polysciences.
2. John A. Riddick, William B. Bunger, and Theodore K. Sakano, Organic solvents, Physical properties and methods of purification, 4th Edition, Wiley-Interscience, 1986
3. Chung-ching Yang, Jack Y. Josefowicz and Lupu Alexandru, *Deposition of ultra thin films by a withdrawal method*, Thin Sold Film, **74**, 117-127 (1980)
4. R. Swanepoel, *Determination of the thickness and optical constants of amorphous silicon*, J. Phy. E-sci. Inst. **16** (12), 1214-1222 (1983)
5. D. B. Kushev and N. N. Zheieva, et al., *A new method for the determination of the thickness, the optical* constants and the relaxation time of weakly absorbing semiconducting thin film, Infrared Phys. **26** (6), 385-393 (1986)
6. Fowles, Grant R, Introduction to modern optics, 2nd Ed, 1975, Chapter 6.
7. H. Kogelnik and V. Ramaswamy, *Scaling rules for thin-film optical waveguides*, Appl. Opt. **13** (8), 1857-1862 (1974)
8. Nitanai, S. Miganaga, *Measurements of dispersion properties of refractive indices and absorption* coefficients in organic-dye-doped thin films by a prism-coupling method, Opt. Eng. **35** (3), 900-903 (1996)
9. J. D. Dwalen, R. Santo, M. Tacke and J. Fischer, *Proerties of polymeric thin film by integrated optical techniques*, IBM J. Res. Develop., Polymeric properties by optical techniques, March, 168-175 (1977)
10. R. J. Gulotty, C. A. Langhoff and S. E. Bales, *Nonlinear optical activity of bisphenol A polycarbonate and related copolymer*, **SPIE 1337**, Nonlinear optical properties of organic materials III, 258-270 (1990)
11. K. Tien, *Light waves in thin films and integrated optics*, Appl. Opt. **10** (11), 2395-2413 (1971)
12. Hans-Joachim Lorkowski, Karl Pfeiffer, et al., *Optical polymers with special birefringent properties, Polymer for Advantage Technologies*, 7, 501-506 (1996)
13. W. M. Prest, Jr. and D. J. Luca, *The origin of the optical anisotropy of solvent cast polymeric films*, J. Appl. Phys. **50**(10), 6067-6071(1979)

14. T. P. Janaky and C. K. Narayanaswamy, *Brillouin scattering in polystyrene thin-film waveguides*, J. Appl. Phys. **58** (7), 2441-2443 (1985)

15. W. M. Prest, Jr. and D. J. Luca, *Molecular weight and plasticizer dependence of the in-plane orientation of solvent cast films*, Bull. Am. Phys. Soc. **22**, 313 (1977)

16. T. P. Sosnowski and H. P. Weber, *Thin birefringent polymer films for integrated optics*, Appl. Phys. Lett., **21** (7), 310-311 (1972)

CHAPTER 4 WAVEGUIDE PHOTODEGRATION OF ORGANIC DYES

Preface

In this chapter the general principles and mechanisms of photodegradation of organic chromophores are presented, attention is focused on measurements of optical stability of the chromophore. Through monitoring the transmitted light out from samples, the optical stability of the chromophore is investigated when the chromophore is exposed to optical radiation, and where photodegradation experiments are carried out under different environments using doped waveguide polymeric films and the two-prism coupling technique. The quantum yields of photodegradation of the chromophore at different wavelengths are obtained from the fitting of the transmission curves. Aggregation of the dye molecules in the waveguide film is described. The photodegradation of non-linear optical (NLO) organic materials investigated is achieved. The results obtained help to improve the properties of the NLO organic materials and lead to a better understanding of photodegradation mechanisms.

4.1 Introduction

Organic chromophore containing polymers have drawn considerable attention during the last few years due to some of their important characteristics, e.g. large nonresonant

nonlinear susceptibility, fast response time and low dielectric constant, and they offer great potentials and have emerged as promising materials in various applications. For example, electroluminescent (EL) devices in information displays and light emitting diodes,[1] optical waveguide components and devices in integrated optics,[2-6] recording materials in holography,[7, 8] fibres in communication systems, [9, 10] solid-state dye lasers,[10-13] high speed electro-optic modulation[14, 15] and electro-optic switching,[16, 17] in nonlinear optical (NLO) applications. For successful implementation in device application, they must satisfy additional requirements and criteria, such as good processability, good optical transparency, acceptable mechanical, thermal and photostabilities. Among all of them, photostability or stability to prolonged light exposure is one of the most important. This means, no matter what these organic chromophore polymers are used as (passive or active systems), the polymer systems must be stable enough in their performance over time when used in devices under operational conditions or environments, or transmit light with little or no degradation over a large range of incident intensities.

4.2 Formation of an organic chromophore polymer system

An organic chromophore polymer system is composed of dye molecules of interest in a polymer matrix. An organic dye with suitable properties can be used in several applications, sometimes it may be used in only one special area. Normally there is more than one choice for a particular application, such as a π-conjugated donor and acceptor system (D-π-A) with different structures in nonlinear optical application. The structure depends on the particular system and device in application. Polymers of interest are typically amorphous glasses because of their high transparency and low scattering of light, at the same time they possess enough mechanical, thermal and photostability and have good processability.

Generally organic dye molecules can be incorporated in a polymer matrix in three ways,[18] guest-host (GH) system, side-chain (SC) polymer and main-chain (MC) polymer as shown in Fig.4.1. Guest-host systems are formed by mixing small unattached chromophores dissolved in high molecular weight polymeric matrix as guest molecules. Side-chain polymers are acquired by covalently linking one end of the chromophore to a polymer backbone, with most of the mass of the chromophore pendant to the backbone as a side-

chain. Main-chain polymers are obtained by incorporating the chromophores into a polymer backbone at both ends of the chromophore, and the majority of the chromophore forms part of the polymer backbone. The chromophores can be linked in a head-to-head, a head-to-tail or in random head-to-tail and head-to-head configurations.

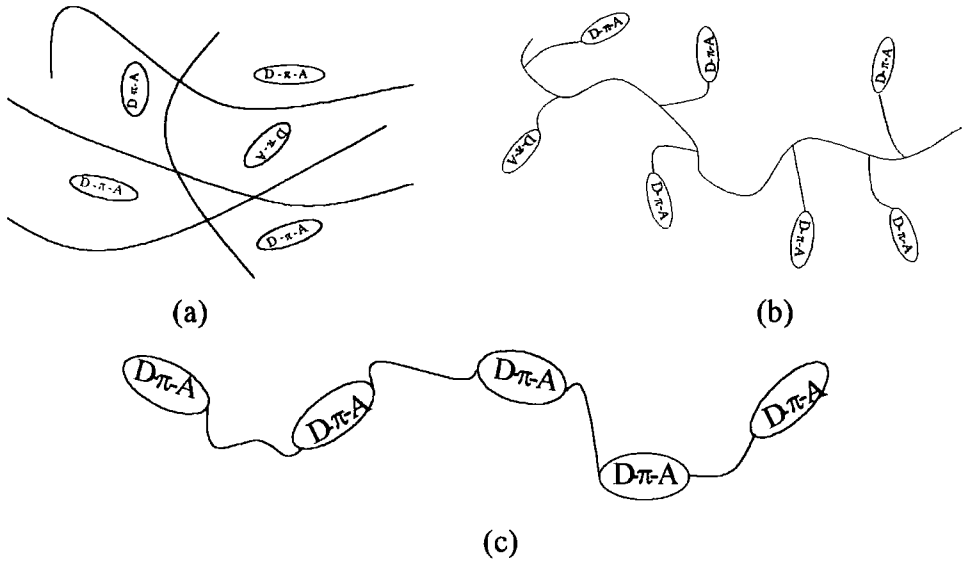

Fig.4.1 Organic polymer systems. (a) Guest-host, (b) Side-chain, (c) Main-chain.

Of these, GH systems are the simplest and easiest to prepare. They are often used in research or other applications where low dye concentration is required. The dye concentration in a polymer matrix is determined mainly by the solubility of the dye in the solvent used. The dye concentration can reach 30% weight to weight concentration in GH systems, however, very often aggregation of dye molecules can occur at ~10% w/w concentration and leads to phase separation in GH systems. Higher doping levels tend to induce phase separation causing scattering of light. Compared with GH systems, SC and MC polymers need to attach dye to the polymer by additional chemical synthesis. Such methods can achieve higher dye concentration due to the increase in the number density of dye molecules, and higher stability than in GH systems, such as thermal stability after poling.

4.3 Light irradiation and photoreaction

A light beam can be thought of as a continuous flow of photons carrying a certain amount of optical energy. The energy of a photon at a given wavelength depends on the frequency of radiation and is determined by

$$E = h\nu = hc/\lambda \qquad (4.1)$$

where h is Plank's constant (6.62×10^{-34} J sec), ν is the frequency of light (s^{-1}), λ is the wavelength of monochromatic light (nm), c is the speed of light (3×10^{8} m/s) in vacuum.

Several relevant definitions are listed below:

The flux of photons (F) is the number of photons (N) emitted per unit time (t)

$$F=N/t \quad \text{(number/sec)} \tag{4.2}$$

The irradiance energy or power of a light beam is the amount of energy (E) emitted per unit time (t):

$$P=E/t=Nh\nu/t=Fh\nu \quad \text{(J/sec or W)} \tag{4.3}$$

The radiation intensity (I) is defined as the flow of radiation incident on a unit area (S) of a given surface

$$I=P/S \quad \text{(J/sec cm}^2\text{ or W/cm}^2\text{)} \tag{4.4}$$

Since the energy of a photon is determined by its frequency, the lower the frequency (the longer the wavelength), the lower the energy of radiation or a photon. For a constant energy of a light beam, there are fewer photons at higher radiation frequency (short wavelength).

Interaction between light and matter is achieved by the photons' interactions with atoms or molecules of the material and exchange of energy between them. The energy available to the reacting atom and/or molecule is the energy possessed by the photon. The energy of the individual photon ($h\nu$) is fixed. The interactions will lead to photoreactions of matter (photophysical or photochemical) through absorption of radiation by atoms or molecules of the matter. Normally, light quanta may only interact with atoms or molecules one at a time (one-photon absorption). Two-photon absorption or multi-photon absorption may occur, once the intensity of incident light is very high.

A photophysical reaction occurs without change in the chemical structure of the organic system, and this process of photoreaction includes formation of excited state molecules and energy transfer processes. The excitation energy of a molecule in its excited state may be dissipated by the following photophysical processes: 1) radiative processes; luminescence (fluorescence and phosphorescence), 2) radiationless processes; which occur when a molecule is back from the singlet excited states (S) or the triplet excited states (T)

to the ground state (e.g. $S_1 \rightarrow S_0$ + heat, $S_1 \rightarrow T_1$ + heat, $T_1 \rightarrow S_0$ + heat); 3) bimolecular deactivation processes (energy transfer processes), 4) dissociation processes, which occur when a molecule is excited from the singlet ground state (S_0) to the repulsive excited state by absorption of a photon.

A photochemical reaction in an organic system means that the process results in change of chemical structure of the system. One typical photochemical reaction includes the following process: 1) formation of an electronically excited state from the absorption of radiation, 2) the primary photochemical process involving the excited states of molecules in the system, 3) the secondary reactions of the radicals, radical ions, ions and electrons induced by the primary process.

4.4 Absorption and emission of light radiation

Absorption of a homogeneous organic system (e.g. a doped polymer film) is described quantitatively by the Beer-Lambert law. The law gives the fraction of monochromatic light transmitted through the system,

$$\frac{I}{I_0} = 10^{-\varepsilon Ml} = e^{-\sigma nl} \quad \text{or}$$

$$A = \lg\left(\frac{I}{I_0}\right) = -\varepsilon Ml \quad \text{and} \quad A = \ln\left(\frac{I}{I_0}\right) = -\sigma nl \tag{4.5}$$

where A is absorbency, I_0 is the incident intensity, I is the transmitted intensity through the sample film, M is the molar concentration of dopant (mol/litre), l is the sample thickness (cm), n is the number density of dopant molecules (cm^{-3}), σ is the absorption cross section of dopant molecules (cm^{-2}) and represents the probability that a photon will be absorbed by a molecule. The extinction coefficient (ε) is defined as

$$\varepsilon = \frac{N_A \sigma}{2.303M} \quad \text{(litre/mol cm)} \tag{4.6}$$

where N_A is Avogadro's number. This equation shows that the absorption cross section of the dopant molecules (σ) is directly proportional to the extinction coefficient (ε).

Atoms or molecules of samples can exist only in certain defined, discrete (separate) energy states (energy levels) because of quantization of their energy. Therefore, the

absorption of radiation by a molecule occurs if the difference between two arbitrary energy levels (E_1 and E_2) of the absorbing bond (or group) in the molecules is exactly equal to the energy of the photon of incident radiation,

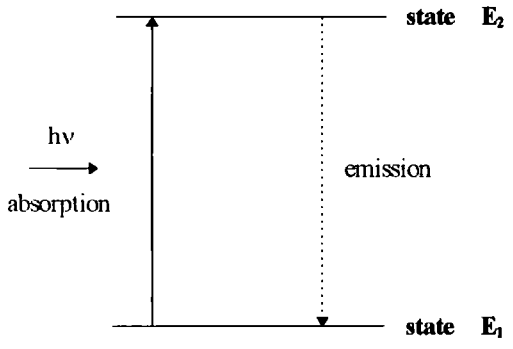

$$\Delta E = h\nu = E_2 - E_1 \qquad (4.7)$$

Fig.4.2. Excitation by absorption of radiation

where ν is the frequency (s^{-1}) at which absorption occurs, E_2 and E_1 are the energy levels of a single molecule of absorbing samples in the upper energy level (final state) and lower level (initial state), respectively.

A molecule can be excited from a lower energy level to an upper one by absorbing a quantum of radiation with frequency ν (a transition). On the contrary, the excited molecule will experience the converse process of absorption, emission, and jumps from the higher energy state to the lower state by giving out a light with same frequency. The probability of a transition for a molecule is proportional to the interaction between the electric field of radiation ($\vec{E}$) and transition dipole moment ($\vec{\mu}$) given by their scalar product, $\vec{\mu} \bullet \vec{E}$. That is, the interaction of atoms and molecules with radiation depends not only on the intensity of incident light but also the electric component of the light (the E field or its polarised direction).[19, 20]

The total energy of a particular energy state of a molecule is the sum of the electronic excitation energy (E_e), the vibrational energy (E_v) and the rotational energy (E_r),

$$E = E_e + E_v + E_r \text{ and } \quad E_e > E_v >> E_r \qquad (4.8)$$

Usually the separations between electronic energy levels are much larger than those between vibrational energy levels and those between rotational levels. As for an atom, it can have only electronic energy and have no rotational or vibrational energy. Any

variations in energy of the atom result from a change in the electronic state as the electron moves between the various available orbitals. When a molecule becomes excited, transitions will be induced between its different electronic levels by absorbing light in the visible or ultraviolet region. However, the near infrared (< 20 μm) and far infrared (> 20 μm) radiation will lead to transitions between different vibrational levels or rotational levels, respectively.

4.5 Waveguide degradation

Organic chromophore containing polymers are exposed to optical radiation when they are used as a device material in practical applications. Photodegradation occurs during the exposure of the polymer system to light, i.e., there are changes in the chemical structure of the chromophore and in the physical properties of the system resulting from photochemical reactions involving bond scission in the chromophore molecule, in the end the properties of the system deteriorate. If the system is exposed to light with short wavelength (e.g. UV radiation), degradation of the polymer matrix may take place and accompany the degradation of the chromophore in the system. The changes of physical properties caused by slow accumulation of the chemical changes in the system include: decrease in molecular weight, tensile strength, impact strength, elongation at break; loss of gloss and transparency.

4.5.1 The laws of photochemistry and quantum yields

Laws have been developed to describe the chemical changes in a system induced by the interaction of molecules with photons having enough energy, and to quantify photochemical reactions in the system. Following the laws, 'Only light which is absorbed by a molecule can be effective in producing photochemical change in the molecule' (the first law of photochemistry)[21]; and 'the absorption of light by a molecule is a one-quantum process, so that the sum of the primary process quantum yields φ must be unity, that is, $\sum \varphi_i = 1$ '(the second law of photochemistry).[21] Where φ_i is the quantum yield of the *i*th primary process, which may include dissociation, isomerization, fluorescence, phosphorescence, radiationless transitions, and all other reaction paths which lead to the destruction and deactivation of the excited molecule.

Therefore, in order to be effective in inducing a chemical change in an organic system, light must be absorbed by the material in the system. The existence of a dye molecule in the system or chromophoric groups in the molecule is a prerequisite for the initiation of photochemical reactions. Each molecule absorbing a photon has a certain probability of transition from its ground state (S_0) to either the lowest excited singlet state (S_1) or lowest triplet state (T_1), the lowest excited singlet and triplet states are the starting point of most organic photochemical processes.[22]

A quantum yield (φ) determined for a given photochemical product resulting from the photodecomposition of molecules, ($A + h\nu \rightarrow B$), is defined as

$$\varphi = \frac{\text{number of molecules (B) formed in a particular process}}{\text{number of photons absorbed by molecules (A) or system}} \tag{4.9}$$

For certain systems φ is equal to unity. There may be a number of secondary processes available for each primary process. The quantum yield defined above is wavelength-dependent and the measured values can range from less than 10^{-6} to more than 10^{6}, depending on the different reaction system. When $\varphi=1$, every absorbed quantum produces one photochemical reaction; when $\varphi > 1$, a chain reaction takes place; when $\varphi < 1$, other reactions compete with the main photochemical reaction. It should be noticed that quantum yields are not a fundamental material property, they may depend on factors such as film thickness, moisture content, and processing conditions.

4.5.2 Material Systems

The guest-host system is chosen for our nonlinear organic material system in film fabrication. The host polymer is PMMA whose molecular structure is shown in Fig.4.3. Poly (methyl methacrylate) (PMMA) is a commercially available polymer, which will be used in experiments, it is a hard, rigid, polar, amorphous and optically homogenous, a transparent polymer with reasonable scratch resistance and low birefringence, its surface hardness is amongst the highest for thermoplastics. The outstanding property of PMMA is its clarity, its transmission is greater than 93% for visible light (400 ~ 700 nm) with absorption in the UV region starting from 260 nm, light scattering is low. It can be

obtained with different molecular weights (from 10,000 to 1,000,000), it has a glass transition temperature in the region 100°C to 120°C, it is soluble in many organic solvents. Its structure is shown in Fig.4.3. At the same time it is very resistant to UV radiation and to weathering and is easy to process. Bulk PMMA dose not show appreciable thermal decomposition below 180°C. These characteristics lead to its use as a very good waveguide material. Comparatively speaking, PMMA is very stable, its disadvantages is high moisture absorption.[21, 22]

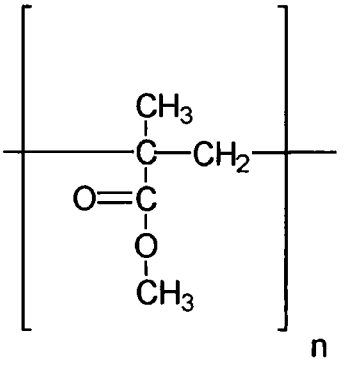

Fig.4.3. Molecular structure of poly (methyl methacrylate) (PMMA)

Two groups of nonlinear optical (NLO) organic materials are doped in the host polymer as guests. The first group are tertiary amide derivatives of tetracyano-*p*-quinodimethane (TCNQ).[25, 26], DEMI-3CNQ (4-[1-Cyano-3-(diethylamino)-2-propenylidene]-2,5-cyclohexadiene-1-ylidenepropanedinitrile) (DEMI), *N*-Acetaldehyde Diethyl Acetal-Piperidyl-DEMI-3CNQ (Ultra-DEMI), Dicyclohexyl-DEMI-3CNQ (4-[1-Cyano-3-(dicyclohexylamino)-2-propenylidene]-2,5-cyclohexadiene-1-ylidenepropanedinitrile) (Dicyclohexyl-DEMI). Their molecular structures are shown in Fig.4.4. These NLO chromophores have been shown to be planar. The tricyanquinodomethane (TCQ) acceptor is separated from an electron deficient amino moiety (donor) by a fairly long delocalised π- electron system. DEMI has a zwitterionic structure with complete conjugation between a dicyano carbanion and a diethyl iminium cation through a benzene ring and two double bonds. This extensively extended zwitterionic structure leads to a large dipole moment and enhances the nonlinearity of the molecules, and as a result, leads to a higher β value.[26-28] The remaining two compounds have similar structures to DEMI. In the case of Ultra-DEMI, a 2,2'-diethoxyethyl group is used to replace one of the ethyls of DEMI, and the iminium nitrogen is embedded in a six-membered ring. Whereas in

Dicyclohexyl-DEMI two relatively bulky cyclohexyl groups are used to replace the two ethyl groups of DEMI. DEMI is crystalline solid with green-gold lustrous needles; both Ultra-DEMI and dicyclohexyl-DEMI are blue powders. The solutions obtained from these materials are blue in colour.

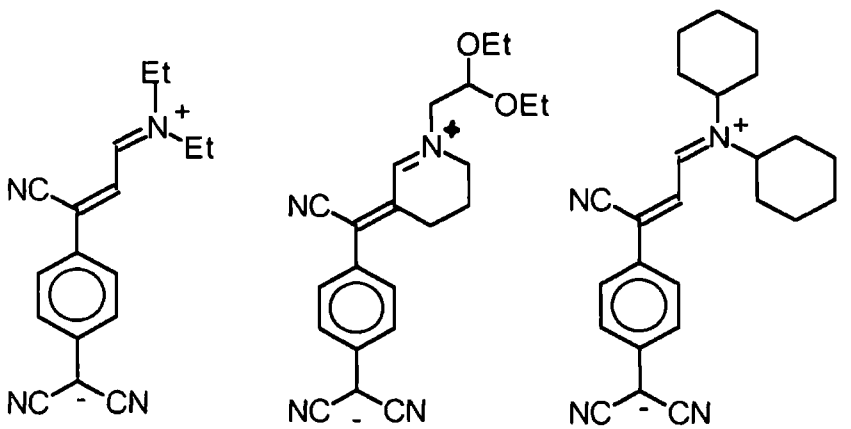

DEMI Ultra-DEMI Dicyclohexyl-DEMI

Fig. 4.4 Molecular structures of DEMI-series materials

The UV absorption spectra of these three molecules measured by a Lambda 19 UV/VIS/NIR spectrometer are shown in Fig.4.5. Because of the similarity of their structures, the electronic spectra for the molecules all consist of intense multiple absorption bands in the mid-visible region between 500 and 850 nm with two major absorption peaks (peak A and B), their peak wavelengths are listed in table 4.1. This unique property suggests they may be suitable for them to be used in frequency doubling applications from the near IR (900 - 940 nm) into the visible (450 - 470 nm), where anomalous dispersion phase matching can be achieved.[29-32]

Table 4.1 Peak wavelengths of DEMI-series materials

Material	Peak Wavelength (nm)	
	Peak A	Peak B
DEMI	720	655
Ultra-DEMI	715	658
Dicyclohexyl-DEMI	724	660

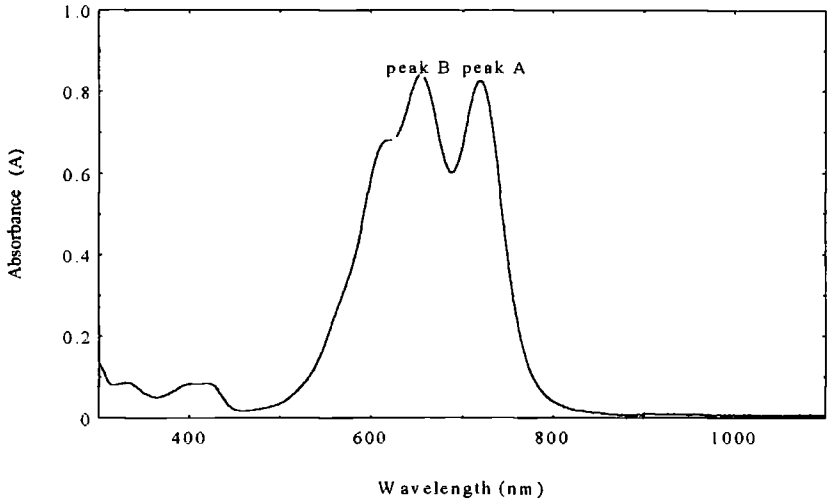

(a)

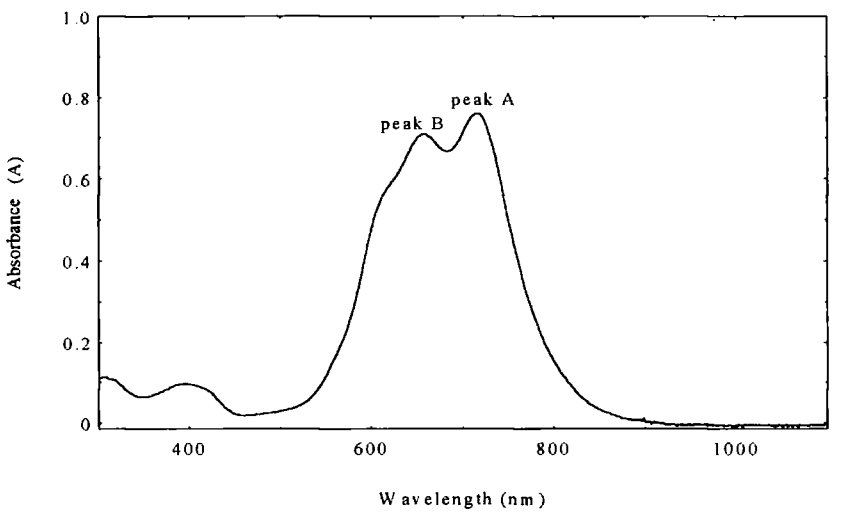

(b)

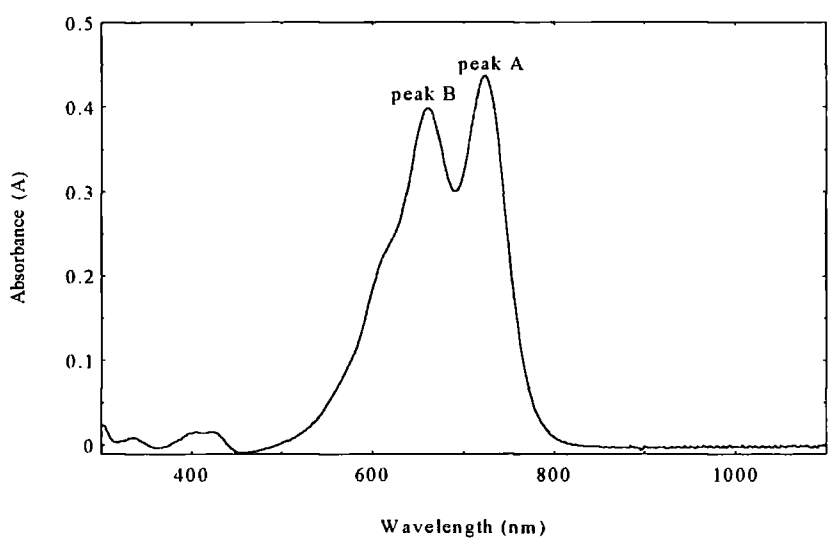

(c)

Fig.4.5. UV absorption spectra of DEMI-series materials doped (1% w/w) in PMMA baked at 60℃ in vacuum for 48 hours. a) DEMI, b) Ultra EMI, c) Dicyclohexyl-DEMI

The second group of NLO organic materials are yellow materials which have high polarity, 7,7-(2,6 dimethylmorpholino)-8,8-dicyanoquinodimethane (mixtures of *cis* and *trans* conformations) (Mor2), 7-(2,6, dimethylmorpholino)-7-(4-methyl piperidino)-8,8, -dicyanoquinodimethane (mixtures of *cis* and *trans* comformations) (Morpip), 4-dicyanomethylene-2-methyl-6-p-dimethylaminostyryl-4H-pyran (DCM). Mor2 and Morpip were synthesised by Yasuyuki Kagawa.[33] Their molecular structures are shown in Fig.4.6. These three NLO chromophores have been shown to be planar. Their high polarity is achieved by their structure consisting of a conjugated electron donating moiety and an electron accepting moiety. The electron accepting moiety of all these three molecules is dicyanomethylene, the electron donating moieties are different dialkyl anion groups directly bonded to the conjugated centre backbones. The amino groups consist of one morpholine and one piperidine group for Morpip, two morpholine groups are used for Mor2, the structure of DCM is different from Mor2 and Morpip in both the amino terminal and the central backbone. Both Mor2 and Morpip are yellow crystals with decomposition temperature in air of 260°C. The solutions obtained from these two materials are yellow in colour. DCM is red powder and the solution obtained from it is red in colour.

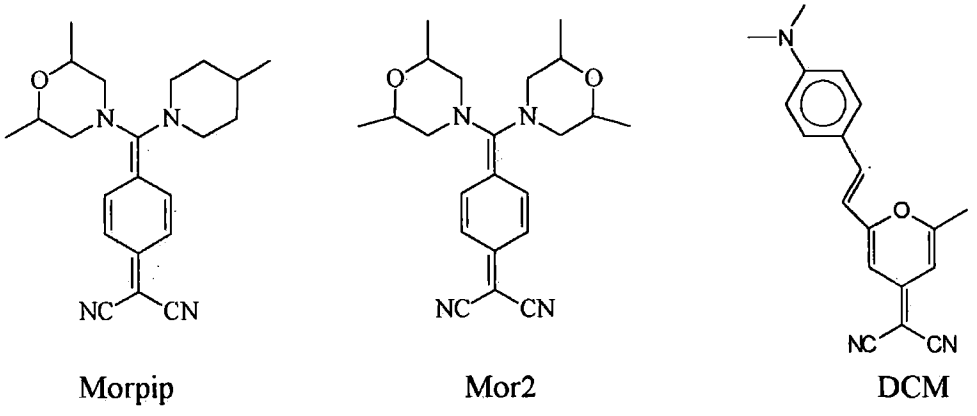

Fig.4.6. Molecular structures of the yellow materials

Table 4.2 Peak wavelength of yellow materials

Material	Peak Wavelength (nm)
Mor2	434
Morpip	432
DCM	460

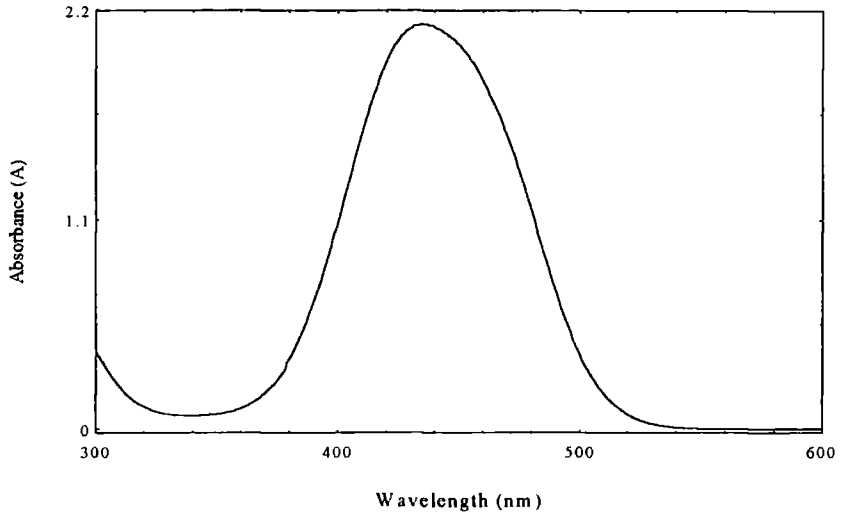

(a)

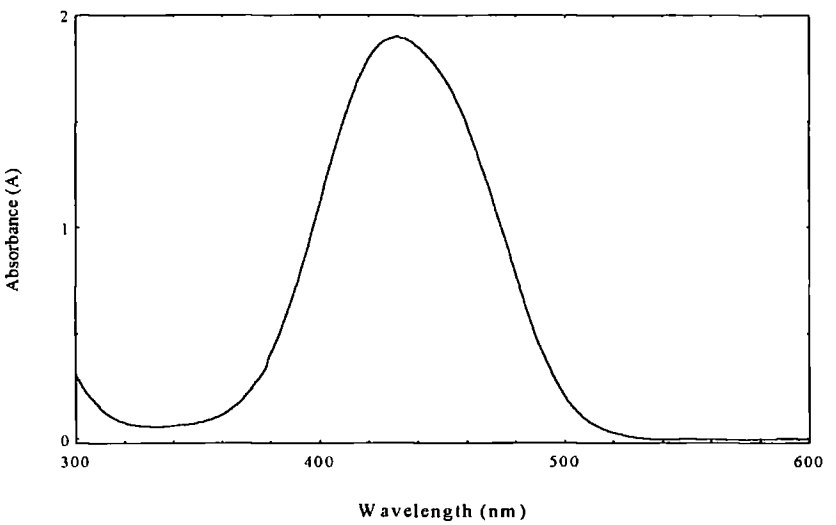

(b)

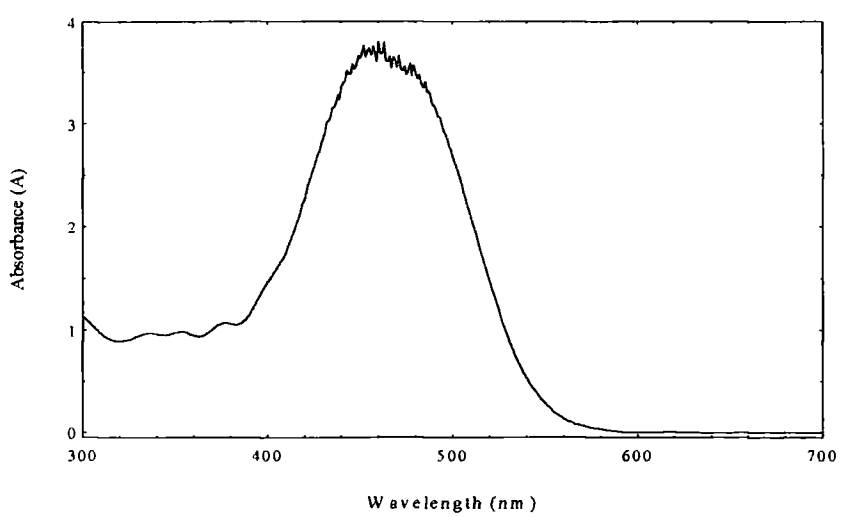

(c)

Fig.4.7. UV absorption spectra of yellow materials doped in PMMA baked at 60℃ in vacuum for 48 hours. a) Mor2 (6.27% w/w), b) Morpip (6.04% w/w), c) DCM (5% w/w)

The UV absorption spectra of these three molecules measured by a Lambda 19 UV/VIS/NIR spectrometer are shown in Fig.4.7. The electronic spectra for the molecules consist of intense an absorption band in the region between 360 and 500 nm with one major absorption peak, their peak wavelength measurements are listed in table 4.2. Their absorption bands have shifted toward the UV region and have no absorption in visible and near infrared bands. This advantage makes them suitable for possible use in telecommunication applications.

4.5.3 Experimental set-up

A chromophore containing system will change or lose its physical and chemical properties because of chemical reaction in the system induced by photodegradation. One typical change of the chromophore properties is its absorbance which leads to significant changes of optical intensity passing through the system during continuous operation by laser beam. As the chromophore or dopant is being degraded, the transmitted light increases gradually due to the decrease of its absorbance. Meanwhile, a reduction in the refractive index of the sample takes place as a result of photodegradation of the chromophore. Thus measurements of transmitted light from samples can provide a useful preliminary picture of the general ways in which a chromophore molecule is breaking down caused by photodegradation, and supply experimental data to evaluate the photostability of the chromophore of an organic system, and to improve its structure, and also, to elucidate the process of photodegradation.

The experimental set-up of photodegradation studies is showing in Fig.4.8. Two visible lasers, an argon ion laser (A_r^+ at 457.9 nm, 488.0 nm and 514.5 nm), a helium-neon laser (He-Ne at 632.8 nm), and two infrared lasers (laser diodes at 780.0 nm and 940.0 nm) were used in experiments. Slab waveguide films were fabricated on silica substrates by spin coating or dip coating as described in chapter 3. The correct thicknesses of the films were achieved to support 3 guided modes for refractive index measurements and to support only 1 mode for degradation studies. The two-prism coupling technique was used to couple the incident laser beam into and out from the waveguide films. Maximum coupling-in intensity and coupling efficiency were achieved by carefully rotating the stage to choose coupling angles. TE and TM modes in the film were excited with polarised light

parallel (for TE) and perpendicular (for TM) to the plane of the film via a polariser. A chopper and lock-in amplifier were utilised to detect minor variations in transmitted light coupled out from the film. The transmitted light in which variations were caused by photodegradation of the doped organic chromophore, was monitored directly by a detector and recorded in a computer.

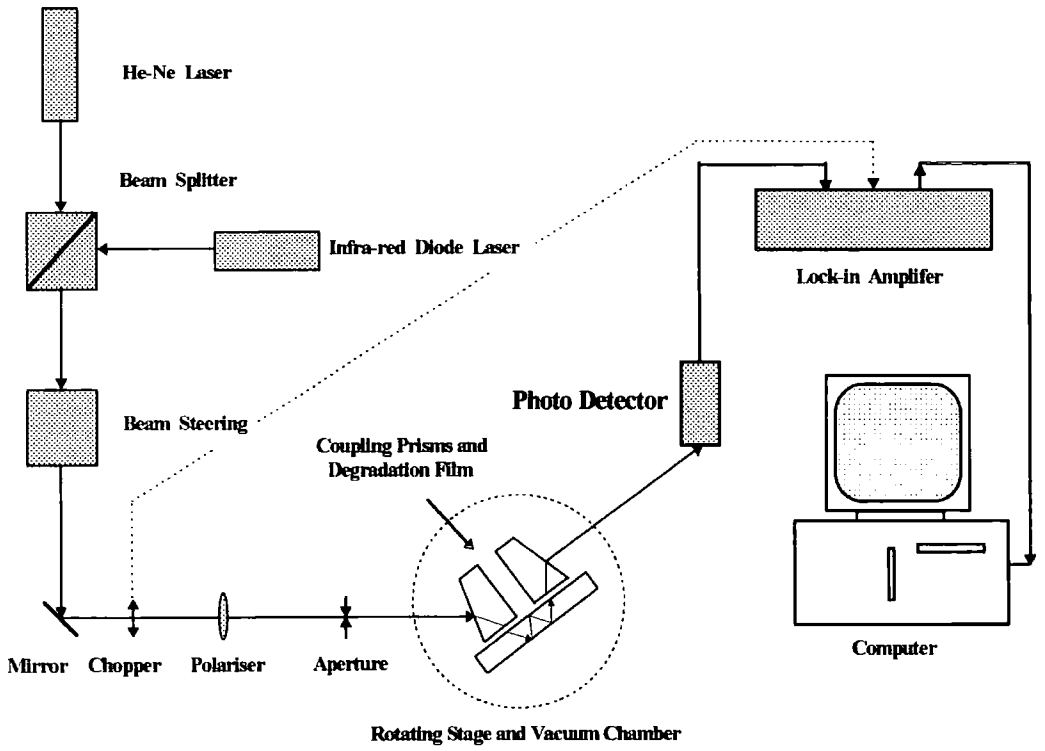

Fig.4.8. Experimental set-up for photodegradation of organic waveguide films

In order to investigate the photostability of organic chromophores in varied environments at different wavelengths and their degradation mechanisms, several measures were adopted in experiments.

1. The TM_0 mode was excited in the films in degradation experiments. In order to record whole change of transmitted light (from minimum to maximum), the appropriate doping concentration was chosen for the films to obtain minimum transmitted light which can be detected by detector at the beginning of degradation. All guest materials in this group were set at the same molar concentration, once the concentration was determined. Different groups of material may have different molar concentration.

2. Slab waveguide films were fabricated from guest-host system. PMMA was used as the host polymer, chromophores from the two groups of organic chromophores, the blue group (DEMI, Ultra-DEMI and Dicyclohexyl-DEMI) and the yellow group (Mor2, Morpip and DCM), were doped into the polymer matrix as guest materials. Sample films were dried in a vacuum oven at 80°C for 24 hours.

3. The output power of the lasers was set at equal photon flux for all those wavelengths of interest to achieve an equal number of photons arriving at the material interface per unit time, when degradation studies were carried out at different wavelengths. The whole system was fixed as firmly as possible to keep the system aligned, as the stability of the alignment was crucial for an extended degradation experiment.

4. The coupling efficiency of two prism coupler was measured in the slab waveguide films. Generally more than 70% efficiency can be achieved in practice for single prism coupler. An average value of coupling efficiency (75%) was used in the calculations.

5. Photodegradation of chromophores was investigated under different environments (air, vacuum or nitrogen atmosphere) at room temperature (~ 20°C) by using a chamber attached with two valves, where the different environments were obtained by pumping and refilling.

6. In order to analyse the effect of the polymer matrix on degradation of the guest material, degradation studies of PMMA were carried out at 632.8 nm under several environments (air, vacuum and N_2) at room temperature.

7. When photodegradation was carried out using an invisible infrared beam (940.0 nm), a wavelength at which the DEMI-series materials have no absorption, a He-Ne laser (632.8 nm, low power) was used as a probe beam to detect absorption changes in films because the DEMI-series materials have strong absorption at this wavelength, thus this probe beam was very sensitive in detecting the change of very small absorption in the films caused by photodegradation. Initially the probe beam

was coupled into the film and its coupled-out intensity was read from a lock-in amplifier. Then the film was exposed to the degrading beam (940.0 nm) by rotating the stage. Data of transmitted light was recorded at different times when the probe beam was coupled into the film to detect the absorption variations of the film at regular intervals.

4.5.4 General mechanism of photodegradation

Photodegradation can be classified into 2 types: photooxidation and photothermal degradation. Photooxidation can occur in the presence of oxygen; photothermal degradation involves reactions carried out at elevated temperatures but below the temperature necessary for purely thermal breakdown of material molecules. In these experiments, only photooxidation is discussed.

The process of photodegradation or photooxidation of an organic system is complicated and is not well understood, it differs from one class of chromophore to another and depends upon many factors (e.g. impurities, chromophore structure and its environment). There have been dramatic advances in the understanding of the mechanism of photodegradation and photooxidation over the last 20 years,[22, 34-39] however there are still many questions which needed to be answered in this field.

In the absence of light, most organic systems (e.g. chromophore, polymer) are stable for long periods at ambient environment. Nevertheless, unstable organic chromophores in the polymer or the polymers themselves degrade and/or oxidise upon exposure to optical radiation that they absorb in the absence or presence of oxygen respectively, their rates of photodeterioration vary greatly with their structures. The physical and chemical changes caused by photodegradation in organic chromophores or organic polymers often take the form of colour changes, loss of absorption, reduction in their molecular weight, etc. A reduction in molecular weight of organic system due to chain scission is the key to changes in their physical and mechanical properties of the system. Photostability of these organic systems is seriously affected by photochemical reactions in the system.

In photodegradation molecules of chromophore or polymer are excited to their excited states directly or indirectly when they obtain energy from the incident light. Then the excited molecules can dissociate into free radicals with low molecular weight (process 1), or optical energy that is absorbed by sensitisers and other intermediates, is transferred to the molecules, and as a result, the molecules are excited (process 2).

$$^{1}M + h\nu \rightarrow M^{*}(^{1}M \text{ or } ^{3}M) \rightarrow R_1^{\bullet} + R_2^{\bullet} \quad \text{(process 1)} \tag{4.10}$$

$$Sen + h\nu \rightarrow Sen^{*}, \qquad Sen^{*} + {}^{1}M \rightarrow Sen + M^{*} \quad \text{(process 2)} \tag{4.11}$$

where ^{1}M indicates singlet molecule (ground state), * represents the excited molecule, $R^{\bullet}$ is the low molecular weight free radical, Sen is sensitiser. From the excited singlet and triplet states, the excited molecules react with other intact molecules in the system, that is, photochemical reaction occurs and bond rupture or chain scission takes place. These chemical reactions lead to molecular decomposition and in polymers a reduction in molecular weight.

Photo-oxidative degradation can be catalysed by a variety of photosensitisers, because oxygen reacts efficiently with organic compounds in a radical chain reaction, resulting in a permanent chain break.

Photodegradation of organic chromophores can undergo free radical mechanisms. Normally, oxygen molecules are in their ground state ($^{3}O_2$) which is a diradical ($\dot{O}-\dot{O}$), which readily react with free radicals, and electronically excited singlet and triplet states of molecules of different chemical nature. Besides molecular oxygen, other oxygen species (singlet oxygen ($^{1}O_2$), atomic oxygen (O_2) and ozone (O_3)) are also reactive with double bonds. Among them singlet oxygen is an important intermediate in many photooxidation reactions,[40, 41] particularly it is quite reactive towards unsaturated substances (e.g. olefins and dienes) and organic compounds containing allylic and/or diene unsaturated bonds.[42, 43] In a photooxidation process, therefore, once the chromophore radicals are formed (from the initiation resulting from different processes such as formation of electronically excited species, energy transfer process or direct photodissociation of chemical bonds), these radicals react with any oxygen present and the surrounding molecules, resulting in a

permanent chain scission via rapid chain reaction and leading to chemical decomposition of the chromophore.

In the solid state the photochemical breakdown of organic molecules often occurs in the amorphous region where oxygen has ready access and the rate of diffusion of oxygen is higher than in the crystalline regions. In general, organic materials in polymers photooxidise more rapidly above their glass transition temperatures than those in the glass state due to the faster rate of diffusion of oxygen in the former.

4.6 Experimental results

4.6.1 Waveguiding in pure host polymer (PMMA)

The possible degradation of pure PMMA films was investigated in order to monitor the behaviour of the polymer matrix under the exposure of visible light in several different environments. Slab PMMA waveguide films were fabricated using PMMA of molecular weight 100,000 and glass transition temperature 105°C, its refractive indices measured at 632.8 nm are 1.48894 (TE) and 1.48951 (TM).

Firstly, pure PMMA film was exposed to a He-Ne beam (632.8 nm) in air or vacuum as shown in Fig.4.9, and the light was set at same photon flux as for the doped films. The transmitted light intensity (TM_0 mode) from the film versus time was monitored.

Secondly, the sample was then monitored under exposure to the beam under air or vacuum alternately to observe the variations of transmitted light of a pure PMMA film as shown in Fig.4.10. At the beginning, the film was under air atmosphere for 17 hours (A $\rightarrow$ B), then the film was under vacuum (< 10 mbar) for 7 hours (B $\rightarrow$ C or D $\rightarrow$ E), and then under ambient atmosphere for a further 17 hours (C $\rightarrow$ D or E $\rightarrow$ F).

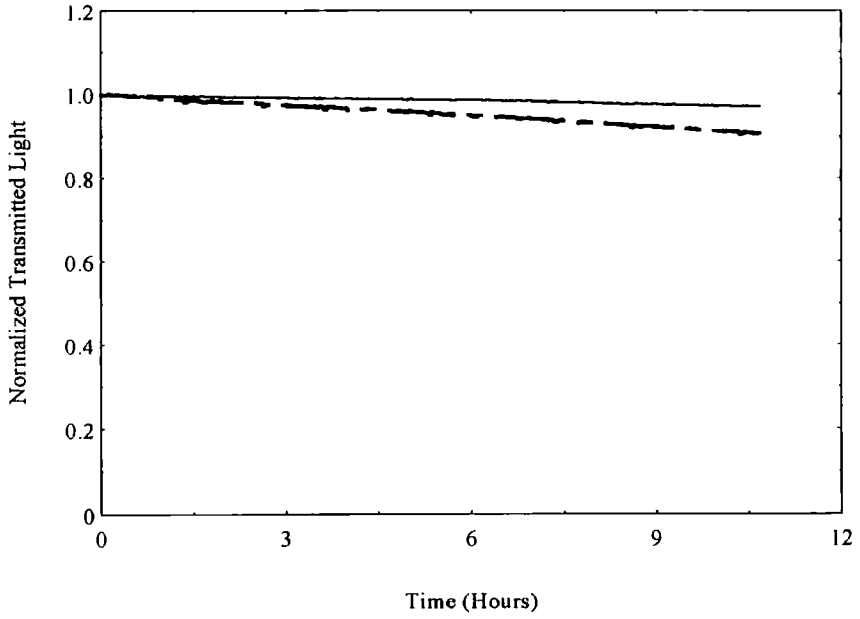

Fig.4.9. Coupled-out transmitted light from pure PMMA film at 632.8 nm (0.84 mW) under different environments at ~ 20℃. Solid line is under air atmosphere, broken line is under vacuum.

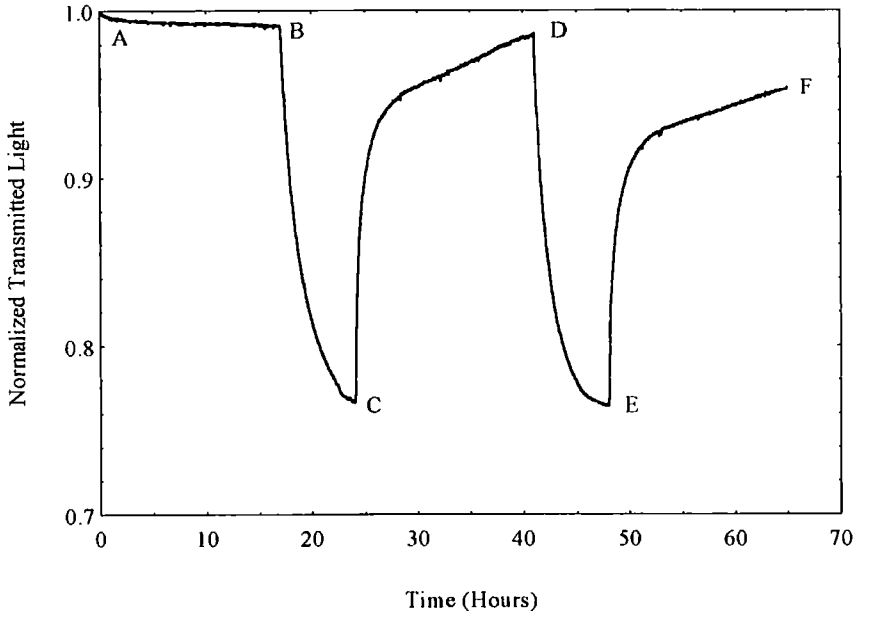

Fig.4.10. Variations of transmitted light of PMMA film at 632.8 nm (0.84 mW) at ~20℃ under air and vacuum alternately.

The changes of coupling angle (TM_0) of the pure PMMA waveguide film under vacuum (< 10 mbar) were measured at varied drying conditions to study the effect of residual solvent and water as shown in Fig.4.11.

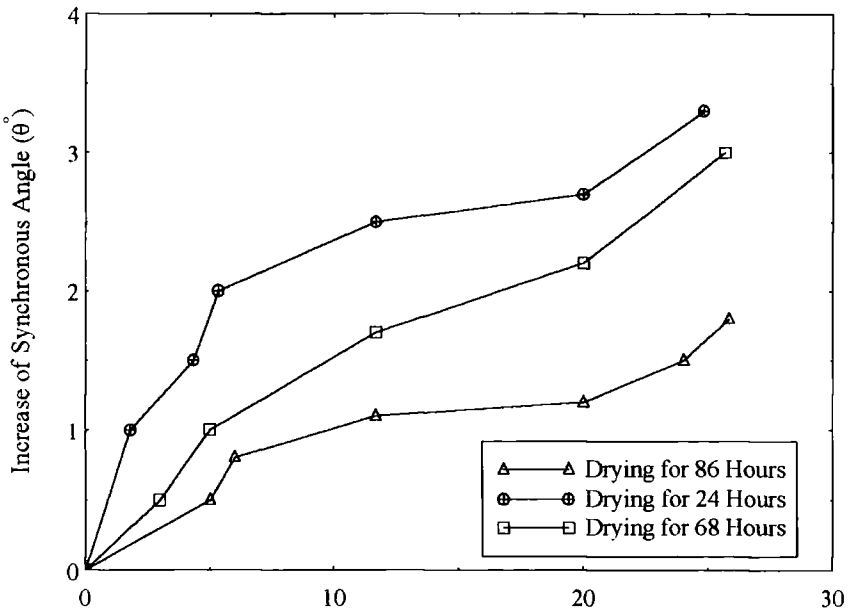

Fig.11. Changes of coupling angle (TM_0) of PMMA films in vacuum at 632.8 nm after samples' drying in vacuum oven at 80℃ for 1) 24 hours, 2) 68 hours, 3) 86 hours.

Thirdly, the changes of refractive index of pure PMMA films were measured under vacuum or a nitrogen environment in order to investigate the rate of index change of PMMA under different environments as shown in Fig.4.12 ~ 4.14. Samples were dried in a vacuum oven at 80°C for 24 hours

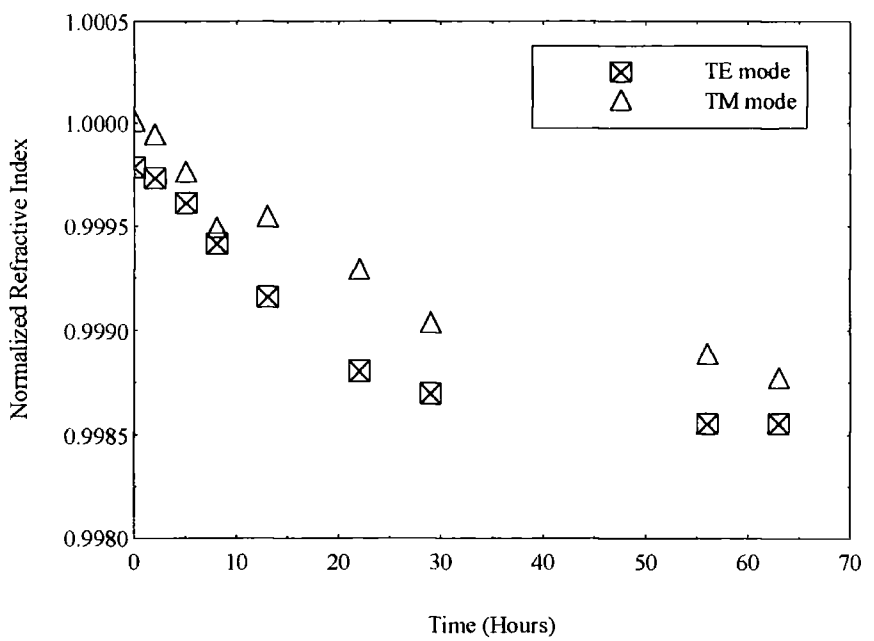

Fig.4.12. Changes of refractive index of PMMA at 632.8 nm under vacuum (< 10 mbar) at ~ 20℃ for TM and TE modes.

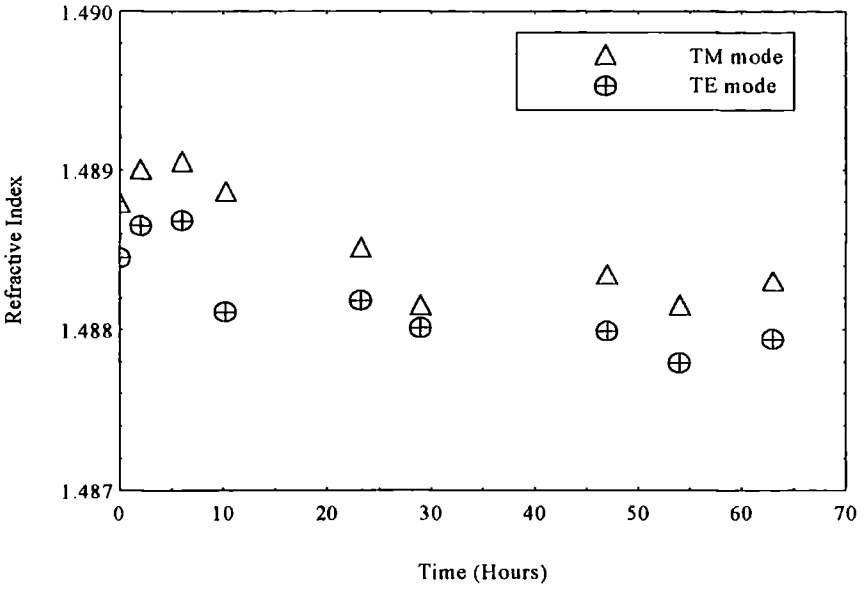

Fig.4.13. Changes of refractive index of PMMA at 632.8 nm under N_2 atmosphere (1 atm pressure) at ~ 20℃ for TM and TE modes.

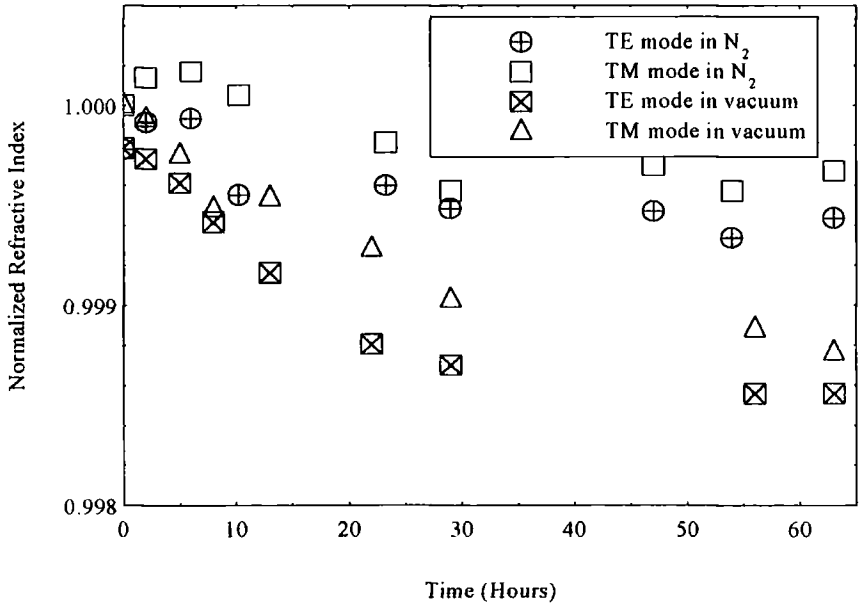

Fig.4.14. Normalised changes of refractive index of PMMA at 632.8 nm under vacuum (< 10 mbar) and N_2 atmosphere (1 atm pressure) at ~ 20℃, 1) TM mode and 2) TE mode in N_2,, 3) TM mode and 4) TE mode in vacuum.

4.6.1.1 Discussion

It is seen that there is a slight decline in transmitted light (0.024%/hr.) of pure PMMA waveguide film as shown in Fig.4.9 and A → B in Fig.4.10, but on the whole the

transmitted light under ambient atmosphere is quite stable if taking into account the experimental errors (e.g. unstability of light source). No large variations in transmitted light from samples indicate that the PMMA matrix is stable enough under low power (0.84 mW) He-Ne radiation, thus the possible photodegradation of the PMMA matrix at 632.8 nm is ruled out, that is, there is no evident influence from the degradation of polymer matrix on the photodegradation of doped chromophores in the polymer at 632.8 nm or at longer wavelengths. The transmitted light under vacuum decreases a little, the decline (0.86%/hr.) in vacuum is larger than in an air environment. This change of transmitted light from the waveguide film is attributed to the change of coupling condition (e.g. dominated by variation of refractive index of the film) due to the relaxation of polymer resulting from residual solvent and water coming out from the sample during exposure to light radiation under vacuum. This is confirmed by measurements of coupling angle changes and index changes of pure PMMA film in vacuum.

As shown in Fig.4.10, when pumping the chamber (B $\rightarrow$ C and D $\rightarrow$ E), the coupling condition of the sample varies and the polymer system begins to relax, the transmitted light decreases as the vacuum gets higher. When the sample is opened to an air atmosphere, the coupling condition relaxes back as water molecules diffuse into the polymer film and the refractive index of the polymer film increases. Transmitted light in turn increases (C $\rightarrow$ D and E $\rightarrow$ F), since most residual solvent has been lost, the coupling condition cannot relax back to its original point, and the transmitted light can not reach its original level either. By tracing changes of the coupling angle and measuring changes of the refractive index of samples, it was confirmed that the coupling condition changes when samples are exposed to radiation in a vacuum. The angle changes less if the sample contains less residual solvent and water. As shown in Fig.4.11, the coupling angle (TM_0) of pure PMMA film under vacuum (< 10 mbar) increases more (curve 1). This means that the refractive index of the film decreases more, when the film is dried in a vacuum oven for less time and contains more residual solvent and water. With drying at the same temperature for an extended time, the coupling angle changes less and the changing rate declines (curve 2 and 3). However, when the sample is dried at the same temperature for the same time and under the same environment, the rate of index change of a pure PMMA film is different under nitrogen and vacuum environments. The change of refractive index is greater initially, then reduces almost to a constant. The rate is larger

when the film is under vacuum than in an N_2 atmosphere as shown in Fig.4.12 ~ 4.14. The final changes of refractive index of PMMA films under vacuum are also larger (Δn_{TE}=0.00183 and Δn_{TM}=0.00184 for 63 hours) than in an N_2 atmosphere (Δn_{TE}=0.00037 and Δn_{TM}=0.00034 for 96 hours), this is attributed to the partial compensation of index change for polymer by diffusion of nitrogen molecules into the film after molecules of residual solvent and water come out from the film.

4.6.2 Photodegradation of DEMI-series materials

As promising nonlinear optical materials with large dipole moment and high β value,[26, 29-31] the DEMI-series materials (DEMI, Ultra-DEMI and Dicyclohexyl-DEMI) need to be fully characterised before putting them into applications. Photostability is one vital requirement for such applications.

The photostability was investigated by exposing the DEMI-series materials to radiation at the wavelengths of interest and measuring their rate of photodegradation. The two-prism coupling technique was used to couple three different wavelengths (632.8 nm, 780.0 nm and 940.0 nm) of light with an equal photon flux into sample films to degrade samples. Slab waveguide films were fabricated by doping DEMI-series materials in PMMA. The solution concentration of these three materials was chosen to be 5.42×10^{-5} mol/l to obtain the minimum transmitted light that can be detected. Among these three wavelengths, 632.8 nm and 780.0 nm wavelengths were nearly at the peak absorption within the absorption band of the DEMI-series materials, 940.0 nm was outside the absorption band of the DEMI-series materials, no absorption was seen at this wavelength on the UV absorption spectra as shown in Fig.4.5. When the materials were degraded at 940.0 nm wavelength, a low power probe beam at 632.8 nm from a He-Ne laser was utilised to detect any possible change in the absorption caused by the exposure to 940.0 nm wavelength. Special attention was paid to avoid inducing any noticeable degrading of the sample from the probe beam by using low power probe beam and probing the sample for a time as short as possible.

In order to assess the role of atmospheric oxygen in photodegradation and to study the mechanism of photodegradation of DEMI-series materials, the experiments were carried

out in both air and oxygen-free environments. Firstly sample films were irradiated at 632.8 nm, 780.0 nm and 940.0 nm wavelengths in air atmosphere at room temperature (~ 20°C) as shown in Fig.4.15 - 4.17.

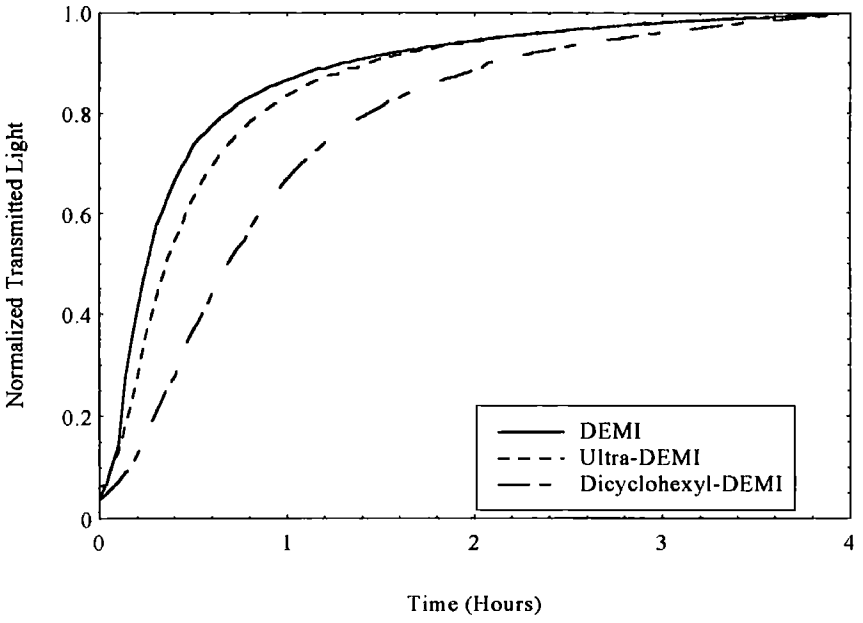

Fig.4.15. DEMI-series materials' degradation at 632.8 nm (2.66×10^{15} photons/s) in air atmosphere (~ 20℃)

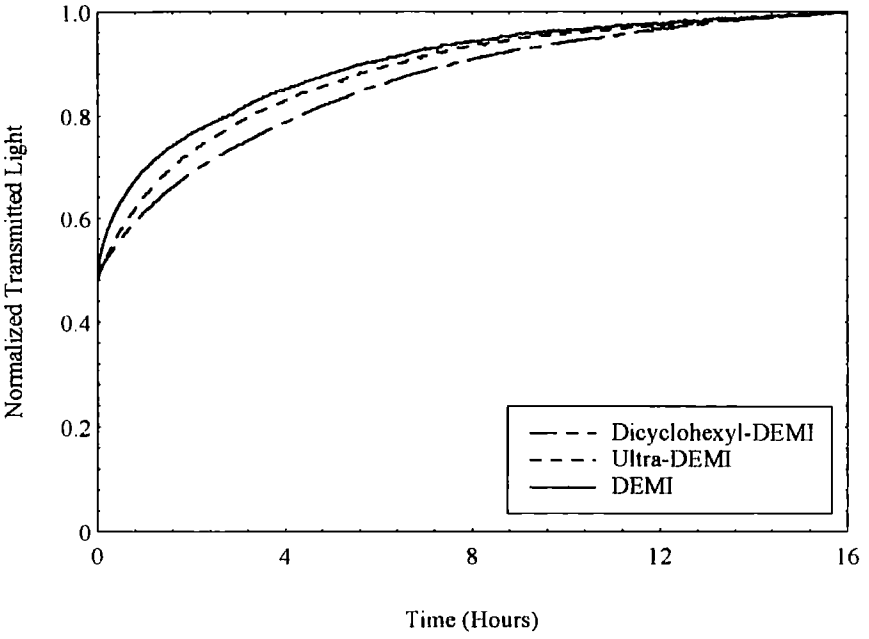

Fig.4.16. DEMI-series materials' degradation at 780.0 nm (2.66×10^{15} photons/s) in air atmosphere (~ 20℃)

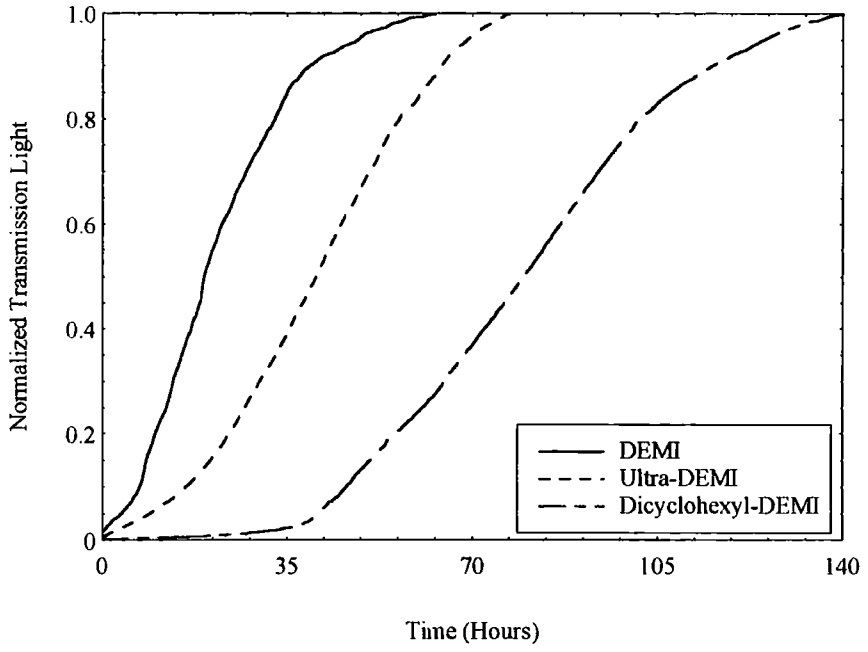

Fig.4.17. DEMI-series materials' degradation at 940.0 nm (2.127×10^{16} photons/s) in air atmosphere (~ 20℃)

Secondly the experiments were carried out in oxygen-free environments (vacuum and nitrogen). DEMI-series materials were then degraded at 632.8 nm and 780.0 nm wavelengths under vacuum and in nitrogen atmosphere as shown in Fig.4.18 and 4.19.

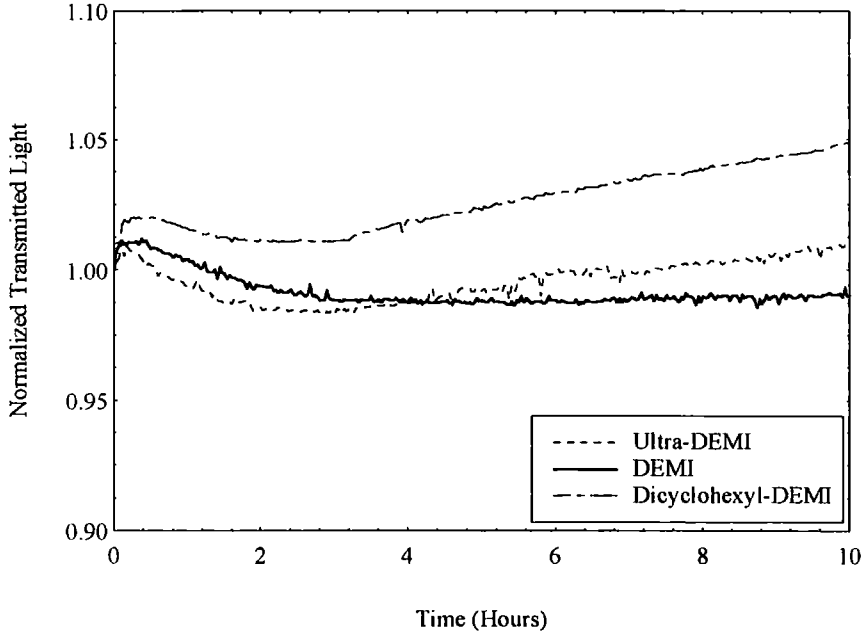

Fig.4.18 DEMI-series materials' degradation at 632.8 nm (2.66×10^{15} photons/s) in vacuum (< 10 mbar, ~ 20℃)

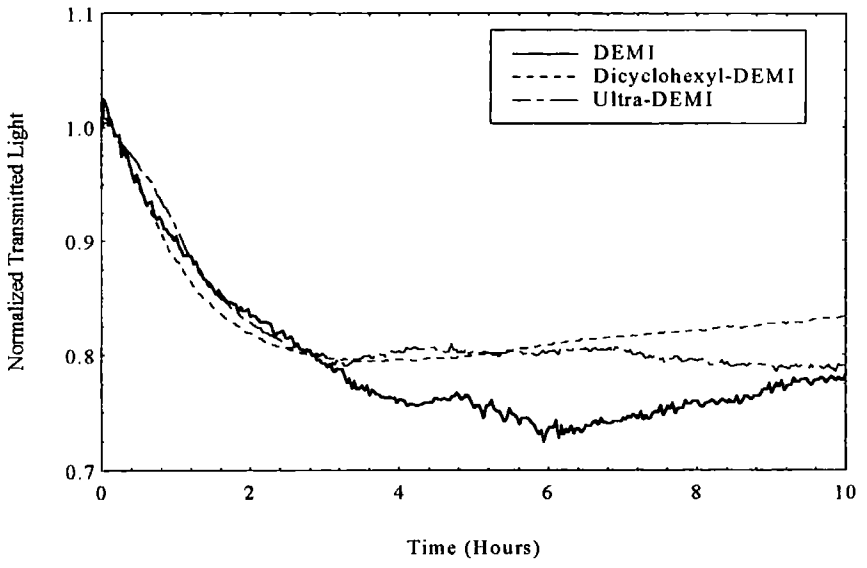

Fig.4.19. DEMI-series materials' degradation at 632.8 nm (2.66×10^{15} photons/s) in Nitrogen (~ 1 atm, ~ 20℃)

It can be seen from Fig.4.15 - 4.19 that the behaviour of photodegradation is quite different when DEMI-series materials are degraded in air or oxygen free atmosphere. A typical photodegradation curve in air is characterised by the fact that the transmitted light from samples displays an auto-accelerating period, and is followed by a rapid quasi-linear increase, the increase slows down and then reaches a steady value. When a material is exposed to light radiation at a different wavelength with an equal photon flux, it takes a different time (the characteristic degradation time) for the normalised transmitted light to reach an equal level (e.g. 60% transmission). The time is dissimilar for these different materials under irradiation by an identical wavelength at an equal photon flux. The degradation rate of DEMI-series materials is different between different members of themselves when they are irradiated by light in air atmosphere, and their rate of photodegradation is wavelength dependent. This characteristic degradation time (the time taken to reach a certain normalised transmission) determines the photostability of these materials. The initial slope is determined by the probability that a given photon is absorbed by a dye molecule, and the transmission saturates when most of the dye molecules have been degraded. However, DEMI-series materials are outstandingly stable when they are exposed to light under vacuum or in a nitrogen atmosphere. As shown in Fig.4.18, the transmitted light increases slightly at the beginning of the exposure, then gradually declines before finally displaying a slow steady increase (< 0.4% /h in vacuum, < 0.85% /h in N_2).

These experimental results strongly indicate that the DEMI-series materials experience a photooxidation process when they are irradiated by light in an oxygen containing environment, the molecules of DEMI-series materials degrade after irradiation, and oxygen plays a very important role in their photodegradation. High photostability can be achieved in an oxygen free environment.

4.6.2.1 Wavelength dependence of the DEMI-series materials' photodegradation

It is generally a disadvantage that organic chromophoric systems change their physical properties as a result of photodegradation, limiting the ultimate usefulness of the systems and the lifetime of devices made from them in applications. However, photobleaching of dye molecules in or attached to polymers, which induce changes in refractive indices of organic systems by exposure of material to light radiation, has been widely used for the fabrication of polymer channel waveguides and active electro-optic waveguide components.[44 - 46]

In order to achieve a better understanding of the kinetics of the photodegradation process and detailed information on the refractive index profiles, several models have been proposed to model the process of light propagation through polymer thin-film waveguides. By analysing the photodegradation processes of isotropic chromophore molecules in a solid (i.e. polymer) matrix, Jan et al,[47] Nadia Capolla et al,[48] R. S. Moshrefzadeh et al[3] have developed their models to describe the refractive index profiles in the film. Other authors like Jang-Joo Kim et al,[49] W. J. Tomlinsom,[50] Jiong Ma et al,[51] James R. Sheats et al,[52] Arnaud Dubois et al,[53, 54] I. P. Kaminow et al[55] generate their models to describe the transmitted light from waveguide film. Among them, Arnaud Dubois' model[53, 54] does not contain any restrictions to its validity, to any specified excitation process and to film thickness. He uses his model in thick films (several millimetres thick) to quantify the efficiency of absorption processes and photochemical reactions of specific photons and chromophores in a given host polymer to predict the operational lifetime for the chromophores. It is similar to the situation in this research, therefore the model is chosen in the analysis of the experimental results. The efficiency of photon absorption and its wavelength dependence are obtained by fitting the data using the model.

We consider the dye molecules to be isotropic and homogeneously distributed in polymer matrices. At time t=0, dye molecules (species 1, absorption across section σ_1) with volume concentration (density) N_0 are contained in a thin film of thickness L. The dye molecules are progressively converted into bleached molecules (species 2, absorption across section σ_2) during exposure to light of wavelength λ with a uniform photon flux n_0. This model assumes:

$$\text{species } 1 \quad ---\frac{h\nu}{(\lambda)}\longrightarrow \quad \text{species } 2 \tag{4.12}$$

1. When illuminated continuously, not all of the dye molecules transform into the bleached molecules, each dye molecule has a certain probability of being transformed into a bleached (degraded) molecule after having absorbed a certain number of photons. This probability is defined as the photodegradation quantum efficiency B^{-1}.

2. The degraded molecules progressively created during irradiation are assumed to be photochemically stable, although having only slight or weak absorption.

3. All dye molecules are always in the irradiated region. The irradiated molecules are not renewed by diffusion in solid matrices, they are permanently excited until they are degraded.

4. The degradation process is a one-photon process. Multiphoton or thermal processes that obviously may occur at high powers are then neglected by using low input power.

5. The transmitted light saturates when most of the dye molecules have been converted into degraded molecules.

6. The errors are dominated by changes of the coupling efficiency in the calculations of B parameters. The errors listed in table 4.3 and table 4.4 corresponde to ±5% changes to the coupling efficiency. Extra estimated experimental or systematic errors (0.1×10^5 or 0.01×10^6) are needed to include it.

Therefore, the transmission from the sample film is given by

$$T(t) = \frac{e^{-\sigma_2 J_0}}{1 + e^{(\Delta\sigma J_0 - 1)} e^{-\sigma_1 B^{-1} n_0 t}} = \frac{T(\infty)}{1 + [\frac{T(\infty)}{T(0)} - 1] e^{-\beta t}} \qquad (4.18)$$

where n_0 is the incident photo flux (photons/sec. m^2), N_0 is volumetric concentration of nondegraded dye molecules at t=0 (mol/m^3), T(0) is the initial transmission, T(∞) is the final transmission, B is the average number of photons absorbed by a dye molecule before it is degraded (photons/molecule), B^{-1} is the quantum efficiency for degradation and other terms are as described below

$$J_0 = N_0 L, \qquad \Delta\sigma = \sigma_1 - \sigma_2, \qquad \beta = \frac{\sigma_1 n_0}{B}, \quad T(0) = e^{-\sigma_1 J_0}, \quad T(\infty) = e^{-\sigma_2 J_0} \qquad (4.18a)$$

The dye concentration (N_0) affects only the initial and final transmission of light. σ_1 affects the initial transmission and affects the rate of photodegradation to a certain extent whereas the final transmission is not affected. σ_2 affects just the final transmission. The B factor affects just the rate of photodegradation (i.e. the slopes of the transmission curve) and determines the photostabilities of the measured materials. By selecting the fit of the initial slope of the transmission from the samples. A good fit of the initial slope provides a β parameter with good precision though there is an obvious differentence between a theoretical curve and a experimental result. B is calculated from the β parameter that can be obtained by fitting the experimental data with the model.[53, 54] A typical measuring and fitting curve is shown in Fig. 4.20.

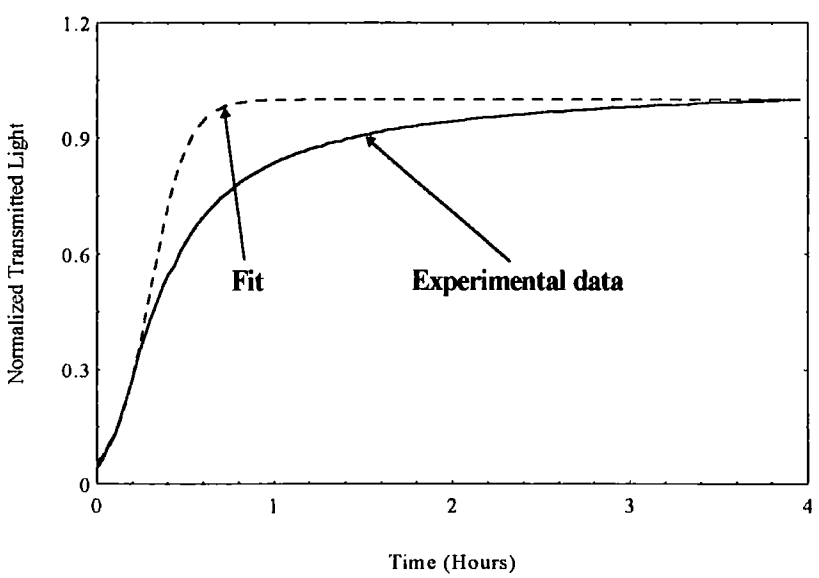

Fig.4.20 A typical fit of the transmission versus degradation time for Ultra-DEMI

This model gives a simple and quick way to analyse the data from photodegradation experiments of waveguide thin films, and supplies a clear picture of the degradation process inside the film. It can be seen from Fig.4.20 that this model has a good fit with the evolution of the transmission at the beginning but does not fit so well at the end. The difference may be due to 1) the dye molecules are actually not isotropic and their orientation may be fixed by matrix surroundings. 2) some dye molecules enter the irradiated region from the unirradiated region by diffusion. 3) the photon flux is greater at the first part of propagation path in the waveguides than the back for a long path or thick film since some photons are absorbed by dye molecules that are not degraded effectively. Because of these, the experimental transmission will not increase as fast as the theoretical transmission. The experimental data of DEMI-series materials are fitted according to this model from equation 4.13, the results are listed in table 4.3.

Table 4.3 B factor of DEMI-series materials doped in PMMA and degraded at different wavelengths in air at room temperature (~ 20°C)

dye	B (photons/molecule)		
	λ=632.8 nm	λ=780.0 nm	λ=940.0 nm
DEMI	$(1.38\pm0.09)\times10^{6}$	$(2.32\pm0.15)\times10^{6}$	$(1.05\pm0.07)\times10^{9}$
Ultra-DEMI	$(2.50\pm0.17)\times10^{6}$	$(4.51\pm0.37)\times10^{6}$	$(2.30\pm0.15)\times10^{9}$
Dicyclohexyl-DEMI	$(5.65\pm0.38)\times10^{6}$	$(9.95\pm0.66)\times10^{6}$	$(4.98\pm0.33)\times10^{9}$

4.6.2.2 Spectroscopic studies

In order to investigate the photodegradation mechanism of the DEMI-series materials, besides UV/VIS absorption spectroscopic studies as shown in Fig.4.22, infrared (IR) spectroscopy was carried out on undegraded and degraded films to detect the changes in the sample films (presence or disappearance of certain functional groups). IR spectroscopy provides a simple way to observe many absorption bands and obtain a wealth of structural information about a molecule or an organic compound from the characteristic frequencies of molecular vibrations, even though many of the absorption bands cannot be assigned accurately. By analysing the characteristic frequencies of a molecule and the typical absorption bands of functional groups, certain functional groups can be distinguished and the process or reaction which happened in the sample films can

be deduced. These characteristic frequencies are determined by the masses of vibrating atoms, the strength of the chemical bonds of a molecule and the geometry of molecules.

During IR spectroscopic studies, Ultra-DEMI was chosen as a representative sample of the DEMI-series materials. Sample films were fabricated according to the method described in chapter 3. Ultra-DEMI at 10% by weight was doped in poly (N-vinylcarbazole) (PVK) and 1,1,3,3-Tetra-Methylurea (TMU) was chosen as solvent. The following steps were employed to achieve good films during film fabrication.

1. TMU was used as solvent to dissolve Ultra-DEMI (dopant) and PVK (polymer matrix) for a higher concentration of Ultra-DEMI obtained in it. In order to reduce the possibility of degradation of Ultra-DEMI caused by water contained in the TMU solvent, distilled TMU (or undistilled TMU boiled for 5 mins before use) was used to eliminate water.

2. In order to avoid the overwhelming absorption from carbonyl functional groups from the polymer matrix at 1735 ~ 1680 cm^{-1} on IR spectra, PVK, whose molecular structure is shown in Fig.4.21, was chosen as the polymer matrix. It is expected to see the carbonyl function group to appear at this region induced by oxidation of Ultra-DEMI in PVK matrix.

3. Sample films were spun on Calcium fluoride (CaF_2) substrates which are transparent to infrared radiation in most of the region of interest.

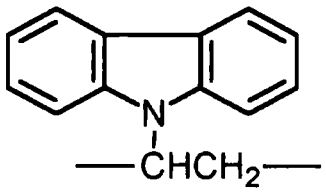

Fig.4.21 Molecular structure of poly (N-vinylcarbazole) (PVK)

The experimental set-up of spectroscopic studies is shown in Fig.4.22. Two lasers, a He-Ne at 632.8 nm and a laser diode at 780.0 nm, were aligned with optical components in the system, the light beam was expanded to a circle with 0.9 cm in diameter. The two lasers irradiated the sample surface with equal photon flux and uniform intensity distribution.

Following drying, Ultra-DEMI doped polymer film on CaF_2 substrate was exposed to light radiation in an air environment (~ 20°C). UV/VIS and IR spectra were recorded at regular intervals as shown in Fig.4.23 and 4.24. As the Ultra-DEMI doped sample film was exposed to radiation for extended time during experiments, the colour of the film under exposure changed from its original blue to colourless and transparent. The colour was not recovered even after the sample was baked at elevated temperature (~ 180°C) in a vacuum oven.

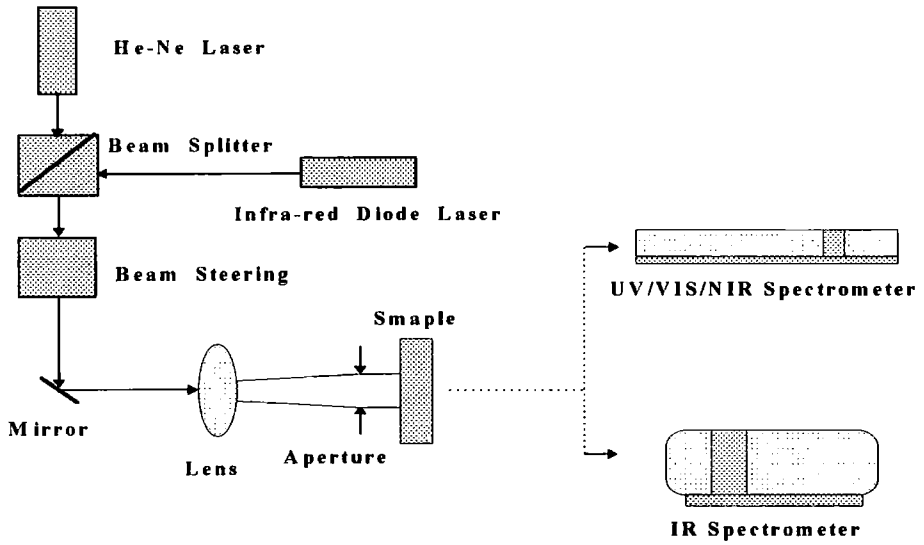

Fig.4.22 Experimental set-up of spectroscopic studies for Ultra-DEMI

Fig.4.23 shows the UV/VIS absorption spectra of the unirradiated (t=0 hr) and the irradiated Ultra-DEMI doped film at different times with laser light of 632.8 nm in air (the result irradiated with 780.0 nm in air is very similar). It is easily noticeable that exposure of the sample film to radiation results in a reduction of its absorption, with the increase of irradiation time, the absorption of Ultra-DEMI decreases drastically in air. Moreover peak B drops faster than peak A. Some absorption still exists in the film and no absorption band shift is seen after irradiation. The above results suggest that some Ultra-DEMI molecules in the film still remain unchanged even after irradiation. The IR spectra as shown in Fig.4.24, provides more information about the photodegradation of Ultra-DEMI doped films.

Assignment of the infrared vibrational energies were taken from the chemical characterisation of Ultra [26] and standard tables of infrared vibrational energies.[56] At the beginning of photodegradation, it can be seen from Fig.4.24 that a characteristic

frequency of Ultra-DEMI, is represented by a strong cyano stretching band (R – C ≡ N) at 2187 cm^{-1}. Initially there is no peak at the 1650 ~ 1760 cm^{-1} region in the unirradiated sample film. Both IR spectra of the films irradiated at 632.8 nm and 780.0 nm in air are very similar and show some differences from the spectrum of an unirradiated Ultra-DEMI doped film. After irradiation, the absorption of the C≡N stretching band reduces drastically, new absorption bands can be seen at around 1715 cm^{-1} due to the presenc of a

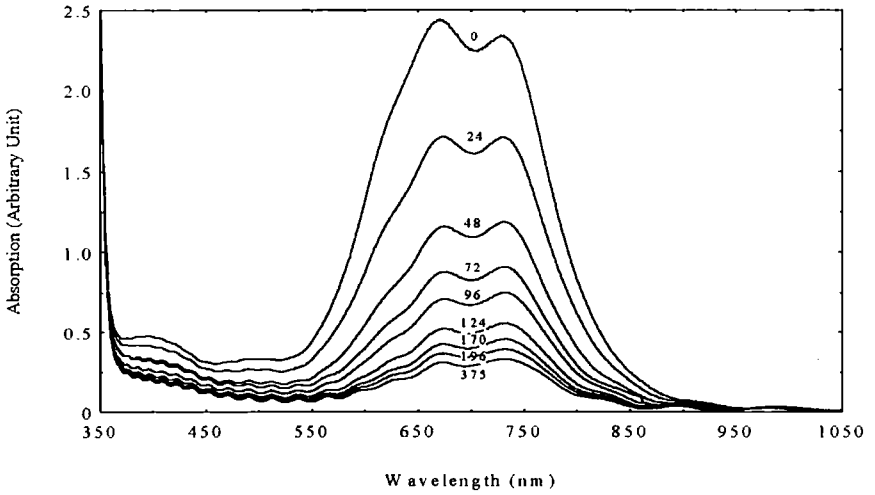

Fig.4.23 UV/VIS absorption spectra of unirradiated (t=0) and irradiated Ultra-DEMI at 632.8 nm wavelength in air atmosphere (~ 20℃) at different time

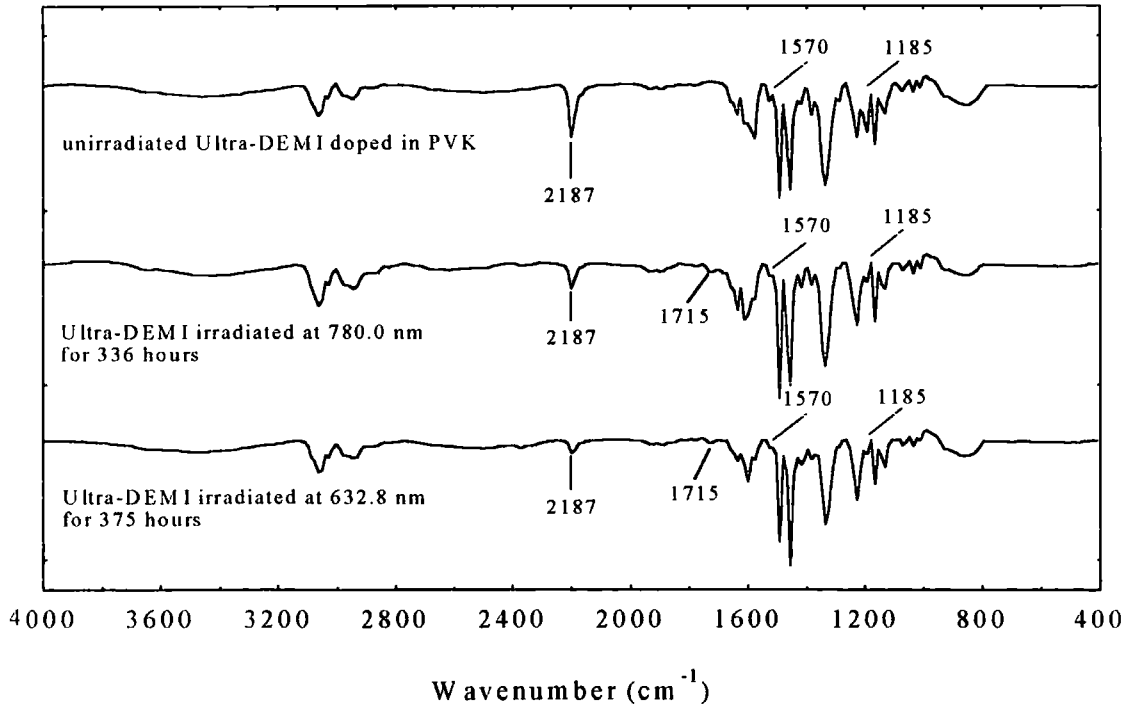

Fig.4.24 Infrared spectra of unirradiated Ultra-DEMI doped in PVK and irradiated in air atmosphere at 632.8 nm and 780.0 nm wavelength respectively

carbonyl group (C=O) in the irradiated film, and a corresponding reduction of the C=C or C=N stretching bands is observed at 1570 cm^{-1}. The feature at 1185 cm^{-1} due to C-O or C-N group in the unirradiated sample suffers a large decrease with irradiation. However, the other absorption bands show no change even after irradiation in air.

Since the wavelengths of radiation (632.8 nm and 780.0 nm) are far away from the ultra violet region, the possible significant influence of polymer matrix (PVK) degradation on dopant degradation (Ultra-DEMI) is excluded. It can be seen from these observations in the UV/VIS and IR spectra:

1. Most cyano groups (C≡N) at 2187 cm^{-1} disappear in the molecular structure of Ultra-DEMI after irradiation.

2. The large reduction at 1570 cm^{-1} means that C=N or C=C bonds in Ultra-DEMI molecules are broken with irradiation.

3. Some increase at around 1715 cm^{-1} corresponds to carbonyl stretching (C=O) and indicates the formation of carbon-oxygen double bond resulting from oxidation in air.

4. All of these chemical reactions occurred in the Ultra-DEMI film induced by photooxidation, which results in the loss of conjugation of molecules, and leads to degradation of Ultra-DEMI molecules and permanent loss in the colour of sample films in air.

4.6.2.3 Conclusions of photodegradation of DEMI-series materials

By analysing the waveguide degradation experiments at different wavelengths in various environments by means of spectroscopic studies, it was found that the effect of polymer matrices on the dopant is negligible and can be ignored, since the energy of the wavelengths used in experiments are not hight enough to induce noticeable degradation of the polymer matrix, the degradation behaviour of dye molecules is mainly determined by their structures. The experimental results clearly show that the degradation of DEMI-

series materials in oxygen free (vacuum or nitrogen) and oxygen present (air) environments is totally different. The degradation of DEMI-series materials is fast in air atmosphere, but they are very stable in the oxygen free environments. This strongly indicates that the degradation process of DEMI-series materials is photooxidation involving oxygen in air with irradiation of light.

This is confirmed by spectroscopic studies of Ultra-DEMI. After irradiation, the carbonyl groups are observed in the IR spectra of Ultra-DEMI; At the same time the characteristic groups of Ultra-DEMI (also DEMI-series materials), the bands due to the cyano group (C≡N) nearly disappear, the C=N or C=C bands in the Ultra-DEMI molecules reduce greatly. Because of the similarity in molecular structure among DEMI-series materials, we have reason to believe that similar reactions and changes occur in all the DEMI-series materials.

Though the exact mechanism of photodegradation in the DEMI-series materials has not been fully understood yet, according to the experimental results obtained, the proposed degradation mechanisms are (irradiation of 632.8 nm and 780.0 nm in an oxygen containing environment):

1. Photoexcitation: the DEMI-series chromophores (D) absorb a photon at these wavelengths and transits to an excited state (D^*).

$$D + h\nu \rightarrow D^* \tag{4.14}$$

2. Photodegradation: i) At its excited state, the excited molecule of DEMI-series materials transfers energy to ground state oxygen ($^3O_2$), forming excited oxygen molecules (O_2^*) that in turn react with or oxide the ground state molecules, this results in degradation or decomposition of molecules of DEMI-series materials.

$$D^* + {}^3O_2 \rightarrow D + O_2^* \ (^1O_2^* \text{ or } {}^3O_2^*) \tag{4.15}$$

$$O_2^* + D \rightarrow \text{degradation} \tag{4.16}$$

During the photochemical reaction, singlet oxygen ($^1O_2^*$) plays a more important role in the photodegradation, since singlet oxygen is very reactive towards olefinically unsaturated bonds in the DEMI-series materials. ii) The excited molecules of DEMI-series materials dissociate into free radicals with low molecular

weight, then the free radicals react with oxygen molecules; What is more, the excited molecules may react with oxygen molecules directly. Finally, all these lead to the chemical decomposition of molecules of DEMI-series materials.

$$D^{\bullet} \rightarrow R_1^{\bullet} + R_2^{\bullet}, \qquad R_1^{\bullet} (\text{or } R_2^{\bullet}) + O_2 \rightarrow \text{degradation} \tag{4.17}$$

$$D^{\bullet} + O_2 \rightarrow \text{degradation} \tag{4.18}$$

At 940.0 nm in an oxygen containing environment, the degradation rate of DEMI-series materials is much lower. Because they have no absorption at this wavelength shown in Fig.4.4, photodegradation process differs to some extent to photoexcitation from that of 632.8 nm and 780.0 nm, but the real reason has not been understood yet.

However, when the DEMI-series materials are degraded in oxygen free environment, these dye molecules are quite stable, but a small and slow degradation is observed. The possible reason may be that the molecules react with small number of oxygen molecules trapped in the polymer matrix and photodegrade, this leads to a small increase of transmitted light at the beginning of degradation and then declines after most of the oxygen is used up as shown in Fig.4.18 and 4.19. Because of lack of the active intermediate (oxygen) in the system, the excited chromophore molecules have very low possibility of reaction with other molecules directly in the system, photophysical deactivation of energy becomes the dominant process. That is, excited molecules dissipate or lose their excess energy through a variety of photophysical processes or through collision with their surroundings, then return back to their ground states.

For DEMI-series materials from the fitting of the results of photodegradation in air, it can be shown that the average number of photons absorbed by a dye molecule (B) before it is degraded is wavelength dependent. The B parameters at 632.8 nm and 780.0 nm in absorption band are in the same order of 10^6, the B of 780.0 nm is greater than that of 632.8 nm. When the excitation wavelength is varied to 940.0 nm at infrared region, B increases by 3 orders of magnitude from 10^6 to 10^9 as shown in table 4.3.

$$B_{633,\,780} << B_{940}\ , \qquad B_{780} > B_{633} \tag{4.19}$$

At the same excitation wavelength.

$$B\ (\text{Dicyclohexyl-DEMI}) > B\ (\text{Ultra-DEMI}) > B\ (\text{DEMI}) \tag{4.20}$$

Finally the photostability of Dicyclohexyl-DEMI is the highest, then Ultra-DEMI and DEMI. If DEMI-series materials are used in devices at IR band (1.3 ~ 1.55 μm), longer lifetimes and higher photostability can be expected.

4.6.3 Degradation of yellow materials

The photostability of the yellow materials, 7,7-(2,6 dimethylmorpholino)-8,8-dicyanoquinodimethane (mixtures of *cis* and *trans* conformations) (Mor2), 7-(2,6, dimethylmorpholino)-7-(4-methyl piperidino)-8,8, -dicyanoquinodimethane (mixtures of *cis* and *trans* conformations) (Morpip), 4-dicyanomethylene-2-methyl-6-p-dimethylaminostyryl-4H-pyran (DCM), were studied by exposure to light radiation in different environments using doped polymer systems. Mor2 and Morpip were synthesised in order that they could be used in polymer optical fibre telecommunication applications and may have improved photostability. Two measures are employed to realise these purposes. 1) the main absorption of the materials occurs outside of the visible and infrared regions, 2) no olefinically unsaturated bonds exist in their structures as shown in Fig.4.6 ~ 4.7.

In experiments, these three yellow materials were irradiated at wavelengths within their main absorption band from an argon ion laser (A_r^+ at 457.9 nm, 488.0 nm and 514.5 nm), and with a He-Ne at 632.8 nm. Slab waveguide sample films were fabricated by dip coating, where the concentrations of these three materials were chosen at equal molar concentration (3.3×10^{-5} mol/l), in order to achieve the minimum transmitted light coupled out by two-prism coupling of 75% coupling efficiency. Materials were exposed to these three wavelengths with the same photon flux (3.223×10^{15} photons/s) in air (oxygen present) or vacuum (oxygen free) environment at room temperature (~ 20°C). DCM was used as a reference material in photodegradation studies of Mor2 and Morpip not because they are very similar in their structures, but mainly because DCM is a commercial laser dye of acceptable photostability.

The transmitted light of sample films irradiated at varied wavelengths in different environments are shown in Fig.4.25 ~ 4.30.

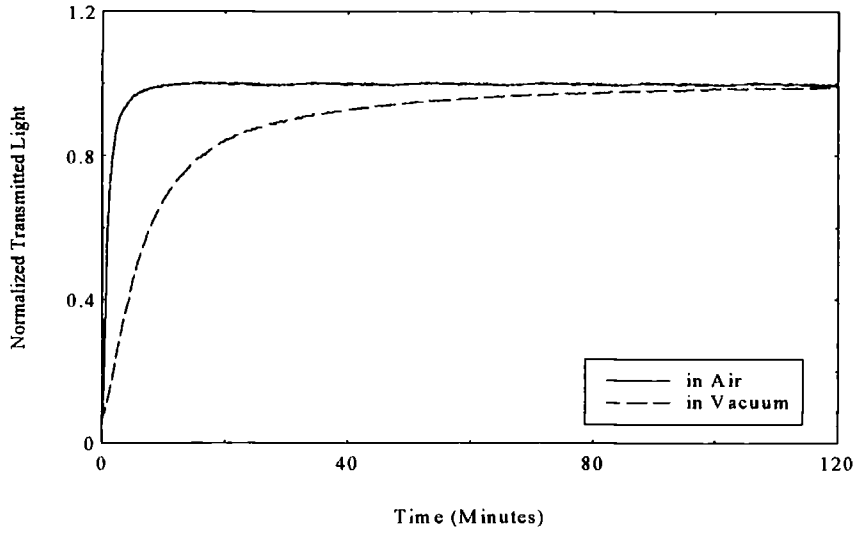

Fig.4.25 Mor2's degradation in air and vacuum (< 10 mbar) at 457.9 nm wavelength

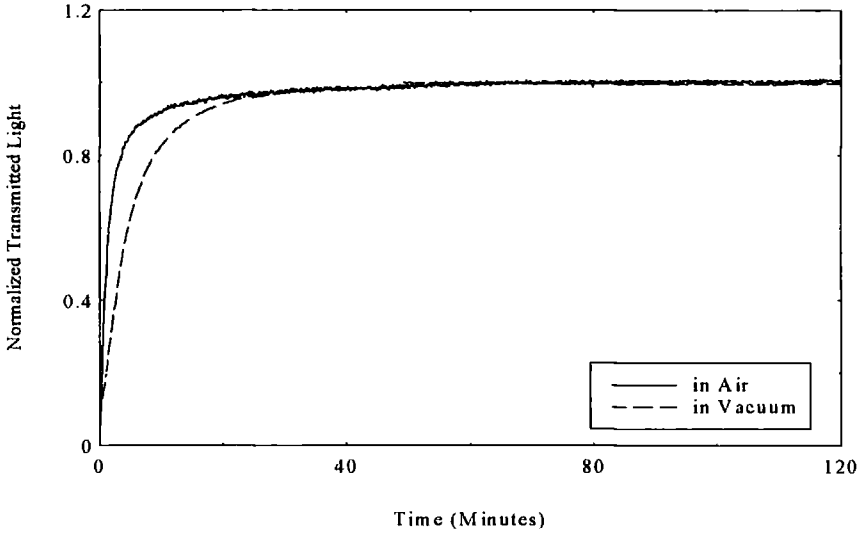

Fig.4.26 Morpip's degradation in air and vacuum (< 10 mbar) at 457.9 nm.

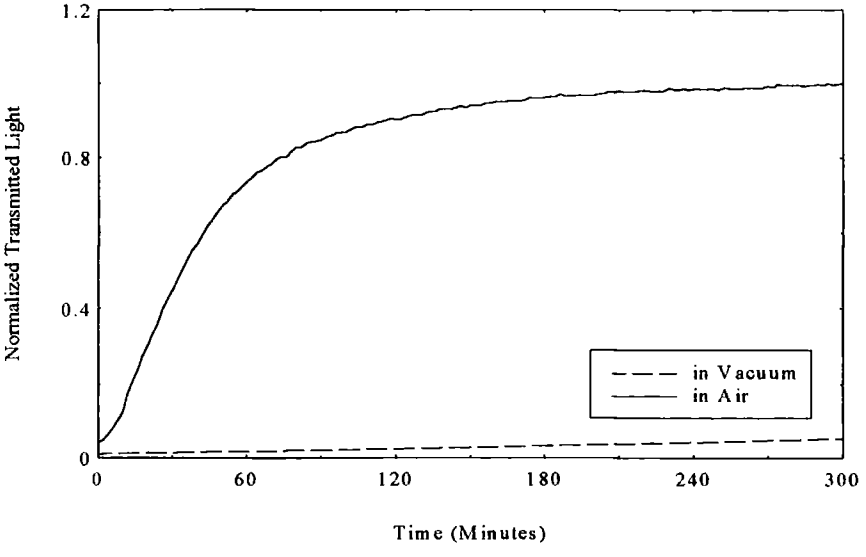

Fig.4.27 DCM's degradation in air and vacuum (< 10 mbar) at 457.9 nm.

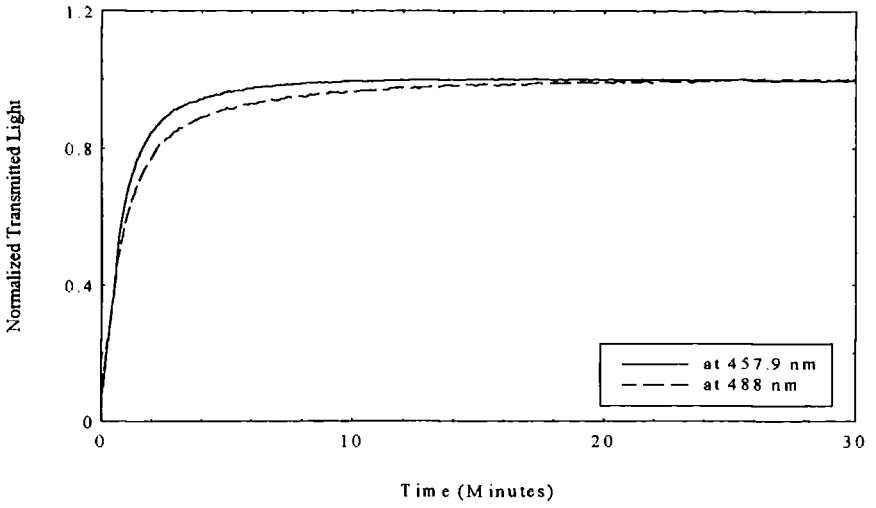

(a)

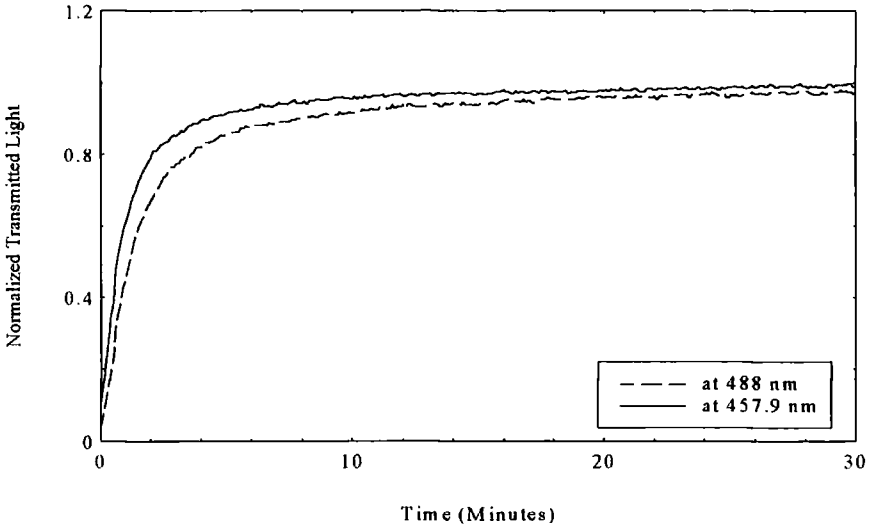

(b)

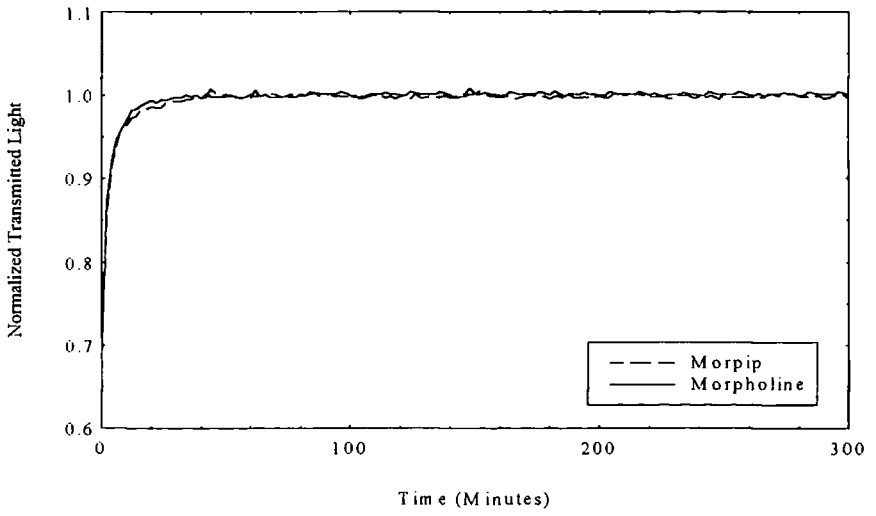

(c)

Fig.4.28 Mor2 and Morpip's degradation in air. a) Mor2 at 457.9 nm and 488.0 nm, b) Morpip at 457.9 nm and 488.0 nm, c) Mor2 and Morpip degraded at 514.5 nm.

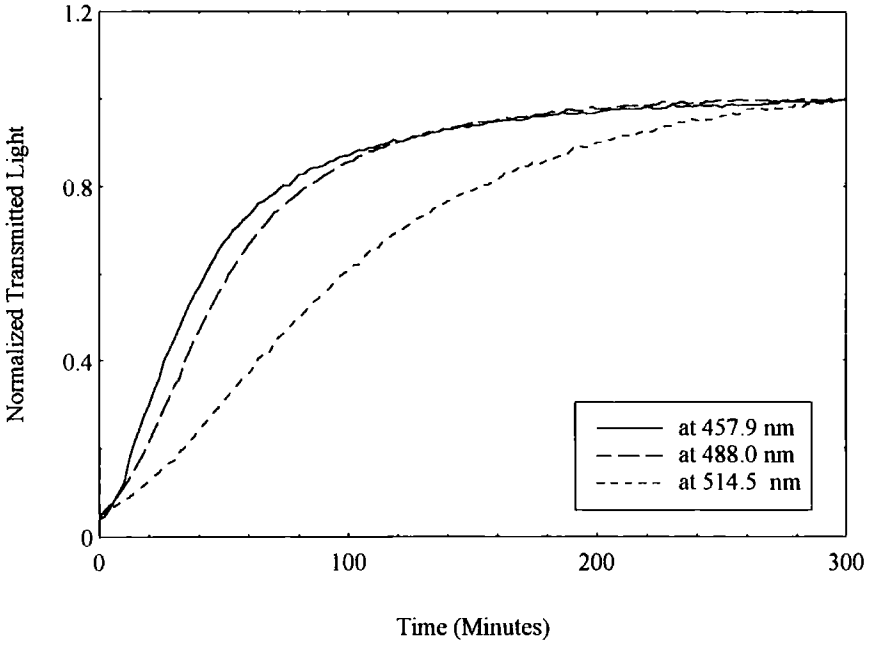

Fig.4.29 DCM's degradation in air at 457.9 nm, 488.0 nm and 514.5 nm.

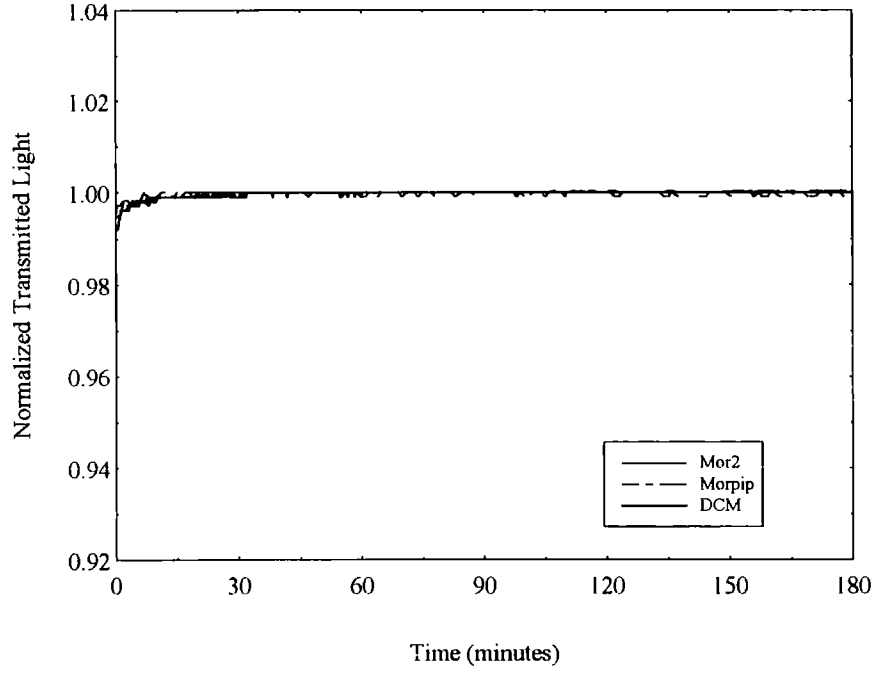

Fig.4.30. Mor2, Morpip and DCM's degradation at 632.8 nm in air

Corresponding to the data above, these curves are fitted using equation 4.13 from the model described in section 4.6.2.1, their wavelength dependencies (B parameter) are listed in table 4.4 below.

Table 4.4 B parameters of yellow materials at different wavelengths in PMMA

dye	B (photons/molecule)			
	457.9 nm in air	457.9 nm in vacuum	488.0 nm in air	514.5 nm in air
Mor2	$(3.01\pm0.20)\times10^{5}$	$(1.78\pm0.12)\times10^{6}$	$(2.44\pm0.16)\times10^{5}$	$(1.10\pm0.073)\times10^{5}$
Morpip	$(3.85\pm0.26)\times10^{5}$	$(1.47\pm0.098)\times10^{6}$	$(2.22\pm0.15)\times10^{5}$	$(1.42\pm0.094)\times10^{5}$
DCM	$(1.89\pm0.13)\times10^{7}$		$(1.28\pm0.085)\times10^{7}$	$(1.43\pm0.096)\times10^{7}$

From the experimental results and fitting of data, it is seen that no matter what environments (air or vacuum) Mor2 and Morpip are degraded in, they all degrade after irradiation by the light they absorb and their degradation behaviour is similar as shown in Fig.4.25 and 4.26. This indicates clearly that:

1. The photodegradation mechanism of Mor2 and Morpip is direct photodecomposition. In vacuum the molecules of Mor2 and Morpip may react with free radicals in the polymer matrix or may be brought to their excited states by absorbing a photon of light, from there these molecules degrade or decompose involving chain scissions and lose their original properties. When these molecules are irradiated in air environment, the rate of degradation is faster than that in vacuum, the photostability of Mor2 and Morpip increases by 1 order of magnitude from 10^5 in air to 10^6 in vacuum. Oxygen in air accelerates the process of photodegradation by reacting effectively with these molecules because of its activity.

2. On the contrary, degradation behaviour of DCM is different from that of Mor2 and Morpip, in vacuum DCM is stable even though it degrades a little in oxygen free environment as shown in Fig.4.27. Thus the mechanism of degradation for DCM is predominantly photooxidation. Oxygen acts as an active intermediate and plays an important role in photodegradation of DCM. The molecules of DCM are excited, from there these excited molecules follow the routes similar to DEMI-series materials to degrade, which was described in the previous section.

3. Taking into account the experimental errors, the photostability of Morpip is slightly better than that of Mor2. Their B numbers are in the same order at those

wavelengths and exhibit no wavelength dependence when they are irradiated at wavelengths within their main absorption band. For DCM, its photostability and degradation exhibit no wavelength dependence either when it is exposed to the wavelengths of which radiation are within its main absorption band. The B parameters of DCM at those wavelengths are in the same order. According to the data collected, DCM doped in PMMA matrix (B ~ 10^7) is much more stable than when doped into a sol gel film (B ~ 10^5).[53] The B parameter is improved about 2 orders of magnitude.

4.7 Molecular aggregation and a beam branching effect

When sample films doped with yellow materials at low concentration (3.3×10^{-5} mol/l) are exposed to the 632.8 nm light, even though 632.8 nm is outside the main absorption band of yellow materials and no absorption is found at this wavelength, a little degradation is still observed and DCM's degradation is the largest among them as shown in Fig.4.29. However, as yellow materials films doped at high concentration (4.12×10^{-2} mol/l) which corresponds to 5% by weight for DCM, 6.27% for Mor2 and 6.04% for Morpip, are irradiated by 632.8 nm at same photon flux (3.223×10^{15} photons/s) as degraded at low concentration, the transmitted light decreases rather than increases photodegradation as shown in Fig.4.31 ~ 4.32.

For Mor2 and Morpip, Fig.4.33 and 4.34 show that most of the energy coupled into the film is confined in the mode which is being excited (TM_0) at the beginning of irradiation in air or in vacuum environment. After irradiation for 48 hours, the energy confined in the TM_0 mode reduces and other modes (TM_1, TM_2) obtain more energy when the TM_0 is being excited. At the same time, the ratios of mode energy (I_1 / I_0, energy in the 1st mode (I_1) to the 0 mode (I_0)) change from 44.51% at t=0 to 73.91% at t=48 hours for Mor2 and from 28.49% to 79.66% for Morpip as listed in table 4.5. The changes in their refractive indices (decreases) are very small before and after irradiation in an air environment. Compared with this, the corresponding mode profiles show little change and only small changes are found in their ratios of mode energy under vacuum conditions. Their refractive indices reduce much more than those in air as listed in table 4.6.

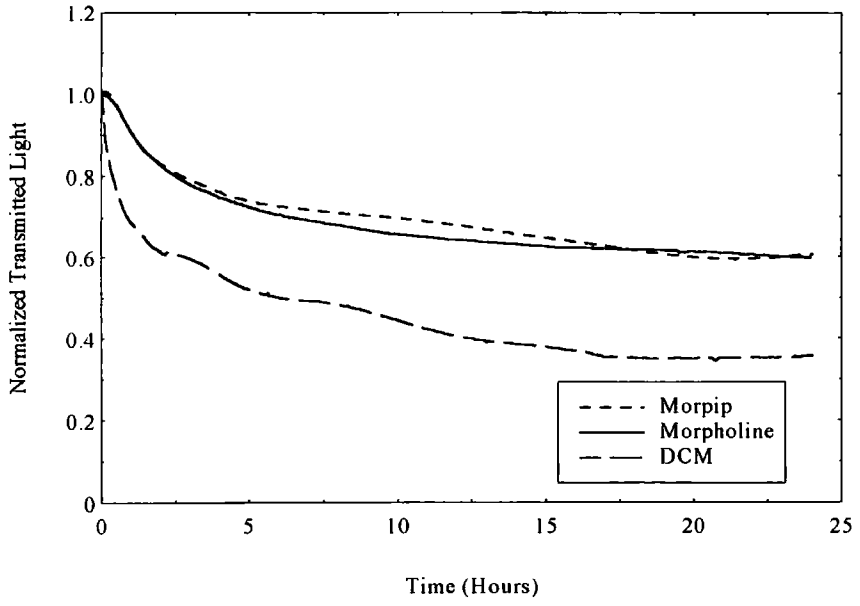

Fig.4.31 Yellow materials' degradation in air at 632.8 nm at high concentration of 4.12×10^{-2} mol/l (corresponding to Mor2 6.27% w/w, Morpip 6.04% w/w and DCM 5% w/w.)

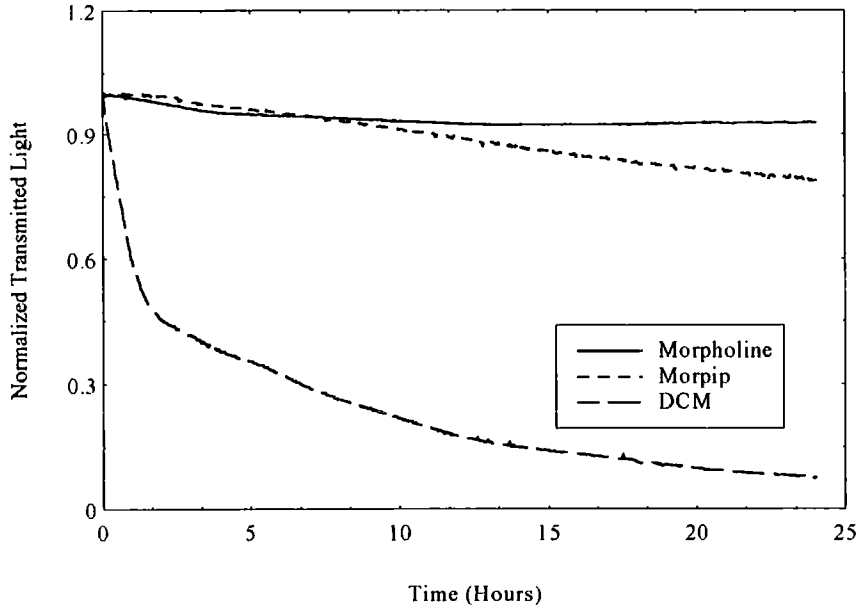

Fig.4.32 Yellow materials' degradation in vacuum (< 10 mbar) at 632.8 nm at concentration of 4.12×10^{-2} mol/l (corresponding to Mor2 6.27% w/w, Morpip 6.04% w/w and DCM 5% w/w)

The light transmitted by Mor2 and Morpip reduces more in air than that in vacuum, but their transmitted light always decreases no matter what environment they are degraded in. In order to investigate this phenomena, the prism outcoupled light from sample films was

scanned using a slit of 0.2 mm in width in air and in vacuum at room temperature (~ 20°C) to obtain the mode profiles as shown in Fig.4.33 ~ 4.35. Meanwhile, the sample films were checked under an optical microscope to monitor their degradation after irradiation for 48 hours and photographs were taken as shown in Fig.4.36 ~ 4.38.

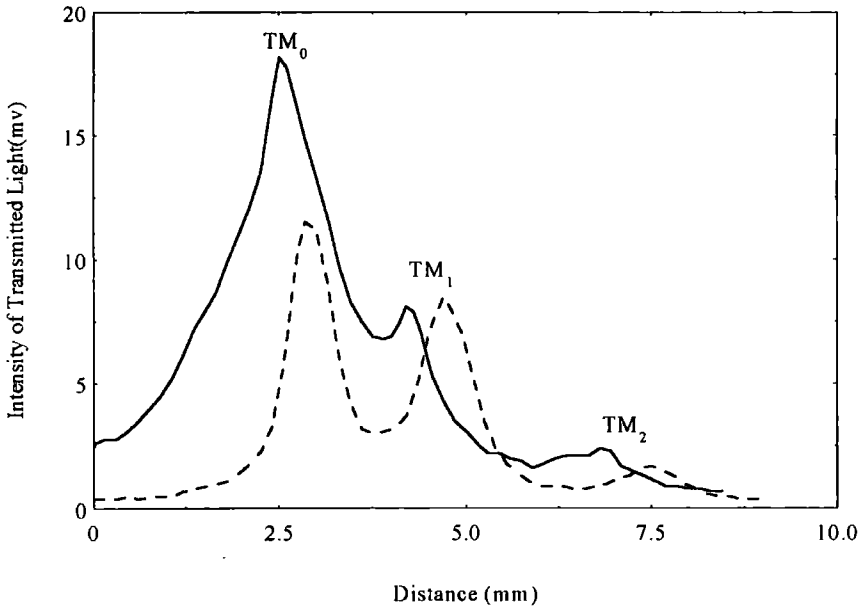

(a)

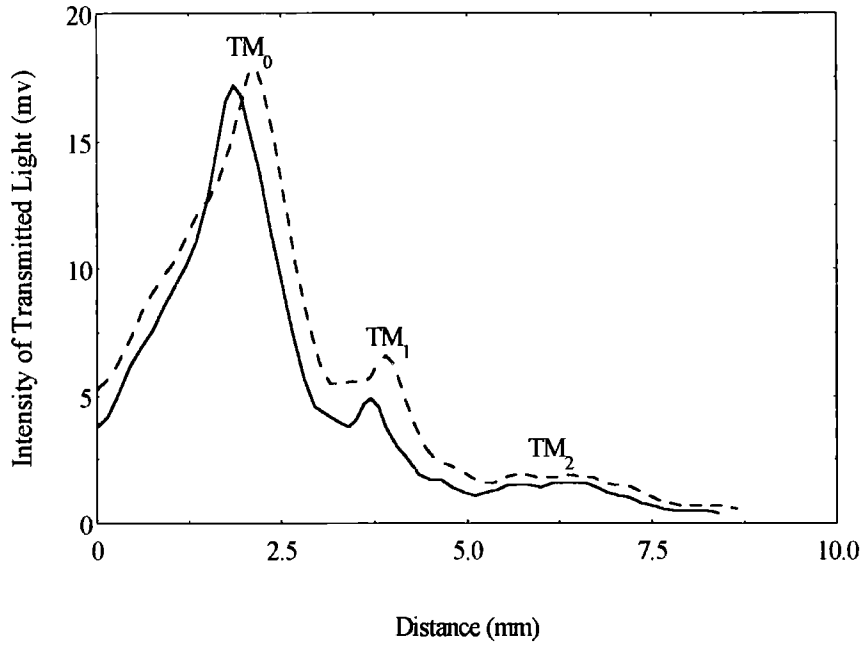

(b)

Fig.4.33 Mode profiles of Mor2 when TM_0 mode is excited in the waveguide film. Solid line indicates profiles at the beginning of degradation (t=0), broken line expresses profiles at t=48 hours. (a) in air, (b) in vacuum.

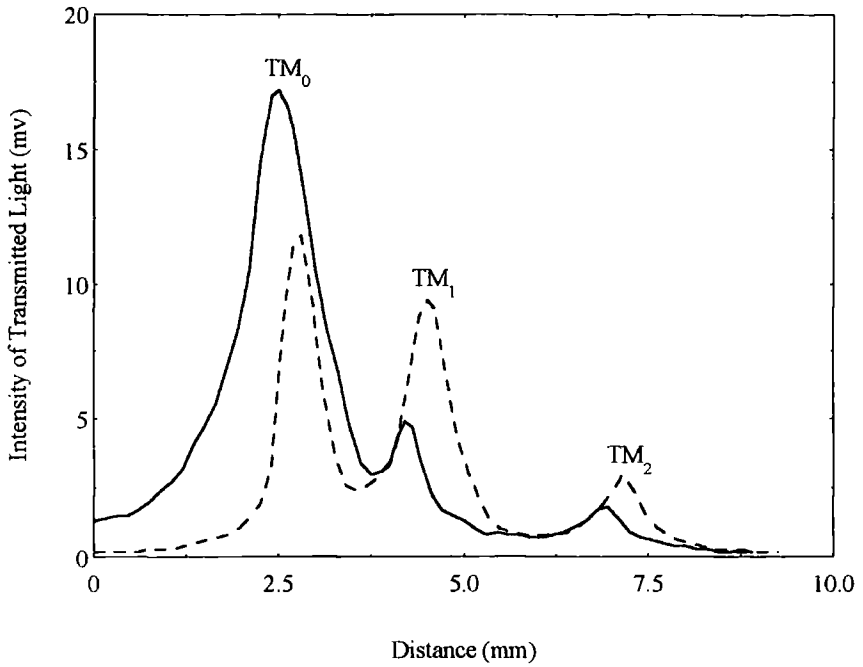

(a)

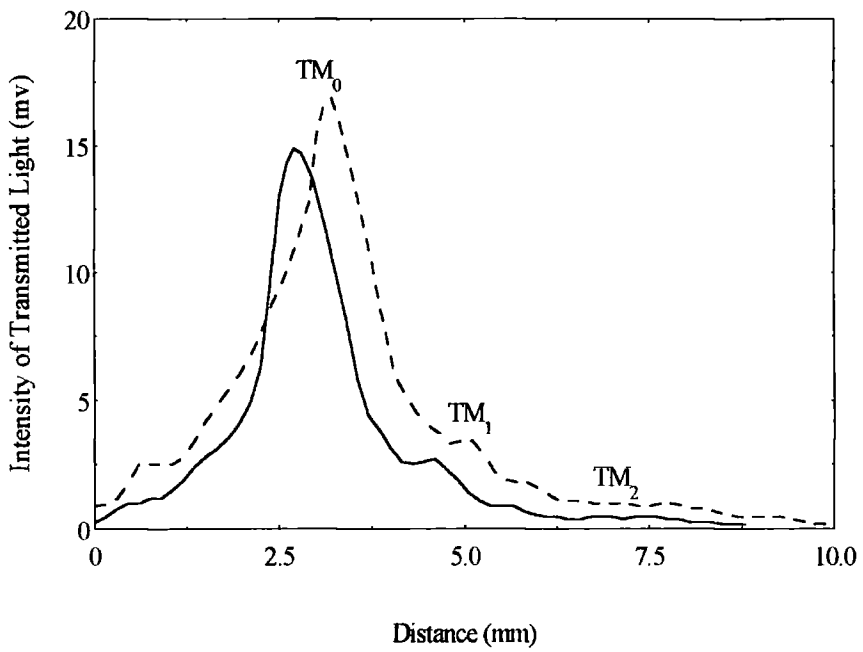

(b)

Fig.4.34 Mode profiles of Morpip when TM_0 mode is excited in the waveguide film. Solid line indicates profiles at the beginning of degradation (t=0), broken line expresses profiles at t=48 hours. (a) in air, (b) in vacuum

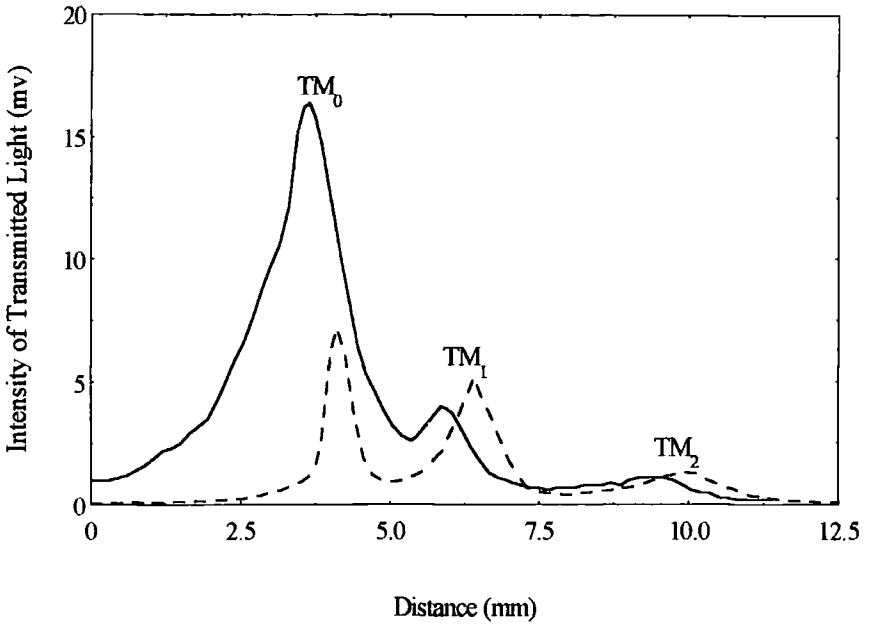

(a)

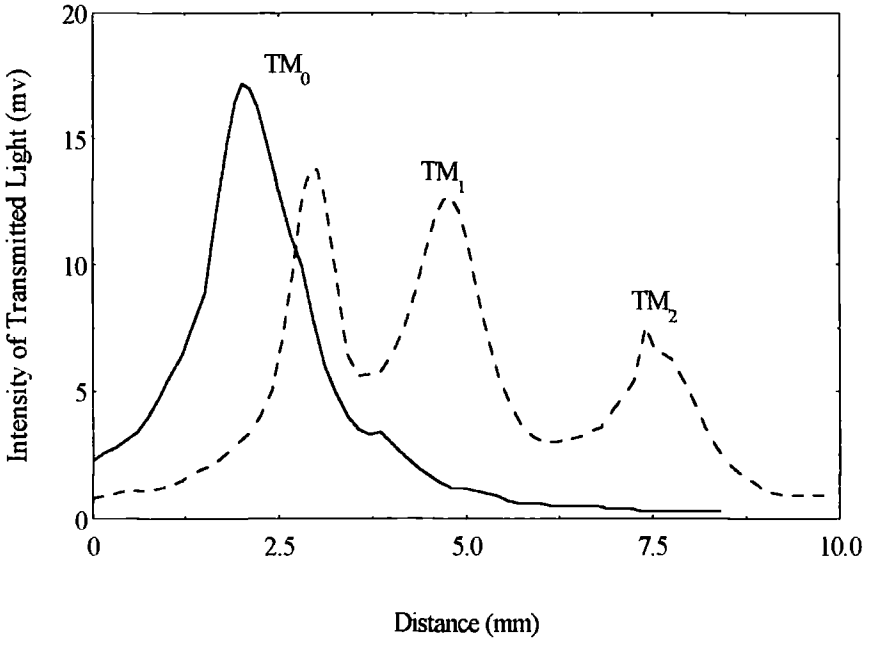

(b)

Fig.4.35 Mode profiles of DCM when TM_0 mode is excited in the waveguide film. Solid line indicates profiles at the beginning of degradation (t=0), broken line expresses profiles at t=48 hours. (a) in air, (b) in vacuum

Table. 4.5 Ratio of mode energy, refractive index of yellow materials doped PMMA waveguide film degraded in air environment at 632.8 nm wavelength (~ 20°C)

dye	I_1/I_0		refractive index				Δn_{TE}	Δn_{TM}
	t=0 (hr)	t=48 (hrs)	t=0 (hr)		t=48 (hrs)			
			TE	TM	TE	TM		
Mor2	44.51%	73.91%	1.50191	1.50200	1.50164	1.50167	-2.7×10^{-4}	-3.3×10^{-4}
Morpip	28.49%	79.66%	1.49864	1.49878	1.49745	1.49815	-8.9×10^{-4}	-6.3×10^{-4}
DCM	24.39%	72.22%	1.51504	1.51510	1.51343	1.51318	-16.1×10^{-4}	-19.2×10^{-4}

where $\Delta n_{TE} = n_{TE}(t=48\text{ hrs}) - n_{TE}(t=0\text{ hrs})$ and $\Delta n_{TM} = n_{TM}(t=48\text{ hrs}) - n_{TM}(t=0\text{ hrs})$.

Table. 4.6 Ratio of mode energy, refractive index of yellow materials doped PMMA waveguide film degraded in vacuum environment at 632.8 nm wavelength (~ 20°C)

dye	I_1/I_0		refractive index				Δn_{TE}	Δn_{TM}
	t=0 (hr)	t=48 (hrs)	t=0 (hr)		t=48 (hrs)			
			TE	TM	TE	TM		
Mor2	28.49%	36.87%	1.50066	1.50105	1.49950	1.50015	-11.6×10^{-4}	-9×10^{-4}
Morpip	17.45%	20.12%	1.49761	1.49763	1.49674	1.49738	-8.7×10^{-4}	-2.5×10^{-4}
DCM	19.77%	92.03%	1.51590	1.51607	1.51272	1.51281	-31.8×10^{-4}	-32.6×10^{-4}

As for the DCM, no matter what environment it is degraded in at 632.8 nm, its mode profiles all change greatly as shown in Fig.4.35 and its refractive index decreases significantly as listed in table 4.5 and table 4.6. The energy in the TM_0 mode decreases and the TM_1 and the other mode, obtains energy. The ratio of mode energy increases from 24.33% to 72.22% in air, and from 19.77% to 92.03% in vacuum. These results suggest that the energy in the TM_0 mode scatters to the other modes.

By analysing the photographs of films containing the yellow materials obtained from the optical microscope as shown in Fig.4.36 ~ 4.38, it can be seen that the surfaces of the films, which are clear and smooth originally before irradiation, becomes rough in small areas after irradiation. Many small spots appear in the area where light is coupled into the film under the in-coupling prism. Microcrystals are observed in this small area through a powerful microscope, whereas hardly any microcrystals are seen outside this area. It is

proposed therefore that changes of mode profile are mainly due to the effect of microcrystals in the films, and an air environment (oxygen, humidity) favours the aggregation of dye molecules in the film, which results in the formation of microcrystals.

Because of the formation of large microcrystals in the in-coupling area in the film and the scattering of light from them, part of the light coupled in a certain mode which is being excited (e.g. TM_0) changes its propagating direction and enters the other modes (e.g. 1st and 2nd modes). This leads to the redistribution of mode profile after the irradiation, in which the zeroth order mode loses part of its energy and other modes obtain some energy. Since the changes in refractive index is small before and after irradiation in air, the scattering of light is dominant in the redistribution of mode profile. As for Mor2 and Morpip in vacuum, it is inferred that few microcrystals form during irradiation and little scattering of light occurs in the film because no noticeable redistribution of mode profile is observed. The changes in their refractive indices are larger in vacuum than in air, which may be due to more residual solvent coming out from the film in the vacuum environment. Thus a little beam divergence occurs for these two materials in vacuum.

For DCM, besides large changes in its mode profile in air and in vacuum at room temperature after exposure to 632.8 nm, photodegradation occurs as can be seen in the large changes (decrease) of refractive index in air and in vacuum environments which are measured in experiments. This photodegradation is induced by upconverted fluorescence which will be discussed in the next section. As a result of degradation, a single beam in the film becomes multibeam (beam branching).

Therefore, scattering of light from microcrystals and beam branching from photodegradation together cause the redistribution or change of DCM's mode profiles in air. In vacuum, beam branching, which also leads to the changes of light direction in the beam, is the dominant factor in the variation of its mode profiles.

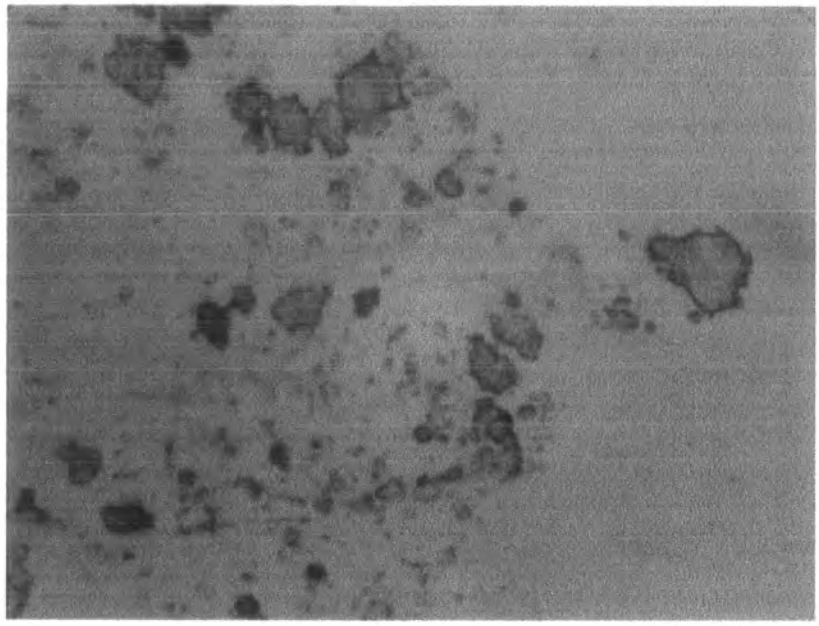

(a)

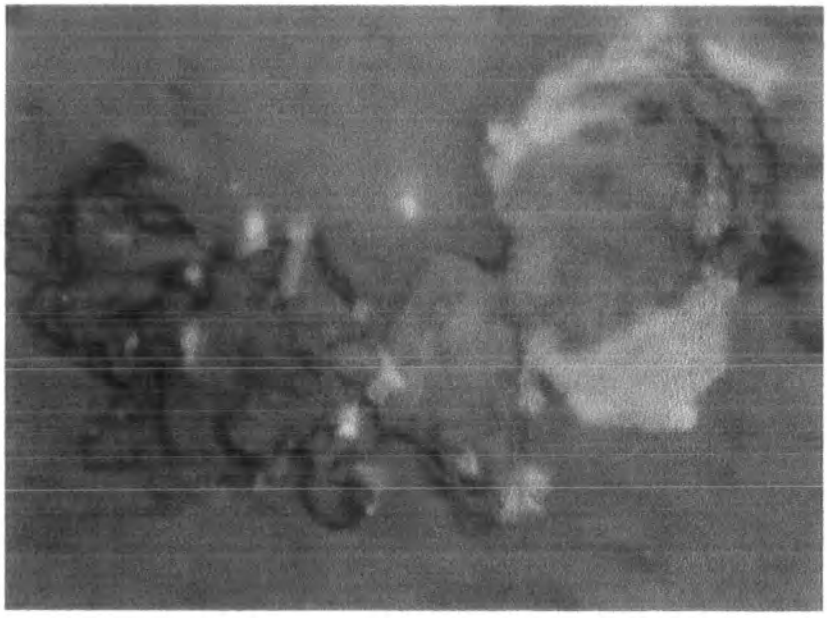

(b)

Fig.4.36 Optical microscope images of microcrystals forming in a Mor2 waveguide film. a) ×20, b)×100, crystal size ~ 4μm.

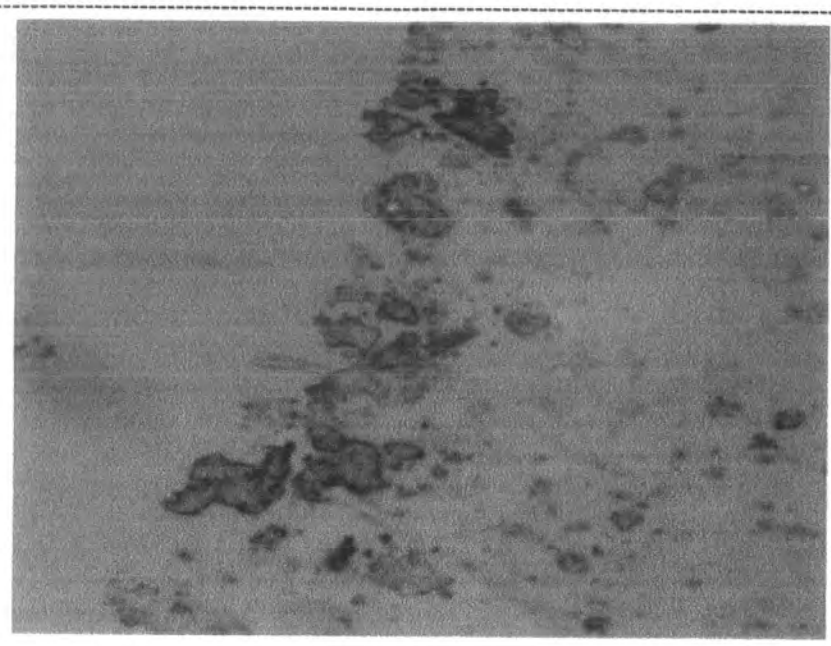

(a)

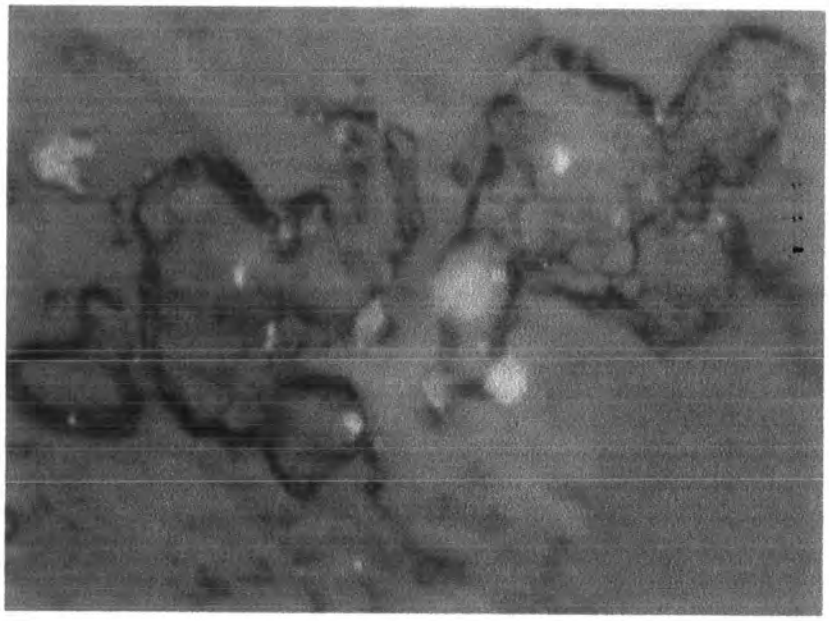

(b)

Fig.4.37 Optical microscope images of microcrystals forming in Morpip waveguide film. a) ×20, b)×100, crystal size ~ 7μm.

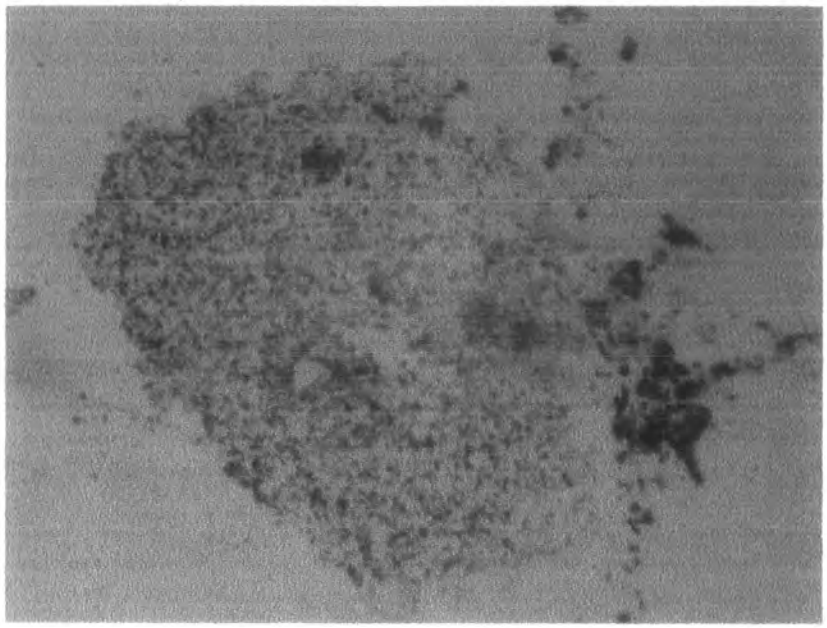

(a)

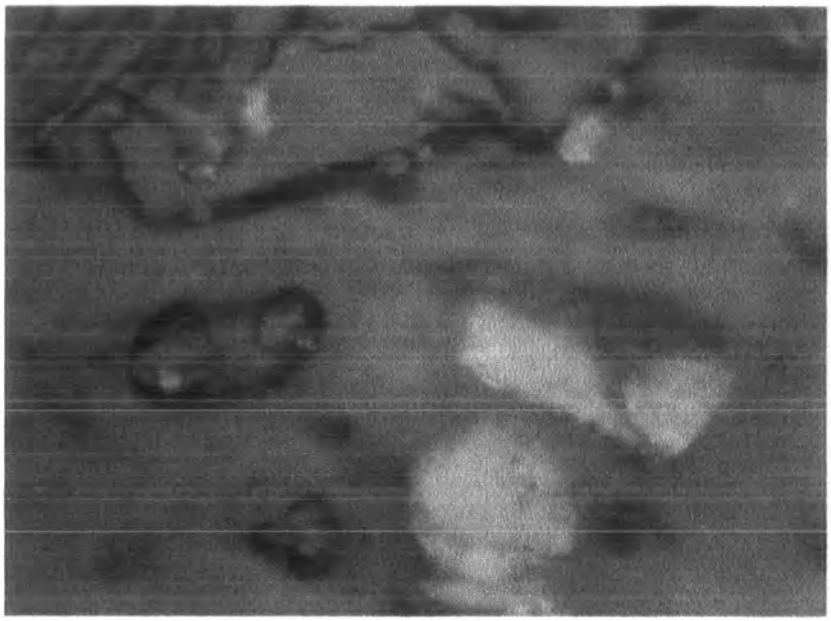

(b)

Fig.4.38 Optical microscope images of microcrystals forming in DCM waveguide film. a) ×5, b)×100, crystal size ~ 6μm.

4.7.1 Beam branching effect in DCM doped waveguide film

When light of 632.8 nm was coupled into a DCM doped PMMA waveguide film at a concentration of 5% by weight in air (~ 20°C) using either a two-prism coupler or a single

prism coupler, the single guided beam propagating in a slab waveguide film split with time into several beams (beam branching effect). This effect has also been observed in Ti:$LiNbO_3$ waveguide film.[57, 58] In experiments this effect was studied with the experimental set-up as shown in Fig.4.39.

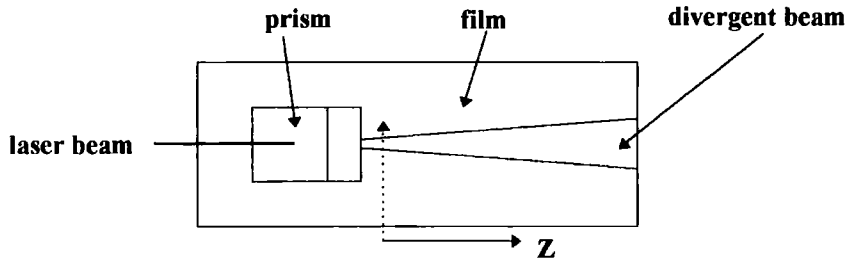

Fig.4.39 Top view of the set-up of beam branching study

As the beam split gradually, the subbeams continued to split, which induced more new beams to grow and led to the beam further spreading with time during irradiation as shown in Fig.4.40 and 4.41. Observing at a distance of about 6 mm from the edge of the in-coupling prism (z=0), it was found that the beam branching effect took place within 2 minutes as the sample film was exposed to radiation (6 mW, TM_0 mode), a multibeam structure was formed, and the whole beam became divergent.

At this position the beam was scanned by a Hamamatsu camera at regular intervals (0, 2, 5, 10, 15, 30, 60 mins), the beam profiles were recorded as a function of time and distance along the beam (z direction) as shown in Fig.4.42 and 4.43. It is seen from these two figures that the intensity distribution of the beam bundle is an approximately Gaussian distribution just at the beginning of irradiation. Several peaks become visible and the beam begins to split 2 minutes later, and the intensity of the beam decreases. With exposure for an extended time, many new peaks (new branchs) appear and their power distribution changes with time, the intensity of the whole beam decreases dramatically, the beam spreads and diverges.

Along the splitting beam, these peaks separate because of beam divergence, the subbeams become more clear, the intensity of beam drops greatly and the beam expands even wider, eventually the total width of the beam disappears in the background.

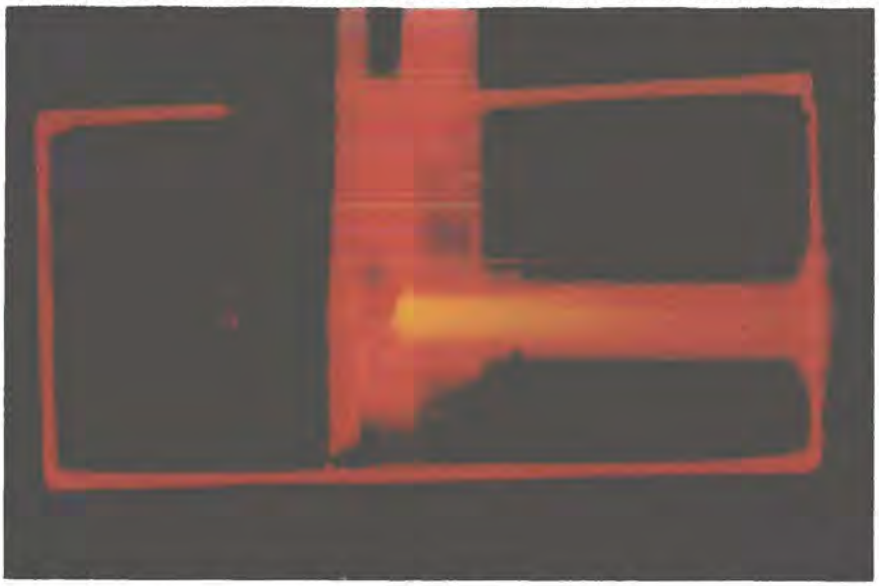

Fig.4.40 Beam branching effect forming in DCM waveguide film within 2 mins.

Fig.4.41 Beam branching effect in DCM waveguide film after irradiation for 30 mins.

Beam branching in DCM doped waveguide films has been studied by several authors.[59 - 61] A mechanism has been proposed that the branching effect is caused by upconverted photodegradation leading to an optical beam splitting into multiple beams. From DCM's fluorescence spectrum, it can be seen that an intensive upconverted fluorescence exists within the band (±100 nm) around the 598 nm peak when the film is irradiated by cw 632.8 nm. The upconverted light will induce photodegradation in a DCM doped waveguide film and this is confirmed by degradation experiments at 514.5 nm here. It was observed in experiments that a trace of yellow coloured emission appears across the sample film when a guided mode was excited by 632.8 nm.

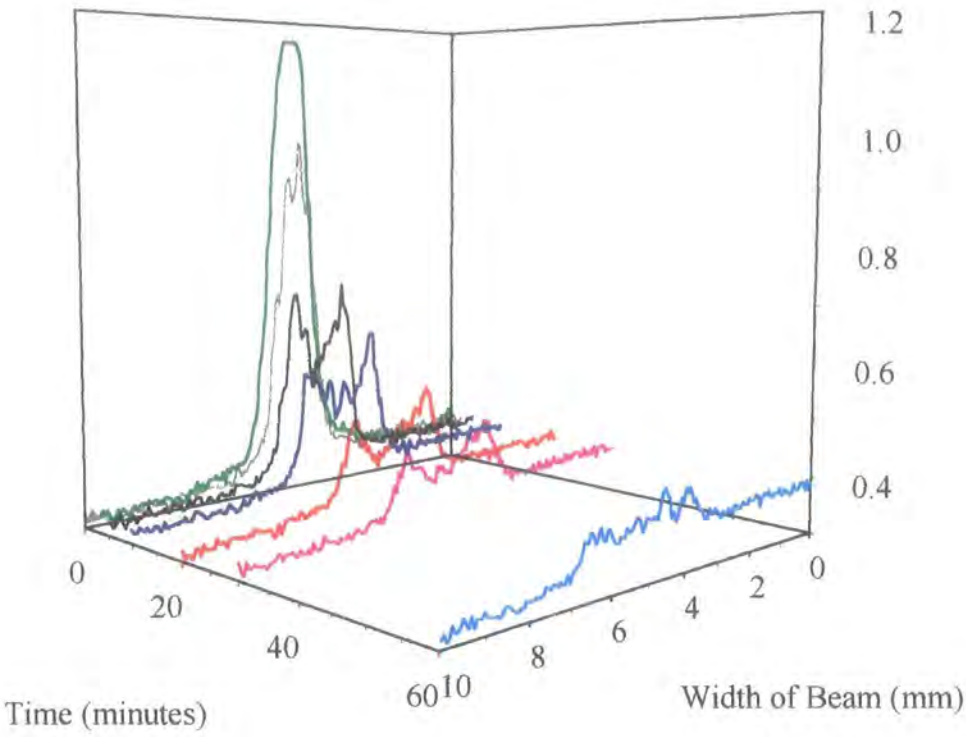

Fig.4.42 Profiles of beam branching at different times at ~ 6 mm away from the edge of the in-coupling prism.

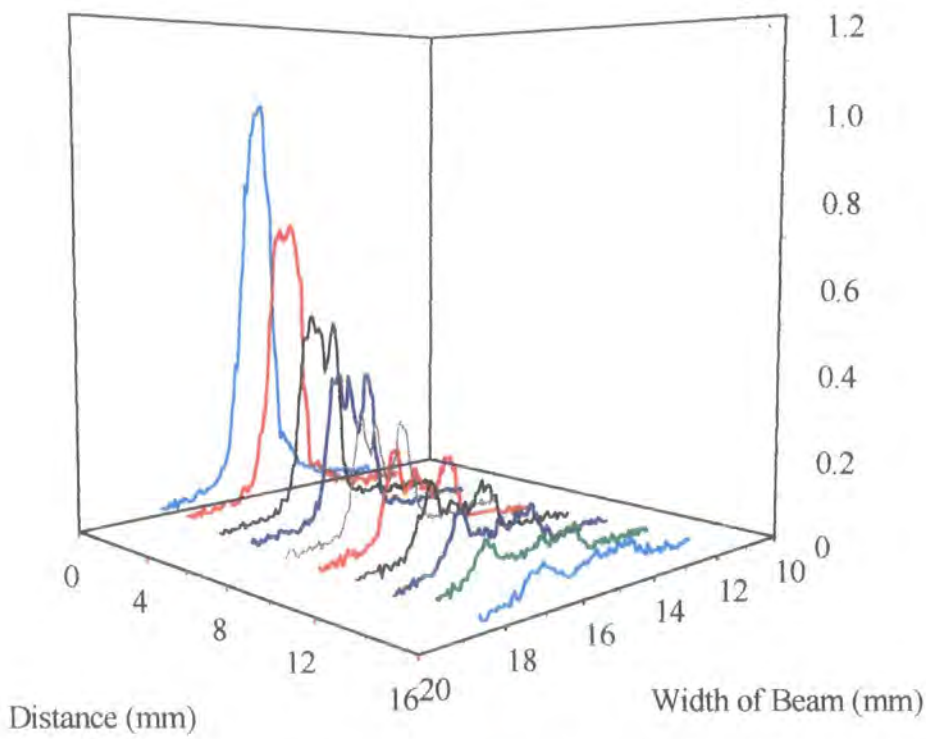

Fig.4.43 Beam profiles along the guided beam (TM_0) in the film after exposure of light (632.8 nm) for 30 minutes.

Thus, the beam branching effect of DCM doped waveguide films is caused mainly by upconverted photodegradation, and combined with strong scattering from microcrystals aggregating in the film. The degradation induces a permanent decrease of refractive index of the sample film and reduction in the colour of the film. The upconverted photodegradation occurs both in air and in vacuum environments, the only difference is that the rate of degradation is much slower under vacuum.

4.8 Summary

Photostabilities of the DEMI-series materials and the yellow materials were investigated in different environments (air or vacuum) at different wavelengths which is within their main absorption band or outside it. Their wavelength dependence of photodegradation was also studied, their B parameters were measured in experiments. As samples of organic semiconductors, it is found that degradation mechanism of the DEMI-series materials is photooxidation. The photostabilities of Dicyclohexyl-DEMI is the highest, then Ultra-DEMI and DEMI. The DCM's degradation mechanism is also photooxidation. However, the degradation mechanism of Mor2 and Morpip is direct photodecomposition by free radicals in the polymer system, the photostability of Morpip is slightly better than that of Mor2. These data supply a better understanding of photodegradation process in organic polymer system and their characterisation, and will be helpful to improve their structure, performance and photostabilities. It is also found that oxygen plays a very important role in the photodegradation of organic materials from this research. An oxygen free environment or system will increase their photostabilities dramatically, this will help to stabilise or improve these organic materials in polymer systems. During this investigation, beam branching effect of DCM doped polymer film is studied also.

4.9 References

1. Taehyoung Zyung and Jang-Joo Kim, *Photodegradation of poly(p-phenglenevinylene) by laser light at the peak wavelength of electroluminescence*, Appl. Phys. Lett., **67** (23), 3420-3422 (1995).
2. M. A. Mortazavi, H. N. Yoon, and C. C. Teng, *Optical power handling properties of polymeric nonlinear optical waveguides*, J. Appl. Phys., **74** (8), 4871-4876 (1993).
3. R. S. Moshrefzadeh, D. K. Misemer, M. D. Radcliffe, C. V. Francis, and S. K. Mohapatra, *Nonuniform photobleaching of dyed polymers for optical waveguides*, Appl. Phys. Lett., **62** (1), 16-18 (1993).
4. Karl W. Beeson, Keith A. Horn, Michael McFarland, *Polymeric materials for guided-wave devices*, SPIE **Vol.1337**, Nonlinear optical properties of organic materials III (1990), 195-202.
5. Theodor Tamir (Ed.), Guided-wave optoelectronics, Springer-Verlag, 1990.
6. R. A. Norwood, D. R. Holcomb and F. F. So, *Polymers for nonlinear optics: Absorption, two-photon absorption and photodegradation*, Nonlinear optics, **6**, 193-204 (1993).
7. W. J. Tomlinson, *Phase holograms in photochromic materials*, Appl. Phys., **11** (4), 823-831 (1972).
8. Lawrence A. Hornak, Polymers for lightwave and integrated optics, Marcel Dekker, Inc., 1992, Chapter 5.
9. Reference 8, Chapter 1 and 2.
10. Roberto Sastre and Angel Costela, *Polymeric solid-state dye lasers*, Adv. Mater., 7 (2), 198-202 (1995).
11. K. M. Dyumaev, A. A. Manenkov, A. P. Maslyukov, et al., *Dyes in modified polymers: problems of photostability and conversion efficiency at high intensities*, J. Opt. Soc. Am. B, **9** (1), 143-151 (1992).
12. A. Costela and I. Garcia-Moreno et al., *Laser performance of coumarin 540A dye molecules in polymeric host media with different viscosities: From liquid solution to solid polymer matrix*, J. Appl. Phys., **83** (2), 650-660 (1998).

13. Edward T. Knobbe, Bruce Dunn, et al., *Laser behaviour and photostability characteristics of organic dye doped silicate gel materials*, Appl. Opt., **29** (18), 2729-2733 (1990).

14. C. C. Teng, *Travelling-wave polymeric optical intensity modulator with more than 40 GHz of 3-dB electrical bandwidth*, Appl. Phys. Lett., **60**, 1538-1540 (1992).

15. Ch. Bosshard, K. Sutter, Ph. Pretre, et al., Organic nonlinear optical materials, Amsterdam: Gordon and Breach Science Publishers, 1995, p181.

16. T. E. Van Eck, A. J. Ticknor, et al., *Complementary optical tap fabricated in an electro-optic polymer waveguide*, Appl. Phys. Lett., **58** (15), 1588-1590 (1991).

17. Reference 8, Chapter 16.

18. Reference 15, p90.

19. Jeffrey I. Steinfeld, Molecules and radiation, An introduction to modern molecular spectroscopy, 2nd Edition, The MIT Press, p23.

20. Andrew Gilbert and Jim Baggott, Forword by Peter J. Wagner, Essentials of molecular photochemistry, Blackwell Scientific Publications, Oxford, 1991, p65.

21. Carol E. Wayne and Richard P. Wayne, Photochemistry, Oxford university press, 1996, p10.

22. Jan F. Rabek. Photodegradation of polymers, Springer 1996, p52.

23. Yasuhiro Hida, and Saburo Imamura, *Influence of temperature and humidity change on optical waveguide circuits composed of deuterated and fluorinated methacrylate polymers*, Jpn. J. Appl. Phys., Part 1, **34** (12A), 6416-6422 (1995).

24. Yasuhiro Hida, and Saburo Imamura, *Moisture-induced drift in thermo-optic phase shifters composed of deuterated and fluorinated methacrylate polymer waveguides*, Appl. Opt. **36** (27), 6828-6837 (1997).

25. Marek Szablewski, *Novel reactions of TCNQ: Formation of zwitterions for nonlinear optics by reaction with enamines*, J. Org. Chem., **59** (5), 954-956 (1994).

26. Marek Szablewski, Philip R. Thomas, et al., *Highly dipolar, optically nonlinear adducts of tetracyano-p-quinodimethane: Synthesis, physical characterisation, and theoretical aspects*, J. Am. Chem. Soc. **119** (13), 3144-3154 (1997).

27. Reference 18, chapter 1-3.

28. D.S. Chemla and J. Zyss, Nonlinear optical properties of organic molecules and crystals, Vol. 1, Chapter II-1.

29. G. H. Cross, D. Bloor, et al., *High dipole, high β molecules with blue window transparency*, SPIE **Vol. 2285**, 11-16 (1994).

30. G. H. Cross, D. Bloor, and Marek Szablewski, *'Blue window' organics for frequency doubling devices*, Nonlinear optics, **14**, 219-223 (1995).

31. Jason C. Cole, Judith A. K. Howard, Graham H. Cross, Marek Szablewski, *(Z)-{4-[1-Cyano-3-(diethyliminio)-1-propenyl]phenyl}-dicyanomethanide, a novel 'blue window' zwitterionic molecule for nonlinear optics*, Acta crystallographica, Sect. C, 715-718 (1995).

32. Roland Dietrich, Klaus Meerholz, et al., *Phase-matched second-harmonic generation due to anomalous dispersion: tailoring of the refractive indices in three-component systems*, Chemical Physics Letter, **280**, 119-126 (1997).

33. Y. Kagawa, *New tetracyanoquinodimethane chromophores, synthesis and physical properties*, Ph.D thesis, University of Durham 1998.

34. W. Lincoln Hawkins (Editor), Polymer stabilisation, Wiley-Interscience, 1972, p159.

35. B. Ranby and J. F. Rabek, Photodegradation, photo-oxidation and photostabilization of polymers, John Wiley & Sons, 1975, Chapter 1-3.

36. W. Schnabel, Polymer degradation, Hanser International, New York, 1981, p95.

37. Norman Grassie and Grerald Scott, Polymer degradation and stabilisation, Cambridge University Press, 1985, p1 and p87.

38. J. F. Rabek, Photostabilization of polymer, Elsevier science publishers. Ltd., 1990, Chapter 1.

39. Norman S. Allen and Michele Edge, Fundamentals of polymer degradation and stabilisation, Elsevier Applied Science, 1992, p75.

40. P. R. Ogilby, M. Kristiansen, D. O. Martire, et al., *Formation and removal of singlet ($a^1\Delta_g$) oxygen in bulk polymers: Events that may influence photodegradation*, Polymer durability, 113-126 (1996).

41. Rodger D. Scurlock, Bojie Wang, et al., *Singlet oxygen as a reactive intermediate in the photodegradation of an electroluminescent polymer*, J. Am. Chem. Soc. **117**, 10194-10202 (1995).

42. Reference 36, p122.

43. Reference 22, p83.

44. K. W. Beenson, K. A. Horn, et al., *Photochemical laser writing of polymeric optical waveguides*, Appl. Phys. Lett., **58** (18), 1955-1957 (1991).

45. Lawrence A. Hornak (Eds), Polymers for lightwave and integrated optics, Marcel Dekker, Inc., 1992, Chapter 4 and 6.

46. Geoffrey A. Lindsay and Kenneth D. Singer (Eds), Polymer for second-order nonlinear optics, American chemical society, Washington, DC 1995, Chapter 28.

47. Jan Vydra, Hanno Beisinghoff, and Theo Tschudi, Manfred Eich, *Photodecay mechanisms in side chain nonlinear optical polymethacrylates*, Appl. Phys. Lett., **69** (8), 1035-1037 (1996).

48. Nadia Capolla and Roger A. Lessard, *Real time bleaching of methylene blue or thionine sensitized gelatin*, Appl. Opt., **30** (10), 1196-1200 (1991).

49. Jang-Joo Kim, Taehyoung Zyung, and Wol-Yon Hwang, *Photochemically formed refractive index profiles in nonlinear optical polymer thin films*, Appl. Phys. Lett., **64** (25). 3488-3490 (1994).

50. W. J. Tomlinson, *Dynamics of photochromic conversion in optically thick samples: theory*, Appl. Opt., **15** (3), 821-826 (1976).

51. Jiong Ma, Sihan Lin, Wei Feng, et al., *Modelling photobleached optical polymer waveguides*, Appl. Opt., **34** (24), 5352-5360 (1995).

52. James R. Sheats, James J. Diamond, and Jonathan M. Smith, *Photochemistry in strongly absorbing media*, J. Phys. Chem., **92**, 4922-4938 (1988).

53. Arnaud Dubois, Michael Canva et al., *Photostability of dye molecules trapped in solid matrices*, Appl. Opt., **35** (18), 3193-3199 (1996).

54. Arnaud Dubois, Michael Canva et al., *Enhanced photostability of dye molecules trapped in solid xerogel matrices*, Synthetic metals, **81**, 305-308 (1996).

55. I. P. Kaminow, L. W. Stulz, E.A. Chandross, and C. A. Pryde, *Photobleaching of organic laser dyes in solid matrices*, Appl. Opt., **11** (7), 1563-1567 (1972).

56. Robert M. Siverstein, G. Clayton Basster, Terence C. Morrill, Spectrometric identification of organic compounds, John Wiley & Sons, 1981.

57. H. Jerominek, R. Tremblay and C. Delisle, *Optical branching effect in photorefractive sensitive Ti:$LiNbO_3$ slab waveguides*, Journal of lightwave technology, **LT-3** (5), 1105-1109 (1985).

58. Hubert Jerominek, Claude Delisle, and Real Tremblay, *Optical branching effect in $Ti:LiNbO_3$ waveguides: near field pattern studies*, Appl. Opt., **25** (5), 732-736 (1986).

59. Anadi Mukherjee, *Two-photon pumped upconverted lasing in dye doped polymer waveguides*, Appl. Phys. Lett., **62** (26), 3423-3425 (1993).

60. Sergey Sarkisov, Abdalla Darwish, William Bryant, and Putcha Venkateswarlu, et al., *Nonlinear optical characterisation of poly (methyl methacrylate) polymer doped with different dyes for laser waveguide fabrication*, SPIE/95, **2527**, 338-349.

61. Sergey Sarkisov, Andre Taylor, Putcha Venkateswarlu, Aaron Wilkosz, *Optical branching in dye-doped polymeric waveguide*, Optics communications, **145**, 265-273 (1998).

CHAPTER 5 WAVEGUIDE SENSORS

Preface

The principle, functions and device structures of humidity sensors are presented in this chapter. Firstly sensing technology, which includes a definition, a classification and the specifications of sensors is described. Attention is focused on optical sensors and optical waveguide sensors as well as relevant techniques. A review of optical sensors, especially detailed waveguide interferometric sensors and devices containing them, optical modulation techniques as well as their advantages are presented. Secondly an extensive study and experiments on multi-layer waveguide interferometric humidity sensors undertaken is presented. This includes principles, design, waveguide fabrication, experiments and analysis. Two multi-layer waveguide sensors were studied. Special procedures and fabrication processes for multi-layer waveguide structures were developed. A new type of integrated humidity sensor with attractive properties was fabricated.

5.1 Introduction

A sensing task can be accomplished by using a variety of principles, methods, and techniques based on optical, electrical, or acoustical responses for example. Sensors are a multidisciplinary area. They involve many subjects, such as physics (phenomena and principles), electronics (signal detecting and processing), chemistry and material sciences (materials synthesis), mechanical engineering and microtechnology (producing and processing materials), system engineering and packaging; Such combinations present considerable challenges. In order to meet the increasing needs on the large quantity of information transfer and processing, developments of sensor devices and their components with a higher capacity, a higher speed, smaller size and lower fabrication cost are urgently

needed. Alongside the development of conventional electric macrosensors and microsensors by means of the miniaturisation and large scale integration in microelectronics, research into optical sensors has also been a rapidly growing.

Waveguides, particularly polymeric waveguides, offer more flexibility of the development of integrated optical sensors which leads to the possibility for point-to-point transportation of optical energy and information carried by it. Although waveguide sensors are relatively new, considerable progress has been made, opening up possibilities for economical use of disposable sensors, possible integration of 'all-optical' sensing and communication of the required information[1, 2, 3]. Many unique and potential advantages are offered by polymeric waveguide sensors. These include:

- Physical compatibility with integrated circuits, interconnection and other components with high capacity.
- High sensitivity and high information transfer capacity.
- Smaller size and light weight.
- High stability, low signal attenuation and low temperature drift.
- Elimination of electromagnetic interference.
- Explosion, ignition and corrosion safety
- Flexibility in the choice of construction materials and dimensions.
- Low-cost with mass production.

Generally a sensor can be defined as a device that receives and responds to a signal or stimulus. Its purpose is to respond to any input physical property (stimulus) and to convert it into any signal which can be detected, measured and understood. A common sensor system will include a sensor and signal detecting and processing devices as shown in Fig. 5.1 in a data process controlling unit. Sensors and actuators mean the application of intelligent electronic systems that are able to do a self-controlled communication with their environment. Roughly all sensors may be divided into passive or active. Passive sensors produce a response to an external stimulus directly. But the active sensors require an external power supply for their operation and this may affect the sensing means (physical processes). Sensors can actually be classified into many classes according to 1) materials used, 2) application field, 3) objective (stimulus) to be detected, 4) detection

means, 5) conversion mechanism[4]. The behaviour of a sensor is determined by its specification and characteristics. The main specifications of a sensor are: sensitivity, stability, selectivity, linearity, the limit of detection.

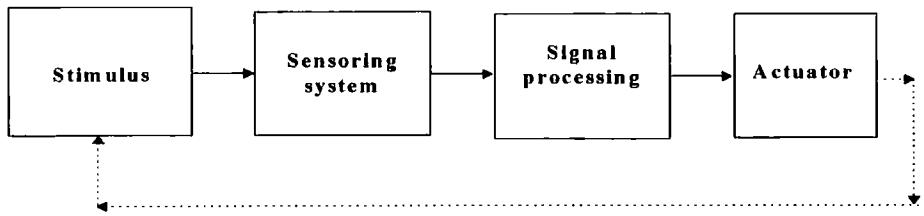

5.1 Schematic a sensor system.

5.2 Optical sensors

An optical sensor is referred to as a device which exploits light (infrared-visible-ultra-violet radiation) to detect an external variation in applications. The primary interaction between the measurand and the sensor needs not be optical, but the sensor must produce an optical output after further transduction. Light can be coherently modulated in phase, frequency, state of polarisation and either coherently or incoherently modulated in amplitude, which gives a variety of methods to modulate light for optical sensors. Since optical sensors can be made in more compact structures with the development of integrated optics and optical fibre technology, and can be operated at a lower voltage, optical sensing methods provide a sensitive and safe means of sensing in chemical sensor, humidity sensor and displacement sensor applications to detect the changes in physical or chemical parameters.[39-41] This is particularly true when combined with other techniques or methods, such as interference technique, evanescent field and surface plasmon generation, where very small changes of displacement, refractive index, disturbances of temperature and vibration can be detected. Optical sensors normally consist of three parts. 1) The light source, 2) The sensing part (modulating structures or agent), 3) A detector or receiver, as shown in Fig. 5.2. Light sources and detectors are electro-opto components that can be controlled and selected in a particular application according to the wavelength range of operation, required spectral line width, incident threshold or damage power, loss, wavelength selectivity; and sensitivity. Signals and information obtained can be displayed and processed by detectors, cameras and computers, and can lead to a convenient output (digital or visual) for the user. The central part of an optical sensor is its sensing part.

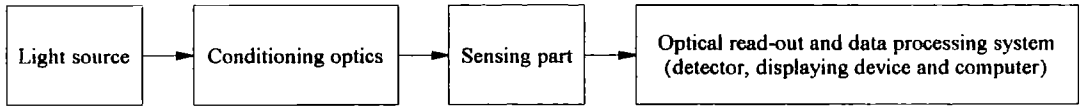

Fig. 5.2 A scheme of a optical sensor system

In the following sections the principles and classification of optical waveguide sensors (particularly waveguide interferometric sensors) are given in detail. Optical fibre sensors have similar principles and classification, more information can be found in other references.[1, 5-8]

5.2.1 Waveguide interferometric sensor

There are two classes of optical waveguide sensors according to the role of waveguides in the sensor. One class is intrinsic, the another is extrinsic.

1) Intrinsic sensors, in which light is modulated in response to the measurand when it is being guided along the waveguide. The waveguide itself plays an essential role in the modulation. The environment disturbs the propagation of light within the waveguide in a measurable way.

2) Extrinsic sensors, in which the waveguide is only used as an easy means to transport light to and/or from a sensing region, light is modulated in polarization, wavelength, phase or intensity in a separate zone. Modulation is based on optical principles, but is not a wavguide property. their configurations are indicated in Fig. 5.3.

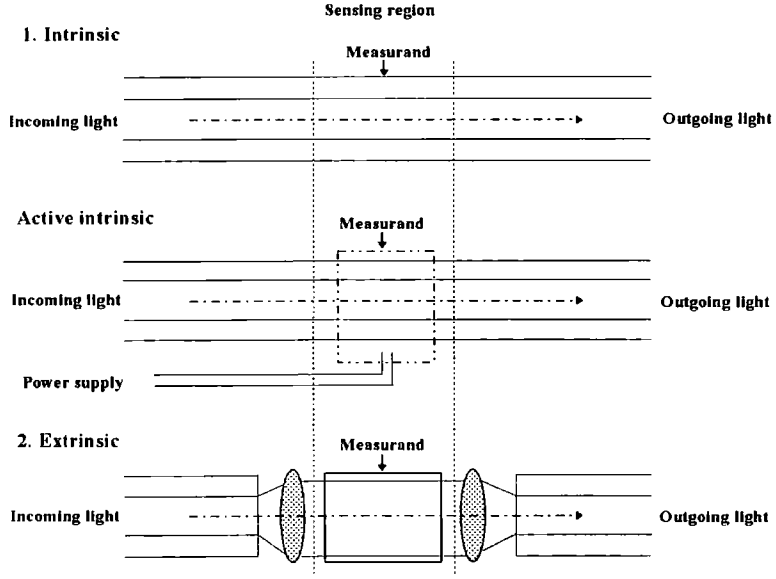

Fig. 5.3 Configuration of waveguide sensor

Interferometry is a very sensitive method used for the measurement, testing and detection in applications. Measurands can be displacement, refractive index, length and irregularity of a surface. Interference occurs when more than two coherent beams of light from a source meet following more than one path. Interference fringes (intensity distributions) are observed in the area where these light beams overlap. Once the phase and/or intensity of a coherent optical beam from any path varies, the position and visibility of the fringe will change. So in principle, any variation in phase or intensity caused by a variety of disturbances, such as vibration, fluctuation of the refractive index, temperature and intensity, can be detected by interferometric methods. Interferometers are vital and common elements in optical systems because they can measure very small changes (about $10^{-4} \sim 10^{-6}$) in optical index and any tiny displacement (about 10^{-7}), therefore they are widely used in sensor applications. Some waveguide interferometers have been built as optical sensors used to do measurements, their operation is based on the optical interference between a reference and a sensitive lightwave.

1) The integrated Mach-Zehnder interferometer sensor:[9,10]

The interferometer consists of two-Y-branches shown in Fig.5.4. Light is coupled into the waveguide and is split into two parts at a Y-branch, where one is guided in one branch (reference) and another is guided in the measuring branch exposed to the environment or covered with a sensing material for a certain length. Two beams of light finally combine at another Y-branch where they interfer and couple out from the waveguide.

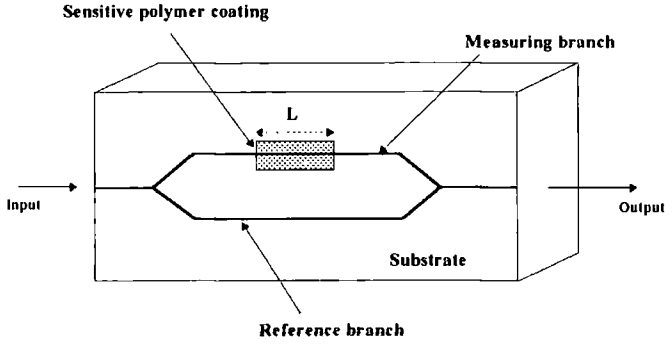

Fig. 5.4 Schematic of a waveguide Mach-Zehnder interferometer

Light is modulated in phase when it travels across the measuring branch where part of the branch (L) interacts with external stimulus. However the rest of the waveguide is optically

and chemically isolated from its surrounding environment completely. The modulation is caused by some external stimulus that is directly related to the physical quantity to be monitored. Sensitive materials can be used to cover part of the measuring branch aimed to detect a specific substance. One can detect a variation in the output intensity that results from a change in the difference of optical path or phase between the two branches.

$$I_{out} = \eta\left[1 + \cos(\theta_0 + \Delta\theta)\right]I_{in} \qquad (5.1)$$

Where I_{in} is input intensity, I_{out} is output intensity, η is a constant related to waveguide coupling efficiency and Y-branch coupling efficiency, θ_0 is intrinsic phase relevant to the waveguide and Y-branch coupler, $\Delta\theta$ is phase change caused by the interaction between the measurand and the guided light.

A variation of the output intensity can also be caused by the fluctuation of the light source in this case. An improved Mach-Zehnder interferometer was proposed to obtain an interference pattern,[11, 12] in which both the sign and the optical phase shift can be measured by monitoring the interference fringes.

2) The Reflecting interferometer sensor[13]

The waveguide structure is irradiated by a white light beam from a side of substrate. Light is partially reflected at waveguide/polymer and polymer/air interface, respectively. The superposition of these two partial beams reflected at parallel interfaces is analysed by interferometry shown in Fig. 5.5.

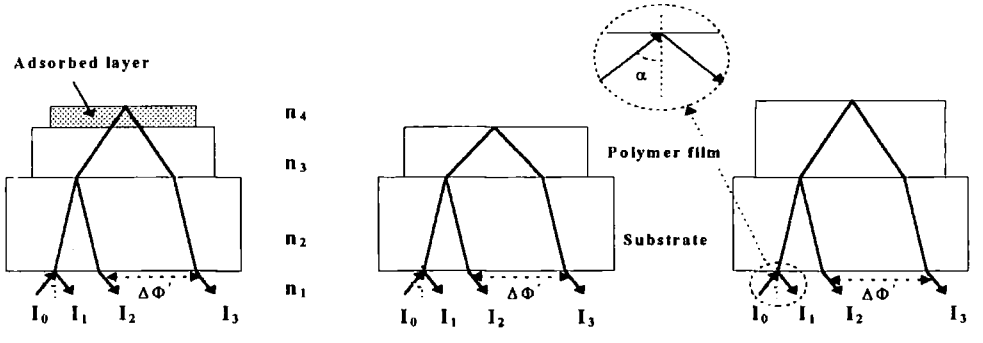

Fig. 5.5 Set-up of reflection interferometer

The interference intensity is

$$I = I_1 + I_2 + I_3 + 2(I_2 I_3)^{\frac{1}{2}} \cos\left[\frac{4\pi}{\lambda}\frac{n_3 d}{\left(1-\frac{n_2^2}{n_3^2}\sin\alpha\right)^{\frac{1}{2}}}\right] \quad (5.2)$$

Their interference pattern can be affected either by swelling of the film caused by permeation of gas or liquid, or by adsorption of molecules of gas or liquid on the top of the film which will introduce an additional reflection. Besides the variation of optical pathlength, the refractive index of the polymer will change because of the interaction between analyte with polymer film.

3) The Young's interferometer sensor[14]

This interferometer is based on the Young's and Mach-Zehnder interferometer as shown in Fig.5.6. It is composed of one Y-branch and two branches, a reference and a measuring branch. The incoming light is divided into two parts guided along the two branches with separation d. Light is modulated when the measuring branch interacts with the measurand, and a phase shift appears in the branch where part of it is exposed or covered by sensitive polymer film. The light is coupled out from both branches and interferes with each other. The output is monitored by a CCD array and the intensity distribution on the array is

$$I = 1 + \cos(\phi - \delta) \quad (5.3)$$

Where $\phi = \frac{2\pi}{\lambda_0}\frac{nd}{f}x$, n here is effective refractive index, δ is additional phase shift caused by refractive-index change.

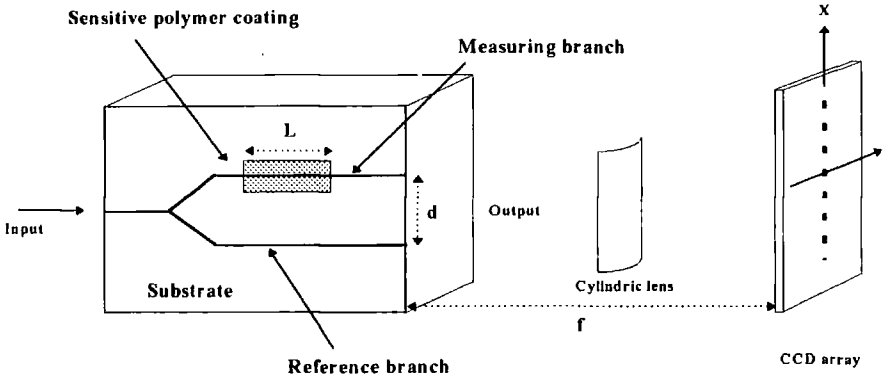

Fig. 5.6 Sketch of Young's interferometer sensor

The spatial period of the fringes (L) is

$$L = \frac{f\lambda_0}{nd} \tag{5.4}$$

n is refractive index. The phase shift resulted from refractive-index variations of the measurand can be obtained by monitoring the interference fringes.

5.2.2 Optical chemical and biochemical sensors[15-18]

Chemical sensors are the area of most active research. Since a chemical sensor is a transducer which provides direct information about the chemical composition of its environment, the need for smaller and easily calibrated chemical sensors is increasing for on-line control of chemical gas mixtures and toxic substances in industry and in environmental protection. Most chemical sensors consist of structures containing the sensitive material which is normally designed for sensing one particular chemical. Optical chemical and biochemical sensors take advantage of the effect of chemical or biochemical reactions on optical phenomena, chemical information can be obtained by means of monitoring the changes in selected optical properties (e.g. absorption, radiation or luminescence) of materials or the medium surrounding them when sensors are subjected to these chemical materials (e.g. gas, liquids).

Waveguide chemical sensors can be built incorporated with interferometer,[12, 13] evanescent field,[19, 20] or surface plasmon[24] techniques or phenomena, where waveguide properties are influenced by the presence of a chemical species and the changes of optical properties may be induced by the following effects:(1) attenuation of the guided light amplitude, (2) variation of the effective refractive index of the mode, (3) modification of the polarisation of the light.

5.2.3 Optical surface plasmon resonance sensor (OSPRS)

The OSPRS is based on the surface plasmon phenomenon.[21, 22] A typical configuration of this sensor is a thin metal film on the dielectric layer (measurand) as shown in Fig.5.7. A prism with higher refractive index n_1 is used to couple light into the metal layer to excite the surface plasmon.

When the wavevector (k_x) of the incident light (wavelength λ) parallel to the surface of the dielectric film equals that of the surface plasmons (k_{sp}) in the metal film, the phase matching condition is reached,

$$\frac{2\pi}{\lambda} n \sin\theta = k_{sp} = \frac{2\pi}{\lambda}\left(\frac{1}{\varepsilon_2} - \frac{1}{\varepsilon_m}\right)^{\frac{1}{2}} \tag{5.5}$$

Where θ is the angle of incident light at resonance, ε_m is the real part of dielectric constant of the metal at a given frequency and ε_2 is the dielectric constant of material with lower index.

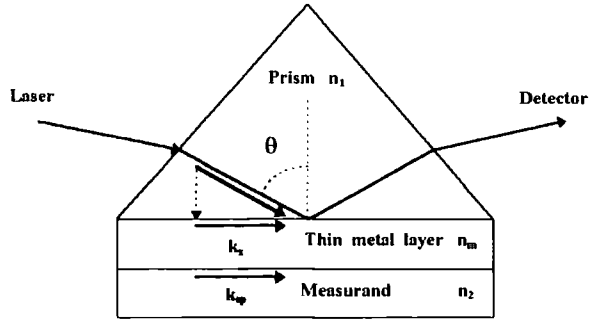

Fig. 5.7 A diagram of surface plasmon arrangement

A surface electromagnetic mode is excited and propagates along the metal/ dielectric layer interface, the energy of the incident light will be coupled into the surface plasmon, the reflected light at the metal/dielectric layer interface will be be attenuated. As a result, the reflected light monitored drops sharply to a minimum at this resonance angle. Because of the lossy character of the metal layer, the surface plasmon is quickly attenuated and dissipated by the metal layer, and the coupling is spread over a small θ interval. The tip of lowest level of reflection (at the resonance angle) will shift as a consequence of the changes in the properties of the sample (dielectric constant).[23, 24] The typical angular resolution is better than 5×10^{-2} degree.[25]

5.3 Optical modulation techniques

Optical modulation techniques are based on the changes of various properties of light which are influenced by the measurand, such as intensity, phase, polarisation, frequency, emission and reflection.. Here the common ones are introduced. Very often more than one type of modulation technique may be employed in a sensor, but the exact considerations in applications for these techniques are different.

1) Intensity modulation

This is defined as the monitoring of the variations of the output light from a sensor with respect to the measurand. It is widely used in many sensors because of its reliability, simplicity, and low cost.[26] However this technique is susceptible to the drift caused by intensity changes in the light source, variation of absorption or scattering in the waveguide and connectors, sensitivity changes of detectors. One reference signal obtained from different techniques is needed to automatically compensate for drifts and to eliminate these variations.[7]

2) Phase modulation

Phase modulation is another commonly used, but indirect modulating technique. Generally it is required in cooperation with other means or devices to convert the phase modulated signal into an intensity-modulated signal for measurement. These phase changes associate with changes of refractive index and optical-path-difference, such as phase shifts of $10^{-4} \sim 10^{-7}$ radians can be detected by interferometric techniques. Phase modulation is a little more complicated compared with the intensity modulation. A fluctuation of wavelength in the light source may cause an undesired phase shift. If measurements are made using interferometers, intensity output may be ambiguous because of its period of sinusoidal signal, the order of interference is not readily obtained. The coherence length of the light source will limit its usage.

3) Polarisation modulation

Polarisation modulation is a useful technique for encoding and decoding the measurand. Its operating principle is that the physical quantity to be measured is converted into a polarisation change, where appropriate effects (e.g. electro- or elasto-optical effects) are utilised to implement the conversion. Sensors based on this modulation are used in measuring stress and temperature. Examples of polarisation sensors can be found in references 27, 28.

4) Wavelength modulation

Wavelength modulation is another concept used in sensing. It utilises the wavelength shift from reflected or transmitted light to detect the measurand. A sensor using wavelength modulation has a wide-band light source, a transducer to encode wavelength depending on its external perturbation, a form of spectrometer (prisms, gratings, or filters) to decode the light and give the appropriate output. This modulation [29, 30] is more complicated than other ones. Errors can be introduced from wavelength fluctuations of the light source as result of changes in temperature or unstability of voltage or current in the power supply. The output from the modulation is less susceptible to loss variations in the device and connectors. The achievable resolution of this kind of sensor depends on the characteristics of the detector (single photodiode or array), and the inherent resolution of the spectrometer.

5.4 Diffusion into polymer materials[31]

Generally speaking, polymers are water and gas resistant macroscopically. Very often they are used as a protecting or packaging material to act as a barrier to vapours and gases. But actually the microstructure of polymers is not so dense, there are some spaces between their molecules. Some microvoids or pores still remain in the polymer, the film will be porous in the case of very thin film. For these reasons, polymers have the ability to absorb a certain quantity of vapour molecules. When there is a partial pressure difference of vapour or gas between the inside and the outside of polymer. the vapour molecules (e.g. water) or gases (e.g. O_2, N_2, etc.) can pass through the air/polymer or polymer/polymer interface and go into the polymer by following two processes: 1) vapour goes into polymer through micropores if film is porous; 2) vapour molecules are adsorbed on the surface of the polymer, then followed by diffusion into the polymer film. The diffusion strongly depends on the size and the shape of the vapour molecules. The diffusion process and quantity of vapours or gases adsorbed differs from polymer to polymer (and gas to gas) because of structural differences.

The diffusion of small molecules (vapours, liquids or gases) occurs by movement of these molecules from one microvoid to another in the polymer. In a microporous polymer film, its refractive index may be written as,[15]

$$n = qn_m + (1-q)n_p \tag{5.6}$$

where q (<1) is the volume fraction of the polymer matrix, n_m is the refractive index of the matrix (polymer) and n_p is the refractive index of the medium (e.g. water or gas) in the pores. When the film is exposed to vapour like water vapour, water molecules will enter the film and fill part of the micropores inside the film, then its index is given by

$$n = qn_m + (1-f)(1-q)n_A + f(1-q)n_W \tag{5.7}$$

where n_A and n_W are the refractive index of air and water respectively. f (<1) is the volume fraction of micropores taken by water molecules. Depending on the filling of the pores with water, n_p can vary from $n_A \cong 1$ (air) to $n_W = 1.33$ (water). This variation leads to an index change of the film by

$$\Delta n = f(1-q)\Delta n_p \tag{5.8}$$

where (1-q) is the relative pore free volume and Δn_p is the change in refractive index inside the pores, $0 < \Delta n_p \leq 0.33$. The more volume the water molecules take (f increases), the larger the increase of the polymer refractive index as shown in Fig.5.8 according to equation 5.8.

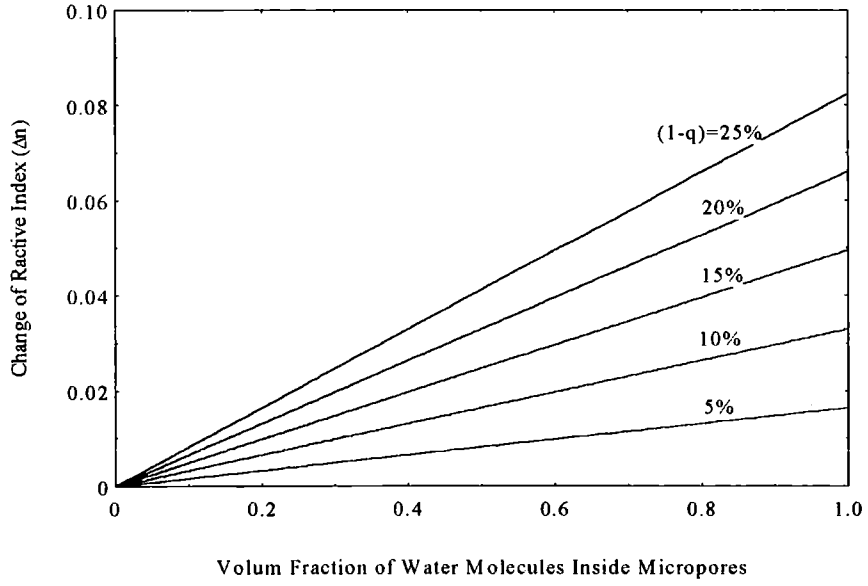

Fig.5.8 Changes of refractive index induced by water molecules inside a polymer

The amount of water taken in by a glassy polymer depends in part on the concentration of hydrophilic groups in the polymer and their accessibility. Water may also be accommodated during the processing of the film. The absorption of water by polymers can also lead to expansion or swelling. However the capacity for swelling varies considerably from polymer to polymer. In some polymers it is significant, in others it can be ignored. Even small volume changes can lead to voids or microcrack formation inside the polymer, which may lead to an increase of diffusion and uptake of water. If the effect

of volume expansion can be ignored, the water vapour diffusion will only induce a change (increase) in its refractive index. If the effect cannot be ignored, but is small, the index of the polymer will still increase during volume expansion. The refractive index will decrease rather than increase, when the increase in the index induced by diffusion is over compensated by the reduction of density caused by the volume expansion.

The absorption of water vapour is very important for a polymer used as humidity sensing material, which dominates the change of refractive index of polymer (Δn). The Δn in turn induces a phase shift in a humidity sensor. The phase shifts are directly proportional to the quantity of water which the polymer absorbed and hence concentration of water in the vapour phase.

5.5 Slab waveguide interferometric sensors for humidity

Atmospheric water content is becoming an increasingly important concern in industry. Humidity control and monitoring is required not only for human comfort, but also in a broad range of application areas, integrated circuits (IC) packages, medical services and textiles. The measurement of humidity has always been a difficult problem, especially at very low concentration levels (<100 ppm), because of its being easily affected by other parameters, e.g. temperature or gaseous component in the air. Stable, reliable and low-cost humidity sensors with fast response time are needed in some fields. The successive deposition on a substrate of films with differing refractive indices enables stacked waveguide structures to be formed. This could enable interferometers to be fabricated with interference taking place between layers. This type of structure has been used in the applications, such as making optical IC elements[32] and a coupling wave optical waveguide sensor.[33]

The polymer waveguide interferometric humidity sensor is based on the principle that the polymer's absorbing and desorbing water molecules leads to a change in refractive index as the ambient relative humidity increases or decreases. The induced phase shifts of modes in an optical waveguide are determined by measuring interference fringe shifts when water molecules enter the waveguides. The longer interaction length, higher sensitivity, easier fabrication and detection of this waveguide interferometric humidity sensor are its main

advantages over other humidity sensors.[42-43] The porosity of the polymer and the absorbance of polymer to water is vital to obtain a large phase change and a rapid response. A good humidity sensor should be stable, reversible, reproducible and low-cost, and should have high sensitivity, good selectivity, and linearity of response.

5.5.1 Young's two beam interferometric theory

Historically Thomas Young's experiment[34] first illustrated true light interference. Consider the configuration of the experiment shown in Fig.5.9 .

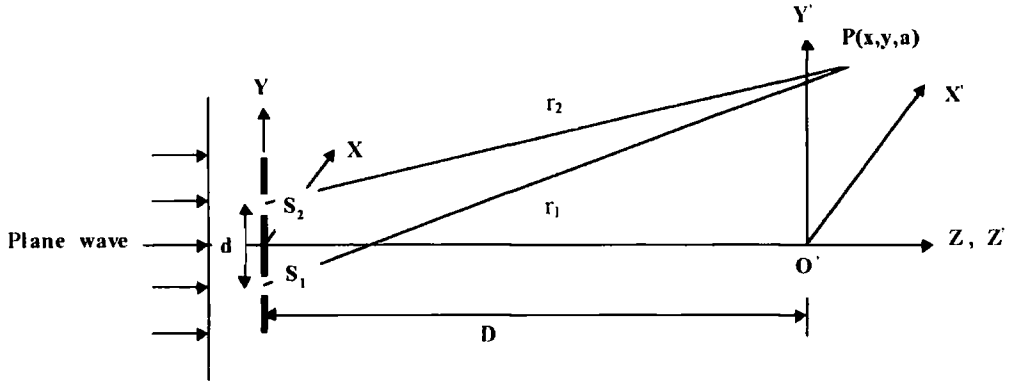

Fig. 5.9 The geometry of Young's experiment

A plane monochromatic wave (e.g. a laser beam) passes through 2 slits s_1 and s_2 with separation d, the width of each slit is small or in the same order of the wavelength used. Two diverging cylindrical waves are formed and spread out through each slit as secondary sources. These series of cylindrical waves come out overlapped in the region where they meet and interfere with one another. A screen or a photo-detector at $Z = D$ is placed at this point and interference fringes can be observed. Two cylindrical fields with the same amplitude can be expressed as the following scalar equations to make the problem simple.

$$E_1(r_1,t) = \frac{A_0}{\sqrt{r_1}} e^{i(kr_1-\omega t+\varphi_1)} = A_1 e^{i(kr_1-\omega t+\varphi_1)} \tag{5.9}$$

$$E_2(r_2,t) = \frac{A_0}{\sqrt{r_2}} e^{i(kr_2-\omega t+\varphi_2)} = A_2 e^{i(kr_2-\omega t+\varphi_2)} \tag{5.10}$$

where A_0 is the amplitude of each cylindrical wave, ω is the frequency of the wave, k is the free space wavenumber; φ_1 and φ_2 are the phase of these two waves, r_1 and r_2 are the travelled distance from each slit to the point P on the screen, respectively. The total optical field in the far field is then the sum of two cylindrical waves from slits,

$E_{total}(\rho) = E_1(\rho_1) + E_2(\rho_2)$. The time averaged intensity of the field at the point P(x,y,a) on the screen is then obtained by the interference of these two fields,

$$I_{total}(\rho) = E_{total}(\rho)E^*_{total}(\rho) = [E_1(\rho_1) + E_2(\rho_2)][E^*_1(\rho_1) + E^*_2(\rho_2)] \quad (5.11)$$

and

$$I_{total} = A_1^2 + A_2^2 + 2A_1A_2\cos[k(r_1 - r_2) + (\varphi_1 - \varphi_2)] \quad (5.12)$$

For a far-field interference in an observation plane ($Z = D$), the point P(x,y,D) is sufficiently far from s_1 and s_2, that the distances r_1 and r_2 can be thought nearly as equal, so that the amplitude $A_0(x,y,D)$ of the two cylindrical waves on the screen is effectively the same, $A_1 = A_2$ or $I_1 = I_2 = I_0$. And $\varphi_1 - \varphi_2 = 0$, provided that two cylindrical waves are in phase at $Z = 0$, when $t = 0$. The point P(x,y,a) is in the vicinity of the centre (O') of the screen ($d << D$ and $(x')^2+(y')^2 << D$). We have

$$I_{total} = 4I_0\cos^2\frac{\delta}{2} = 2I_0(1+\cos\delta) = 4I_0\cos^2\frac{1}{2}[k(r_1 - r_2) + (\varphi_1 - \varphi_2)] \quad (5.13)$$

The phase difference is

$$\delta = k(r_1 - r_2) \quad (5.14)$$

Maxima (bright fringes) occur when

$$\delta = 2\pi m \qquad \text{or} \qquad r_1 - r_2 = m\lambda \quad (5.15)$$

provided that m=0, ±1, ±2,..... Similarly, minima (dark fringes) occur when

$$\delta = \pi(2m+1) \qquad \text{or} \qquad r_1 - r_2 = \frac{(2m+1)}{2}\lambda \quad (5.16)$$

Now consider the point P(x,y,a) in the $Y'O'Z'$ plane, all the plane parallel to yoz plane will have same situation under the approximation above. Noting that $y \cong \theta d$ and $\sin\theta \cong \theta$ when θ is small, therefore we have

$$r_1 - r_2 = \frac{d}{D}y \quad (5.17)$$

the position of the *m*th maximum point is

$$y_m = \frac{D}{d}m\lambda \quad (5.18)$$

From here we know a series of maxima are the points situated at Y' axis with same separation ($D\lambda/d$) from one another in yoz plane. So the interference fringes in the observation plane at $Z = D$ ($X'OY'$ plane) are a set of straight lines parallel to the X' axis and one another. The central fringe (X',O,D) is a bright one. The separation of two

consecutive maxima or minima (Δy) in the observation plane is determined by the original separation of the aperture (d), and the distance to the observation plane (D)

$$\Delta y = \frac{D}{d}\lambda \tag{5.19}$$

The spatial distribution of Young's fringes is decided by the optical phase differences between the distance from the two slits to the observation point. The phase shifts, and more specifically, changes of refractive index (negative or positive) in the path r_2 can be determined by monitoring the direction of fringes movement (up or down), and calculating the fringe shifts.

5.5.2 Structure, material and modelling

A multi-layer waveguide system is chosen to form an integrated Young's interferometer with two guiding layers with higher refractive index separated by a polymer layer with lower index. Modes are excited and propagate along the guiding layers, when coherent light is cast into the waveguide. Two diverging beams are produced and spread out at the output facet from the structure, they overlap and interfere with each other. A stable, clear interference pattern (Young's fringes) is obtained on a screen or a detector which is situated far enough from endface of the interferometer (far field interference pattern).

Firstly a 5-layer symmetric waveguide, PMMA/P-4VP/PMMA/P-4VP/PMMA (structure P4VP-I) was chosen. Two commercially available polymers, poly(4-vinylpyridine) (P-4VP), and poly(methyl methacrylate) (PMMA), were chosen as the guiding layer and cladding layer, respectively. Both PMMA and P-4VP are amorphous and optically homogenous, they are characterised by a very high optical transparency which leads to their use as waveguide materials.

The main purpose in employing a symmetric structure is to try to obtain equal mode intensities propagating in each guiding layer and therefore to achieve maximum contrast of fringes which will be crucial to measurements and detection. Once the choice of polymers used for the waveguide is made, the profile of refractive index of the waveguide is fixed. It is necessary to select the correct thickness for each individual layer in the light of the numbers of modes which need to be supported in the structure. The larger the difference in refractive index between the guiding layer and the cladding layer, the thinner the

thickness of the guiding layer. In this case the less the tail of a guided mode field extends into the cladding layer. For a well defined mode, the majority of its energy will be confined in the guiding layer and thus a higher mode intensity can be achieved.

Modelling of the sensor structure is necessary for a determination of the parameters of sensor configuration. The thickness of each layer in this 5-layer waveguide was decided and the field profile (symmetric and asymmetric distribution) of the modes acquired from modelling using SLAB®[35] software in order to obtain two output modes from the structure. The waveguide structure is selected as:

upper cladding layer:	PMMA (3 μm, n=1.49)
upper guiding layer:	P-4VP (0.7 μm, n=1.57)
middle cladding layer:	PMMA (3 μm, n=1.49)
lower guiding layer:	P-4VP (0.7 μm, n=1.57)
lower cladding:	PMMA (3 μm, n=1.49)

The refractive index profile of the waveguide is shown in Fig.5.10. There are 4 TE modes (TE_0, TE_1, TE_2 and TE_3) in this waveguide structure from the modelling, their field distributions are obtained from calculation as shown in Fig.5.11 below,

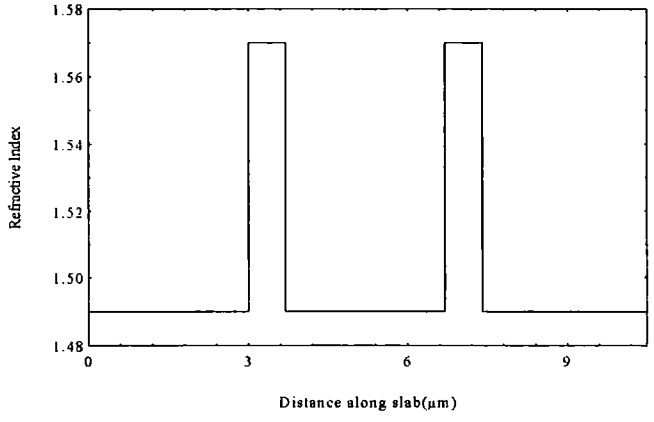

Fig. 5.10 Refractive index profile of 5-layer waveguide (P4VP-I)

Fig. 5.11 shows that the effective index of TE_0 and TE_1 modes are the same and their energy is mostly confined in each guiding layer. Despite the amplitude of one part of TE_1 being negative, they are identical for their overlapping intensity distributions. They produce two degenerate output modes which are not distinguishable. These two modes give the same far-field interference pattern when coupled out from the waveguide. However, the field of TE_2 and TE_3 modes is distributed largely at the cladding layers. They

undergo poor coupling of field profile with coupling-in light (Gaussian beam). In addition they will suffer from moderate loss and are dissipated during their propagation because of their poorly confined mode profile in the guiding layers. Therefore TE_2 and TE_3 will have no serious affect on the interference pattern formed by TE_0 and TE_1, and their effect can be ignored.

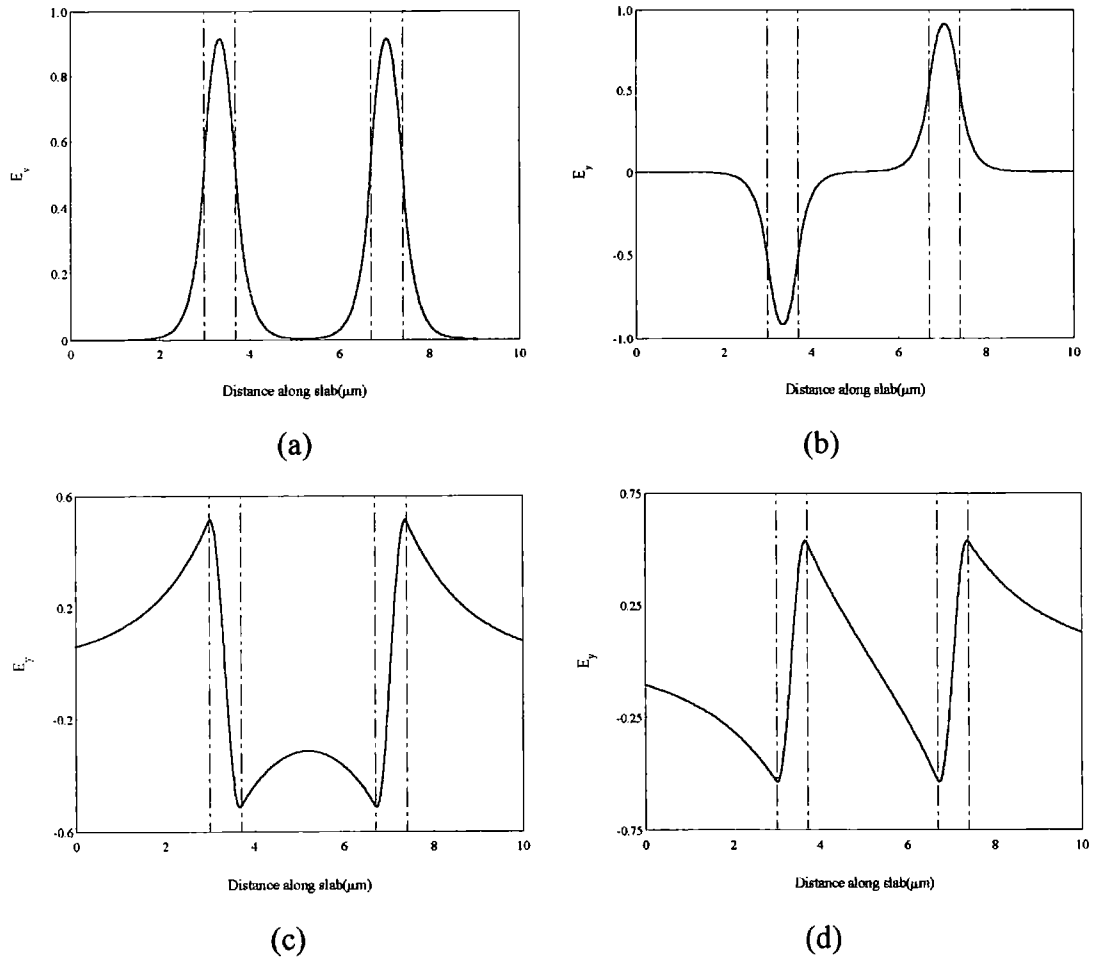

Fig.5.11 Normalised field profile of TE modes calculated for the 5-layer waveguide at 632.8 nm wavelength. (a) TE_0 mode with n_{eff}=1.544946, (b) TE_1 mode with n_{eff}=1.544946, (c) TE_2 mode with n_{eff}=1.491697, (d) TE_3=1.491080

The input light beam (Gaussian distribution) is coupled in the structure, its energy is passed onto the modes supported in the waveguide. As it travels further, the Gaussian mode redistributes, several maxima appear in the region illuminated. Two major guided modes (TE_0 and TE_1) gradually evolve from the initial Gaussian mode, other maxima (corresponding TE_2 and TE_3) decay sharply with distance. Finally the 5-layer waveguide gives two guided mode outputs as shown in Fig.5.13, even though the overall amplitude of the guided modes reduces over the propagation length by diffraction.

The process by which a Gaussian beam propagates in the waveguide is also modelled using GLAD Pro® [36] shown in Fig. 5.12, which is done by G. H. Cross.

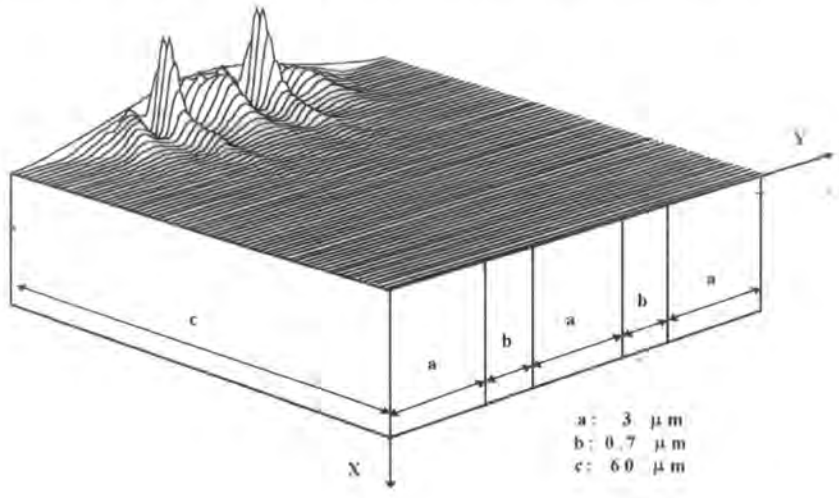

Fig. 5.12 Evolution of a Gaussian mode in 5-layer waveguide. The length of waveguide modelling is 60 μm.

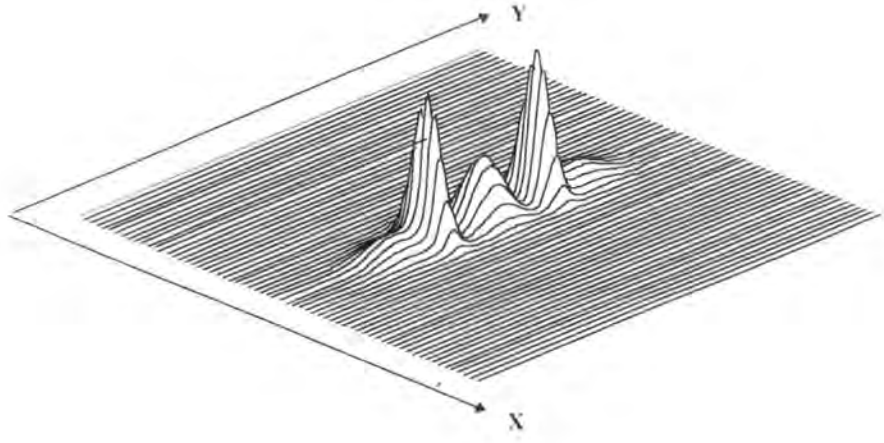

Fig.5.13 Field profile of guided modes at 60 μm along the propagation length

Secondly an improved 5-layer waveguide comprising SiO_2/P-4VP/Zeonex/P-4VP/Air (P4VP-II), is used as an asymmetric structure. Zeonex, a commercially available polymer with very low absorption of water, suitable index and good clarity, is selected to replace the PMMA as the middle cladding layer in the waveguide. The physical constants are shown in table 5.1. SiO_2 and air act as the lower and upper cladding layer, respectively. The intention to utilise Zeonex in this unsymmetric structure is based on, 1) Zeonex acts as a strong barrier to prevent water molecules from the upper layer going down to lower

guiding layers by diffusion. This will bring about a larger index difference between the two guiding layer resulting from diffusion of water molecules. This will induce a larger phase shift. 2) Water molecules can easily go into the upper guiding layer from the humidity in the surroundings without an upper cladding layer as a protecting layer, which will possibly develop a faster response of the sensor.

Table 5.1 Comparison of some properties between PMMA and Zeonex

Property	PMMA	Zeonex
Water absorption (%)	0.30	< 0.01
Refractive index (at 632.8 nm)	1.49	1.52
Glass transition temperature(T_g) (°C)	105	138
Linear expansion coefficient (K^{-1})	7×10^{-5}	7×10^{-5}
Light transmittance (%)	93%	92%

The thickness of each layer of the improved waveguide and its field profile of modes are determined by the software[35], The layer structure is as

upper cladding layer	Air (∝, n=1)
upper guiding layer	P-4VP (0.7 μm , n=1.57)
middle cladding layer	Zeonex (3 μm, n=1.52)
lower guiding layer	P-4VP (0.7 μ m, n=1.57)
lower cladding layer	SiO_2 (1 μm, n=1.46)

5.5.3 Fabrication of multi-layer waveguide structure

PMMA and P-4VP were tried as possible multiple layer film components of the waveguide structure. Their thicknesses were determined to support 2 modes for the structure from the modelling. In order to obtain the stacked integrated Young's interferometer, coating techniques must be applicable to combinations of layers with differing optical and chemical properties into a multi-layer film. Although a multi-layer waveguide, in principle, can be fabricated by repeating the process several times (successive deposition) on a substrate using appropriate coating methods, the following requirements should be followed for a multiple polymer waveguide:

- Solvents used must not dissolve the layer underneath
- The former deposited layer should be as wettable as the substrate and give good adhesion between each layer
- Good waveguide interfaces

Normally polymers can be dissolved in not only one organic solvent, they tend to be dissolved in a common solvent. In the practical waveguide fabrication, it is very difficult to fabricate multi-layer structures using a solvent which can dissolve only one polymer rather than other one. Therefore, this leads to a severe restriction on the solvent selection and the choice is very limited. Even though the solvent used in one polymer layer does not dissolve the other layer just underneath, the solvent still can penetrate this thin layer by diffusion and attack other polymer layers further down. Good adhesion between each layer is important for improvement of surface condition which produces better waveguide interfaces. Good interfaces will finally reduce the optical loss and provide good confinement to modes in the structure.

PMMA and P-4VP solutions were made following the methods described in section 3.3 and prepared by dissolving in appropriate solvents in table 5.2. Once fully dissolved, the solutions were filtered through 0.5 μm Millipore filters to remove impurities and undissolved contaminants. The filtered solutions were left to stand for approximately 30 minutes to allow any bubbles to escape from the solutions before deposition. The first PMMA layer was deposited directly onto bare silicon wafers by dip coating as a lower cladding layer with a thickness of approximately 3 μm, the second P-4VP layer was then coated on the PMMA layer by dip coating as a guiding layer with a thickness of about 0.7 μm after the previous PMMA layer had dried. Afterwards the remaining layers were cast either by dip coating or by spin coating from solutions successively (see section 3.2). The appropriate parameters of each layer are shown in Fig. 5.14. These thicknesses were calibrated from measurements of the total thickness of the structure after each deposition.

Dip coating produced much better film surface when compared to spin coating. Spin coating often produced dots and tiny traces onto the surface of the film or 'fish eyes' with poor adhesion. The situation was even worse when coating very thin films, a high degree of roughness occurred. Because the two P-4VP layers (the 2nd and the 4th layer) were so

thin, spin deposition of the PMMA layer (the 3rd and the 5th layer) above them was an attempt to reduce the time of coating and to protect the solvent in wet PMMA film from attacking the PMMA layer below by the penetrating the P-4VP layer. After each deposition, films were put in a vacuum oven for drying (<60°C).

Table 5.2 Parameters for preparing solutions for multi-layer waveguide structure

Polymer	Quantity of polymer (g)	Solvent added	Quantity of solvent added (ml)	Coating method
PMMA	5.5	DCM (dichloromethan)	20	dip
PMMA	2	chlorobenzene	7	spin
P-4VP	1.8	IPA (Isopropyl alcohol)	20	dip

PMMA	5
P-4VP	4
PMMA	3
P-4VP	2
PMMA	1
Silicon	

No.5 ~3 μm, spin coating, drying for 15 mins (<60°C)

No.4 ~0.7 μm, dip coating, drying for 15 mins(<60°C)

No.3 ~3 μm, spin coating, drying for 15 mins (<60°C)

No.2 ~0.7 μm, dip coating, drying for 10 hrs (<60°C)

No.1 ~3 μm, dip coating, drying for 10 hrs (<60°C)

Fig.5.14 Structure and fabrication parameters for the P4VP-I structure

The drying process was found to be very critical for a good multi-layer structure. Each preceeding layer needed to be dried to an extent where it contained no more solvent before the next coating could be applied. The possibility of dots or cracks appearing increased as each successive layer was coated (>3 layers), particular attention was paid to thick films. Very often reticular cracks occurred initially from dots and fisheyes on the surface because of stresses within the layers. There were differences in the coefficient of thermal expansion between differing polymers, as in the stress between dry and wet films. Violent changes of drying temperature would cause accumulation of the stresses in the films beyond the limit to which the film could resist and these would induce cracks. High temperature and extended heating at higher temperature favoured the evolution of stress.

More cracks were observed on the surface of films in experiments. As the waveguide increased in thickness or more layers were coated, it tended to crack easily. Drying multi-layer waveguide films at lower temperature (<60°C) for shorter time (<15 mins) in the later stages of deposition was found to decrease the stress within the films and to reduce cracks effectively. A 5-layer waveguide with good interfaces without any cracks in it was fabricated successfully following the procedures above and this was used in experimental measurements.

When fabricating the improved structure (P4VP-II) by spin coating, P-4VP was coated onto a silicon wafer with a thin SiO_2 layer on its surface. The Zeonex and other P-4VP layers were then coated on one by one by spin coating. A hot plate was used to dry the film in the first instance during the coating of each layer, furthermore the waveguide was moved into the vacuum oven at higher temperature (>150°C) to expel the resident solvent in the film. The waveguide films were placed directly onto the hot plate, the temperature (~50°C) of which was chosen appropriately. The hot plate passed heat through the waveguide from its bottom to its surface, stopping the solvent penetrating and attacking the other polymer layer underneath by diffusion just after spinning, it expelled most solvent inside the waveguide within a short time. Attention was paid to the temperature of the hot plate. Good films with smooth surfaces were achieved when the correct temperature was chosen for drying. Otherwise many dots or orange peel would appear on the surface of the film if the temperature of the hot plate is too high (>100°C). The appropriate parameters of each layer are shown in Fig. 5.15.

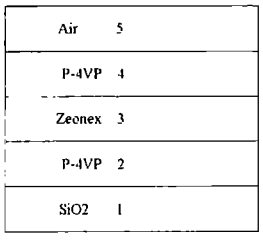

No.4 ~0.7 μm, spin coating, drying for 1~2 mins (50°C, hot plate)
No.3 ~3 μm, spin coating, drying for 1~2 mins (50°C, hot plate) then in vacuum oven for 30 mins
No.2 ~0.7 μm, spin coating, drying for 1~2 mins (50°C, hot plate)

Fig.5.15 Structure and fabrication parameters for the P4VP-II structure

Sometimes the surface of the Zeonex film needed special treatment to improve adherance when necessary using concentrated H_2SO_4, the waveguide with dry Zeonex film was immersed into the acid for 15 seconds at room temperature, then rinsed in deinised water and washed with isopropylalcohol (IPA) and finally dried with dry nitrogen.

5.5.4 Formation of sensor chips

Sensor chips were obtained and their endfaces were prepared by scribing and cleaving the silicon wafers. Once a multi-layer waveguide structure with good optical quality (uniform layer, clean surface, scratch free) was prepared successfully on the silicon wafer (either the whole wafer or a strip of wafer), trace marks were scribed onto the wafer using a diamond tipped scribe. The wafer was cleaved at the trace mark along one of the cleave lines (crystal surface of silicon wafer) in favourable cases. Waveguide silicon wafers were cleaved into narrow strips at the beginning, then into approx. 10×10 mm square sensor chips for use. Dust free gloves were worn to prevent sensor chips from any damage and dusting during the whole operation.

5.5.5 Optical test of sensor end face and its structure

The multi-layer polymer on the silicon wafer fractured along the line of the cleave during the cleaving of the silicon wafer. The endface of the polymers would be smooth enough optically to produce good Young's fringes, if the polymer was fragile enough and gave a sharp fracture. Actually most of the polymers were a little tough because of their elastic behaviour or plastic deformation. Consequently an uneven polymer facet was formed using this method to produce sensor chips, which would affect the future Young's fringes to a certain extent.

Several scanning electron microscope (SEM) images were taken to check the end face of sensor chips and the quality of multi-layer structures on the wafer substrate. From Fig.5.16 it was confirmed that a good 5-layer stacked waveguide structure had been obtained using the method described in section 5.5.3. The individual polymer layers and their interfaces were very clear, though some small unevenness appeared at the end face of waveguide. The interfaces from dip coating were better than those of spin coating in our experiments according to the SEM images. The bright line on the surface of structure (at the right) was a charging effect due to charges accumulating on the non-conducting polymer layer.

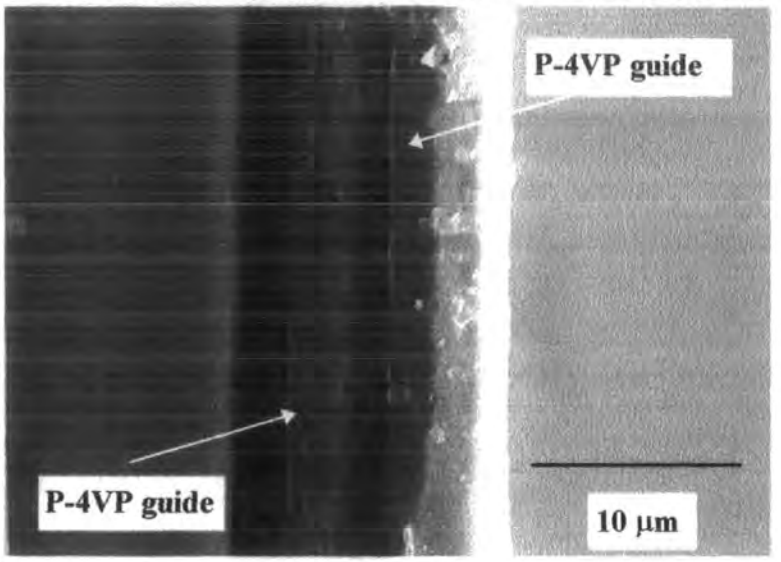

(a)

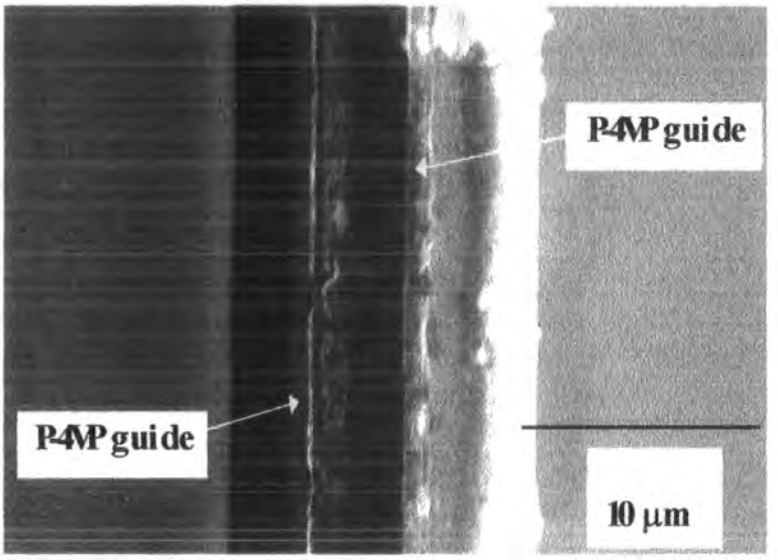

(b)

Fig.5.16 SEM images of the endface of 5-layer waveguide structure. a) Separation between the centres of the two guiding layers is 4.5 μm. b) Separation is 5.03 μm. Images are taken using a JSM IC848 scan electron microscope (SEM) at 15 KV, ×3000, beam current 2×10^{-10}A.

5.6 Experimental set-up for the humidity sensor system

The experimental setup for humidity sensing consisted of two parts as shown in Fig.5.17. One part consisted of Young's fringe generation, data detection and recording systems which included a laser source, sensing cell, detector, camera and computer. Light from a helium neon(He-Ne, 632.8 nm wavelength) laser was coupled into a sensor chip using the

end-fire technique. A ×10 microscope objective lens was used to focus the laser beam onto the input cleaved endface of the sensor chip through a window in the sensing cell, where the two guiding layers of the structure were illuminated uniformly to excite the guided modes in the structure. Microtranslation stages fixed on the support of the objective lens and a microalignment stage were used to align the lens, the waveguide and the laser beam. The sensor chip was placed in a special sensing cell which was designed to supply a uniform concentration of humidity to be measured and to isolate the sensor chip from its outside environment to reduce its influence or interference. The coupled-in light diverged when it propagated along the waveguide and diffracted out from the output endface of the waveguide. The interference fringe distribution was imaged onto either a screen for direct observation or for taking photographs, or onto a pin-holed silicon photodiode for detection or recording. A lock-in amplifier and chopper were used to pick out the responses when the intensity of transmitted light was too low for a direct recording, although the light and fringe shifts were very clear to see.

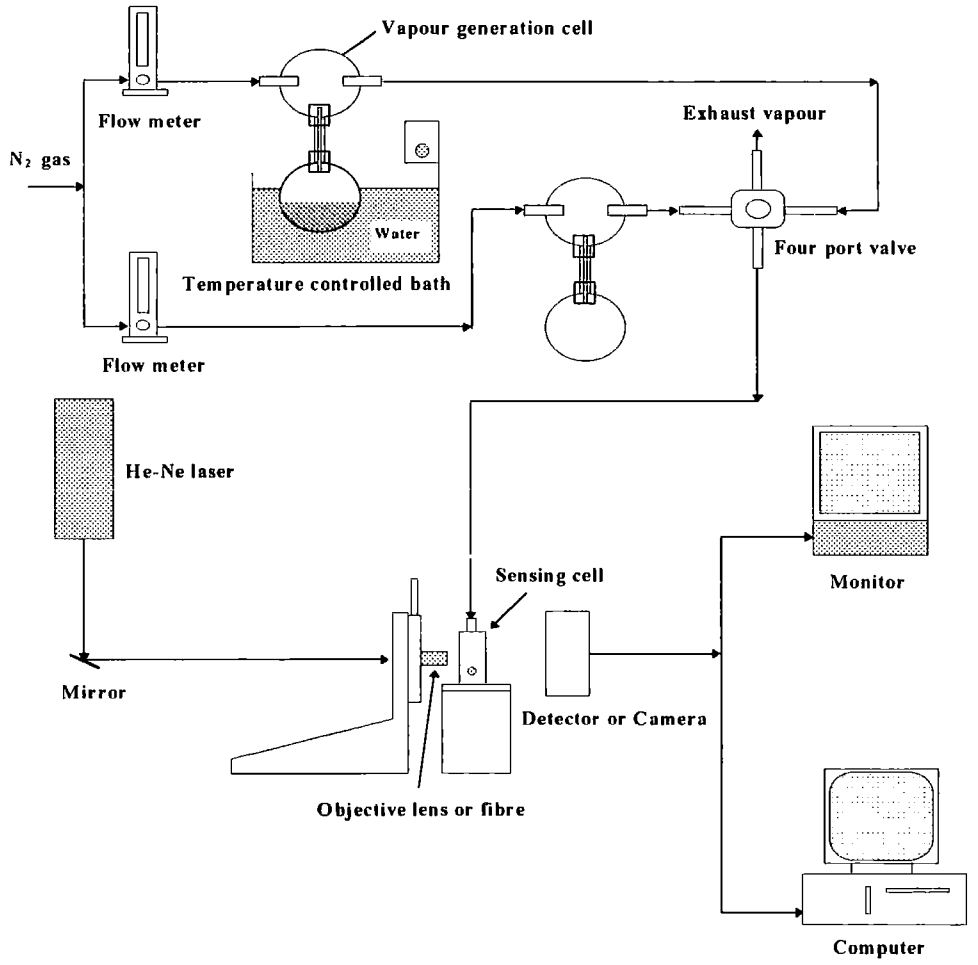

Fig.5.17 General set-up of humidity sensing experiments

The second part was a humidity generation system,[37] designed to produce a very low concentration of humidity. It comprised two flasks connected by a capillary tube, water bath and flow meters. Water molecules diffuse from the lower flask partially filled with water to the upper one through the tube, where they are mixed with nitrogen molecules to form a certain concentration and carried away by a carrier gas (dry nitrogen) and sent to the sensing cell. Two channels, reference (dry nitrogen) and measuring channels, were connected with the sensing cell through a four port valve for measurements. Tens of ppm concentration of water vapour was obtained from this system in these experiments.

The concentration of water vapour generated from the system depends on the flow rate of carrier gas and diffusion quantity of water molecules. Different concentrations can be achieved by: i) changing the flow rate of carrier gas to dilute the water molecules at a constant diffusion quantity of water molecules. ii) changing the diameter or length of the capillary tube or, iii) varying the water temperature to change the diffusion rate of water molecules using a temperature controlled water bath. Once the capillary tube and temperature were fixed, the rate of water molecule diffusion from the lower flask to the upper one is constant. A low concentration of humidity in a certain range can be obtained either by increasing the flow rate of carrier gas, using a thinner capillary tube or by reducing the temperature. The humidity generation system had to be calibrated before experiments could be carried out.

5.6.1 Calibration of humidity system

The actual concentration of water vapour generated from the system could be measured from calibration for a given diameter capillary tube. All concentrations of water vapour were given in ppm by molecules. The concentration could be changed in a particular range by using a tube with a different bore size, but the system had to be calibrated when changing it. Calibrations were carried out by measuring the weight loss of water (or solvent) from the lower flask at regular time intervals for a constant flow rate of carrier gas and at various temperatures. A constant in the diffusion equation was determined from the calibration curve, then various concentrations at different temperatures, shown in Fig.5.18, could be calculated from the equation.

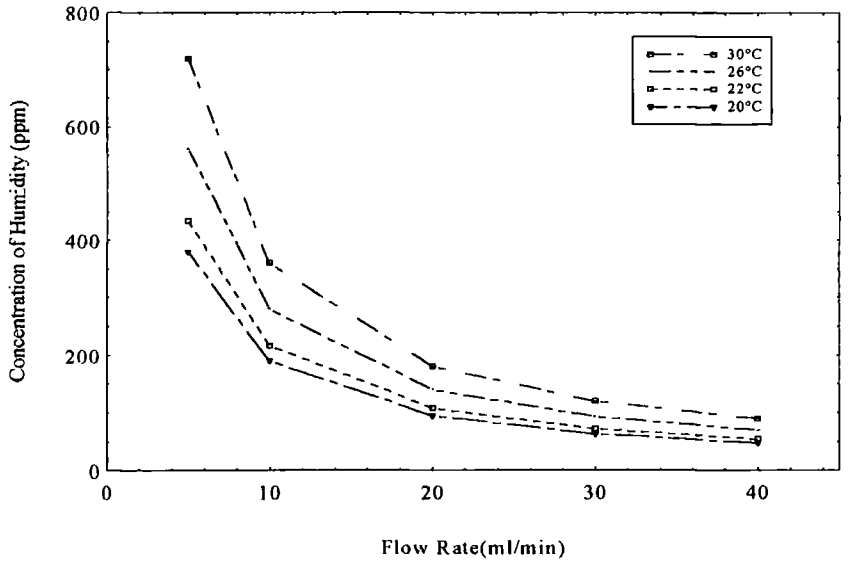

(a)

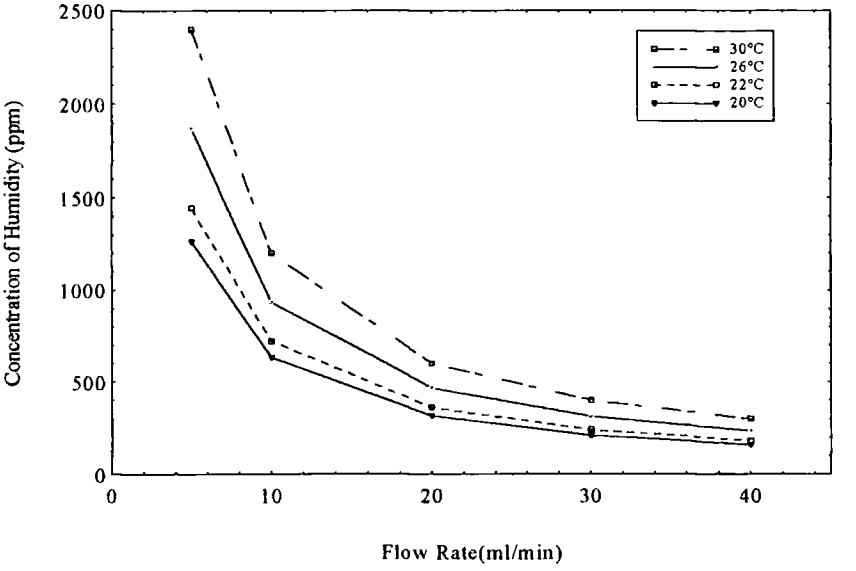

(b)

Fig.5.18 Concentration of the vapour system from calibration. a) Diameter of capillary tube is 2.6 mm and its length is 10 cm. b) Diameter is 5 mm and length is 10 cm.

5.6.2 Modelling and measuring of Young's interference fringes

A 632.8 nm wavelength He-Ne laser beam was focused onto the input endface of the waveguide by end-fire coupling after the whole system had been aligned. Light coupled-in excited 4 modes in the multi-layer waveguide structure, two degenerate modes were excited and propagated along it as modeled in section 5.5.2. Each guiding layer gave one mode output from the output endface eventually. Microscope objective lenses with

different magnifying powers and numerical apertures were replaced in an attempt to supply the two guiding layers with uniform illumination and to optimise the coupling which depended critically on the alignment in accordance with the thickness or numerical aperture of the waveguide.

Guided light in each guiding layer diffracted out of the output endface of the structure and formed two cylindrical waves. The distribution of fringe patterns were obtained when these two waves met and interfered with each other. This process was modelled by G. H. Cross using a computer program.[36] Two ideal Gaussian modes with separation of 4.2 μm were assumed at the output endface of the waveguide, each mode expanded to 6 mm (in the Y direction) and 0.8 μm in width (in the X direction) in Fig.5.19 (a) because of divergence of the beam. The fringe pattern was calculated at a distance (approx. 10 cm) from the output end face of the waveguide and was scanned to give an intensity profile of fringes in Fig.5.19 (b) and (c), these could be used to compare with the results in experiments.

To test the multi-layer waveguide structure and to confirm Young's theory and results from modelling, fringe distribution was imaged on a screen at a distance of 9.65 cm behind the output endface of waveguide shown in Fig.5.20. The intensity distribution of fringes was scanned across the fringes using a Hamamatsu camera. Two guiding layers served as two slits and the distance between them was the separation of the slits, respectively. Separation of fringes from experiments, calculation and modelling are listed in table 5.3.

Table 5.3 Measurement of Fringe Separation

d (μm)	λ (nm)	D (cm)	ΔX_m (cm)	ΔX_1 (cm)	ΔX_2 (cm)
4.5	632.8	9.60	1.7	1.35	1.45
		15.0	2.5	2.11	
		21.0	3.4	2.95	

Where the distance (d) between two the guiding layers was measured from the SEM image, fringe separation, ΔX_m were measured from experiments, ΔX_1 were calculated using Young's theory, ΔX_2 was from modelling.

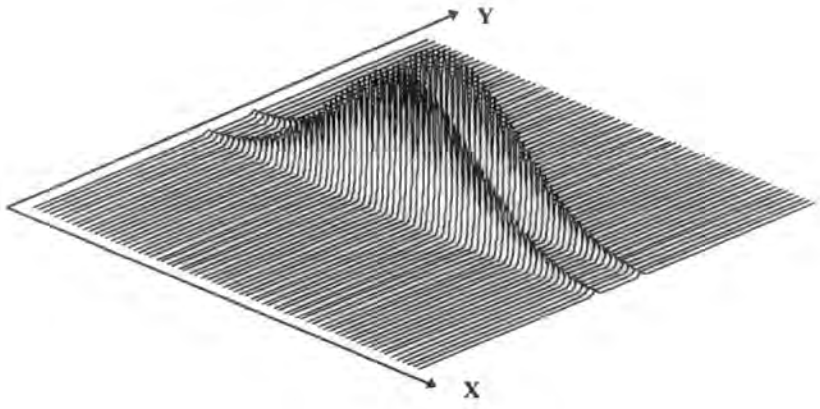

(a)

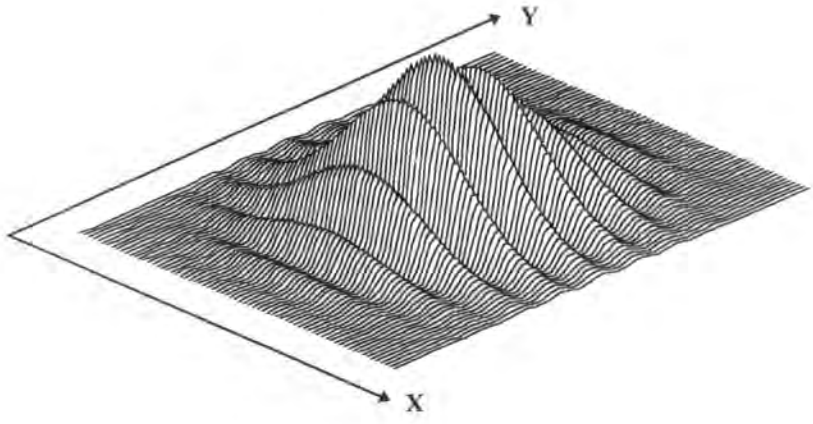

(b)

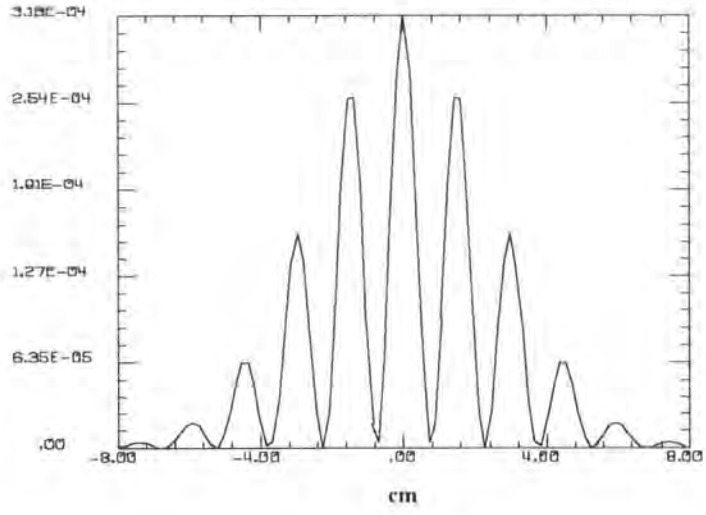

(c)

Fig.5.19 Modelling results of Young's fringes. (a) Intensity profile of two guided modes at the end face of waveguide. (b) Fringe distribution at a distance 9.65 cm away from the end face. (c) Fringe profile

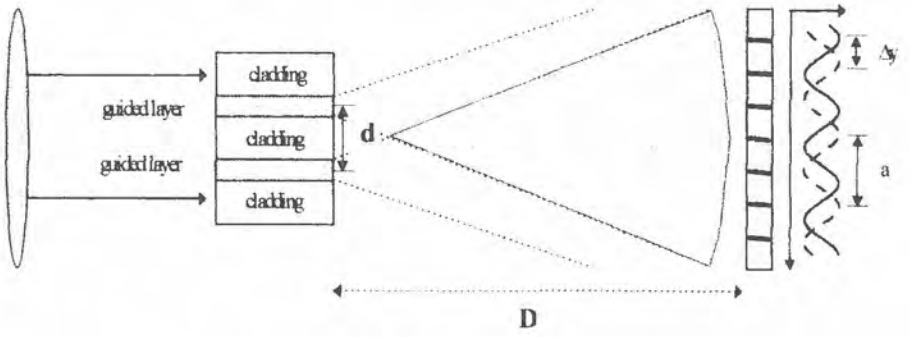

Fig.5.20 Set-up for fringe profile measurement

(a)

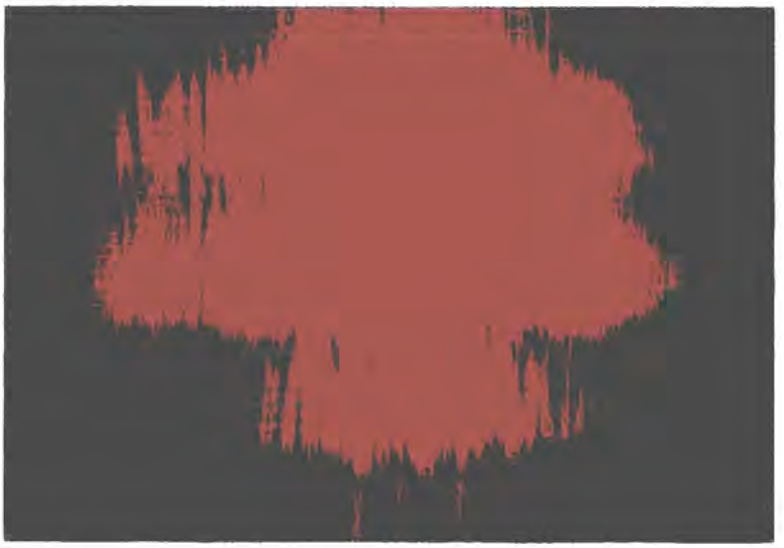

(b)

Fig.5.21 Images of Young's fringes from 5-layer waveguide structure

Images of Young's fringes were taken and are shown in Fig.5.21. A group of horizontal fringes parallel to the guiding layer (Y direction) was obtained from interference between the two guided modes just as Young's theory predicted and the program modelled. The separation of two adjacent fringes measured in the experiments is in good agreement with the expected value from theory or modelling, which is confirmed by the Young's two beam interference theory.

According to the modelling in Fig.5.19 (c), at least 9 fringes should be seen. As the order of fringe increases, the intensity of fringe drops down quickly. These fringes were confirmed from experiments. 9 fringes were seen very clearly and several more could be distinguished on a large screen, but the side fringes were dim. Only parts of the fringes were detected in Fig.5.22 and recorded in pictures in Fig.5.21 because of their limited detecting level. Obviously observable Young's fringes were seen from almost all samples examined.

From the pictures in Fig.5.21, a distinguishing feature of the fringe pattern is that many roughly parallel vertical lines overlap the overall interference fringe pattern in all samples. Sometimes some displacement and distortion of fringes appear in different samples or the same sample at different position. These vertical lines are mainly attributed to the cleavage lines and other fabrication imperfections. Cleavage lines appear on the cross section of the waveguide along from the top to the bottom during their fracture which is induced by cleaving of the silicon wafer substrate. The same phenomena were observed on the other cleaved samples.[38] These cleavage lines separate the endface of the waveguide into a large number of small narrow strips and form steps on it. Two adjacent surfaces separated by the cleavage line may not be parallel and they may have a relative slope along the direction of line in their microstructures. These haphazard lines together with imperfections, such as local irregularities and damage on the end face of the structure, generate an uneven end face. They are of great optical irregularity and produce vertical lines, discontinuities, distortion and optical noise which sometimes overwhelm the Young's fringes in some extreme cases. The less uneven the cross section of the waveguide, the better the fringes. This is demonstrated and observed clearly in experiments by translating the sample across the beam after optimising the vertical coupling alignment. In the case when a perfect area with least irregularities, which is big

enough for the focusing spot on the end face, is chosen, sharp and smooth fringes with high contrast are presented on the screen.

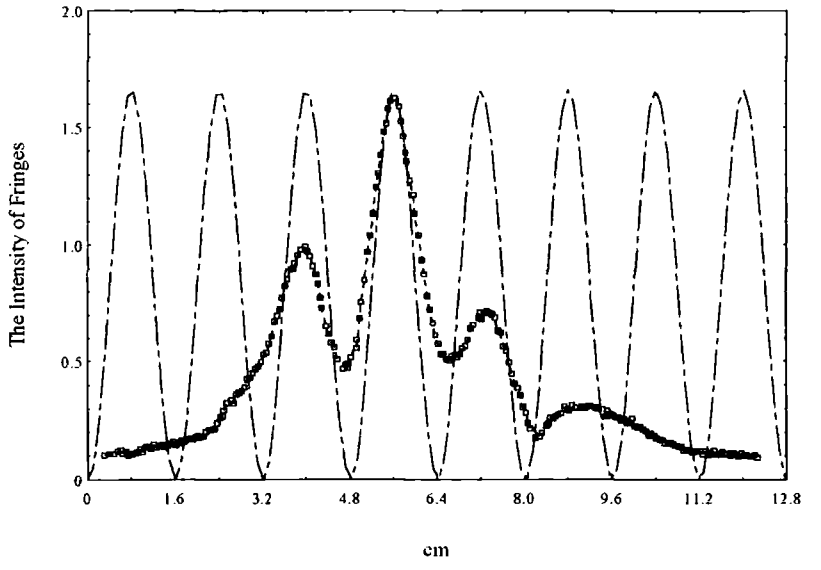

(a)

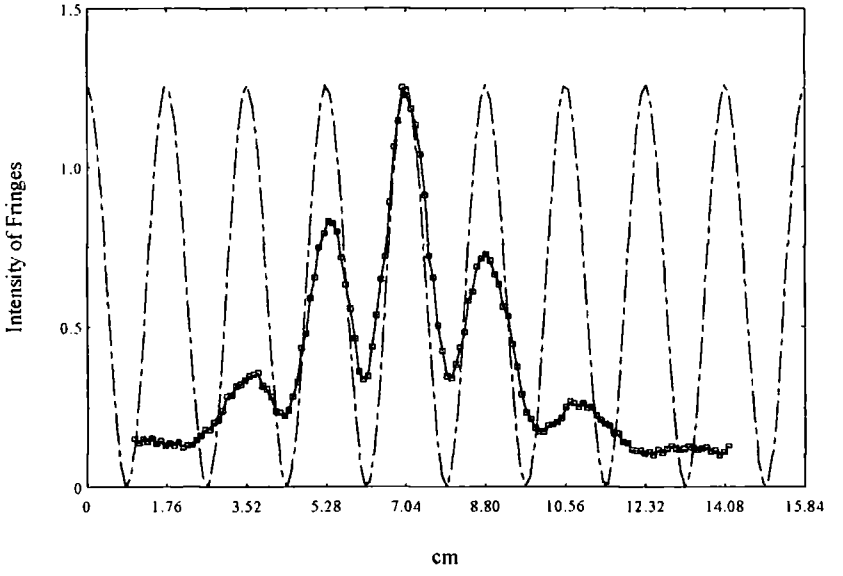

(b)

Fig.5.22 Profiles of interference fringes produced from 5-layer waveguide structure. (a) Symmetrical structure P4VP-I. (b) Unsymmetric structure P4VP-II.

5.6.3 Stability investigation of sensors

Stability is a key parameter of a sensor, particularly long term stability. Therefore the stability of the fringes over an extended period is measured using a pin-holed detector, a

chopper and a lock-in amplifier. Fig.5.23 shows the change in intensity of P4VP-I sensor when a single fringe is monitored by the detector over a period of 24 hours at room temperature. Though the intensity change of transmitted light is about 30%, it corresponds to only around 1/3 to 1/4 of a fringe shift.

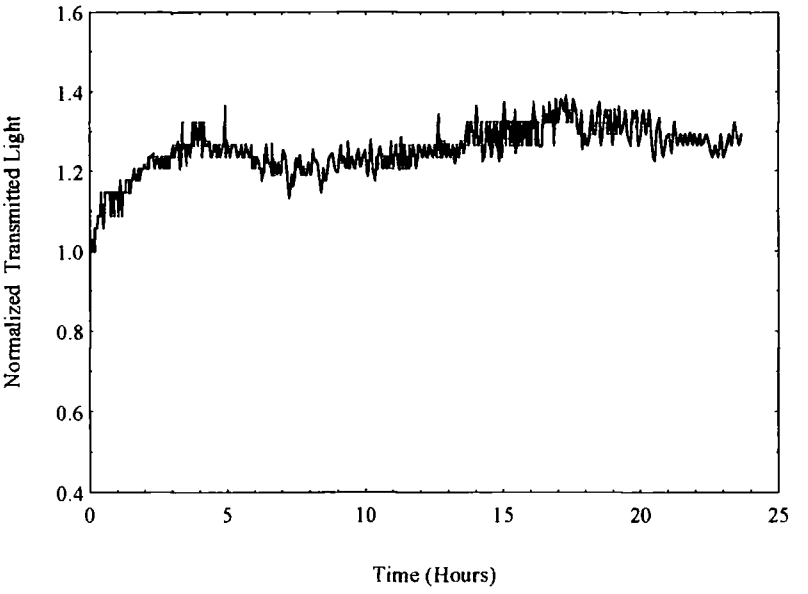

Fig.5.23 Stability measurement of P4VP-I sensor

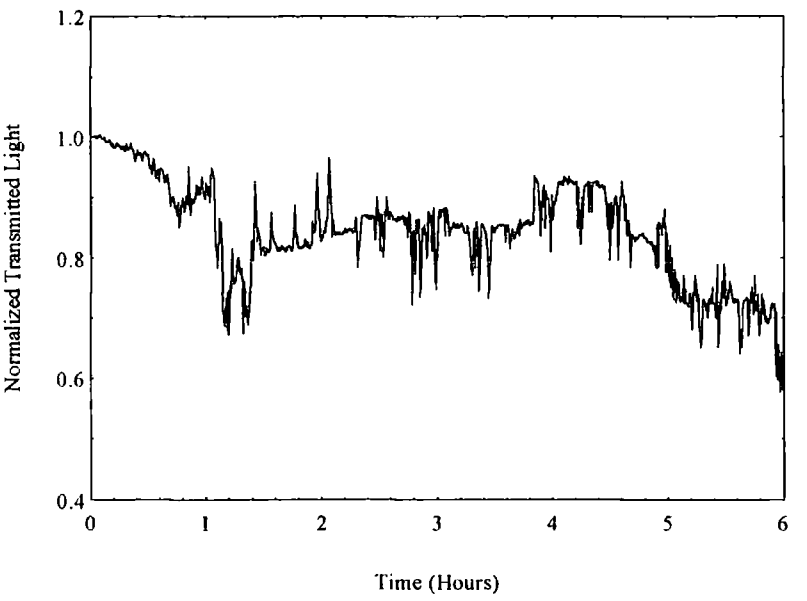

Fig.5.24 Stability measurement of P4VP-II sensor

Fig.5.24 shows the stability measurement of improved sensor, P4VP-II, under the same experimental conditions as P4VP-I. The intensity changes corresponding to one fringe

shift. From these two figures, we can see the intensity changes are small when P4VP-I sensor reaches its stable state, but are larger for P4VP-II sensor which combined with slow drift of fringe. The P4VP-I sensor is more stable than P4VP-II. For P4VP-II, the fringe shifts more with improvements of its sensitivity. Here monitoring is carried out for only 6 hours as shown in Fig.5.24, contrast and intensity of fringes dropped significantly and the fringe would shift away at extended monitoring.

Since the fringe drift in optical interference is a common and frequent phenomena which is affected by environmental factors (density, temperature, pressure of ambient atermosphere) and associated with the light source and detector used. The stability of these two sensors is good considering these factors, and is enough for practical measurements. In most cases, measurements can be finished in less than tens of minutes, stability is mainly limited by detector noise and laser output stability over this short period.

5.6.4 Reversibility of sensors

The reversible behaviour of sensors was decided under continuing and repeating measurement condition. The distribution of the fringe pattern was recorded before and after exposing the samples to water vapour. At the beginning, the flow rate was fixed for both flow meters in reference and measuring channels, the sample was opened to reference (dry nitrogen), careful adjustments were made to the stages supporting the sensing cell and objective lens by micromanipulators to obtain the best fringes.Their contrast, and fringe distribution was recorded. Samples were then exposed to water vapour for the measurements at room temperature when switching to the measuring channel. After that dry nitrogen flowed over the sample when switching back to the reference channel. Fringe distribution was recorded again for comparison with the previous distribution before exposing to vapour. Between each measurement the sample was exposed to dry nitrogen for long enough time (longer than 5 minutes in experiments). Measurements were made on both P4VP-I and P4VP-II sensors, their results are shown in Fig.5.25 and Fig.5.26.

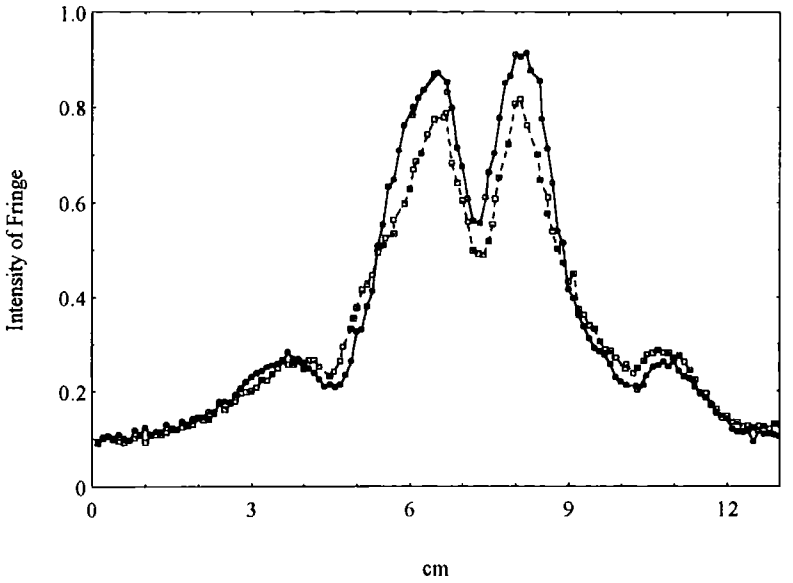

Fig.5.25 Reversibility of P4VP-I sensor. Solid line represents the fringe distribution before exposing to vapour, dash line represents the one after exposing to vapour and returning to dry nitrogen.

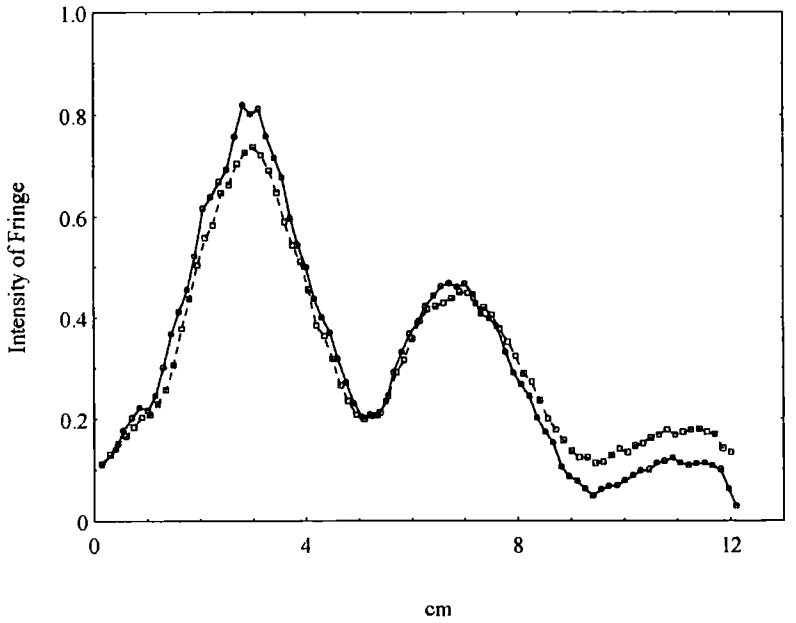

Fig.5.26 Reversibility of P4VP-II sensor. Solid line represents the fringe distribution before exposing to vapour, dash line represents the one after exposing exposing to vapour and returning to dry nitrogen.

The reaction of both structures to water vapour is reversible as seen from Fig.5.25 and 5.26. Diffused water vapour induces a refractive index change in the structures and leads to a fringe shift. Finally the fringe patterns return to their original position after shutting

off water vapour, but are of lower overall intensity. A difference is observed in experiments for these two types of sensors, where the time to recover for the fringe of P4VP-I sensor is shorter than that of P4VP-II sensor, also the contrast of fringes changes less for P4VP-I structure rather than for P4VP-II structure.

5.6.5 Sensitivity study of sensors

The sensitivity to water vapour is one of the most important indications of merit for a humidity sensor. Responses of the sensors were determined by monitoring fringe shifts. Concentrations of water vapour from tens of ppm to thousands of ppm generated from the system were transported to the sensing cell through a four port valve by means of a soft PVC tube. The reference channel (dry nitrogen) or measuring channel was opened individually by switching the valve. The dry nitrogen served to produce a zero reference concentration from which to compare the concentration of water vapour 'on' and 'off' in order to distinguish the possible phase shift.

Phase changes determined by the fringe shifts were measured either by recording the spatial intensity distribution of interference fringes and scanning along the cross section of fringes distribution using a Hamamatsu camera, or by measuring intensity changes using a pin-holed detector. In the first case the interference fringes were imaged onto a diffuser screen which smoothed out the fine structure of the fringes, especially the vertical lines that overlapped on the Young's fringes, and generated uniform distribution of the fringes. The fringe distributions were displayed on a monitor for measurements and/or data were transferred to a computer. A comparison was made between the intensity distributions of the reference (before the start of the sensing experiment) with that recorded by measuring water vapour (after sensing experiment). The phase shift $\Delta\Phi$ was determined from the lateral shift Δy of the fringes. The relation when the shift was within 2π is as shown in equation 5.20.

$$\Delta\Phi = 2\pi\frac{\Delta y}{a} \tag{5.20}$$

where a is the spatial period of the interference fringes. In the second case the fringes were allowed to fall onto the detector directly with a pin hole which was aimed at a dark

or bright fringe. Intensity change was recorded with a computer when a phase shift greater than 2π was observed or more than one fringe shifted.

Before or between each measurement, the sample was exposed to an atmosphere of dry nitrogen at room temperature (~20°C) as a zero reference for a period of time. This would result in a stable reference state for the sample and create a phase difference in the experiment when water vapour was introduced thereafter. In order to maintain the flow an equality in the two channels (reference and measuring) connected to the sensing cell stability, two identical flasks were used in the two channels and the same PVC soft tubes with nearly same length were used in both of them. Before measurements, the two lower flasks in each channel were kept empty and the system was left for a long enough time to reach equilibrium. Observations were carried out when the valve was switched to the measuring channel and back to the reference channel. Fringes should remain stable if the flow rate in each channel was set the same, because of the same gas (dry nitrogen) in both channels. Otherwise slight adjustment was made on setting the rate. In Fig.5.27 two channels are balanced after calibration, but there is a difference between their overall intensity.

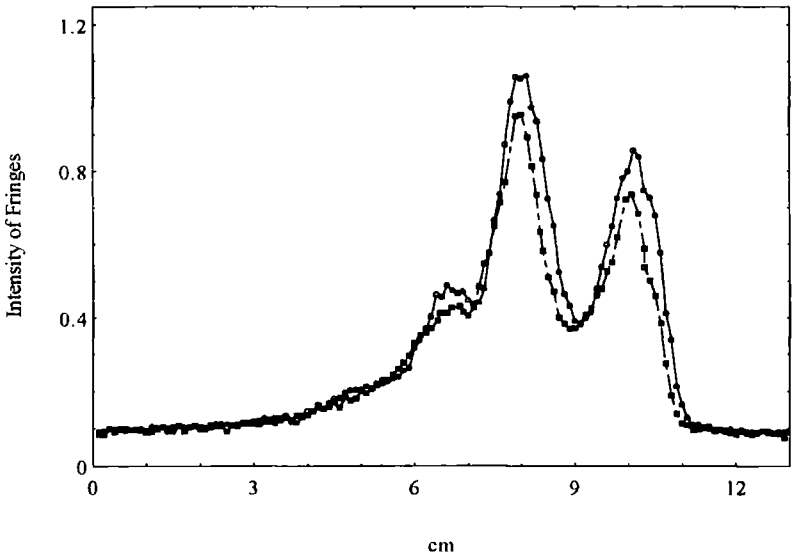

Fig.5.27 A typical calibration of reference and measuring channel

Firstly, measurements were made on the P4VP-I sensor. Turning to the measuring channel, a 0.3π (0.94 radians) phase shift was observed at about 150 ppm concentration of water vapour which corresponded to 40 ml/min at 20°C in the vapour system when the water vapour passed over the sample as shown in Fig.5.28.

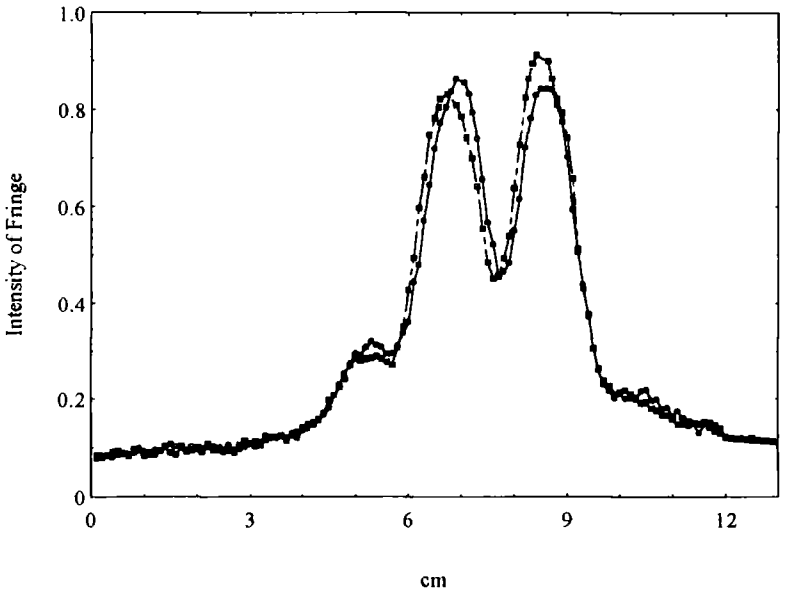

Fig.5.28 Lateral fringe shift from the sensor after exposure to 150 ppm concentration of water vapour. The solid line is before exposure and the dash line is after exposure.

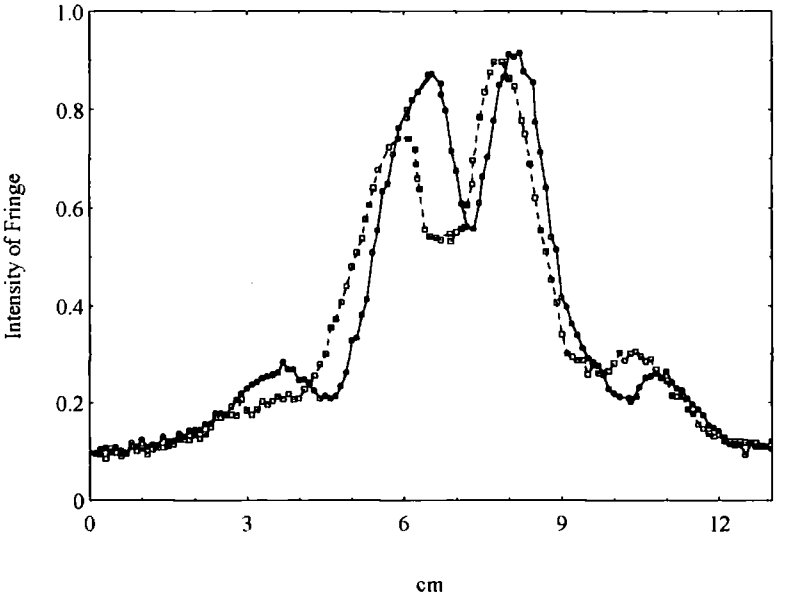

Fig.5.29 Fringe shift of the sensor when exposed to 600 ppm concentration water vapour. The solid line is before exposure and the dash line is after exposure.

At a lower flow rate for dry nitrogen carrier gas, a higher concentration can be generated from the system. The response of the sensor, a 0.53π (1.57 radians) phase shift, was measured at a concentration of 600 ppm (correspond to 10ml/min, 20°C) as shown in Fig.5.29. The sensitivity of this structure was limited, as it was difficult to observe a noticeable phase shift between 150 ppm and 600 ppm concentration.

Secondly, a series of tests were performed on the improved structure, P4VP-II. When exposing the sample to water vapour, responses were measured from the concentration of 30 ppm to 1100 ppm by changing the capillary tube and reducing the flow rate. Fig.5.30 shows the typical response time of the P4VP-II sensor recorded by a pin-holed dector at different concentration (300 and 1100 ppm concentration, respectively). A phase shift from 0.1π (0.314 radians) to 8.4π (26.4 radians) was obtained corresponding to the changes of concentration within that range in experiments as shown in Fig.5.31.

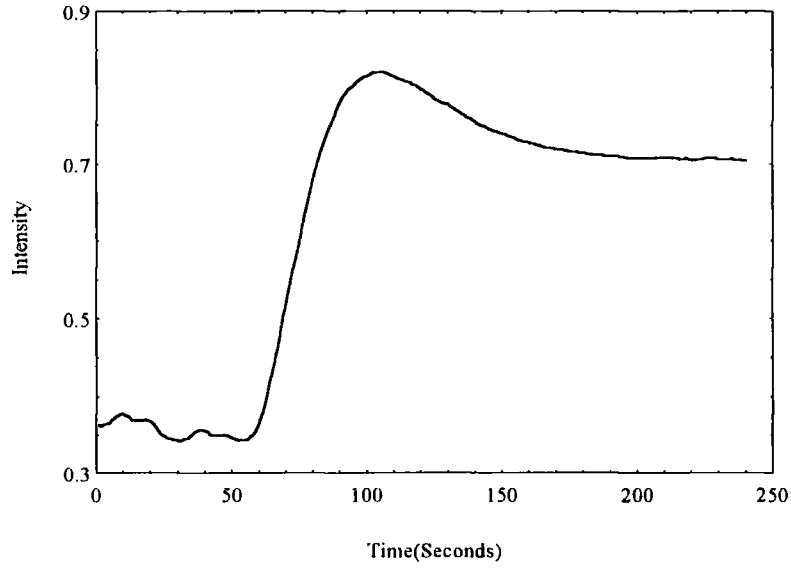

(a)

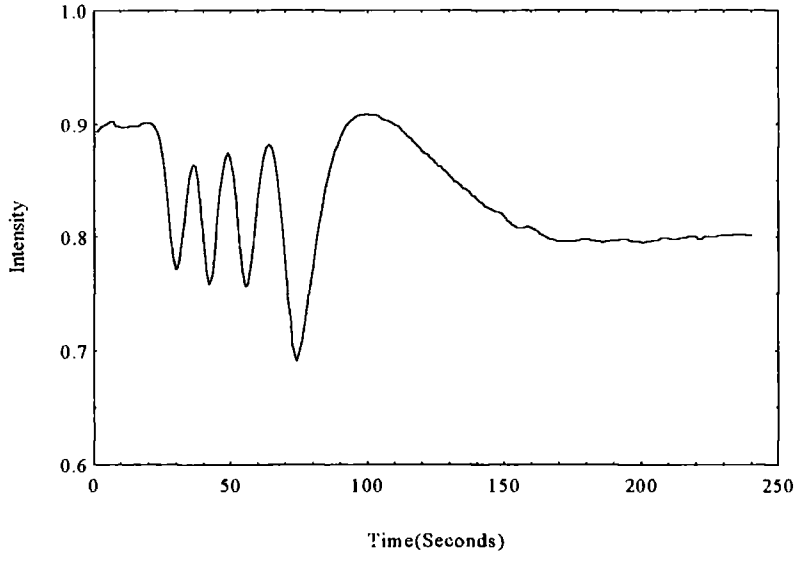

(b)

Fig.5.30 Responses to different concentration of water vapour recorded by a pin-holed detector. a) at 300 ppm concentration. b) at 1100 ppm concentration.

The overall response of the P4VP-II sensor is basically linear as shown in Fig.5.31 taking into account errors in experiments. The fringes all move upwards during experiments when both structures (P4VP-I and P4VP-II) are exposed to water vapour indicating an increase in refractive index in the sensing waveguide. After each measurement, the valve is switched back to the reference channel which allows dry nitrogen to flow over the sample, water molecules to desorb from the surface of the sensor and to diffuse out of it. The flow rate is then changed to vary the concentration of vapour. The system is left for enough time, to reach a new equilibrium before the next measurement. As it is relatively difficult to set accurate flow rates and exactly equal values for both flow meters each time, an error of concentration is introduced. The errors are comparatively large (up to 20%) at higher concentration compared with that at lower concentration (3~5%). This larger error is introduced because of nonuniform graduation on the flow meters.

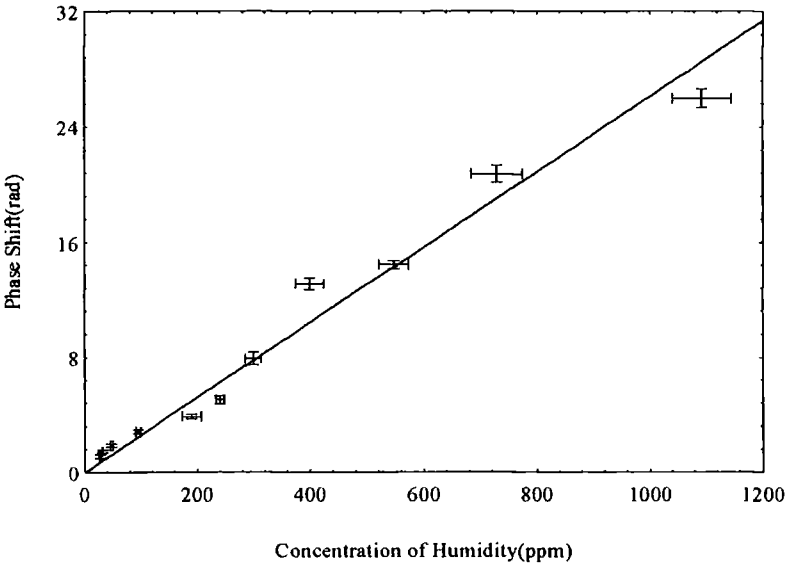

Fig.5.31 Phase shift versus concentrations of water vapour in improved structure (P4VP-II)

5.7 Discussion and conclusion

From the direction of the fringe displacement, moving upwards, it is evident that the refractive index of the upper guiding layer increases when the sensor chips are exposed to water vapour; or the index of the upper guiding layer increases more than that of the lower guiding layer, if that the index of the lower guiding layer increases also. This indicates that a change happens inside the waveguide and induces index difference in polymer layers during the process. Meanwhile, the fringes move back to their original

positions after a period of time to recover in experiments, that is, the interference fringes shift upwards and downwards when turning water vapour 'on' and 'off' and present a good reversibility. It is strongly suggested that the whole process is reversible and mainly a physical one.

From the experimental evidence above, the reason for fringe shifts can be interpreted in terms of water entering the polymer, which increases the refractive index and causes the movement of interference fringes. More specifically, the process can be divided into two steps: i) initially water molecules are adsorbed and form an adlayer on the superstrate of waveguide, which are transported by convection or diffusion from water vapour outside the waveguide. ii) water molecules pass the air/polymer interface and enter the polymer layers of the waveguide by diffusion, they occupy positions of micropores in the polymer, these water molecules may even pass the polymer/polymer interfaces inside the multi-layer waveguide and go further down. Consequently these molecules are absorbed and distributed inside the polymer layers homogeneously.

Since water is more dense than air, this indiffusion of water molecules causes an increase in the density of the polymer and leads to the raising of refractive index of the polymer. Accordingly it induces phase changes of the interference fringe. Water molecules go into the polymer layer in a steady stream because there is a concentration difference of water vapour (partial pressure difference) between air/polymer interface of the waveguide. A higher vapour concentration increases the number of water molecules available to interact with the superstrate of the waveguide, more molecules will diffuse into the waveguide and a higher percentage of micropores in it will be occupied by them with the increase of vapour concentration outside it.

Particularly for the diffusion of water molecules, it will take time for them to go out from the polymer layer, so the recovery process for a sensor is longer at the higher concentration range. In this case, the phase shifts resulting from the index changes of polymer strongly depend on and are proportional to the quantity of water absorption by polymer or the filling percentage of the pores with water molecules. More micropores in the waveguide will favour this effect and enhance the sensitivity of a humidity sensor, thus a drawback of polymer in other applications become an advantage here.

Referring to structure (P4VP-I) with symmetric structure, water molecules have to pass through the top cladding layer (PMMA) first when they enter the upper guiding layer (P-4VP). The PMMA upper cladding layer hinders and reduces the diffusion of water molecules into P-4VP upper guiding layer, which results in a long response time and low sensitivity because of small index change or phase shift. Because PMMA is known to absorb water and is a relatively polar polymer, if provides a poor barrier to water. It cannot therefore be excluded that a small proportion of water molecules diffuse into the lower guiding layer, which will reduce the absolute phase shift between the two guiding layer in the waveguide and lower the sensitivity of the sensor.

Inevitably the index change of the upper cladding layer (PMMA) will lead to intensity redistribution of the guided mode in the structure. On one hand it does not affect the measurements of phase shift and induce extra phase change because there is only one mode in each guiding layer. On the other hand however, the intensity change of the mode is small and the effect can be neglected. The effect of water molecules which are adsorbed to form an adlayer on the superstrate of the waveguide is also small and neglected owing to symmetric structure of sensor, where the upper cladding layer acts as a protecting layer.

Turning to the improved structure, P4VP-II, since its guiding layer is exposed to the water vapour directly, it is much easier for water molecules to enter the guiding layer for their interaction with P-4VP layer, more molecules diffuse into the guiding layer without a layer acting as its protection. In addition a polymer with very lower water absorption, Zeonex, is applied as the middle cladding layer in the structure. Zeonex separates the two guiding layers (reference, measuring), and it prevents water molecules from diffusing further by acting as a barrier. This renders the reference inactive as much as possible and maximises the difference between the reference and measuring layers, which can increase the sensitivity of the sensor. Consequently both the sensitivity of the P4VP-II sensor and the absolute phase shift are increased or enhanced greatly. Its response time is much faster.

Comparing these two structures, the limit of detection for water vapour increases by 5 times from 150 ppm (for P4VP-I) to 30 ppm (for P4VP-II). The corresponding sensitivity to water vapour increases from the 100s of ppm range to the 10s ppm. Since the response

of P-4VP-II to water vapour exhibits a good linear increasing tendency over the concentration range used in experiments, the expansion or swelling effect of the waveguide is neglected. Both structures produce interference fringes with a separation of about 1.53 cm at a distance about 9.7 cm from the output endface of waveguide. This fringe separation is much larger than that in other devices[114] and make measurements simpler and detection of fringe easier in practical applications.

5.8 References

1. J. Fluitman and Th. Popma, *Optical waveguide sensor*, Sensors and Actuators, **10**, 25-46 (1986)
2. F. J. Gutierrez Monreal and Claudio M. Mari, *The use of polymer materials as sensitive elements in physical and chemical sensors*, **12**, 129-144 (1987)
3. Michael T. Gale, Rino E. Kunz, Hans P. Zappe, *Polymer and III-V transducer platforms for integrated optical sensors*, Opt. Engineering, **34** (8), 2396-2406 (1995)
4. J. Fraden, AIP handbook of modern sensor--physics, designs and applications, American Institute of Physics, New York, 1993, pp.6-8
5. B. Culshaw and J. Dakin(eds.), Optical fiber sensors, Artech House, Norwood, MA,1989
6. Y. N. Ning, K. T. V. Grattan, W. M. Wang and A. W. Palmer, *A systemic classification and identification of optical fibre sensors*, Sensors and Actuators A, **29**, 21-36 (1991)
7. B. Culshaw, *Optical systems and sensors for measurement and control*, J. Phys. E: Sci. Instrum., **16**, 978-986 (1983)
8. R. Narayanaswamy and F. Sevilla, *Optical fibre sensors for chemical species*, , J. Phys. E: Sci. Instrum., **21**, 10-17 (1988)
9. N. Fabricius, G. Gauglitz and J. Ingenhoff, *A gas sensor based on an integrated optical Mach-Zehnder interferometer*, Sensors and Actuators B., 7, 672-676 (1992)
10. R. G. Heideman, R. P. H. Kooyman and J. Greve, *Performance of a highly sensitive optical waveguide Mach-Zehnder interferometer immunosensor*, Sensors and Actuators B., **10**, 209-217 (1993)
11. Isabelle Schanen Duport, Pierre Benech and Roger Rimet, *New integrated-optics interferometer in planar technology*, Appl. Optics., **33** (25), 5954-5958 (1994)
12. R. Kherrat, N. Jaffrezic-Renault, P. Greco, H. Helmers, P. Benech, R. Rimet, *Integrated optical enlarged-field interferometer used as a chemical sensor*, Sensors and Actuators B., **37**, 7-11 (1996)

13. G. Gauglitz, A. Brecht, G. Kraus and W. Nahm, *Chemical and biochemical sensors based on interferometry at thin(multi-)layers*, Sensors and Actuators B., **11**, 21-27 (1993)

14. A. Brandenburg and R. Henninger, *Integrated optical Young interferometer*, Appl. Opt. **33** (25), 5941-5947 (1994)

15. W. Lukosz, *Integrated optical chemical and direct biochemical sensors*, Sensors and Actuators B., **29**, 37-50 (1995)

16. Paul V. Lambeck, *Integrated opto-chemical sensors*, Sensors and Actuators B., **8**, 103-116 (1992)

17. Z. A. Ansari, R. N. Karekar, R. C. Aiyer, *Planar optical waveguide with $PbCl_2$ cladding: a chlorine sensor*, J. Materials science: materials in electronics, 7, 255-259 (1996)

18. Jay N. Zemel, Jan Van der Spiegal et al., *Recent advances in chemically sensitive electronic devices*, Fundamentals and applications of chemical sensors, American chemical society, Washington, DC 1986, p2-38.

19. Shin-Won Kang, Keisuke Sasaki, and Haruyuki Minamitani, *Sensitivity analysis of a thin-film optical waveguide biochemical sensor using evanescent field absorption*, Appl. Opt., **32** (19), 3544-3549 (1993)

20. Hakon Helmers, Pierre Greco, Rolf Rustad, Rochdi Kherrat, Gerard Bouvier, and Pierre Benech, Performance of a compact, hybrid optical evanescent-wave sensor for chemical and biological applications, App. Opt., **35** (4), 676-680 (1996)

21. Andreas Otto, *Spectroscopy of surface polaritons by attenuated total reflection*, in Optical properties of solids: new developments (Editor: Seraphin), North-Holland Publishing Company1976, p677.

22. E. Burstein, W. P. Chen, et al., *Surface polaritons-propagating electromagnetic modes at interfaces*, J. Vac. Sci. Technol., 11 (6), 1004-1018 (1974)

23. A. V. Kabashin, P. I. Nikitin, *Interferometer based on a surface-plasmon reasonance for sensor applications*, Quantum electronics, **27** (17), 653-654 (1997)

24. K. Choi, H. J. Youn, Y. C. Ha, K. J. Kim, J. D. Choi, *Detection of cholera cells using surface plasmon reasonance sensor*, J. Microbiology, **36** (1), 43-48 (1998)

25. Pockrand, I., Swalen, J. D., Gordon, J. D. and Philott, M. R., *Surface plasmon spectroscopy of organic monolayer assemblies*, Surface Science, **74**, 237-244 (1977)

26. H. Bezzaoui and E. Voges, *Integrated optics combined with micromechanics on silicon*, Sensors and Actuators A, **29**, 219-223 (1991)

27. W. Lukosz, *Integrated optical nanomechanical devices as modulators, switches and tunable fitlers, and as acoustical sensors*, Integrated optics and microstructures, Proc. SPIE, **1793**, 214-234 (1992)

28. S. Fujita, T. Kihara, M. Aoki, A. Hiroe, and K. Yokomori, *Integrated waveguide device for magneto-optical disk signal detection and its/fabrication techniques*, Miniature and micro-optics and micromechanics, Proc. SPIE, **1992**, 140-149 (1993)

29. H. Ghafoori-Shiraz and T. Okoshi, *Fault location in optical fibres using optical frequency domin reflectometry*, IEEE J. Lightwave Technol., **LT-4**, 316 (1986)

30. R. B. Dyott, *Fibre-optic Doppler anemometer*, IEEE J. Microwaves Opt. Acoust., **20**, 13-18 (1978)

31. J. H. Briston, Plastics films, third edition, Longman Scientific and Technical, 1988, p117.

32. I. Kato and M. Komatsu, *Multistructured optical I.C. elements by polymer thin films*, Electronics and conmunications in Japan, **66-C** (2), 106 (1983)

33. De-Kui Qing, Kiminori Itoh, and Masayuki Murabayashi, *A coupling wave optical waveguide chemical sensor constructed by combining the ion-exchange and the sol-gel methods*, Chemistry Letters, 623-624 (1996)

34. E. Hecht and A. Zajac, Optics, Addison-Wesley publishing company, 1982

35. SLAB(BBV software, 1997)

36. GLAD Pro. Ver. 4.4 (Optima Research 95)

37. James M. Mckelvey and H. E. Hoelscher, *Apparatus for preparation of very dilute gas mixtures*, Anal. Chem., **29** (1), 123 (1957)

38. S. Tolansky, Multiple-beam interferometry of surfaces and films, Oxford University Press, 1948, p45-73

39. Albrecht Brandenburg and Rainer Edelhauser, Frank Hutter, *Integrated optical gas sensors using organically modified silicates as sensitive film*, Sensors and Actuators B, **11**, 361-374 (1993)

40. Rene G. Heideman, Rob P. Kooyman, et al., *Simple interferometer for evanescent field refractive index sensing as a feasibility study for an immunosensor*, Appl. Opt., **30** (12), 1474-1479 (1991)

41. R. E. Kunz, Miniature integrated optical modules for chemical and biochemical sensing, Sensors and Actuators B, **38-39**, 13-28 (1997)

42. S. Middelhoek, S. A. Audet, Silicon sensors,. Academic press 1989, p271-277.

43. Noboru Yamazoe, Yasuhiro Shimizu, *Humidity sensors: principles and applications*, Sensors and actuators, **10**, 379-398 (1986)

CHAPTER 6 CONCLUSIONS AND FUTURE WORK

The aim of this work was to investigate and characterise potential optical materials (chromophore doped polymer systems) for nonlinear optics and optoelectronics, and to explore new sensor applications for polymer optical waveguides. The measurements carried out in this research were divided mainly into three parts; linear optical measurements, photostability measurements and waveguide humidity sensing measurements.

In this research a series of photodegradation studies were carried out to investigate the photostabilities of the DEMI-series (DEMI, Ultra-DEMI and Dicyclohexyl-DEMI) and the yellow (Mor2, Morpip and DCM) chromophores in a waveguide structure. This research has shown that the DEMI-series materials have good photostabilities as promising nonlinear materials; the data provide helpful information to improve their structures further. In different environments at room temperature the doped slab waveguide films were exposed to optical wavelengths lying within these materials' main absorption bands (or their peak wavelengths) or near infrared region. It is concluded from the experimental results that the photodegradation mechanism of the DEMI-series materials is primarily photooxidation. This has been confirmed by IR spectroscopic studies of Ultra-DEMI and it has been proved that the degradation of the DEMI-series materials in an air environment is induced mainly by oxidation of olefinically unsaturated bonds in the molecular structure, which leads to the decomposition of these chromophores by a permanent chain scission and loss of colour in the sample films. Singlet oxygen plays a more important role in this reaction since it is quite reactive towards olefinically unsaturated bonds. Besides this the solubility of oxygen in the polymer matrix and the rate of diffused atmospheric oxygen into the polymer are also vital factors in the photodegradation of the DEMI-series materials. The degradation rate of the DEMI-series materials is very low in vacuum or nitrogen environments, as a result, an oxygen free

environment (vacuum or nitrogen) is ideal for the DEMI-series materials and their devices in applications to achieve high photostability and longer operational life. Eliminating the unsaturated bonds in their molecular structures is also of importance to improve their photostabilities. However this would affect their other optical properties. A proposed mechanism of photodegradation of DEMI-series materials has been presented in detail in section 4.6.3 according to the experimental results in this work.

It has been shown that within the series of molecules studied the photostability of Dicyclohexl-DEMI is the highest, then Ultra-DEMI and DEMI, according to the calculation of their B numbers at 632.8 nm, 780.0 nm in air environment.

As for the photodegradation exhibited by Mor2 and Morpip, their degradation is different from their reference material (DCM). There is no significant difference for Mor2 and Morpip degraded in air and vacuum at wavelengths within their main absorption bands (457.9 nm, 488.0 nm and 514.5 nm). These two materials presumably degrade or decompose directly by chain scission when they are exposed to light. The rate of degradation for Mor2 and Morpip is faster in air than in vacuum. However their photostabilities increase by only 1 order of magnitude in a vacuum environment. For DCM it has been shown that its photodegradation is dominated by photooxidation. The photodegradation shows no wavelength dependence at the wavelengths within its main absorption band.

Because photodegradation of organic chromophores is a complicated process which is different from one chromophore to another and involves many factors (e.g. the physical and chemical properties of the dye molecules, the intrinsic physical and chemical properties of the polymer), the process has not been fully understood, more work needs to be done to clarify it. For the DEMI-series chromophores, only limited information is obtained about the changes in molecular structure during and after photodegradation from the IR spectroscopic study on Ultra-DEMI in this research. Even so the possible influence of polymer matrix (PMMA) on the photodegradation of doped polymer system is excluded based on the experiments of the pure PMMA film under exposure of 632.8 nm at the same condition as the doped waveguide films. In order to enhance the photostability of these chromophores and their systems, further work needs to be done. Such as,

analysing the products of photodegradation in the films by electron spin resonance or other methods to achieve more information about exact changes in the chromophores and new structures occurring in the system; doping these chromophores into other polymer matrices (e.g. polycarbonate, etc.) to fully elucidate the interaction between the chromophore molecules and the matrix molecules on the process of photodegradation and to explore a higher possible photostability in different polymer systems.

On the techniques of waveguide degradation, doped slab waveguide structures and two-prism coupling have been used to perform the experiments. However, to achieve more accurate results and better characterisation, channel waveguiding is a solution to do these experiments, which provides a better confinement of the beam and the waveguide modes. This means that microprocessing on slab waveguide is needed to form channel structures. At the same time some work needs to be undertaken to maintain the consistency of coupling efficiency during photodegradation by changing or improving coupling techniques, since prism coupling is related to the surface condition of the waveguide and the pressure applied on the prism, which will lead to the variation of the coupling efficiency, errors may be introduced in the calculations of the quantum yields.

As an application to explore for a polymer waveguide structure, a stacked waveguide (multi-layer structure) is investigated as a humidity sensor and it has reached nearly to the stage to launch a commercial product, because it has shown promising prospect for its attractive advantages (e.g. a very low limit of detection humidity value (ppm), good linearity and reversibility). Two types of these waveguide structures, P4VP-I (symmetric) and P4VP-II (unsymmetric), were designed to form an integrated Young's interferometric sensor. Using this vertically stacked slab structure waveguides were fabricated to achieve single mode output from the each guiding layer.

The P4VP-I and P4VP-II sensors have shown that they have good reversibility and enough stability from the experiments, if the instability of the light source is considered. The P4VP-I structure, which can detect 150 ppm of water vapour, proves the feasibility of vertically stacked waveguide (integrated Young's interferometer) as a kind of humidity sensor with good properties and potential. The sensitivity of P4VP-II is improved significantly by using different polymers in the structure. It can detect as low as 30 ppm of

water vapour using a simple observation of phase shifts. A phase shift of 0.1π (0.314 radians) has been measured at this low concentration of water vapour in experiments. The results have shown that the overall response of the P4VP-II sensor exhibits good linearity with increase in the concentration of water vapour. Since both P4VP-I and P4VP-II structures cannot only measure the values of fringe phase shift, but also the direction of movement of the interference fringe, and can produce interference fringes with a separation about 1 cm at a distance about 10 cm behind the output endface of the waveguide, they have advantages compared with other sensors.

In order to achieve a better performance in applications and to open up new markets, increasing the sensitivity and improving the endface condition of the sensor chips are two major pieces of work needed for this waveguide sensor. Because the sensitivity of the sensor depends on the measured amount of phase shift of fringes, this is proportional to the changes in the refractive indices between the upper and lower guiding layers and is induced by the quantity of water vapour absorbed by the upper guiding layer. By using either a larger sample due to its longer interaction length or different combinations of materials in the waveguide structure (a highly water absorbing polymer as the upper guiding layer, no water absorbing materials as the middle cladding layer), a larger absolute phase shift of the interference fringes can be induced between the two guiding layers, eventually the sensitivity of the waveguide sensors can be improved significantly.

The quality or condition of endface of the sensor chips affects the quality of the produced interference fringes and coupling efficiency of the illuminating beam, more important is that the accuracy and sensitivity are influenced to a certain degree by reading the shifts of the fringes from the background noise. Further effort needs to be paid to the improvement of the endface quality of the sensor to obtain the sharp contrast of the fringes and to suppress the background noise. In conclusion, this integrated waveguide humidity sensor will hopefully become a low cost, small size sensor.

At the moment the selectivity of the waveguide sensor in this research has not been investigated. Its humidity sensing ability is increased greatly by using a polymer which has degree of water absorption. Sensing organic vapour is important research work which needs to be done for this sensor. It has a potential market and is facing a great challenge.

The selectivity of the sensor can be realised by choosing a suitable polymer or by selecting a sensitive dopant in the polymer, a large change of refractive index in the sensing layer can be induced when an organic vapour is introduced. Therefore the sensor will provide a quick and sensitive response to the vapour, and may be used to detected some vapour which the available techniques are unable to do at present or at a high price.